Study of the endoplasmic reticulum proteostasis network during ageing

A thesis submitted to the University of Manchester for the degree of Doctor of Philosophy in the Faculty of Life Sciences

2012

ALINA - RUXANDRA MARES

Faculty of Life Sciences

University of Manchester

Table of Contents

List of Figures

List of tables

Abbreviations

3D – three-dimensional
α1-AT – alpha-1 antitrypsin
Aβ – amyloid beta peptide
Aip-1 – actin interacting protein 1
ALS – autophagic-lysosomal system
ANOVA – analysis of variance
ATF – activation transcription factor
Atg – autophagy-related genes
BAG – Bcl-2-associated athanogene
BiP – immunoglobulin binding protein
cav – caveolin
CFTR – cystic fibrosis transmembrane conductance regulator
CHIP – C-terminus of Hsc-70 interacting protein
CHOP – C/EBP (CCAAT/enhancer binding)-homologous protein
CHX – cycloheximide
CMA – chaperone-mediated autophagy
CNX – calnexin
conA – concanavalin A
crt – calreticulin
COPII – coat protein complex II
Da – Dalton
daf - abnormal dauer formation protein
DAPI – 4,6-diamine-2-phenylindoledihydrochloride
Der – Derlin
DMEM – Dulbecco's modified Eagle's medium
DTT – dithiothreitol
E1 – ubiquitin-activating enzyme
E2 – ubiquitin-conjugating enzyme
E3 – ubiquitin ligase
EDEM – ER degradation enhancing -mannosidase-like protein
EDTA – ethylenediaminetetraacetic acid
EGTA – ethylene glycol tetraacetic acid
eIF2α – eukaryotic translation initiation factor 2 alpha
ER – endoplasmic reticulum
ERAD – ER-associated dergradation
ERdj – ER-associated dnaJ protein
ERES – ER exit sites
ERGIC – ER-Golgi intermediate compartment

ERQC – ER quality control
ERp – endoplasmic reticulum resident protein
EndoH – endoglycosidase H
GADD34 – growth arrest and DNA damage-inducible protein 34
Glc – glucose
GRP – glucose-regulated protein
HA – hemagglutinin
HCl – hydrochloric acid
HEK –human embryonic kidney
HEPES – 4-(2-hydroxyethyl)-1-piperazineethanesulfonic acid
HPD – high population doubling
HRD-1 – HMG-CoA reductase degradation protein 1
Hsc – heat shock cognate
Hsf-1 – heat shock factor 1
Hsp – heat shock protein
γINF – gamma interferon
IGF - insulin-like growth factor
IRE-1 – inositol-requiring protein-1
LAMP-2 – lysosomal-associated membrane protein 2
LB – Luria Bertani
LC3-II – microtubule associated protein 1A/1B-light chain 3-II
LPD – low population doubling
MEM – Minimum Essential Medium Eagle
MW – molecular weight
mTOR – mammalian target of rapamycin
MTT – 3-(4,5-Dimethylthiazol-2-yl)-2,5-diphenyltetrazolium bromide
NEM – N-ethylmaleimide
NHK – alpha 1 anti-trypsin Null Hong-Kong variant
Npl4 – nuclear protein localisation 4
OD – optical density
ops – opsin
OST – oligosaccharyl transferase
OS9 – osteosarcoma 9
p5 – protein disulfide-isomerase A6 precursor
p97 – valosin-containing protein AAA-ATPase
PAGE – polyacrylamide gel electrophoresis
PCR – polymerase chain reaction
PD – population doubling
PDI – protein disulphide isomerase

PERK – protein kinase RNA-like ER kinase 1

pK – proteinase K

PMSF – phenylmethylsulphonyl fluoride

PNG – protein N-glycanase

polyQ – polyglutamine

polyUb - polyubiquitinated

pPL – pre-prolactin

QC – quality control

qPCR – quantitative PCR

RFP2 – E3 ubiquitin-protein ligase TRIM13 isoform 2

RIPA – radio-immunoprecipitation assay

RMA1 – RING finger protein with membrane anchor 1

Rpl17 – large-subunit ribosomal protein L17A

Rpn – proteasome regulatory particle non-ATPase-like

Rpt – large ribosomal subunit protein

RT-PCR – reverse-transcription PCR

SDS – sodium dodecyl sulphate

SDO – sodium deoxycholate

SeL-1L – sel-1 suppressor of lin-12-like

s.e.m – standard error of the mean

SPC – signal peptidase complex

SPP – signal peptide peptidase

SRP – signal recognition particle

TCR – T-cell receptor

TRAM – translocation-associated membrane protein

TRAP – translocon-associated protein

TRC40 – arsenical pump-driving ATPase

Tris – tris(hydroxymethyl)aminomethane

Tn – tunicamycin

ts – temperature sensitive

TGN – trans-Golgi network

Ub – ubiquitin

Ufd – ubiquitin fussion degradation

UGGT – UDP-glucose glycoprotein glucosyltransferase

UPR – unfolded protein response

UPS – ubiquitin – proteasome system

VIMP – VCP-interacting protein

v/v – volume per volume

VSV-G – vesicular stomatitis virus G glycoprotein

WB – western blotting

WRB – tryptophan-rich basic protein

WT – wild-type

w/v – weight per volume

XBP-1 – X-box binding protein 1

*XBP1*1u/s – unspliced/spliced Xbp1 mRNA

XTP3B – XTP3-transactivated gene B

Abstract

The functional integrity of the proteome is essential for proper cell functioning. Protein homeostasis, or proteostasis, is maintained by a network of pathways that mediate the biosynthesis, folding and degradation of proteins. Accumulating evidence suggest that ageing is associated with a general decline in protein homeostasis. Proteins are synthesised in the cytosol as extended polypeptide chains, which must then be folded in to their native conformation, before moving to their site of function. Protein folding occurs in different subcellular compartments, such as the cytosol and the endoplasmic reticulum (ER). Due to the nature of the proteins that are processed in the ER (e.g. ionic channels, receptors, hormones, signalling molecules), the function of this compartment can be seen to be of vital importance to the cells. However, the effect of age on ER protein homeostasis is virtually unknown.

A combination of post-mortem mouse tissues and cell-based models were used to examine the impact of age on ER protein folding, quality control and the ER stress response. Analysis of the expression level of ER-resident and ER-linked proteins showed a number of age-related changes in mouse tissues, in human fibroblasts aged *in vitro* by serial passage, and human fibroblasts obtained from young and old donors (*in vivo* aged cells). Overall, the pattern of changes was variable between different tissues and cell systems. However, a common feature of aged tissues and both cellular models of ageing, was a significant increase in phosphorylation of eIF2α, indicating that ER protein homeostasis is affected with age. In addition, ageing in several tissues and in both cellular systems was associated with accumulation of polyubiquitinated substrates, suggesting that degradation of abnormal proteins via the proteasome is deficient. More detailed investigation of ER proteostasis using the cellular models showed that *in vitro* aged cells had a decreased capacity to fold a temperature sensitive model membrane protein (ts O45 VGV-G) and were less efficient at degrading two model substrates of the ER-associated degradation pathway. Since the ER protein folding and degradation pathways are modulated by ER stress response signalling to restore ER homeostasis, therefore their malfunctioning would impact on the ability of aged cells to cope with stress. Indeed, in the aged cells both PERK and IRE-1 signalling were perturbed. In addition, the level of BiP was not upregulated following ER stress in the aged cells. Moreover, ER stress induction led to decreased cell survival in the case of aged cells, showing that the inability of aged cells to maintain ER protein homeostasis results in increased susceptibility to cell death. All these data together shows how perturbed ER proteostasis can occur with increased age and its impact on overall cell wellbeing, therefore provide new insight into mechanisms of cell ageing.

Declaration

No portion of the work referred to this thesis has been submitted in support of an application for another degree or qualification of this or any other university or other institute of learning.

Copyright statement

Acknowledgements

I wish to express my deepest gratitude and admiration to my supervisor, Dr. Lisa Swanton for her continuous support in the pursuit of this thesis, excellent guidance and extensive knowledge. I am thankful to you for allowing me a great degree of professional freedom, but always being close with help or good advice whenever I have needed it. Also, thank you for your suggestions on the writing of this thesis and for the fact that you made it an enjoyable experience as was all of the time spent in your lab. Many thanks to Professor Ray Boot-Handford for his guidance during my work with animal models and for his useful suggestions on my project.

Special thanks to my advisor, Professor Steven High for sharing many constructs and antibodies, and especially for the valuable discussions and experienced assessment of my working progress.

I owe a lot of thanks to my colleagues, members of the Swanton and Pool labs, for creating a pleasant working environment. I will never forget the help provided by Dr. Lydia Wunderley and our stimulating discussions, when we were working together side by side, and all the good time we have had in the last four years. I would like to thank to the members of the High, Lowe, Smith, Woodman and Allan for sharing reagents, protocols and lab equipment.

I am fortunate to have a loving family that was close to me when times got stressful. Thank you for your unconditional support. I would like to thank to my loving partner, Jonathan for supporting me throughout my research and writing times, and for believing in me even when I did not believe in myself. Your joyful spirit was refreshing after the long days of work and commuting.

Many thanks to all my friends, from abroad and from England, for the encouragement and for the good time that we had together.

At last, I would like to dedicate this thesis to two exceptional women: my grandmother that surely discovered the secret of healthy ageing and to Lucette Penant, my Belgian ‘adoptive’ mother that will never be touched by age.

Grateful thanks to Biotechnology and Biological Sciences Research Council for funding.

CHAPTER 1

Introduction

1.1 Protein homeostasis and quality control

The functionality of the cell depends on maintaining an appropriate balance between protein synthesis, folding and protein trafficking or degradation. This balance of protein biosynthesis and degradation pathways has been named protein homeostasis or 'proteostasis'. These key cellular pathways act in a coordinated manner as a network (Figure 1.1), to ensure proper protein maturation and efficient degradation of misfolded or otherwise damaged proteins (Roth & Balch 2010).

Proteins are initially translated as extended polypeptide chains that must be folded into their correct 3D native conformation. Protein folding occurs in many different subcellular compartments (e.g. cytosol, endoplasmic reticulum) (Fig 1.2). Here the extended, polypeptide chain, is progressively packed to minimise the exposure of hydrophobic patches to the hydrophilic folding environment (Hartl *et al.* 2012). Thermodynamically, protein folding is illustrated by a funnel-shaped energy landscape, where the unfolded state, representing an unordered structure characterised by high-entropy state is at the top of the funnel and progresses downhill through several folding intermediates to acquire the native, highly ordered state characterised by the lowest energy (Vabulas *et al.* 2010). As proteins fold in a crowded cellular environment, this process is assisted by molecular chaperones that shield the hydrophobic regions of the polypeptide chain and promote its folding (Lindquist & Kelly 2011).

Protein translation and folding are error prone processes and therefore improperly folded (misfolded) proteins are continually produced as a normal consequence of cellular growth and maintenance (Herczenik & Gebbink 2008; Drummond & Wilke 2009). It has been estimated that almost 30% of newly synthesised proteins are misfolded (Schubert *et al.* 2000). In addition, an important fraction of cellular proteins – called metastable proteins, have an increased requirement for chaperone function to acquire their proper conformations (Naeem & Fazili 2011). Since they are very sensitive to the folding environment/resources, metastable proteins are more prone to misfolding, and can be used as 'sensors' for the functional capacity of the proteostasis machinery in live cells and model organisms such as C. *elegans* (Ben-Zvi *et al.* 2009). Furthermore, many situations such as genetic mutations and adverse environmental or cellular conditions can further disrupt folding and increase the production of misfolded proteins. Misfolded proteins may expose hydrophobic regions, therefore making them prone to aggregation (Vabulas *et al.* 2010; Olzscha *et al.* 2011). These non-native proteins can also sequester chaperones or engage in inappropriate interactions with other proteins and cellular membranes, and can also potentially perturb the cellular redox balance (Olzscha *et al.* 2011). Therefore, the cell possesses quality control (QC) systems that operate throughout the cell to identify and remove misfolded, damaged or otherwise abnormal proteins. The protein quality control machineries within the endoplasmic reticulum and cytosol are currently well characterised, and will be discussed in more detail later.

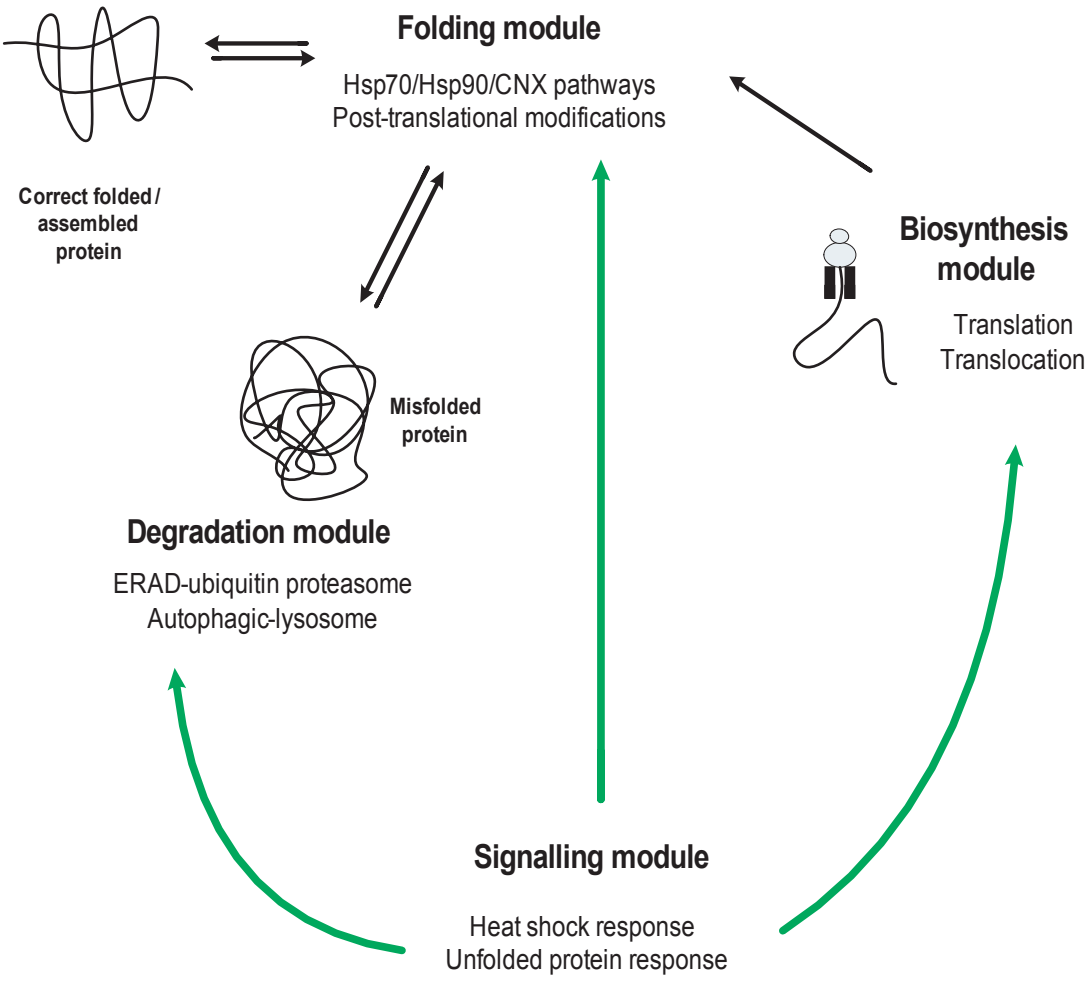

Figure 1.1: Protein homeostasis network
Proteostasis consists of numerous interacting and competing biological pathways (black arrows). These include pathways that control protein synthesis, folding, assembly, traffic and degradation. If proteostasis is disrupted, aberrant proteins accumulate and can lead to cellular dysfunctions and diseases. Stress signalling pathways (green arrows) detect accumulation of misfolded proteins and function to restore homeostasis by regulating the pathways influencing proteostasis. Adapted from Balch et al. 2008

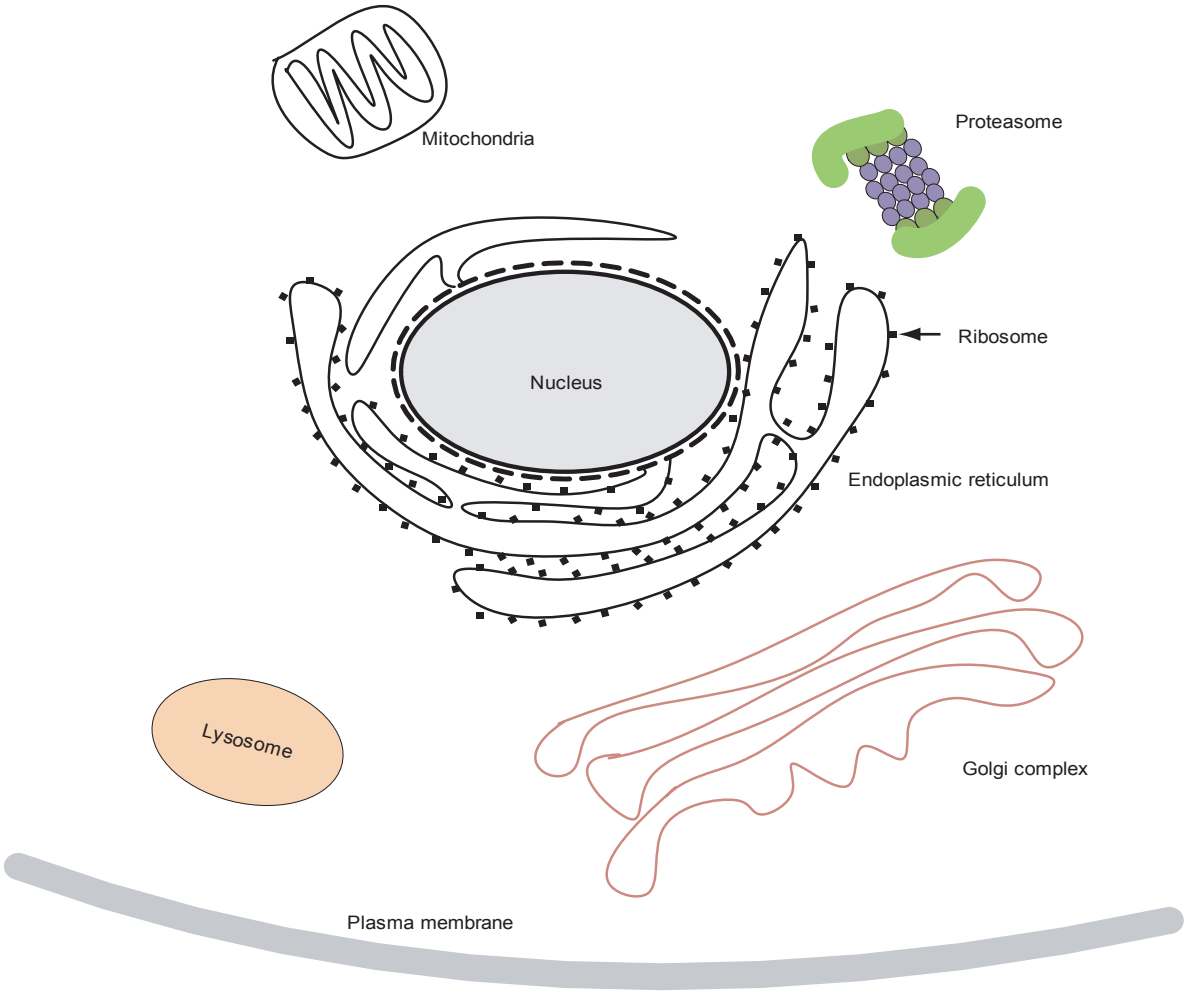

Figure 1.2: Cellular compartmentalisation.
In eukaryotic cell DNA is separated from the cytosol by a double membrane (nuclear envelope), creating the the nucleus. Continuous with the outer membrane of nucleus is a membranous network of tubules - endoplasmic reticulum (ER). The rough ER has membrane bound ribosomes and is involved in protein processing; the smooth ER, without ribosomes is not involved in protein maturation.
The Golgi apparatus is a stack of flattened cisternae, which also has also an important role in further protein modification, sorting and transport. It has a receiving face (cis-Golgi complex) closest to the ER and a secretory face (trans-Golgi complex) closest to the plasma membrane.
The abnormal proteins can be degraded by the lysosome or proteasome.
The mitochondria has an inner and an outer membrane separated by an intermembrane space. It is an important subcellular organelle since it generates the ATP used by the cell in various other processes. Adapted from Kourtis and Tavernarakis 2011.

In the cytosol the folding of newly synthesised proteins is carried out by specific molecular chaperones, generically called heat shock proteins (Hsp) (Hartl *et al.* 2012). These cytosolic chaperones are classified into families according to their molecular weight (e.g. Hsp40, Hsp70, Hsp90). The co-translational folding of polypeptide chains is mediated by interactions with Hsp70, while for posttranslational folding steps the substrate is transferred from Hsp70 to Hsp90 (Taipale *et al.* 2010; Vabulas *et al.* 2010). Most of the proteins require multiple folding cycles before reaching their native conformation, and substrate binding and release from Hsp70 or Hsp90 is mediated by various co-chaperones (Hartl *et al.* 2012). One of these co-chaperones is carboxyl terminus of Hsc70-interacting protein (CHIP), a ubiquitin ligase, which by binding to Hsp70 or Hsp90 mediates the selection of their client protein for degradation (Connell *et al.* 2001; Muller *et al.* 2012). The ability to degrade abnormal proteins is essential to maintain cellular proteostasis. There are two main proteolytic systems in mammalian cells – the proteasomal systems and the lysosomal system, both of which play important roles in removing aberrant proteins. CHIP can bind to either BCL2-associated athanogene 1 (BAG1) or to BAG3 to promote proteasomal, or lysosomal degradation respectively (Luders *et al.* 2000; Gamerdinger *et al.* 2009; Lamark & Johansen 2012).

Proteins are targeted to the proteasome by the attachment of ubiquitin (Ub). The majority of 26S proteasome substrates are polyubiquitinated (polyUb), having at least 4 Ub residues attached in a chain (Finley 2009). Ubiquitination is mediated by a set of enzymes: E3 ubiquitin ligases, E2 ubiquitin conjugating enzymes and E1 ubiquitin-activating enzymes (Guerriero & Brodsky 2012). In an ATP-dependent step Ub is activated by the E1 enzyme which then transfers the Ub to the E2 conjugating enzyme. With the assistance of the E3 ligase, the Ub is then covalently attached to the substrate protein (Fig 1.3A) (Yang *et al.* 2010). E3s can bind both the E2 and the misfolded substrate and is believed that the E3 enzyme provides substrate specificity to the ubiquitination reaction (David *et al.* 2011). The 26S proteasome contains the 20S core particle flanked by the 19S regulatory particles (Fig 1.3B), each of which is composed of multiple subunits. The 20S core contains the proteolytic sites that mediate the hydrolytic activities. Each regulatory 19S particle contains six AAA-ATPase (Rpt 1-6) and several Rpn subunits (Fig 1.3B) (Gallastegui & Groll 2010). The 26S proteasome clients are recognised and deubiquitinated by the Rpn subunits (Fig 1.3C). The entry and release from the 20S proteasome is mediated by the Rpt2 subunit (Kim *et al.* 2011). Proteasomal degradation generates short peptides of up to 30 amino acids (Fig 1.3C), which are released into cytosol for further degradation into constituent amino acids to be used in the biosynthesis of new proteins.

Defective proteins can also be degraded via autophagic pathways, which deliver them to the lysosome (Fig 1.4). Most of the substrates of the autophagic pathway substrates are sequestered in vesicles and delivered to lysosomes for degradation. Lysosomes are specialised vesicles containing hydrolytic enzymes from the aspartic, cysteine, or serine proteinase families

(Mizushima 2007). In mammalian cells, three types of autophagy have been described: microautophagy, macroautophagy and chaperone-mediated autophagy (CMA). Of these, more is known about the mechanisms of the latter two pathways. CMA substrates are soluble cytosolic proteins that exhibit a pentapeptide motif that contains a conserved charge (Asn/Gln – acidic – basic – hydrophobic – basic/hydrophobic residue), and is important for substrate selection (Bejarano & Cuervo 2010). When proteins misfold this targeting sequence is exposed and is bound by the constitutive expressed heat shock protein Hsc70. The complex is delivered to the lysosomal receptor LAMP-2A (Fig 1.4A) (Orenstein & Cuervo 2010). Following binding, the substrate is translocated across the lysosomal membrane, possibly through a complex formed by LAMP-2A multimers and with the assistance of lysosomal chaperone lys-Hsc70 (Fig 1.4A). Once in the lysosome lumen the substrate is degraded by the lysosomal proteases (Arias & Cuervo 2010; Kaushik *et al.* 2011). The macroautophagic, also called the autophagic pathway, is responsible for degradation of bulk cytoplasmic debris, such as organelle fragments or protein aggregates (Ravikumar *et al.* 2010). The substrates for autophagic degradation are isolated in double coated vesicles named autophagosomes, before being delivered to the lysosome (Fig 1.4B) (He & Klionsky 2009). The formation and maturation of autophagosomes requires the recruitment of multiple Atg (autophagy related genes) proteins, such as Atg5, 7, 12 and Atg8 - also known as LC3 (microtubule associated protein 1A/1B-light chain 3). The Atg8/LC-3 exists in two isoforms: the soluble protein (LC3-I) and the membrane bound form (LC3-II) (Kabeya *et al.* 2000). Upon initiation of autophagosome assembly, LC3-I is converted to LC3-II by the addition of a phosphatidylethanolamine group to C-terminus (Kabeya *et al.* 2004). Subsequently, the fusion of autophagosomes with the lysosome, which is mediated by the lysosomal membrane protein LAMP-2 and the GTPase Rab7 delivers the autophagic content to lysosomes for degradation (He & Klionsky 2009; Trocoli & Djavaheri-Mergny 2011). Polyubiquitination can also act as a signal for autophagy, suggesting that cross-talk between different degradative pathways exists (Ding & Yin 2008). Two Ub binding proteins have been shown to be required: p62 (also called sequestrin) and histone deacetylase 6 (HDAC6). P62 binds to the Ub residues and then by interacting with LC3-II, promotes autophagosome assembly (Shaid *et al.* 2012). HDAC6 can bind polyUb misfolded proteins and dynein-motor proteins, mediating the transport on microtubules of damaged proteins to the site of autophagosome formation (Kawaguchi *et al.* 2003; Lamark & Johansen 2012). At the later stage in autophagy, HDAC6 regulates the remodelling of actin filaments to aid autophagosome - lysosome fusion (Lee *et al.* 2010).

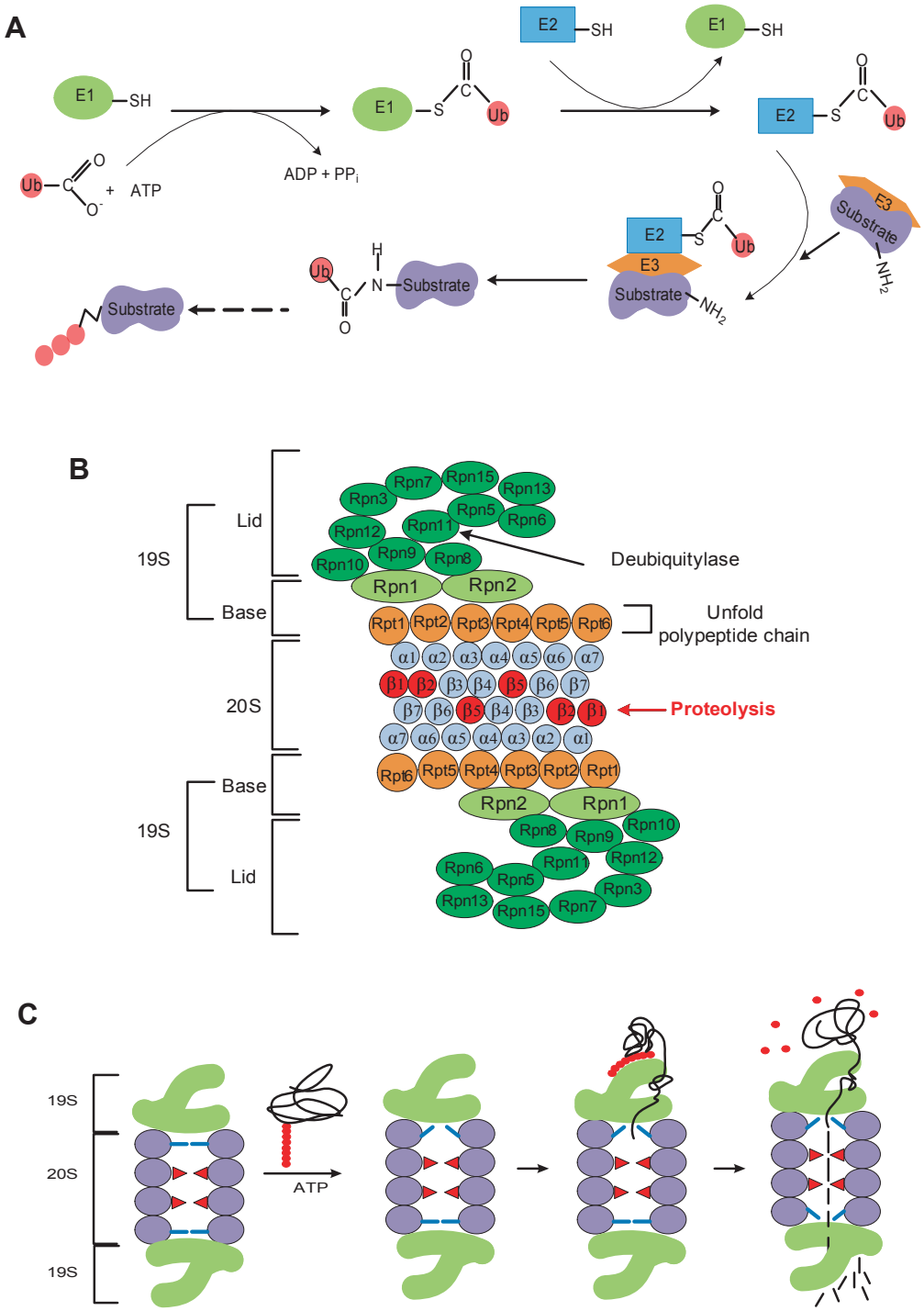

Figure 1.3: Ubiquitin conjugation and 26S proteasome degradation systems
(A) The ubiquitin residue (Ub) is attached to an E1 ubiquitin-activating enzyme in an ATP-dependent reaction, then transfered to an E2 ubiquitin-conjugating enzyme. The recruitment of E2-Ub thioester to E3 ubiquitin lygase initiates the transfer of Ub to a Lys residue of the E3 bound substrate.
(B) Structure of the 26S proteasome. The19S subunit is formed by 15 non-ATPase subunits (Rpn) and 6 ATPase subunits (Rpt). The barrel-shaped 20S subunit includes 4 heptameric rings: two alpha and two beta. Three β-type subunits in each ring have proteolytic activity.
(C) ATP binding mediates the opening of 20S gate. The substrate is bound by Rpn1, Rpn10 and Rpt5 and following unfolding, the polypeptide chain enters in the 20S lumen to be cleaved. The resulting 2-30 amino acid peptides are released in to the cytosol.
Adapted from Goldberg 2007 and Brooks 2010

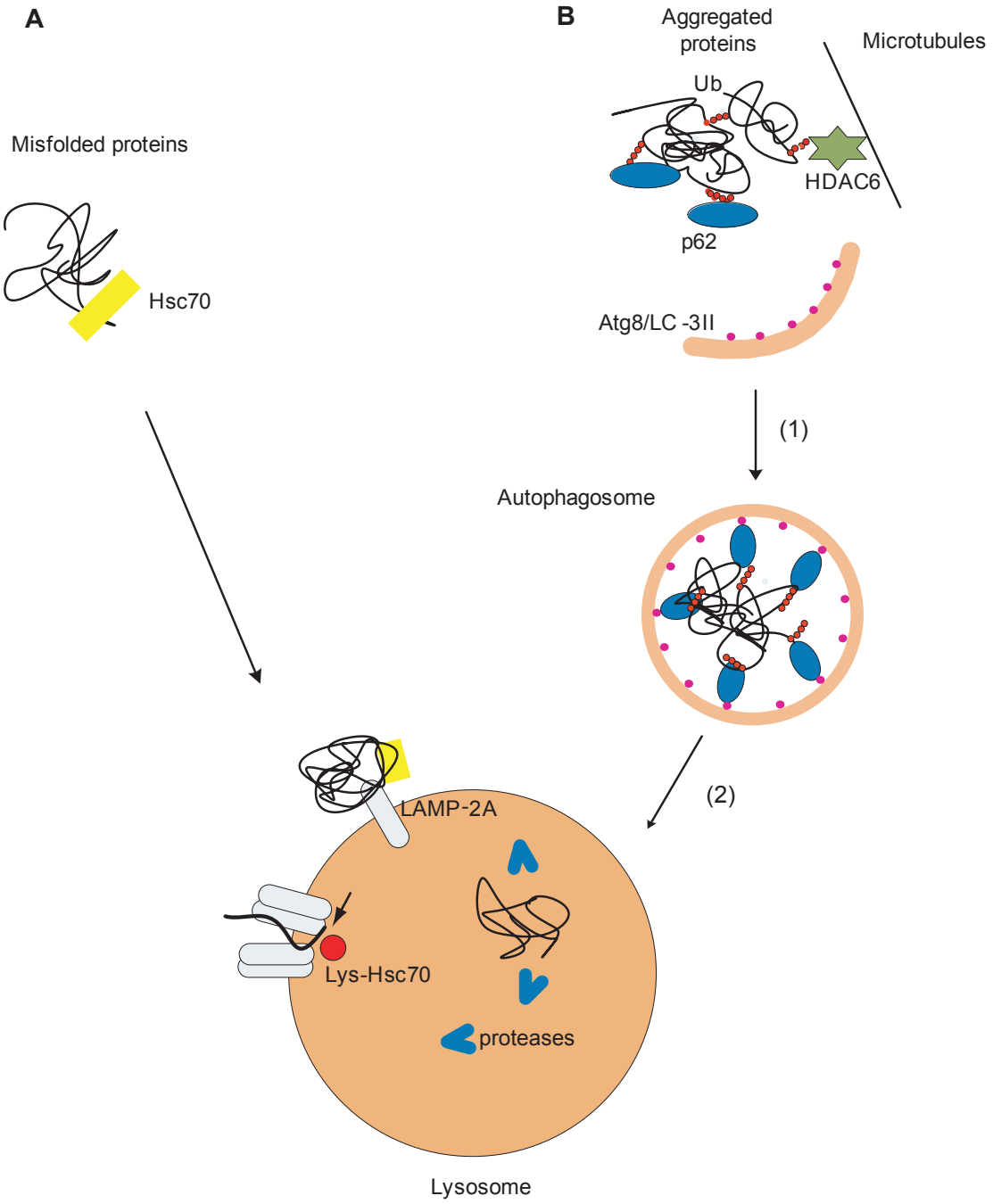

Figure 1.4: Autophagic pathways
Chaperone-mediated autophagy (CMA) **(A)** and selective autophagy **(B)** are two proteolytic pathways. The degradation via CMA requires a recognition motif that is bound by Hsc70 and targeted to lysosomes. Transport into the lysosome is mediated by the lysosomal receptor LAMP-2A and lysosomal Hsc70 (lys-Hsc70).
Selective autophagy (’aggrephagy’) is involved in the degradation of extra- and intracellular cargo, including polyUb aggregated proteins. The p62 acts as an adaptor that binds the Ub residues and also recruits Atg8/LC3-II and promotes the formation of the autophagosome. HDAC6 is another protein with Ub binding domains that is involved in autophagosome maturation (1). At a later step HDAC6 mediates autophagosome - lysosome fusion by modulating the cytoskeleton microfilaments (2).
Adapted from Lamark and Johansen 2012, and Kang 2010.

Removal of non-native proteins by these pathways ensures that the fidelity of the proteome is maintained. However, certain conditions, such as chemical insult, heat shock, and somatic mutations, can disrupt protein folding and/or degradation, favouring the accumulation of aberrant proteins. In these cases, the stress response pathways of the proteostasis network are activated. These function to coordinate and adjust the rates of proteins synthesis, folding and degradation in response to environmental changes, thereby restoring proteostasis (Fig 1.1) (Hartl *et al.* 2012). The fundamental importance of these homeostatic responses is highlighted by the correlation between the capacity of cells to respond to proteotoxic stressors and the ability to survive such challenges (Lindquist & Kelly 2011). Cytosolic proteostasis is regulated by a stress response pathway generically called the heat shock response (HSR). Following stress induction, the heat shock transcription factor (HSF1) is released from a complex with Hsp90/Hsp70 and activates Hsp genes (Vabulas *et al.* 2010). The upregulation of molecular chaperones, including Hsp70 and Hsp90, promotes the folding and/or degradation of aberrant proteins accumulated under stress conditions (Buchberger *et al.* 2010). When the ratio of Hsp70/Hsp90 to unfolded proteins increases, the HSF1 is again trapped in a complex with these chaperones and the HSR is attenuated (Akerfelt et al. 2010). In addition to protecting the cell against the accumulation of toxic misfolded proteins, the HSR has an important role in normal physiology (e.g. during development) (Jedlicka et al. 1997; Xiao et al. 1999).

Defects in the proteostasis network have been implicated in a number of important pathological conditions such as neurodegenerative diseases e.g. Alzheimer's, Huntington's, and Parkinson's diseases that are caused by aggregation of aberrant proteins (Marciniak & Ron 2006). Moreover, these protein-folding diseases are triggered or exacerbated with age suggesting that protein homeostasis might be perturbed during ageing (Morimoto 2008). In addition, several studies provide more direct evidence that global protein homeostasis is disrupted with age (Ben-Zvi *et al.* 2009; David *et al.* 2010).

1.2 Protein homeostasis and ageing

There is evidence that ageing is associated with a global decrease in the functioning of the protein homeostasis machinery (Koga *et al.* 2010). As a result, damaged and misfolded proteins accumulate in aged cells and/or tissues. Aggregated proteins can disrupt the folding of unrelated proteins, leading to a general decline in protein homeostasis. These observations are consistent with the network model of protein homeostasis and suggest an interdependence of the component pathways (e.g. folding, trafficking, degradation, signalling) (Roth & Balch 2010). Therefore, an imbalance of any one of these has the potential to affect the entire network by perturbing the other pathways (Balch *et al.* 2008). For example, when proteins containing glutamine repeats (polyQ) which tend to form insoluble aggregates are expressed in *C. elegans,* they inhibit the folding of other metastable proteins, providing the first evidence that the presence of aggregated proteins disrupts cellular folding capacity (Gidalevitz *et al.* 2006). In

cultured mammalian cells, aggregates formed by expression of beta-sheet containing proteins sequester a range of essential cellular proteins (Olzscha *et al.* 2011). The endogenous proteins that are sequestered have large unstructured regions, suggesting that they represent a distinct metastable population of the proteome (Olzscha *et al.* 2011) providing further evidence that aggregated proteins are able to perturb cellular protein folding capacity. These studies also suggest a mechanism through which protein aggregates promote a loss of protein homeostasis and disrupt cell function. A similar decrease in folding of metastable reporter proteins is also seen to occur in aged *C. elegans* (Ben-Zvi *et al.* 2009), suggesting age reduces the efficiency of the folding proteostasis. In support of this idea, a recent study in *C. elegans* has shown that ageing is associated with the widespread aggregation of a range of endogenous proteins (David *et al.* 2010). Importantly, protein aggregation was found to be reduced by IGF mutations that increase the *C. elegans* lifespan, suggesting that accumulation of aggregates may impact on longevity and contribute to the ageing process (David *et al.* 2010; Kourtis & Tavernarakis 2011). In contrast to these studies using short-lived model organisms, there is no direct demonstration that an age-related decline in general proteostasis is conserved in mammals. Nevertheless, the idea is supported by the observation that accumulation of misfolded and aggregated proteins occurs in degenerative age-associated proteinopathies affecting mice brain, muscle, liver (Page *et al.* 2009; Gupta *et al.* 2011; Lamark & Johansen 2012). In addition, a number of factors might contribute to the decline in proteostasis with age, such as decreased chaperone function, decreased degradation capacity, and inability to respond to proteotoxic stress. Indeed several studies in *C. elegans* and *D. melanogaster* have shown that decreased chaperone expression was paralleled by an accelerated aggregation of proteins with age (see table 1.1). Conversely, increasing chaperone expression has been found to increases lifespan and/or reduce age-related pathology in several model organisms – (table 1.1) (Hsu *et al.* 2003; Walker & Lithgow 2003; McArdle *et al.* 2004; Morley & Morimoto 2004; Morrow *et al.* 2004).

In addition to folding pathways, protein degradation plays a critical role in maintaining protein homeostasis (Koga *et al.* 2010). Several studies have shown that protein degradation mechanisms are impaired by age (summarised in table 1.2). Studies using various mouse tissues (heart, brain, hippocampus, liver) revealed an accumulation of polyUb proteins (Ohtsuka *et al.* 1995; Mura *et al.* 1996; Paz Gavilan *et al.* 2006), suggesting that the activity of the cytosolic proteasomal system declines dramatically with age. Indeed, the function of the 26S proteasome has been found to be impaired with age, due to altered composition of the proteasome (Ferrington *et al.* 2005) and/or reduced protease activity (Low 2011). In contrast, in long-lived *C. elegans* mutants, increased proteasomal activity correlating with high levels of RPN-6 were observed (Vilchez *et al.* 2012). In contrast, studies in human fibroblast and mouse liver found that ageing had no significant effect on the levels of components of the ubiquitination system including those of E1 and E2 enzymes and Ub (Carrard *et al.* 2002). On the other hand, experimental down-regulation of CHIP (cytosolic E3-ubiquitin ligase) expression levels was associated with accelerated age-related (patho)physiology and premature senescence (Min *et al.* 2008; Sisoula & Gonos 2011).

Protein	Function	Observations	References
Hsf-1	Transcription factor, regulates expression of heat shock proteins	Decreased expression reduces *C. elegans* lifespan. Overexpression improves stress-resistance and provides protection from toxic protein aggregation	(Hsu *et al.* 2003; Morley & Morimoto 2004; Volovik *et al.* 2012)
Hsp-70	Cytosolic chaperone, stress inducible	Over-expression increases lifespan in both *D. melanogaster* and *C. elegans* Overexpression maintained function of muscle in aged mice	(Tatar *et al.* 1997; Yokoyama *et al.* 2002; McArdle *et al.* 2004; Broome *et al.* 2006)
Hsp-90	Cytosolic chaperone, stress inducible	Lower expression in liver of aged rats	(Nardai *et al.* 2002)
Hsp-16	Small heat shock proteins, unknown function	Overexpression increase lifespan in *C. elegans*	(Walker & Lithgow 2003)
Hsp-23 Hsp-26 Hsp-27	Small heat shock proteins, unknown function	Upregulated in aged *D. melanogaster*	(Tower 2009)

Table 1.1 Relationship between cytosolic chaperone expression and ageing

The autophagic - lysosomal degradation system is also compromised by age (Hubbard *et al.* 2011). Notably, a decline of chaperone-mediated autophagy has been observed in the liver of aged rats, due to reduced expression of the substrate receptor LAMP-2A (Cuervo & Dice 2000). This plays a causal role in age-related liver pathology since overexpression of LAMP-2A improves liver function in age (Zhang & Cuervo 2008). The age-dependent accumulation of oxidatively-damaged macromolecules in the lysosomes of postmitotic cells (neurons, cardiac myocytes) has been suggested to reduce the efficiency of lysosomal degradation (Terman & Brunk 2005). Furthermore, reduced expression levels of various Atg proteins (Atg 1, 9, 7, 12) decreases lifespan in *C. elegans,* and *D. melanogaster* (Hubbard *et al.* 2011). Additionally Atg 5 knockdown in mouse neurons and cardiomyocytes induced age-related pathologies and reduced cell survival (Taneike *et al.* 2010). In the same study, it was also observed that the levels of Atg8/LC3-II decreases with age in cardiac tissue, suggesting a decrease in autophagy. Interestingly, treatments that extend the lifespan by modulating stress signalling pathways have also been shown to upregulate the autophagic pathway in *C. elegans* and *D. melanogaster* (Rubinsztein *et al.* 2011). Moreover, a recent study using *in vitro* aged human fibroblasts suggested that cellular ageing is associated with a switch from proteasomal to lysosomal degradation (Gamerdinger *et al.* 2009).

Protein	Function	Observations	References
LAMP-2A	Lysosomal receptor, component of the chaperone-mediated autophagy pathway	Levels of LAMP-2A decrease with age. CMA function is decreased in liver of aged rats. Overexpression of LAMP-2A in liver of aged mice protects against accumulation of misfolded proteins and maintain tissues function.	(Cuervo & Dice 2000; Zhang & Cuervo 2008)
20S 19S	Enzymatic and regulatory subunits of proteasome	Increased levels of 20S and decreased content of 19S in muscle of old mice. Increased content of oxidized subunits in muscle of old mice. Decreased protease activity in spinal cord of aged rats. Increased level of Rpn-6 and increased proteasomal activity in long-living *C. elegans*.	(Keller *et al.* 2000; Ferrington *et al.* 2005; Vilchez *et al.* 2012).
BAG1 BAG3	Chaperones from proteasomal (BAG1) and autophagic (BAG3) pathways	Decreased level of BAG1 and increased level of BAG3 in human senescent fibroblasts.	(Gamerdinger *et al.* 2009)
Atg	Proteins from macroautophagic pathway	Pertubation of Atg5 and Atg7 reduces lifespan in *C.elegans,*and *D. melanogaster*, and induces premature senescence in human fibroblasts. Overexpression of Atg8 in the brain of the wt *D. melanogaster* reduced protein aggregation and increased lifespan.	(Juhasz *et al.* 2007; Simonsen *et al.* 2008; Toth *et al.* 2008; Kang *et al.* 2011)
CHIP	Cytosolic E3 ubiquitin ligase	Knockdown induces premature aging in mice and cultured cells. Overexpression decreases the accumulation of aggregated proteins and ameliorates symptoms in diseased mice.	(Adachi *et al.* 2007; Juhasz *et al.* 2007; Min *et al.* 2008; Sisoula & Gonos 2011)

Table 1.2 Correlations between components of the degradation pathways and ageing

Maintenance of protein homeostasis depends on efficient stress responses (Morimoto 2008). Considerable amounts of data have shown a direct correlation between the capacity to respond to stress and longevity. Studies in *C. elegans* have shown that increased lifespan induced by loss of function mutations in IGF signalling pathway (Fig. 1.5) is mediated through upregulation of *hsp* genes (Hsu *et al.* 2003; Halaschek-Wiener *et al.* 2005). IFG signalling pathway is highly conserved in evolution. Ligand binding to the IGF receptor (daf-2 in C. elegans, InsR1 in mammalians) initiates a signalling cascade via of inositol 1,4,5-trisphosphate 3-kinase (age-1 in nematodes, PI3K in mammalians) ending with phosphorylation of transcription factor (daf-16 in worms, FOXO in mammalians) (Fig 1.5). This modification of daf-16/FOXO prevents it transport to nucleus and thus activation of its transcriptional programme (Kenyon 2010b), Also, the transcription factor hsf-1 is negative regulated by the IGF pathway, by preventing its release from the inhibitory complex (Chiang *et al.*). Deletion of daf-2 (Kenyon *et al.* 1993) activates both transcription factors daf-16 and hsf-1, while mutations of age-1 (Johnson 1990) only upregulates transcriptional program mediated by daf-16 (Fig 1.5). In addition, these long-lived worms also exhibit an increased resistance to heat (Lithgow *et al.* 1995) or to oxidative stress (Larsen 1993), and efficiently upregulated the *hsp* genes following exposure to the stresses (Walker & Lithgow 2003). Loss of function mutations in the IGF receptor also extended the lifespan of *D. melanogaster* (Tatar *et al.* 2001). Similarly, the link between mutations in IGF receptor and longevity has been observed in mice (Bartke & Brown-Borg 2004; van Heemst 2010). In addition, the long-lived mice also presented increased resistance to oxidative stress (Holzenberger *et al.* 2003). Therefore, the stress-regulated mechanisms that mediate longevity appear to be conserved in mammals.

Another mechanism that regulates lifespan is the caloric restriction (CR) (Partridge *et al.* 2005; Walker *et al.* 2005). Although the exact pathways that are modulated by CR are not completely elucidated, it is suggested that extension of lifespan is the result of the activation of a genetic programme (e.g. longevity genes), rather than of a reduced cellular damage (e.g. oxidative stress) due to low metabolic activity (Sinclair 2005). By using compounds that mimic CR, such as resveratrol - a natural polyphenol found in grapes - it has been discovered that increased lifespan is mediated by the activation of sirtuins, especially Sir-2 in a daf-16 dependent manner (Wood *et al.* 2004; Viswanathan *et al.* 2005). Sirtuins are NAD^+-dependent deacetylases involved in various cellular such as cell growth, differentiation stress response (Chalkiadaki & Guarente 2012), However, whether this mechanism is also valid for CR is still under debate (Bass *et al.* 2007).

In conclusion, perturbation of protein homeostasis may result from effects on different pathways that influence protein synthesis and folding capacity, protein quality control and protein degradation, as well as the ability to respond to disturbances in folding homeostasis. An important feature of eukaryotic cells is that they are compartmentalised (Fig 1.2). Therefore, organelle-specific mechanisms exist to maintain the protein homeostasis in many of these subcellular compartments (Roth & Balch 2010). Although the proteostasis machinery in various

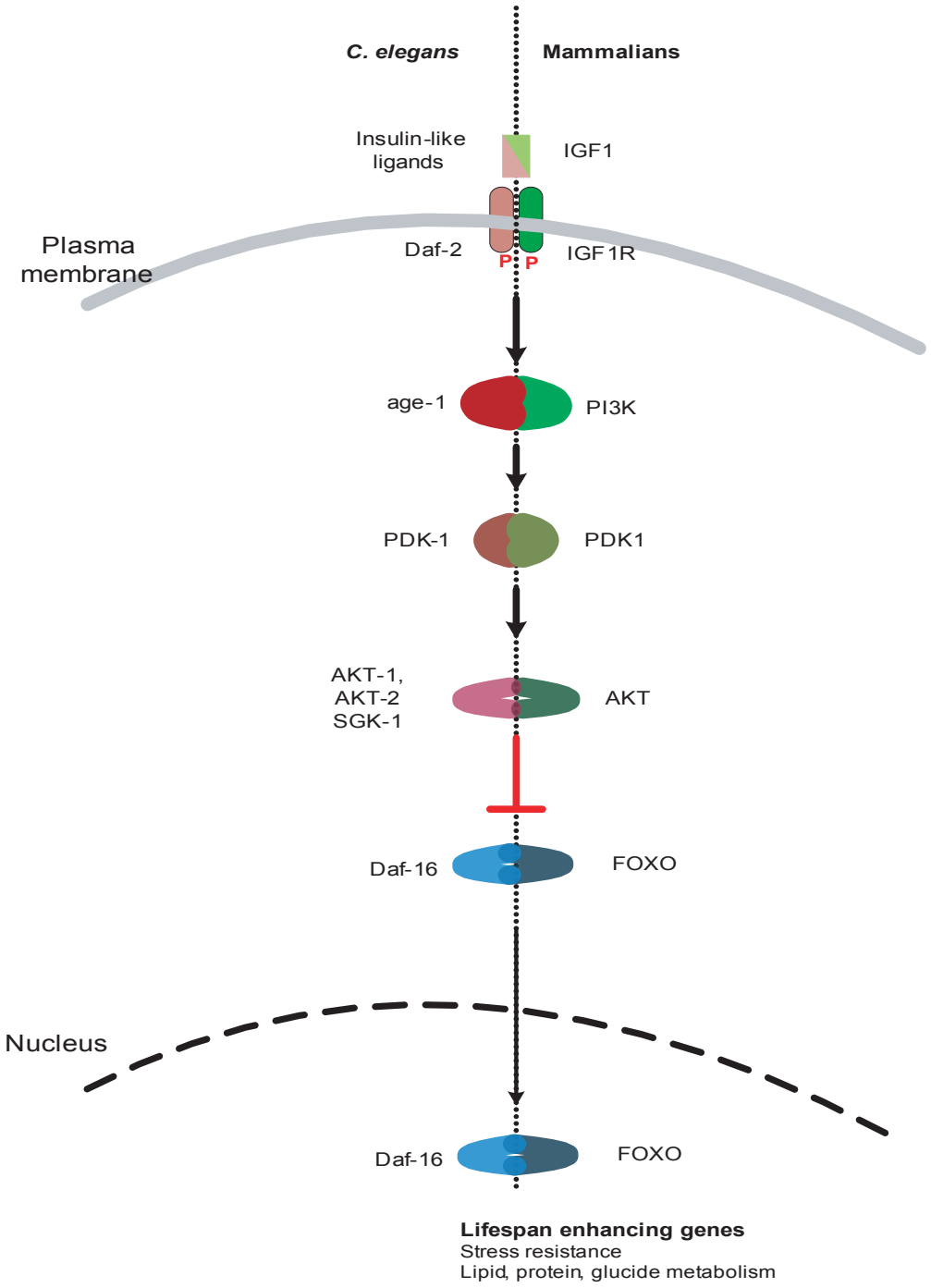

Figure 1.5: IGF pathway in nematode and mammalians.
Ligand binding to the IGF receptor initiates a cascade of phosphorylation ending with the transport to nucleus of the trascription factor daf-16. The dimerisation of the IFG receptor activates age-1, a phosphatidylinositol 3-kinase. As result, the downstream PDK-1 kinase is activated and in turn phosphorylates and activates the ARK serine/threonne kinase. The active ARK-1directly phosphorylates the transcription factor daf-16 and prevents its nuclear entrey.
Adapted from Christensen et al. 2006.

organelles may have distinct components, they also use common machineries such as the proteasome, and therefore cellular compartments are intimately linked and operate as an integrated system to maintain overall proteostasis (Roth & Balch 2010; Bernales *et al.* 2012). The proteostasis machinery of the ER is well described, and disturbances in ER folding and proteostasis are linked to many diseases, including age-related neurodegenerative diseases.

1.3 The endoplasmic reticulum protein homeostasis network

The ER is an important compartment for protein folding in the eukaryotic cell, representing the major site for the synthesis of integral membrane proteins, secreted proteins, and those destined for intracellular organelles. In the secretory pathway, proteins travel from the ER through the Golgi apparatus to arrive at the cell surface (Fig 1.6). The ER lumen has a unique oxidizing environment that supports disulphide bond formation and contains numerous chaperones and folding enzymes that prevent aggregation, thus allowing more efficient folding (Roth *et al.* 2008). The ER also has a QC system that monitors the folding and assembly of nascent proteins, helping to ensure that only proteins that acquire the native conformation are allowed to leave the ER (Buchberger *et al.* 2010). Proteins that fail to fold may interfere with ER function, and are therefore targeted for degradation. This process is called ER associated degradation (ERAD) and ensures that the ER does not become congested with misfolded proteins. However, if unfolded or misfolded proteins do accumulate in ER, then a homeostatic stress response termed the unfolded protein response (UPR), is activated (Hetz 2012). The UPR modulates the rate of protein synthesis and the expression of various ER proteins in response to changes in the load of unfolded/misfolded proteins in the ER and therefore ensures a proper balance between protein biosynthesis and folding and protein degradation (Walter & Ron 2011). Therefore, the ER can be seen as the gatekeeper of the secretory pathway, delivering natively folded and assembled proteins to various subcellular compartments whilst minimising the exit of non-native or misfolded proteins that are harmful for the cell function (Benham 2012).

1.3.1 Protein biosynthesis at the ER

Proteins destined for the secretory pathway are translocated across the ER membrane through an aqueous channel formed by the heterotrimeric Sec61 complex (composed of Sec61 α, β, δ) (Park & Rapoport 2012). In mammalian systems, most of these proteins are thought to be imported into the ER cotranslationally (Fig 1.7A). In lower eukaryotes such as yeast, proteins may also be translocated after the complete synthesis of the polypeptide chain (posttranslational translocation). Recent evidence suggests that post-translational pathways also operate in higher eukaryotes for the translocation of a number of proteins, including tail-anchored proteins (Shao & Hegde 2011; Johnson *et al.* 2012). Proteins are targeted to ER by virtue of a hydrophobic targeting signal sequence. This is often located at the N-terminus of the protein and may be removed following translocation, or may function as a transmembrane

domain following integration into the ER membrane (Fig 1.7A). As the signal sequence emerges from the translating ribosome it is recognised and bound by the signal recognition particle (SRP). Translation is paused temporarily while SRP interacts with its receptor docking the ribosome to the translocon complex at the ER membrane. (Fig 1.7A) (Saraogi & Shan 2011). SRP and the SRP receptor are now released to engage in further rounds of targeting and translation of the nascent chain resumes (Cross *et al.* 2009b). The interaction between the emerging signal sequence and translocon creates a seal on the cytosolic face of the channel, protecting the nascent protein from exposure to cytosol and mediating the opening of the translocon towards the ER, allowing the nascent chain to be transferred into the ER (Park & Rapoport 2012). As the elongation of the polypeptide chain continues, structural modifications within the translocon create an opening through the lateral wall of the channel, allowing the signal sequence to move through the opening into the ER membrane (Shao & Hegde 2011). For soluble proteins, the signal peptide complex (SPC) on the lumenal side of ER membrane will cleave the signal sequence and the rest of the chain is released into the ER lumen (Fig 1.7A). The intramembrane protease signal peptide peptidase (SPP) cleaves the signal peptide once it has been removed from the protein, and allows the signal peptide to be removed from the ER membrane (Weihofen *et al.* 2000). In the case of membrane proteins, the signal peptide can function as a transmembrane domain or can also be cleaved (Fig 1.7A) depending upon the topology of the protein (Shao & Hegde 2011).

Some proteins require the presence of Sec61 associated proteins such as TRAM (translocating chain-associating membrane) and TRAP (translocon associated protein) for efficient translocation (Gorlich *et al.* 1992; Hegde *et al.* 1998; Fons *et al.* 2003). The mammalian post-translational translocation pathway is yet to be completely elucidated (Fig 1.7B). Studies performed using tail-anchored proteins have revealed that the transmembrane domain may be shielded from the cytosol by the interaction with various proteins, such as the Hsp70/Hsp40 complex, SRP, or the BAG6 complex (Rabu *et al.* 2008; Leznicki *et al.* 2010; Mariappan *et al.* 2010; Shao & Hegde 2011). However, the subsequent steps leading to integration into the ER membrane are not established. Some proteins that interact with the BAG-6 complex can be delivered to TRC40, and by the interaction of TRC40 with its receptor WRB, the protein can be delivered to an integration channel (Fig 1.7B), possibly the Sec61 complex (Leznicki *et al.* 2010; Johnson *et al.* 2012). Two other proteins, Sec62 and Sec63, may also be required to assist Sec61 in mediating post-translational translocation (Lakkaraju *et al.* 2012; Lang *et al.* 2012). In addition, the possibilities of direct integration of the transmembrane domain into the ER membrane, as well as the existence of another integration channel have been considered (Cross *et al.* 2009b).

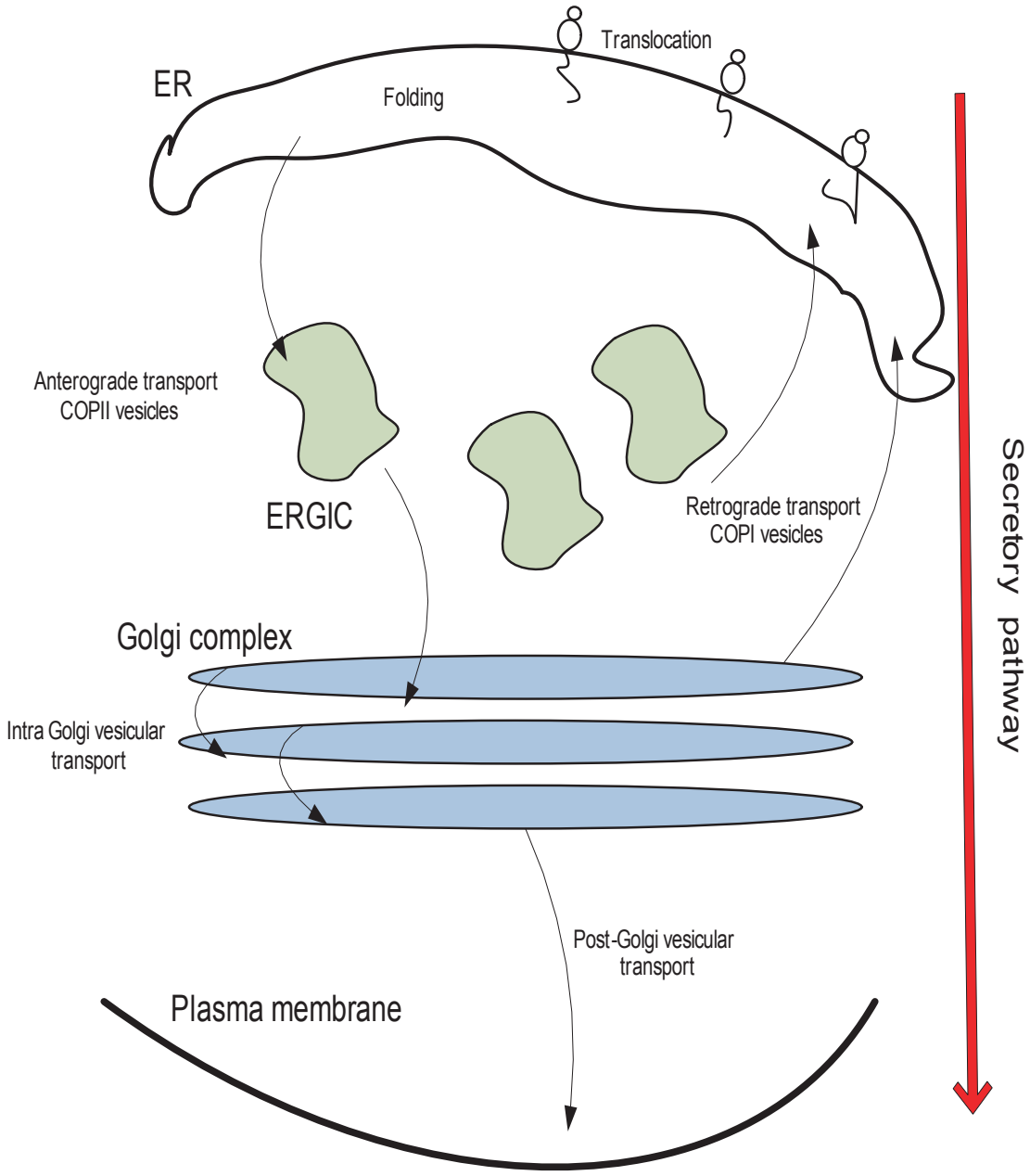

Figure 1.6: The secretory pathway
Secreted proteins are synthesised by ER bound ribosomes and translocated into ER lumen. In the ER proteins are subjected to co-and post-translational modifications such as cleavage of the signal sequence, glycosylation, disulphide bond formation. Proteins that acquire the correct 3D structure are selected and exported to the Golgi apparatus via COPII coated vesicles. They pass through the ER-Golgi intermediate compartment (ERGIC) where they can oligomerise or initiate O-glycosylation. In the Golgi apparatus proteins are subject to further modifications (e.g. glycan proccesing, lipidation), prior to transport to their site of function. Some of the ER resident proteins are retrieved from ERGIC or from cis-Golgi compartment by COPI vesicles (retrograde transport).

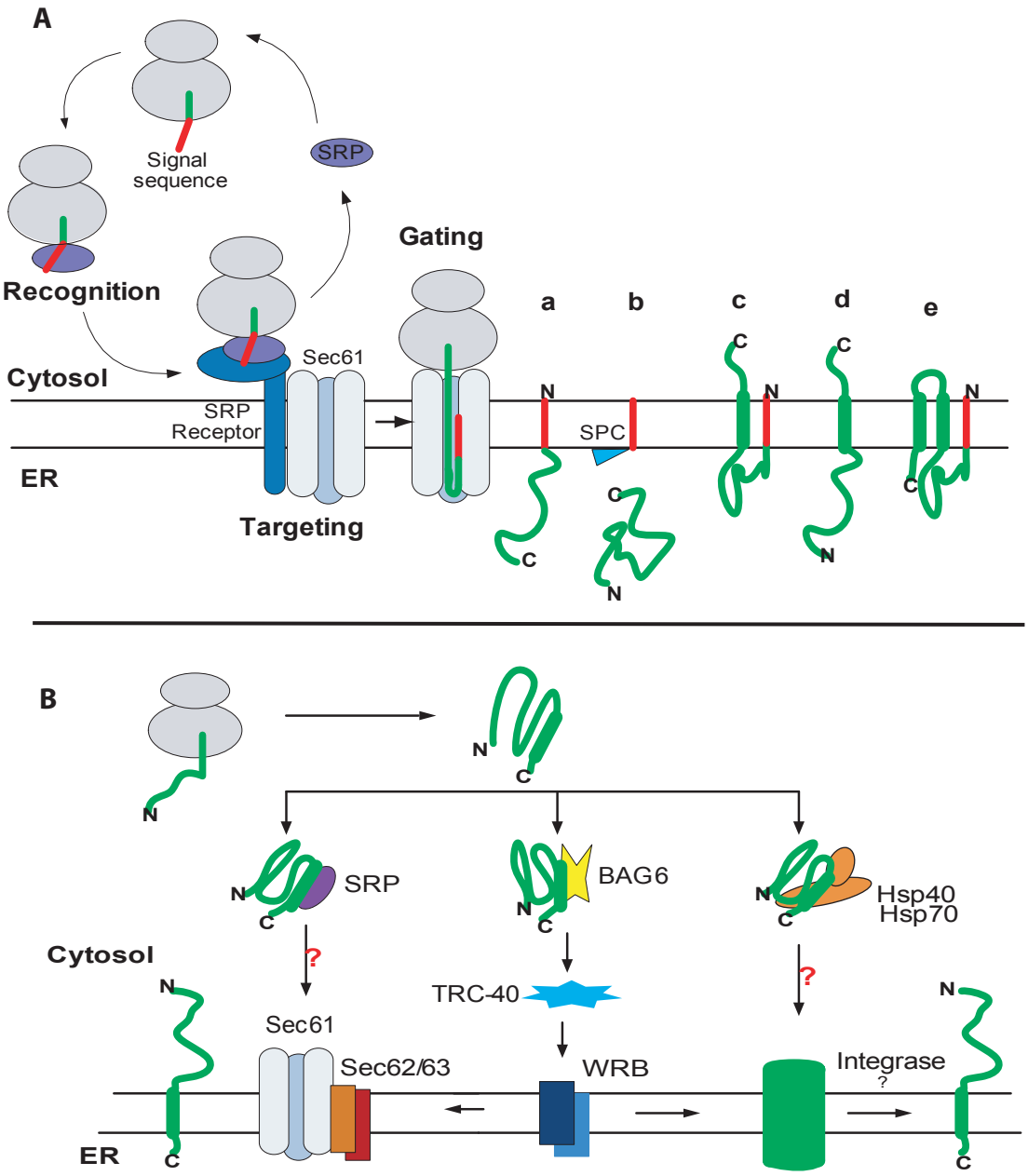

Figure 1.7: Translocation into ER lumen.
(A) Cotranslational translocation: When the signal sequence emerges from ribosome it can bind SRP and the translocation of the polypeptide is coupled with its synthesis. The SRP-ribosome complex is docked to the translocon by the interaction of SRP with its receptor. The transfer of the signal sequence into the translocon channel releases the SRP and SRP receptor. When the translation is finished, the signal sequence is transferred from the translocon lumen into the ER membrane through a lateral opening in the Sec61 channel. The signal sequence can function as a TM (transmembrane domain) for some type I proteins (**a**) or can be cleaved for secreted or soluble proteins (**b**), or for other type of TM proteins (**c** - **e**). The presence of a TM in the translocon can also mediate the lateral opening and release into ER membrane. In this way type III (**c**), the type II (**d**) and the multispanning membrane proteins (**e**) are obtained.
(B) Posttranslational translocation: Some proteins, such as tail anchored proteins, are translocated after their synthesis. Some of the polypeptide chains are bound by BAG6 and transferred to TCR-40 that interacts with its receptor WRB and brings the complex next to the ER membrane. The integration can be facilitated by the Sec61 complex or another unknown integrase. Other cytosolic factors can act as intermediates in posttranslational translocation (e.g. SRP, Hsp40/ Hsp70 complex), but the exact mechanism is still unclear.
Adapted from Rabu and High 2007 and Cross et al. 2009.

1.3.2 ER posttranslational modifications and oxidative folding

Numerous components have been identified in the close vicinity of the translocon, such as the Hsp70 molecular chaperone BiP, SPC and the oligosaccharyl transferase (OST) complex, and these are involved in the further maturation of the polypeptide chain as it enters the ER lumen (Fig1.8). As the polypeptide chains enter the ER lumen, an oligosaccharide structure may be added to specific Asn residues (consensus Asn-X-Ser/Thr, where X ≠ Pro) by the OST complex (Aebi *et al.* 2010). The addition of N-linked glycans promotes folding by allowing interactions with the lectin-chaperones calnexin and calreticulin, which help prevent aggregation of the polypeptide chain (Braakman & Bulleid 2011). Calnexin and calreticulin specifically bind to monoglycosylated N-linked oligosaccharides, and thus association with calnexin/calreticulin requires the removal of two glucose residues from the core oligosaccharides by glucosidase I and II (Fig 1.8). Associated with calnexin/calreticulin is ERp57, an oxidoreductase that interacts specifically with glycoproteins and catalyses formation of disulphide bonds (Oliver *et al.* 1997). Proteins are released from calnexin and calreticulin by the action of glucosidase II which removes the last glucose residue of the N-glycan (Aebi *et al.* 2010), allowing them to enter COPII coated vesicles for transport to the Golgi apparatus. However, some glycoproteins require multiple cycles of calnexin/calreticulin binding and release for proper folding (Hebert & Molinari 2007). To this end, UGGT (UDP-glucose glucosyltransferase) acts like a folding sensor by mediating the re-glucosylation of N-glycans adjacent to unfolded regions of the polypeptide chain (Sousa *et al.* 1992; Sousa & Parodi 1995). As a result, the unfolded glycoprotein rebinds calnexin or calreticulin, and re-enters the folding cycle (Ritter & Helenius 2000; Taylor *et al.* 2004).

In addition to the glycan binding chaperones (calnexin, calreticulin), other ER-resident chaperones contribute to protein maturation. For instance, BiP, an Hsp70 chaperone, binds to hydrophobic domains and keeps the polypeptide chain in a soluble conformation (Molinari & Helenius 2000). However, BiP has multiple roles in the ER, including in degradation and the stress response that will be discussed in the following sections. The formation of disulphide bonds is an important step in the maturation of many secreted proteins and the ER contains a large number of oxidoreductases with various specificities (Braakman & Bulleid 2011). While ERp57 catalyses the formation of disulphide bond in calnexin/calreticulin client proteins, another oxidoreductase, p5, was shown to have specificity for BiP substrates, although it may only act on a select number of substrates (Jessop *et al.* 2009; Rutkevich *et al.* 2010). On the other hand, PDI which is also involved in the selection of misfolded proteins for degradation (Braakman & Bulleid 2011) has a broad specificity, overlapping with that of ERp57 (Rutkevich *et al.* 2010). In addition to catalysing the formation of disulphide bonds, PDI also has reductase activity, allowing for their isomerisation.

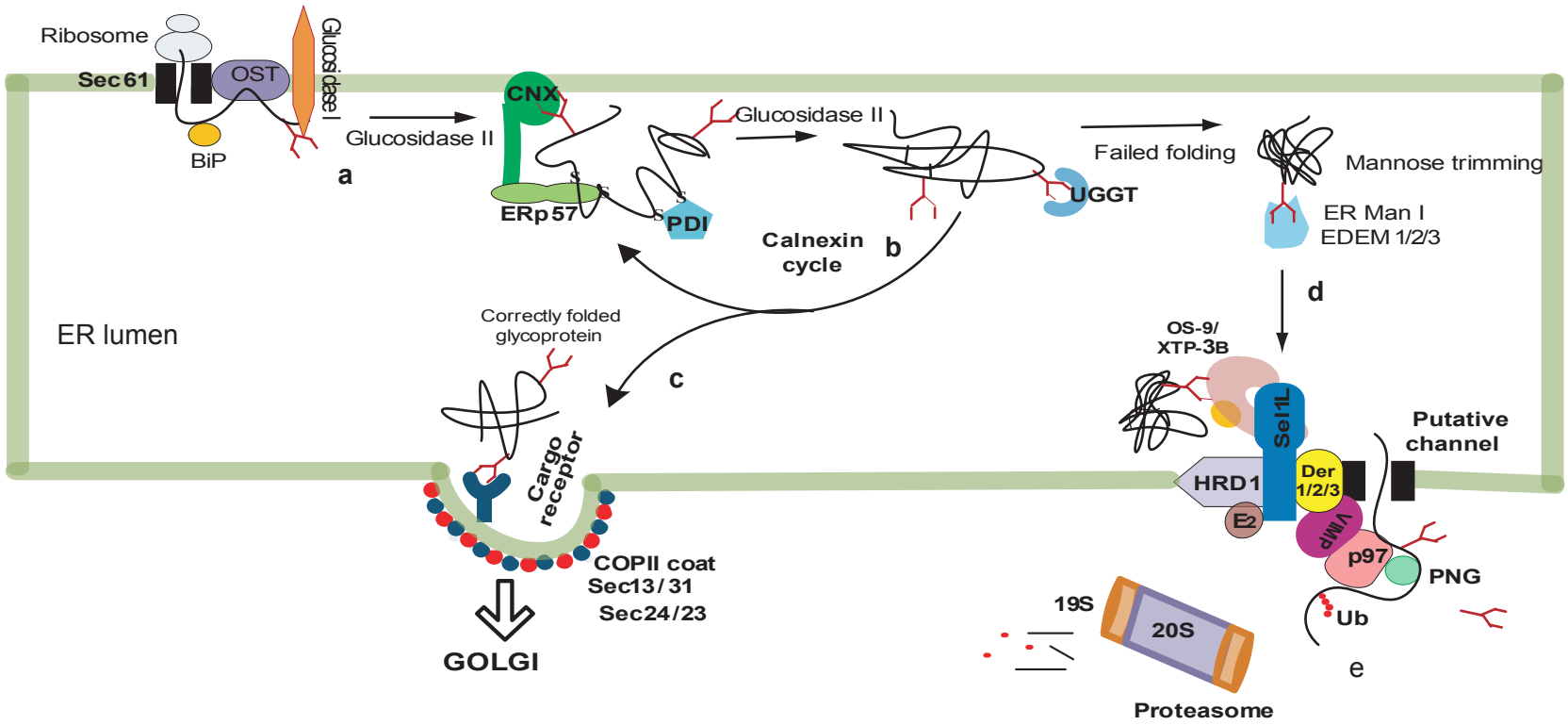

Figure 1.8: ER folding and ER-associated degradation.
The polypeptide chain is translocated in ER and an N-glycan is added. Then the two outer glucose residues are trimmed by glucosidase I and II (**a**). The resulting form of the glycan binds the calnexin (CNX) or calreticulin that interact with the oxidoreductase ERp57 to promote disulfide bond isomerisation. Release of the folded protein from the CNX/CRT cycle occurs upon glucosidase II catalyzed removal of the last glucose residue (**b**). The correctly folded glycoproteins are exported to the Golgi compartment in COPII coated vesicles (**c**). Proteins that fail to acquire the biologically active conformation even after consecutive folding attempts are targeted to degradation via ERAD. EDEMs, OS-9 and XTP-3B interact with ERAD substrates and escort them from folding cycle to the retro-translocation machinery (**d**). The retro-translocation complex is formed by the retrotranslocation pore (Derlins or Sec61), E3 ubiquitin ligase (HRD1), E2 ubiquitin activating enzyme, p97 ATPase and p97 co-factors (VIMP). Following retro-translocation to the cytosol proteins are polyubiquitinated, deglycosylated and degraded by the proteasome (e). Adapted from Määttänena et al. 2010.

If the native conformation is acquired, the nascent proteins can exit the ER and be transported to the Golgi apparatus then sorted to their final destination by vesicular transport (Fig 1.8). Properly folded and assembled proteins are recruited to specialized sites in the ER (ER exit sites, ERES), where the formation of vesicles is initiated by the assembly of cytosolic proteins into COPII coat (Gillon *et al.* 2012). COPII assembly is initiated by the activation of small Ras-like GTPase (Sar1) that further recruits the Sec23/24 complex (Barlowe *et al.* 1994; Bi *et al.* 2002). The binding of Sec13/31 complex to Sec23/24 complex completes the formation of COPII coated vesicles (Barlowe *et al.* 1994; Stagg *et al.* 2006). The selection of cargo proteins for incorporation into ER exit sites for Golgi apparatus traffic is promoted by the presence of specific ER export signals, but bulk flow may also contribute (Gillon *et al.* 2012). Export signals are identified directly or indirectly by the Sec24 subunit of the COPII coat (Sato & Nakano 2007). For some proteins, membrane receptors such as ERGIC-53 mediate recruitment to ERES and the interaction with COPII (Fig 1.8) (Appenzeller *et al.* 1999; Sato & Nakano 2007). While passing through the Golgi apparatus, proteins are subject to further post-translational modifications including processing of N-linked glycans, addition of sulphate and phosphate groups, O-glycosylation, and lipidation to acquire their mature functional state. Proteins then undergo sorting in the trans-Golgi network (TGN) before being transported to various destinations such as the plasma membrane, endosomal compartments or secretory granules (Reynders *et al.* 2011). Due to the nature of proteins that are synthesized in the ER, including cell surface receptors, ion channels, signalling molecules and growth factors, it is clearly of vital importance to prevent export of non-native proteins that could potentially malfunction and affect neighbouring cells, surrounding tissues or the whole organism (Guerriero & Brodsky 2012). Therefore, a strict QC at level of ER is employed to help ensure only properly folded proteins are exported.

1.3.3 Protein quality control at the ER

Proteins synthesised at the ER may fail to obtain the correct conformation for a variety of reasons including genetic mutations (e.g. protein folding diseases), errors in translation or folding, absence of partner subunits, adverse external conditions, or situations that perturb the environment of the ER, including mutations in ER chaperones or altered redox state. The ER quality control (ERQC) system functions to retain and target for degradation proteins that are unable to achieve their properly folded state. An important role is played by the components of the folding machinery that interact with unfolded proteins. The improperly folded proteins are retained in the ER lumen by repetitive associations with calnexin/calreticulin, mediated by the UGGT (Sousa & Parodi 1995; Taylor *et al.* 2004). Similarly, hydrophobic patches exposed by the incorrectly folded proteins are recognised and bound by the molecular chaperones such BiP and GRP94, preventing their exit from ER (Chillaron & Haas 2000; Braakman & Bulleid 2011). In addition, misfolded proteins can be excluded from ER exit sites, through a mechanism that is not yet clear (Pagant *et al.* 2007). All of these mechanisms prevent the unfolded, biologically inactive proteins from exiting ER and proceeding through the secretory pathway. By keeping the unfolded proteins in the ER lumen, the components of QC mainly aim to fold these proteins.

However, the terminally misfolded proteins may be harmful to the ER, therefore they must be moved into the cytosol for degradation by the proteasome (Hebert *et al.* 2010).

The ERAD process is very complex in mammals, given the vast array of different types of proteins that potentially need to be degraded, and many different components of ERAD have been identified (table 1.3). However, the overall process can be seen as a multistep event including recognition of terminally misfolded proteins as substrates for ERAD, targeting the substrate to the degradation machinery, movement across the ER membrane into the cytosol (termed retrotranslocation) and polyubiquitination of the substrate, release into the cytoplasm (termed dislocation), and finally proteasomal degradation (Fig 1.9) (Guerriero & Brodsky 2012). A decisive step in the ERAD pathway for the vast majority of substrates is the attachment of multiple copies of Ub (Mehnert *et al.* 2010), generating a polyUb chain which is recognised by components of the proteasome (Finley 2009). The E3 ubiquitin ligases play a central role in the ERAD network (Smith *et al.* 2010). A number of E3s have been implicated in ERAD in mammals (table 1.3), the best studied of which are HRD1 and gp78. These are proposed to act as platforms for assembly of the various adaptors and ERAD components on both sides of membranes (see table 1.3) (Mehnert *et al.* 2010; Christianson *et al.* 2012). E3 complexes can be 'adapted' for degradation of particular substrates by recruitment of different interaction partners (e.g. E2 enzyme, ERAD components) (Mehnert *et al.* 2010). These factors facilitate the different stages in ERAD including recognition, targeting, retrotranslocation, ubiquitination, dislocation, and degradation.

How different ERAD substrates are recognised as terminally misfolded (as opposed to being engaged in productive folding), and targeted to the E3 complexes is best understood for N-glycoproteins with misfolded domains within the lumen. For such proteins, the ER mannosidase I and ER mannosidase-like proteins (EDEM1-3) release terminally misfolded glycoproteins from the calnexin/calreticulin cycle by removing mannose residues from the oligosaccharide, thereby inhibiting recognition by UGGT and preventing reglucosylation (Molinari *et al.* 2003; Hosokawa *et al.* 2010). The EDEM1 trimmed oligosaccharide also acts as a degradation signal, allowing recognition by ER lectins OS-9 and XTP3-B, which deliver the misfolded glycoproteins to the HRD1 E3 ligase complex (Sel1-HRD1) complex (Fig 1.9) (Christianson *et al.* 2008; Bernasconi *et al.* 2010). These ER lectins also promote delivery to the ERAD machinery by recognition of peptide-based signals (Christianson *et al.* 2012). Other routes for recognition of ERAD substrates and delivery to ERAD E3 complexes are less well defined. Some of these ERAD substrates may require the recognition of exposed hydrophobic domains by molecular chaperones, such as BiP or GRP94 that will further mediate the transfer to the retrotranslocation complex (Okuda-Shimizu & Hendershot 2007; Kriegenburg *et al.* 2012).

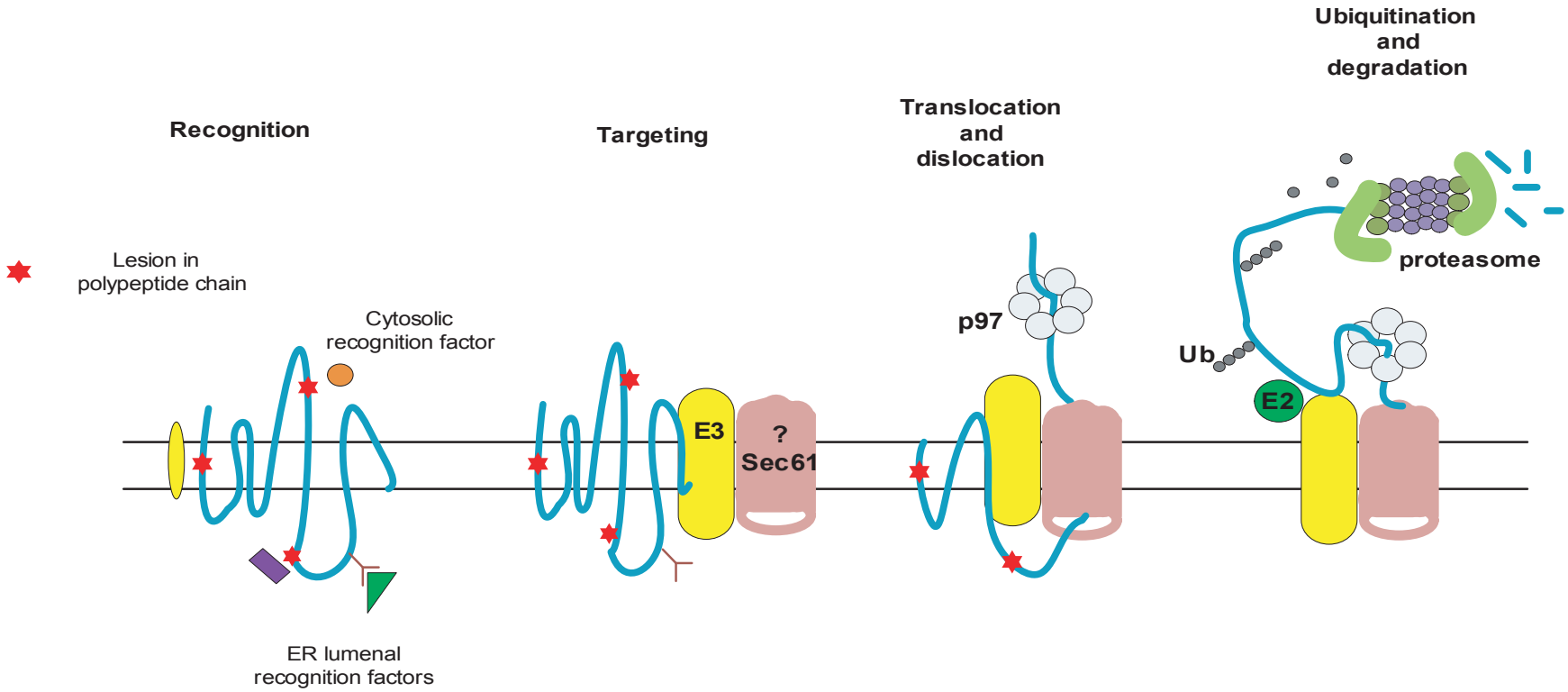

Figure 1.9: Steps in ER-associated degradation (ERAD).
(a) A misfolded lesion (red star) of the polypepide chain localised in the membrane, cytosol or ER lumen is identified by cytosolic, lumenal or intramembrane factors. N-glycans with trimmed mannose residue are also recognised by ER lectins (green triangle).
(b) The resulting complexes are escorted to the retro-translocation machinery, by interaction with other components of ERAD (e.g. OS9, XTP-3B, ERdj5)
(c)The removal of the protein from the ER may involve a retrotranslocation pore (Derlins or Sec61). The energy required for the retro-translocation and dislocation of ERAD substrate from the ER is provided by the p97 ATPase.
(d) Following retro-translocation to the cytosol proteins are polyubiquitinated, a process mediated by an E2 ubiquitin conjugating enzyme and E3 ubiquitin ligase, deglycosylated and degraded by proteasome. Adapted from Guerriero and Brodsky 2012.

Module of ERAD network	Protein	Function
Recognition and targeting	ER Man I	α-Mannosidase
	EDEM 1/2/3	α-Mannosidase-like lectins
	Calnexin	ER chaperone
	BiP	ER chaperone
	GRP94	ER chaperone
	ERdj5	Oxidoreductase
	OS-9	Mannose-6-phosphate receptor-like
	XTP-3B	Mannose-6-phosphate receptor-like
	Sel1L	HRD1 adaptor
Ubiquitination and dislocation	HRD1	E3 ubiquitin ligase
	Gp78	E3 ubiquitin ligase
	RMA1	E3 ubiquitin ligase
	TEB4	E3 ubiquitin ligase
	RFP2	E3 ubiquitin ligase
	TRC8	E3 ubiquitin ligase
	RNF170	E3 ubiquitin ligase
	Kf1	E3 ubiquitin ligase
	Derlin 1/2/3	Multispaninng transmembrane proteins
	Sec61	Multispaninng transmembrane complex
	Ube2g2	E2 ubiquitin activating enzyme
	Ube2j1	E2 ubiquitin activating enzyme
	Ube4a	Ubiquitin extension
Extraction and processing	p97	AAA-ATPase
	Ufd1–Npl4	p97 adaptors
	VIMP	p97 recruitment factor
	Ubxd8	p97 recruitment factor
	Ubxd2	p97 recruitment factor
	VCPIP135	De-ubiquitylating enzyme
	Ataxin-3	De-ubiquitylating enzyme
	PNG	Deglycosylating enzyme

Table 1.3: Established components of the mammalian ERAD network

Studies in *S. cerevisiae* suggested that proteins with misfolded domains within the ER membrane can be recognised directly by Hrd1p (the yeast homolog of HRD1) (Sato *et al.* 2009). In contrast, recognition and degradation of proteins with misfolded cytoplasmic domains is assisted by cytoplasmic chaperones (Zhang *et al.* 2001; Ahner *et al.* 2007). However, considerable overlap or redundancy exists between these different ERAD pathways (Christianson *et al.* 2012). Furthermore, multiple mechanisms may contribute to the recognition and degradation of topologically complex multidomain proteins. For example, degradation of the misfolded polytopic protein CFTRΔ508, requires the coordinated action of ER and cytosolic quality control including Hsp90, Hsp70 and CHIP in cytosol and RMA1 and gp78 in ER membrane (Guerriero & Brodsky 2012).

Following recognition and targeting to the E3 ERAD complex, the misfolded protein must then be transferred from the ER lumen or membrane to the cytosol. This process of retrotranslocation is tightly coupled with polyubiquitination of the substrate protein (de Virgilio *et al.* 1998; Kikkert *et al.* 2001). The retrotranslocation process is thought to require a proteinaceous channel, although its exact composition is still under debate (Hampton & Sommer 2012). The first proposed candidate was the Sec61 complex, mainly due to its demonstrated role as channel through the ER membrane and the observation that in yeast, mutations in the components of the SEC61 complex inhibit degradation of various ERAD substrates (Shao & Hegde 2011). In mammalian cells, the Sec61 complex may assist degradation of the major histocompatibility complex class I heavy chain and amyloid β-peptide (Wiertz *et al.* 1996; Schmitz *et al.* 2004). The multispanning transmembrane proteins Derlin-1, -2 and -3, have also been shown to facilitate the retrotranslocation of various soluble and membrane integrated substrates, suggesting that Derlins could form an alternative retro-translocation channel (Lilley & Ploegh 2004; Oda *et al.* 2006; Younger *et al.* 2006). Moreover, Derlin proteins form complexes with Sel1L, EDEM1 and the AAA-ATPase p97 (Lilley & Ploegh 2004; Ye *et al.* 2004; Lilley *et al.* 2006; Oda *et al.* 2006), further implicating them in ERAD (see below). The multispanning E3 ubiquitin ligases have also been proposed to form the retrotranslocation channel (Carvalho *et al.* 2010). Their interactions with both ER luminal and cytosolic components of the ERAD pathway make them attractive candidates, but there is currently no direct experimental evidence to support this model (Mehnert *et al.* 2010; Hampton & Sommer 2012). The energy required for polypeptide chain extraction from the ER is provided by p97, a hexameric AAA-ATPase (Ye *et al.* 2001). P97 has many cellular functions (Meyer *et al.* 2012), but for ERAD it associates with the adaptors Npl4 and Ufd1, forming a complex which interacts with the polyUb substrates (Ye *et al.* 2003). The p97-Npl4-Ufd1 complex is recruited to the ER membrane either by auxiliary proteins such as VIMP, Ubxd2 and Ubxd8 (Mehnert *et al.* 2010; Christianson *et al.* 2012) or by direct interaction of p97 with some of the E3 ubiquitin ligases (Ballar *et al.* 2006). At the ER membrane, p97 interacts with a number of co-factors which mediate further processing of the substrate, such as Ub chain extension (UBE4A), deubiquitination (ataxin-3, VCIP135, YOD1) and deglycosylation (N-glycanase1) (Christianson *et al.* 2012; Meyer *et al.* 2012). Following extraction, the polyUb substrate is delivered to the proteasome for degradation. The ERAD substrate extraction and proteasomal degradation are tightly coupled, so that proteins are not usually released into the cytoplasm, but are shuttled from ER membrane directly into the proteasome (Guerriero & Brodsky 2012). In fact, proteasomes can be localised to ER and there is evidence that proteasome activity contributes to the driving force that promotes extraction of some substrates (Bagola *et al.* 2011). Thus, cytosolic retrotranslocated ERAD substrates are not typically observed in large quantities. Under conditions of reduced proteasome activity ERAD substrates accumulate primarily in the ER lumen, although detection in the cytosol has been reported (Kelly *et al.* 2007).

Some proteins that misfold in the ER and fail to be cleared by ERAD can form toxic aggregates which are eliminated from the ER by autophagosomes generated by the ER membrane (Bernales *et al.* 2007). This process is called 'ER-phagy' and was first described for yeast under conditions of cellular stress, such as misfolded protein stress (Bernales *et al.* 2006) or starvation (Hamasaki *et al.* 2005). Formation of autophagosomes from ER membranes was also observed in the mammalian cells, but the exact nature of the cargo is still unknown (Axe *et al.* 2008; Hayashi-Nishino *et al.* 2009; Yla-Anttila *et al.* 2009).

1.3.4 Protein homeostasis in the ER and the unfolded protein response

The accumulation of misfolded proteins in the ER activates a signalling pathway called the UPR, a critical pathway for responding to changes in cellular status. Many external and intracellular conditions can perturb protein folding, therefore the folding status in the ER can be considered a sensor for general cellular homeostasis, and UPR signalling a homeostatic mechanism to respond to this disturbance (Wang & Kaufman 2012). Besides responding to pathological or chronic misfolding, the UPR also plays an important role in normal physiology. For instance, the differentiation of plasma cells requires UPR activation to adapt ER function enabling the production of high levels of antibodies (Reimold *et al.* 2001; Ma *et al.* 2009; Rutkowski & Hegde 2010). Similarly, in liver the UPR can regulates the status of lipid and cholesterol metabolism (Lee *et al.* 2008), whilst glucose/energy homeostasis mediated by beta pancreatic cells is also dependent on UPR signalling (Scheuner *et al.* 2001).

There are three branches of UPR named after the ER stress sensors that are activated: IRE1 (inositol-requiring protein-1), PERK (protein kinase RNA-like ER kinase) and ATF6 (activating transcription factor 6) (Fig 1.10). PERK and IRE1 are both transmembrane kinases that require autophosphorylation and oligomerisation for activation (Shamu & Walter 1996; Harding *et al.* 1999). ATF6 is transported to the cis-Golgi apparatus where it is cleaved by two proteases to release a cytoplasmic N-teminal domain which comprises a bZIP transcription factor (Shen *et al.* 2002). The sensors are switched off and maintained inactive by binding of BiP. The accumulation of misfolded proteins in the lumen of the ER indirectly activates ER stress-sensors by interacting with BiP and mediating the dissociation from ER stressors (Bertolotti *et al.* 2000; Ma *et al.* 2002; Shen *et al.* 2002). Recent evidence suggests that IRE1 is actually activated directly by misfolded proteins in a two step fashion whereby BiP dislocation induces oligomerisation of IRE1, followed by binding of misfolded proteins to cause IRE1 activation (Gardner & Walter 2011). However, this model is not yet validated in mammals. Whether PERK and ATF6 can bind misfolded proteins is also unclear and under investigation.

Following activation of the stress sensors, a series of events is initiated to restore proteostasis (Ron & Walter 2007) (Fig 1.10). An early event in the UPR is a global attenuation of translation, mediated by the PERK arm of UPR, which acts to decrease input into the ER thereby relieving the folding burden upon it (Shi *et al.* 1998; Harding *et al.* 2000b). Activated PERK

phosphorylates eIF2α, the α-subunit of eukaryotic translation factor-2, and inhibits the generation of the active translation initiation complex eIF2-GTP-tRNA^{Met} (Harding *et al.* 1999). Another mechanism to reduce the input of cargo into the ER is the degradation of ER localised mRNAs via the RNase activity of IRE1 (Hollien & Weissman 2006; Hollien *et al.* 2009). However, the mechanisms controlling this non-selective RNA degradation and its physiological significance are not clear (Hetz 2012). The selective exclusion of newly synthesised membrane and secreted proteins and their re-routing to degradation (pre-emptive QC) also reduces the influx of proteins into ER (Kang *et al.* 2006). Other events initiated by UPR activation involve upregulation of expression levels of ER chaperones and ERAD components (Okada *et al.* 2002; Lee *et al.* 2003) to increase its folding/degradation capacity. This is mediated by all three branches of the UPR (table 1.4). As well as inhibiting global translation, phosphorylation of eIF2α results in increased translation of certain mRNAs including the transcription factor ATF4 (Harding *et al.* 2000a) which promotes expression of genes, such as those encoding proteins involved in amino acid synthesis and transport (Harding *et al.* 2003). PERK also phosphorylates another transcription factor, nuclear erythroid 2 p45-related factor 2 (NRF2) that forms dimeric complexes with other transcriptional factors, including ATF4 (He *et al.* 2001) to induce the antioxidative stress response genes (Nguyen *et al.* 2000). The activated RNase domain of IRE1 induces the splicing of Xbp1 mRNA (Yoshida *et al.* 2001) that encodes the active form of the transcription factor, XBP1(s). XBP1(s) functions to regulate the expression of a range of ER chaperones (Lee *et al.* 2003). The cleaved form of ATF6 migrates to the nucleus (Haze *et al.* 1999) and upregulates the expression of genes encoding components of protein folding and degradation machinery (Okada *et al.* 2002; Yamamoto *et al.* 2007)

UPR branch	Protein	Function	References
IRE-1	ERdj5 EDEM 1/2/3 HRD1 Derlin-2, -3 RAMP- 4	Folding – quality control ERAD ERAD ERAD ER translocation	(Okada *et al.* 2002; Kaneko & Nomura 2003; Lee *et al.* 2003; Oda *et al.* 2006)
ATF6	Calnexin Calreticulin GRP94 ERp57 ERp72	Folding – quality control Folding – quality control Folding – quality control Folding – quality control Folding – quality control	(Okada *et al.* 2002)
PERK	XBP1	Transcription factor in UPR	(Walter & Ron 2011)
PERK and ATF6	CHOP OS9	Apoptosis mediator ERAD	(Okada *et al.* 2002)
IRE1 and ATF6	BiP PDI P5	Folding – quality control Folding – quality control Folding – quality control	(Okada *et al.* 2002; Lee *et al.* 2003)

Table 1.4: List of targets of the different branches of the UPR that are involved in ER folding/QC/ERAD

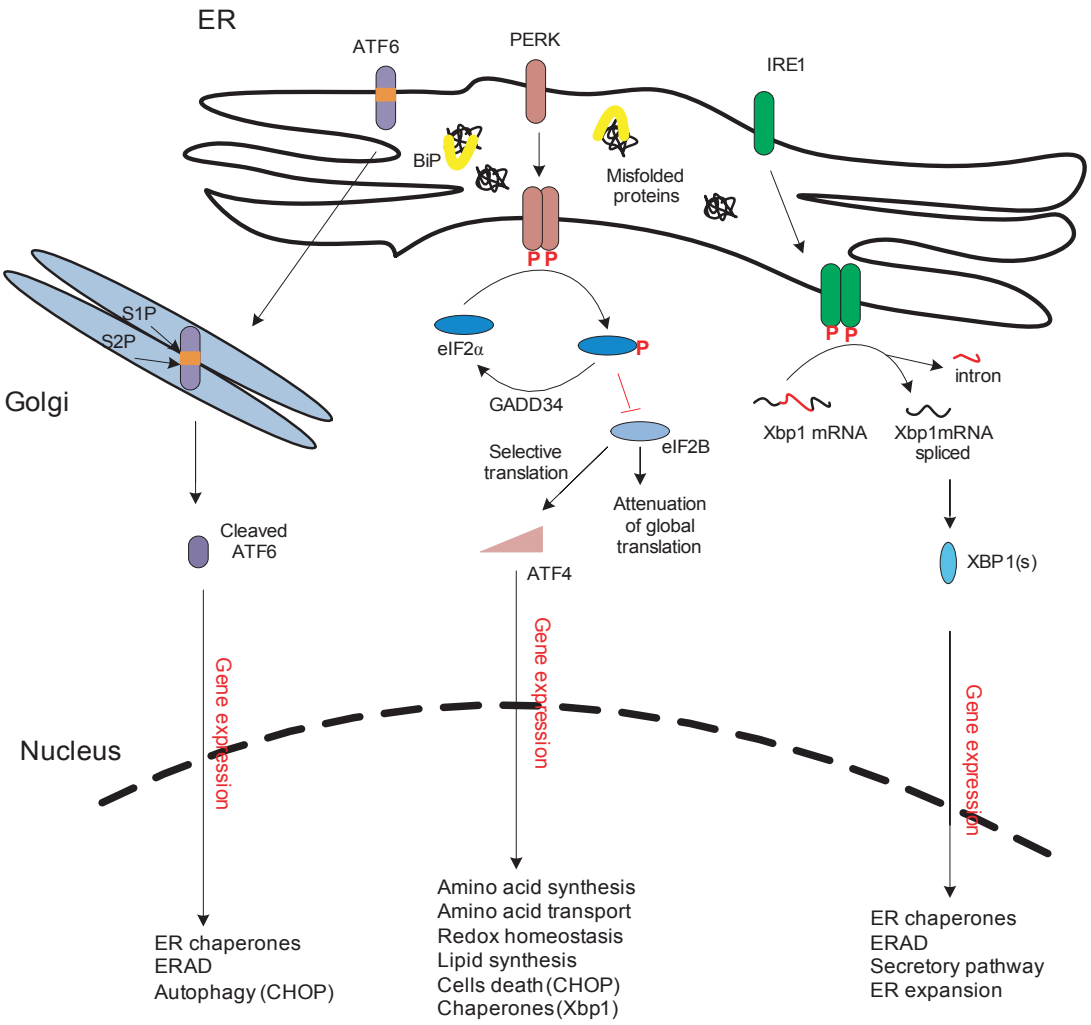

Figure 1.10: Unfolded protein response pathways.
The misfolded proteins activate ER stress sensors either by inducing BiP release or by direct binding to the sensor (e.g. IRE1). ATF6 is transported to the Golgi apparatus and cleaved by the proteases S1P and S2P. Then cleaved ATF6 migrates to the nucleus, where it upregulates the expression of genes encoding components of protein folding and degradation machinery. PERK dimerises and phosphorylates eIF2α. The eIF2α-P temporarily blocks global translation, therefore reducing ER loading. Phosphorylation of eIF2α also activates the transcriptional program mediated by ATF4. ATF4 also initiates the expression of GADD34 that mediates eIF2α dephosphorylation and deactivation of PERK signalling. Similarly, IRE-1 oligomerises and autophosphorylates and induces Xbp-1 splicing. The spliced Xbp-1 activates the UPR-induced genes encoding ER chaperones and ERAD components.
Adapted from Walter and Ron 2011.

Cell fate is decided based on the UPR output. If the perturbation in ER homeostasis cannot be solved by the adaptations described above, prolonged UPR signalling initiates pro-apoptotic pathways, leading to cell death (Walter & Ron 2011). The apoptotic UPR signalling activates the caspase cascade responsible for degradation of key cellular proteins resulting in programmed cell death (Kim *et al.* 2008). One of the promoters of apoptotic pathways is the PERK branch of the UPR via ATF4-induced expression of C/EBP-homologous protein (CHOP). CHOP modulates the expression of apoptosis-related genes including the downregulation of anti-apoptotic B cell lymphoma 2 (BCL-2) and upregulation of the pro-apoptotic BCL-2-interacting mediator of cell death (BIM) (Tabas & Ron 2011). In addition, CHOP upregulates expression of GADD34 which mediates eIF2α dephosphorylation and restores translation (Novoa *et al.* 2001). GADD34 might induce pro-apoptotic pathways by promoting ER overload with misfolded proteins (Marciniak *et al.* 2004). The IRE1 branch is another driver of apoptotic pathways through its association with tumour necrosis factor-receptor-associated factor 2 (TRAF-2) and activation of apoptosis-signal-regulating kinase (ASK1) (Nishitoh *et al.* 2002). ASK1 initiates Jun amino-terminal kinase (JNK) signalling, thus enhancing the activity of pro-apoptotic factors (Urano *et al.* 2000). The IRE1 mediated mRNA decay of key components of folding machinery may also promote cell death (Han *et al.* 2009).

The exact mechanisms that mediate the transition from the pro-survival to pro-apoptotic UPR pathways are not established. Several studies have suggested that differences in the duration of signalling of various UPR branches could decide the cell's fate. Prolonged chemically induced stress was shown to result in attenuation of IRE1 signalling, while PERK signalling was maintained, leading to activation of genes from the pro-apoptotic program such as CHOP (Lin *et al.* 2007; Lin *et al.* 2009). Other studies reported that unmitigated UPR induces prolonged *Xbp1* splicing and attenuation of PERK resulting in reduced survival (Chawla *et al.* 2011). UPR signalling is also able to adapt the response based on the intensity of ER stressor. It was shown that low levels of ER stress, while inducing full activation of UPR (*Xbp1* splicing, eIF2α phosphorylation and ATF6 cleavage) did not activate the CHOP and GADD34 genes, therefore only the pro-survival pathways were active (Rutkowski *et al.* 2006). Thus, both timing and the amplitude of ER stressors signalling have an important role in the output of the UPR.

Recent data indicate that the ability to attenuate or modify UPR signalling outputs may determine cell fate in response to ER stress. For instance, maintaining phospho-eIF2α and translational attenuation by inhibition of GADD34 phosphatase activity reduces ER stress induced cell death (Boyce *et al.* 2005; Tsaytler *et al.* 2011). In contrast phospho-eIF2α dephosphorylation increased the neurotoxicity of prion protein in mice, whilst overexpression of GADD34 was protective (Moreno *et al.* 2012). This suggests that long term eIF2α phosphorylation may promote cell death in certain situations (e.g. prion disease). Similarly, studies in yeast have shown that inactivation of IRE1 kinase activity may be important in determining cell fate in response to ER stress. Mutation of the kinase domain of IRE1 inhibits

deactivation of the mutant IRE1, and results in chronic ER stress, prolonged *Hac1* (yeast Xbp1) splicing and decreased cell survival (Chawla *et al.* 2011; Rubio *et al.* 2011). In addition, IRE1 signalling can be controlled through association with various adaptors (generically called 'UPRsome') independent of PERK signalling (Hetz *et al.* 2006). Most of these proteins (e.g. Bcl-2 associated X protein - BAX, ASK1-interacting protein 1 - AIP1, heat shock protein 72 - HSP72, Bcl-2 homologous antagonist/killer - BAK) appear to enhance IRE1 activity (Hetz *et al.* 2006; Luo *et al.* 2008; Gupta *et al.* 2010), whilst others such as BAX-inhibitor 1 (BI-1) may inhibit IRE-1 activity (Lisbona *et al.* 2009). Activation of the different UPR sensors might be modulated by additional mechanisms, possibly on a cell-type specific basis. For example, ATF6 may be subject to redox regulation (Nadanaka *et al.* 2007), and IRE1 may sense imbalance in the lipid composition of the membrane (Promlek *et al.* 2011). All of these examples suggest that UPR signalling is fine-tuned at different levels to customize the cellular response depending upon the intensity, nature and duration of ER stress, thereby making it prepared for many situations.

1.4 ER protein homeostasis and ageing

The proteostasis pathways in different subcellular compartments are inter-linked, and therefore severe misfolding in one compartment can disrupt protein homeostasis in other compartments (Roth & Balch 2010). The mechanisms underlying such events are not clear, but may relate to a requirement for common machineries (e.g. the proteasome). Thus, the age-related decline in proteostasis leading to aggregation of cytoplasmic proteins has the potential to disrupt proteostasis pathways in other subcellular compartments such as the ER (Roth & Balch 2010). Indeed, activation of the UPR has been observed in many age-related neurodegenerative diseases, including AD, PD and HD (Douglas & Dillin 2010). In several cases, ER stress and UPR signalling has been implicated in contributing to the disease pathology (Duennwald & Lindquist 2008; Morimoto 2008; Wang & Kaufman 2012). The mechanisms leading to UPR activation in these diseases is not well understood, though may be due in part to the ability of cytoplasmic protein aggregates to interact with ERAD components, including Derlin and HRD1 (Duennwald & Lindquist 2008; Nishitoh *et al.* 2008) thereby inhibiting ERAD and promoting UPR. In addition, cytoplasmic aggregates can also globally inhibit the activity of the proteasome (Hipp *et al.* 2012). Furthermore, many of the membrane proteins synthesised at the ER have large cytoplasmic domains which require the assistance of cytoplasmic chaperones e.g. CFTR. Therefore, a reduced cytoplasmic folding capacity could affect folding of such proteins at the ER, thereby contributing to a perturbation of ER protein folding.

Due to the nature of proteins synthesized at the ER (ion channels, hormones, lysosomal proteins, receptors and signalling molecules) any disruption of ER proteostasis with age could have a wide ranging impact on the function of cells and tissues. Furthermore, as described above, perturbation of ER proteostasis and accumulation of misfolded proteins in the ER activates the UPR, which in turn can have a major impact on cell function and fate. Thus,

defects in ER folding homeostasis and/or UPR signalling have the potential to have widespread effects on cells and the organism as a whole. Indeed, the UPR has been linked to a variety of diseases, including diabetes, cancer and age-related neurodegenerative diseases (Wang & Kaufman 2012). In addition, several studies have found that the levels of individual ER chaperones are changed in aged animals (summarised in table1.5), suggesting that the ER chaperone network is altered with age. In rat liver and hippocampus, levels of ERp44, ERp55, ERp57, PDI and calnexin all decrease with age (Erickson *et al.* 2006). Similarly, BiP was found to decrease in various tissues form aged mice (brain, liver) (Rabek *et al.* 2003; Naidoo *et al.* 2008) or rats (hippocampus, liver, heart, brain, kidney, spleen) (Hussain & Ramaiah 2007). In addition, an increase in oxidised forms of some ER proteins (BiP, PDI, calreticulin) has been documented in the liver of aged mice (Rabek *et al.* 2003; Nuss *et al.* 2008), suggesting a decrease in function of these chaperones with age. These changes in the levels and activity of components of ER folding/QC systems might favour the accumulation of aberrant proteins in aged organisms/tissues, and could potentially promote ER stress and activation of the UPR.

Protein	Observations	References
PDI	Reduced enzymatic activity in liver of old mice. Increased carbonylation in aged liver Decreased mRNA and protein expression in aged rat hippocampus	(Rabek *et al.* 2003; Paz Gavilan *et al.* 2006; Nuss *et al.* 2008)
ERp55, ER57, ERp 44	Decreased expression levels in liver form old mice	(Erickson *et al.* 2006)
CNX	Decreased protein level in liver and hippocampus of old mice	(Erickson *et al.* 2006; Paz Gavilan *et al.* 2006)
CRT	Protein level is not affected by age in mouse liver Increased carbonyl content in aged liver	(Rabek *et al.* 2003)
BiP	Decreased expression level in various tissues of old rats Decreased activity in aged mouse liver Increased oxidative damage with age in mouse liver	(Rabek *et al.* 2003; Hussain & Ramaiah 2007)

Table 1.5: The effect of ageing on ER chaperones.

The increased basal level of eIF2α-P observed in hepatocytes from aged mice supports this hypothesis (Li & Holbrook 2004). However, other studies have reported decreased levels of phosphorylated eIF2α in aged mice/rats (Hussain & Ramaiah 2007; Naidoo *et al.* 2008),

suggesting impairment of UPR signalling. In addition, a small number of studies have indicated that the functioning of the UPR may be affected by ageing. In one study, ER stress was induced in the hippocampus of young and old rats by in situ injection of the proteasome inhibitor lactacystin, and upregulation of BiP and PDI was observed in young but not aged animals (Paz Gavilan *et al.* 2006). Furthermore, Xbp1 splicing was higher in the young animals than in their old counterparts which were treated in parallel, suggesting that the UPR was less efficiently activated in the brain of aged rats (Paz Gavilan *et al.* 2006; Paz Gavilán *et al.* 2009). Sleep deprivation has been found to induce activation of the UPR (Naidoo *et al.* 2008). However, in aged mice, this response appears to be defective since sleep deprivation does not result in increased phosphorylation of eIF2α (Naidoo *et al.* 2008). This reduced eIF2α phosphorylation correlated with increased levels of pro-apoptotic markers (e.g. CHOP, GADD34, c-Jun) in both aged mice and rats (Naidoo *et al.* 2008). Together these data indicate that ER proteostasis pathways may be perturbed during ageing, and furthermore that the functioning of ER stress signalling pathway may also be disrupted.

Two studies in C. *elegans* provide evidence that ER proteostasis and UPR signalling may in fact be important components of lifespan determination. Studies examining the mechanism of life span extension by resveratrol found that members of the abu (activated in blocked UPR) family of ER stress related proteins (Urano *et al.* 2002), were upregulated following treatment (Viswanathan *et al.* 2005). Knockdown of abu-11 eliminated the increased longevity conferred by resveratrol, whilst overexpression of abu-11 significantly extended lifespan in C. *elegans* (Viswanathan *et al.* 2005). Thus abu-11 is necessary and sufficient to extend lifespan, providing evidence that the ability to maintain ER homeostasis and/or ER stress signalling contribute to longevity. Loss of function mutations in the insulin/IGF-1 signalling pathway extend lifespan in many organisms including mammals (Dillin & Cohen 2010), and a recent study suggests that ire1/*xbp1* may contribute to the long lifespan of such mutants (Henis-Korenblit *et al.* 2010). They found that mutations in daf-2 (the *C. elegans* insulin/IGF-1 receptor) which increases lifespan resulted in lower activity of the ire1/*xbp1* pathway and increased resistance to ER stress. These results strongly suggest that these manipulations that extend lifespan also improve ER homeostasis. However is not known if these mechanisms are conserved in mammals

1.5 Aims of this thesis

An increasing amount of data reveals that global protein homeostasis declines with age. This may result from deficiencies in the pathways responsible for maintaining proteostasis, such as the folding and degradation machinery, or the function of the stress responses that detect disturbances in proteostasis. The ER is the main site of synthesis and folding of secretory proteins that are directed to different intra- or inter-cellular compartments. Therefore any alteration of its proper function could have an impact on cell function. However, there is a lack of information on the effect of age on ER homeostasis and the ER stress response, particularly in mammals.

The aim of this project was to examine whether ER proteostasis is affected by age in various models of mammalian ageing. Specifically, this study aimed to investigate whether the ER folding capacity, ERAD, and UPR are altered with age. To address these topics the following aspects were investigated:

1. The expression level of components of ER protein homeostasis pathways in tissues harvested from young and old mice, and two cellular models of ageing.
2. The capacity of the ER translocation, folding and degradation pathways in human primary fibroblast aged *in vivo* or *in vitro*.
3. Activation of the UPR in response to ER stress in the cellular models of ageing.

CHAPTER 2

Material and methods

2.1 Materials and general reagents

2.1.1 Antibodies

All antibodies used in this study are listed in the table 2.1 and 2. 2. Antibodies were used at the specified dilution for immunoblotting (WB), immunofluorescence (IF) or immunoprecipitation (IP).

Antibody	Host	Application	Dilution	Source
actin	mouse	WB	1:1000	Abcam (ab3280)
BAG3	rabbit	WB	1:2000	Abcam (ab37751)
BAG6	chicken	WB	1:2000	Abcam (ab37751)
BiP	goat	WB	1:500	Santa Cruz (sc-1050)
Calnexin (CNX)	rabbit	WB	1:1000	Sigma (C4731)
Calnexin (CNX)	rabbit	IF	1:200	Stressgen (ADI-SPA-865)
Calreticulin (crt)	rabbit	WB	1:1000	David Llewellyn The University of Cardiff
caveolin	rabbit	WB	1:1000	Abcam (ab2910)
Derlin-1	rabbit	WB	1:500	Abcam (ab93341)
Derlin-2	rabbit	WB	1:2000	Stephen High The University of Manchester, UK
eIF2α - P	rabbit	WB	1:1000	Cell Signaling (119A11)
eIF2α total	mouse	WB	1:500	BioSource/Invitrogen (AHO0802)
ERGIC-53	mouse	IF	1:300	Alexis Biochemicals (ALX 804-602)
ERp57	rabbit	WB	1:1000	Neil Bulleid The University of Glasgow, UK
FLAG	mouse	WB	1:1000	Sigma (F3165)
GM-130	rabbit	IF	1:100	Martin Lowe The University of Manchester, UK
OS9	rabbit	WB	1:300	Sigma (SAB4200021)
p5	rabbit	WB	1:1000	Neil Bulleid The University of Glasgow, UK
p97	rabbit	WB	1:2000	Bernhard Dobberstein University of Heidelberg, Germany
PDI	rabbit	WB	1:1000	Neil Bulleid The University of Glasgow, UK
Rpl17	rabbit	WB	1:3000	Martin Pool The University of Manchester, UK
Rpt6	mouse	WB	1:1000	Enzo (BML-PW9265-0100)
Sec24c	rabbit	IF	1:200	David Stephens The University of Bristol, UK
Sec61β	rabbit	WB	1:1000	Bernhard Dobberstein University of Heidelberg, Germany
Sel1L	goat	WB	1:500	Santa Cruz (SC-48081)
SPC25	rabbit	WB	1:1000	Stephen High The University of Manchester, UK
Tubulin	rabbit	WB	1:500	Abcam (ab 4074)
Ubiquitin (P4D1)	mouse	WB	1:1000	Santa Cruz (sc-8017)
VSVG (P5D5)	mouse	WB/IF	1:1000	Sigma (V5507)

Table 2.1: List of primary antibodies

Antibody	Host	Application	Dilution	Source
DyLight 488 anti-rabbit IgG	donkey	IF	1:500	Jackson Immuno Research Laboratories (711-485-145)
DyLight 594 anti-mouse IgG	donkey	IF	1:200	Jackson Immuno Research Laboratories (715-515-150)
IRDye800 anti-rabbit IgG	donkey	WB	1:5000	Li-Cor Bioscience (92632213)
IRDye 680 anti-rabbit IgG	goat	WB	1:5000	Li-Cor Bioscience (92668023)
IRDye800 anti-mouse IgG	donkey	WB	1:5000	Li-Cor Bioscience (92632212)
IRDye 680 anti-mouse IgG	donkey	WB	1:5000	Li-Cor Bioscience (92668022)
IRDye800 anti-goat IgG	donkey	WB	1:5000	Li-Cor Bioscience (92632214)
IRDye 680 anti-goat IgG	donkey	WB	1:5000	Li-Cor Bioscience (92632224)

Table 2.2 List of secondary antibodies

2.1.2 Reagents

Cell culture media and reagents were from Sigma or Gibco (Invitrogen Life Science). Restriction enzymes and DNA polymerases were purchased from New England Biolabs and Roche. RNA polymerases, rabbit reticulocyte lysate and methionine free amino acids were from Promega. RNase inhibitor and DEPC water were from Fermentas. The primers and the dT oligomers were provided by Eurogentec. Tunicamycin was from Ascent Scientific and DTT from Melford. All the other reagents were provided by Sigma or Fisher Scientific, unless otherwise stated.

2.2 Mouse tissue methods

2.2.1 Animals

All experiments were conducted under the aegis of the 1986 Home Office Animal Procedures Act (UK) and following the University Animal Ethical Review Group. All animals were reared at 20 – 22°C and maintained on standard rodent breeder or maintenance chow, under 12 hr light: 12 hr dark lighting schedules. Pairs of female mice (C57/BL6) of 3 months (young animals) and 24 month old (old animals) were sacrificed in parallel by cervical dislocation. The brain, heart, lung, liver, kidney, spleen and muscle were removed, rinsed twice in cold PBS with 1mM PMSF and snap frozen in liquid nitrogen and stored at -80^{o}C as stock or used for tissue extract preparation.

2.2.2 Tissue extracts

Frozen tissues were homogenized using a Mikro-Dismembrator U (B.Braun Biotech International) 1,500 rpm, 1 min. The resulted powder was resuspended in 6 M urea extraction

buffer (6 M urea, 1% w/v SDS, 5 mM EDTA, 20 mM Tris-HCl, pH 8, 0.1% mercaptoethanol, and 1 mM PMSF) and incubated at room temperature for 1 h. The samples were centrifuged at 1,500g for 15 min at room temperature to remove any insoluble material, and then sonicated for 5 min to shear the DNA. Protein concentration was determined using the Bradford method.

2.2.3 SDS-PAGE

Protein samples were denaturated in SDS sample buffer with 100 mM DTT for 10 minutes at 100^{o}C. Then the samples were loaded on polyacrylamide Tris-glycine gels and separated at 30 mA. Non-radioactive gels were further transferred onto nitrocellulose membrane (see immunoblotting) or Coomassie stained. Gels containing radiolabelled samples were fixed in 10% methanol (v/v), 10% acetic acid (v/v) for 20 minutes at room temperature, and dried for 1 hour at 80^{o}C. The dried gels were exposed to a Phosphorimager plate (Fuji Photo Film Ltd) and the bands were visualised using a Fuji BAS 2000 Phosphorimager System.

2.2.4 Coomassie staining

For detecting the total amount of protein, gels were placed in 20 ml of colloidal Coomassie (10% w/v phosphoric acid, 10% w/v ammonium sulfate, 0.12% Coomassie Brilliant Blue G250, 20% v/v methanol) and incubated overnight at room temperature on rocker. The next day the gels were destained in 10% methanol (v/v), 10% acetic acid (v/v) the protein bands were seen without background.

2.2.5 Immunoblotting

After SDS-PAGE proteins were transferred onto Odyssey nitrocellulose membrane (LI-COR Biosciences) using Tris-glycine transfer buffer (20 mM Tris-Hcl, pH 7.5, 150 mM glycine and 20% (v/v) methanol) and a wet transfer system (TE 22 Mini Tank Transfer Unit, GE Healthcare) at 300 mA for 2 hours. Membranes were blocked against non-specific binding with 5% (w/v) milk in TBS, Tris-buffered saline (20 mM Tris, 150 mM NaCl, pH 7.4), then incubated with primary antibodies in TBS containing 2% (w/v) milk or 5% (w/v) BSA with 0.1% (v/v) Tween (eIF2α-P antibodies) at 4^{o}C overnight. The list of primary antibodies used in this study is shown in table 2.1. Membranes were washed 3 times with TBS, then incubated with IRDye secondary antibodies (LI-COR Biosciences) diluted 1:5000 in TBS containing 2% (w/v) milk. The infrared signal was detected using an Odyssey scanner (LI-COR Biosciences) and densitometry was performed using the Odyssey 2.1 Image Analyzer software (LI-COR Biosciences).

2.2.6 Analysis of protein aggregation

An adapted protocol based on (David *et al.* 2010) was used to examine protein aggregation in muscle and liver. Frozen tissue powder was solubilised in 10 volumes of RIPA buffer (50 mM Tris, pH 8, 150 mM NaCl, 5 mM EDTA, 1% NP40, 1 mM PMSF) with 0.5% SDO and 0.5% SDS (for liver samples) or 1% SDO and 1% SDS (for muscle samples). A tenth of the resulting homogenate was mixed with 8M urea buffer to generate the 'total' protein extract (including the aggregated detergent insoluble proteins). The remaining homogenate was sequentially centrifuged at 4^{o}C for 20 minutes at 3,000g, 50,000g and respectively 80,000g. The pellets

resulting after first centrifugation were resuspended in 2 volumes/weight, whereas the next two resulting pellets were resuspended in 1 volume/weight 6 M urea buffer and incubated for 1 hour at room temperature prior to mixing with SDS-PAGE sample buffer.

2.3 Cell culture methods

2.3.1 Cell culture

Primary cells used in this study are human skin fibroblasts (AG), and human embryonic lung fibroblasts (IMR90). All cells were purchased from Coriell Institute for Medical Research, Camden, NJ. Skin fibroblasts are from a young donor of 32 years old (catalog number AG06962), and his father, aged 71 years (catalog number AG05807). IMR90 cells were purchases as low population doubling line (LPD, catalog number I90-78) and high population doubling line (HPD, catalogue number I90-52).

Cells were routinely cultured in Minimum Essential Media Eagle (MEM) supplemented with 15% heat inactivated fetal bovine serum, 10% non-essential amino-acids, 5% L- glutamine, 5% MEM essential amino acids, and 5% MEM vitamins. The media was changed every 3 days during cultivation. At confluency, cells were passaged by trypsinization and population doublings (PD) were calculated as (log cell number harvested – log cell number seeded)/log 2.
In this study I90's with PD below 30 were considered as young, whereas cells with PD between 52 and 58 were considered old. The skin fibroblasts were used at a similar PD and not higher than 18. For experiments, cells were seeded at a $2x10^4$ cells/mm^2 cell density with 24 hours before any treatment.

2.3.2 Cell transfection

Primary cells were transfected by electroporation using the NEON transfection system (Invitrogen), according to manufacturer's instructions. Briefly, 1 x 10^5 cells were resuspended in 10 µl reaction mix containing 3 µg DNA and buffer R provided in the kit, then a pulse of 1100 mV was applied for 30 seconds. The cells were seeded into a well of a 12 well plate using MEM culture media containing 15% FBS and incubated at 37^oC and 5% CO_2 for 48 hours before analysis.

2.3.3 VSV-G trafficking

VSV-G was introduced in to the cells using an adenoviral vector. The stock of virus was prepared by infecting HEK293 cells with 50 µl virus in 15 ml Dulbecco's modified Eagle's media with 5% foetal bovine serum. Four days post-infection, when most of the cells were dead, the culture media was removed and freeze – thawed 6 times using liquid nitrogen. After a 10 minutes centrifugation at 1,500 g at 4^oC, the supernatant was aliquoted and stored at -80^oC. The amount of HEK virus preparation needed for optimal infection was determined empirically by using serial dilutions.

Fibroblasts were plated in 6 cm dishes and the next day the culture media was replaced with 1.5 ml of MEM with 5% FBS containing the appropriate volume (e.g. 15 µl) of adenovirus and the cells were incubated at 37^{o}C for 1 hour. The virus-containing media was replaced with 5 ml of MEM media with 15% FBS and the cells were placed overnight in a tissue culture incubator at 40^{o}C. The following day, the culture media was replaced with pre-warmed media containing 1mg/ml cycloheximide and cells were shifted to 32^{o}C and chased for up to 4 hours. Prior to harvesting cells were rinsed twice in cold PBS. Then cells were lysed in HKMT buffer (20 mM HEPES, 100 mM KCl, 5 mM $MgCl_2$, 0,5% Triton X-100) with 1 mM PMSF for 30 minutes on ice, followed by 15 minutes centrifugation at 14,000g at 4^{o}C. The resulting samples were mixed with SDS-PAGE sample buffer with DTT and heated at 100^{o}C for 10 min, EndoH treated overnight then separated by SDS-PAGE and analysed by immunoblotting.

2.3.4 Immunofluorescence

Cell growing on glass coverslips were rinsed with PBS then fixed in pre-chilled (-20^{o}C) methanol for 5 minutes. Following three washes in PBS, the coverslips were incubated with the appropriate primary antibodies diluted in PBS (table 2.1) for 30 minutes at room temperature. Coverslips were washed 3 times with PBS and incubated with the appropriate secondary antibodies (table 2.2) and 50 ng/µl DAPI (4,6-diamine-2-phenylindoledihydrochloride) to stain the DNA for 30 minutes at room temperature. Coverslips were washed twice in PBS and once in distilled water then mounted onto glass slides using 7 µl Mowiol. The mounting media was allowed to dry overnight at 4^{o}C in the dark and analysed on an Olympus BX60 upright microscope using a PlanApo 60X 1.4 N.A. oil objective. The images were captured using a CoolSNAP EZ camera (Photometrics, US) and Metamorph software (University Imaging Corporation).

2.3.5 Preparation of semi-permeable cells

The protocol was adapted from that established by Wilson et al (Wilson *et al.* 1995). Cells were trypsinised and resuspended in 8 ml ice cold KHM buffer (110 mM KOAc, 20mM HEPES, 2 mM magnesium acetate, pH 7.2). Cells were pelleted at 300 g for 3 minutes at 4^{o}C then resuspended in 6 ml ice-cold KHM buffer with 20µg/ml digitonin, and incubated on ice for 5 minutes. Cells were spin down as above then resuspended in 10 ml of cold HEPES buffer (50 mM KOAc, 90 mM HEPES, pH 7.2) and incubated on ice for 10 minutes. The resulting semi-permeabilised cells were collected by centrifugation and resuspended in 100 µl KHM buffer containing 100 µM $CaCl_2$ and 10 µg/ml micrococcal nuclease, then incubated 12 minutes at room temperature. The nuclease was inhibited by addition of 4 mM EGTA and 900 µl of ice-cold KHM buffer. Cells were counted and resuspended in KHM to obtain 0.5 x 10^5 cells/µl cell density and used as source of ER membranes.

2.3.6 *In vitro* transcription

In vitro mRNA synthesis was carried out as previously described (Gurevich *et al.* 1991). Linear DNA was obtained by enzymatic digestion or by PCR (table 2.3) The PCR reactions contained 50 ng of DNA, 100 pmol of each primer, 5 units Pwo DNA polymerase (Roche), 10 µl reaction

buffer (100 mM Tris-Hcl pH 8.8, 250 mM KCl, 50 mM $(NH_4)_2SO4$ and 20 mM $MgSO_4$) and 2.5 mM of each dNTP (BIOLINE) in a total volume of 100 µl. The thermal cycling parameters were 95^oC for 3 minutes, followed by 30 cycles of 94^oC for 1 minute, 60^oC for 1 minutes and 72^oC for 1 minute ended by 10 minutes at 72^oC for the final extension. The PCR was followed by Dpn I treatment for 2 hours at 37^oC to eliminate the template. For the *in vitro* transcription 200 µl reactions were prepared by adding 8 µg linear DNA or 20 µl of PCR product, 80 mM HEPES – KOH pH 6, 12 mM $MgCl_2$, 4 mM DTT, 12 mM ribonucleotide mix (Promega), 160 units of RNAse inhibitor (Fermentas), 40 µl reaction buffer (40mM Tris pH 7.9, 6mM MgCl2, 2mM spermidine and 10mM NaCl) and 150 units of T_7 or SP_6 (for signal peptide peptidase – SPP) RNA polymerase (Promega). The reactions were incubated at 37^oC for 4 hours, followed by phenol/chloroform extraction and ethanol precipitation. The RNA pellet was resuspended in 50 µl RNAse-free water containing 40 units of RNAse inhibitor.

Gene	Vector	Restriction enzyme / Primers	Source
Pre-prolactin	pGEM3	Eco R I	Neil Bulleid University of Glasgow, UK
Hemagglutinin	pGEM3	Bam H I	Neil Bulleid University of Glasgow, UK
Signal peptide peptidase	pSV SPORT	Hind III	Stephen High University of Manchester, UK
Gamma interferon	pGEM T easy	Not I	Werner Muller University of Manchester, UK
Opsin	pZeo	**F**: CCAGTTCCGCCCATTCTCCG **R**: TAGAAGGCCACAGTCGAGG	Stephen High University of Manchester, UK
Human cytomegalovirus US_2	pCR4	**F**: TCAAGCGTAGTCTGGGACGTCGTATG GGTAGCACACGAAAAACCGCATCC **R:** TGTAAAACGACGGCCAGT	Stephen High University of Manchester, UK

Table 2.3 ***List of enzymes and primers used to linearise the cDNA***

2.3.7 *In vitro* translation/translocation

mRNAs encoding membrane or secreted proteins were translated in the presence of SP cells and ^{35}S labelling. In each reaction 14 µl rabbit reticulocyte lysate, 0.5 mM amino acids without methionine, 11 µCi [^{35}S] methionine/cysteine EasyTag protein labelling mix (PerkinElmer, US), 1µl RNA transcript and 1 x 10^5 semi-intact cells were used. Translation was allowed to proceed for 1 hour at 37^oC, and then SP cells were pelleted by centrifugation (1 minute 15,000g). The pellet was washed once with KHM buffer and centrifuged as before. The SP cells were resuspended in 20 µl SDS sample buffer with 100 mM DTT and heated at 100^oC for 10 minutes.

2.3.8 EndoH and proteinase K treatment

EndoH cleavage of high mannose forms of *N*-linked glycans was carried out by adding 500 units of EndoH (New England Biolabs) to the samples already resuspended in sample buffer with 100 mM DTT. The samples were incubated overnight at 37°C then heated for 10 min at 100^{o}C.

For proteinase K digestion, 500 µg/ml proteinase K was added to the samples resuspended in KHM buffer. Samples were incubated for 60 min on ice and then the enzyme was inactivated by adding PMSF to 1mM final concentration. An equal volume of 2 times SDS-PAGE sample buffer with DTT was added and the samples were heated at 100^{o}C for 10 min

2.3.9 Isolation of total RNA

Cells from a 6 cm culture dish were harvested in 1 ml of Tri Reagent (Sigma) at room temperature. Then a volume of 200 µl of chloroform was added and samples were vigorously shaken for 30 seconds, followed by 3 minutes incubation at room temperature. Samples were centrifuged for 30 minutes at 14,000g, 4^{o}C and the upper phase was transferred in new Eppendorf tubes. Next 500 µl of isopropanol were added and samples were vigorously shaken for another 30 seconds and incubated at RT for 10 minutes. The total RNA was pelleted by centrifugation and washed once with 75% ethanol. The pellet was air dried, resuspended in 10 µl of DNase mix containing 9 µl DNase buffer (10 mM Tris-HCl pH 7.6, 2.5 mM $MgCl_2$, 0.5 mM $CaCl_2$) (NEB) and 2 units of DNase (NEB), and incubated at RT for 15 minutes. The DNase was inactivated by heating at 60^{o}C for 10 minutes. After cooling on ice, the RNA concentration and purity was determined by using the nanodrop and a value of OD_{260}/OD_{280} ratio of at least 2 was required for RNA with minimal DNA contamination.

2.3.10 Xbp1 RT-PCR

First-strand cDNA was synthesised using an oligo dT primer and 20 units of AMV reverse transcriptase (Roche), 5x reaction reaction buffer (250 mM Tris-HCl pH 8.5, 40 mM $MgCl_2$, 150 mM KCl, 5 mM dithiothreitol) (Roche) and 5 µg total RNA isolated as above. A quater of the first strand was used as template for PCR. Each PCR reaction contained the first strand, 5 mM of each dNTP, 10 nmol of each primer, 10x reaction buffer (100 mM Tris-HCl pH 8.3, 15 mM MgCl2, 500 mM KCl,) (Roche) and 0.5 µl Taq polymerase (Roche) in a total volume of 25 µl. The primers used in PCR flank the *Xbp1* intron in order to amplify spliced and unspliced *Xbp1* are: ACAGCGCTTGGGGATGGATG (forward) and TGACTGGGTCCAAGTTGTCC (reverse). PCR conditions were as follows: 3 min at 95 °C, followed by 35 cycles of 45 s at 95 °C, 40 s at 58 °C, and 45 s at 72 °C for amplification, and 10 min at 72 °C. PCR products were resolved on 2% agarose gels.

2.3.11 Metabolic radiolabelling

Cells growing in 6 cm or 6-well dishes were washed once with PBS, then incubated with 'starvation' media (DMEM without methionine plus 10% FBS) for 20 minutes at 37^{o}C. Cells were then incubated with starvation media containing 45 µCi/ml of [^{35}S] methionine*/*cysteine EasyTag

protein labelling mix for 30 minutes. Cells were washed twice with PBS before being further processed as described below.

2.3.12 Concanavalin A binding

Cells were metabolically labelled as described above, then incubated for 5 minutes on ice with KHM buffer containing 40 µg/ml digitonin to extract the cytosol, and then washed once with HEPES buffer. The cells were lysed in 1 ml of immunoprecipitation (IP) buffer (10 mM Tris-HCl, pH 7.6, 140 mM NaCl, 1 mM EDTA, 1% Triton X-100 and 1 mM PMSF) for 30 minutes on ice and the lysate was centrifuged at 18,000g, 4^{o}C for 15 minutes to remove non-soluble debris. The resulting supernatant was incubated with 120 µl (25% v/v) concanvalin A sepharose beads (Sigma) for 1 hour on a roller at room temperature. The beads were washed 3 times with IP buffer, each time collecting the beads by centrifugation at 150g for 1 minute. Bounded glycoproteins were eluted from the beads by incubation with 100 µl 0.25 M α-methylmannosidase (Sigma) in IP buffer for 1 hour at 25^{o}C with shaking. The eluate was collected by centrifugation as above. Samples of the total cells, the digitonin extract (cytosol), the conA eluate and the unbound fraction were analysed by SDS-PAGE and phosphorimaging.

2.3.13 Cell viability

Cells were plated in a 96 well plate at a density of 5 x 10^3 cells per well and incubated overnight at 37^{o}C. The next day the cells were treated with the drug of interest. Different concentrations of tunicamycin (Tn) were used for 16 hours, whereas for DTT the same concentration (2 mM) was used for up to 8 hours. Each treatment was performed in triplicate. Following treatment, cells were washed once with PBS and 200 µl of 0.5 mg/ml 3-(4,5-Dimethylthiazol-2-yl)-2,5-diphenyltetrazolium bromide (MTT) solution in MTT media without red phenol and containing 15% FBS was added per well, then the plates were incubated for 2 hours at 37^{o}C and 5% CO_2. The MTT solution was discarded and 100 µl DMSO was added in each well to solubilise the formazan crystals. The absorbance was read at 550 nm using a microtiter plate reader (Synergy H1 hybrid reader, BioTek, US). An empty well was used as blank, and the value of blank reading was deducted from all the readings. The cell viability was calculated as mean of the triplicate readings and plotted relative to the control (untreated cells).

2.4 Molecular biology techniques

2.4.1 Purification of plasmid DNA

One colony was placed in 100 ml of LB media containing the appropriate antibiotic and cultured at 37^{o}C overnight. Plasmid DNA was obtained from the overnight culture using QIAGEN Plasmid Midi Kit, according to the manufacturer's protocol. The concentration and the purity of plasmid DNA was measured using nanodrop (NanoDrop Technologies, US), and a value of 1.8-2 for OD_{260}/OD_{280} ratio was required for a DNA with minimal protein contamination.

2.4.2 Agarose gel electrophoresis

RT-PCR products were separated by horizontal electrophoresis in 2% w/v agarose gel, in 1X TBE buffer (45 mM Tris-borate, 1mM EDTA, pH 7.8). Ethidium bromide at a final concentration of 1µg/ml was added directly to the gel. DNA samples were mixed with loading buffer (BIOLINE Ltd) then subjected to electrophoresis at constant voltage of 70 V for 90-120 minutes. The DNA fragments were visualised using a uv transluminator (UVITEC) and the images were obtained using a Fuji Film box equipped with LAS1000 camera (Fuji Photo Film Ltd).

2.5 Antibody validation, quantification, and statistical analysis

The linearity of fluorescence detection for each of the used antibody was tested to allow an accurate quantification of each antigen. Serial dilutions of liver extract and cell lysates ranging from 0.5 µg to 150 µg total protein were detected with the primary antibody of interest and the appropriate IRDye 800CW secondary antibody. The images were acquired using the Odyssey scanner. The bands of infrared western blots were quantified using Odyssey 2.1 Image Analyzer software (LI-COR Biosciences). The bands of interest were selected and the background border was chosen at width 2. The displayed integrated intensity represents the background-corrected total intensity of the pixels enclosed in the selected area multiplied by the area of the shape. The background correction was calculated using the average intensity of pixels at the top and bottom of the selected area for being multiplied by the numbers of pixels form the selected area and by the area of the shape.

The bands from radioactive polyacrylamide gels and ethidium bromide stained agarose gels were acquired using Fuji equipment and were quantified using AIDA software (Raytest Isotopenmessgeräte GmbH, Germany). The bands of interest were selected and the local background border was set to 2 pixels width. Bands signals were evaluated as background-subtracted integrated peak intensities.

Data were plotted as mean ± error bars showing standard error of the mean (s.e.m). The statistical significance of differences between samples was determined using JMP9 software (SAS Institute Inc.). The data were tested for uniform distribution using Shapiro-Wilk test. Also, for the data sets analysed using ANOVA (analysis of variance), the homogeneity of variances was tested using the Bartlett and Levene tests. To determine whether the differences between two samples were significant a Student's t test was performed. When comparison between two groups required the integration of two variables (e.g. age and treatment) a two way ANOVA was used. The two way ANOVA permits one to test whether both, only one or none of the variables affect the outcome. When both variables contributed to the final effect and the effect of one variable depended on the levels of the other variable (interaction effect), a post-hoc test called slice test was performed. This test allows analysing simple effects of a factor (e.g. age) at the each level of the other factor (e.g. treatment).

CHAPTER 3

Perturbations in ER proteostasis with age studied using mouse tissues

3.1 Introduction

A large amount of data generated by high-throughput transcriptomic studies, using mice as a model organism for mammalian ageing, has shown that numerous molecular pathways are affected by age. Some gene sets, such as genes encoding for stress response, for inflammatory response and for protein degradation (lysosomal and proteasomal pathways) are age-affected in multiple tissues including brain, heart, lung, kidney, liver, spleen, and muscle (Dhahbi *et al.* 2006; Zahn *et al.* 2007; de Magalhaes *et al.* 2009). Genes encoding ribosomal subunits have been also shown to undergo changes in expression levels in aged liver (Papaconstantinou *et al.* 2005), muscle (Beggs *et al.* 2004; Edwards *et al.* 2007), brain (Godbout *et al.* 2005), heart and lung (Zahn *et al.* 2007). Age-related changes in the transcriptional pattern have also been reported for ER-associated pathways. For instance, gene sets involved in protein synthesis, protein folding and response to unfolded proteins are downregulated with age in lung, heart and spleen (Zahn *et al.* 2007). The same study suggested that the ribosomal genes are upregulated in aged lung, heart and spleen, but down regulated in aged brain. Distinct transcriptional changes in old mice have been reported for the *Hspa5* gene, encoding the ER chaperone BiP, in different tissues. *BiP* mRNA is upregulated in old brain, liver, spleen and muscle (Beggs *et al.* 2004; Rodwell *et al.* 2004; Edwards *et al.* 2007; Zahn *et al.* 2007), but is decreased in heart, kidney and lung (Zahn *et al.* 2007). Another ER pathway that might be affected by age is ER-associated degradation (ERAD), e.g. *Derl1* (Derlin-1) mRNA is upregulated with age in lung, muscle and hippocampus (Verbitsky *et al.* 2004; Misra *et al.* 2007), whilst *Vcp* (p97) is lower in aged lung (Misra *et al.* 2007). Interestingly, the gene set regulating protein ubiquitination, comprising genes coding for ubiquitin-ligases and ubiquitin-conjugating enzymes, are decreased in multiple tissues, including lung (Misra *et al.* 2007), heart (Dhahbi *et al.* 2006), liver (Papaconstantinou *et al.* 2005), muscle (Lee *et al.* 1999) and brain (Lee *et al.* 2000; Godbout *et al.* 2005). Thus, in mice at least, there is strong evidence that molecular pathways important for the cellular protein homeostasis are altered with age. Many of these changes appear to be tissue specific, which may reflect the notion that different tissues may age at a different rates (Zahn *et al.* 2007). The number of age-regulated genes may provide a measure to predict the extent of homeostasis perturbation during ageing in different tissues.

However, changes in transcription and mRNA level are not the only factors to affect protein expression levels. In addition, translation efficiency and posttranslational events such as degradation may be altered and may have a significant impact on protein expression. Thus, in order to get a clearer picture of how protein function may be changed with age, it is important to measure protein levels directly. To this end, several proteomics studies have investigated changes in global protein expression in brain (Butterfield & Poon 2005), muscle (Piec *et al.* 2005) or kidney (Chakravarti *et al.* 2009). Like the transcriptome analyses, these also highlight changes in metabolic, stress response and transport pathways with age. However, none of these studies has specifically focused on the changes in particular subcellular compartments such as the ER. To date, a small number of studies have examined the changes with age in the

expression level of ER chaperones and oxidoreductases. Whilst these have identified some age-related changes, they fail to give a comprehensive picture of how the ER folding and quality control machineries may be affected with age. For instance, levels of ERp57, ERp55, ERp72 and calnexin were found to decrease by 50% in the liver of aged mice (Erickson *et al.* 2006), whereas the levels of calreticulin and PDI were unchanged (Rabek *et al.* 2003; Erickson *et al.* 2006). However, a separate study demonstrated that levels of calnexin, PDI and BiP declined with age in rat hippocampus (Paz Gavilan *et al.* 2006). Several studies have assessed age-related changes in BiP expression, and found that it decreases in several tissues: brain, liver (Rabek *et al.* 2003; Naidoo *et al.* 2008), hippocampus (Paz Gavilan *et al.* 2006), heart, kidney and spleen (Hussain & Ramaiah 2007). Thus, in order to obtain an integrated view of how ER protein homeostasis network may be altered by age the expression levels of a wide range of proteins, covering the major function of ER, as well as various ER-linked processes (protein biosynthesis and protein degradation) were examined in seven different tissues from young and old mice.

3.2 Effect of age on expression level of ER proteostasis pathway components

To analyse whether the expression level of components of protein synthesis, translocation, folding and degradation pathways varies with age, 7 different tissues (liver, lung, kidney, brain, heart, muscle and spleen) were harvested from 5 young (3 months) and 5 old (22-26 months) female C57/BL6 mice. Mice were sacrificed by cranial dislocation, the tissues rapidly collected and snap-frozen in liquid nitrogen, then used to prepare protein extracts for western blot analysis (see section 2.4.2). Equal amounts of total protein were loaded for each tissue extract, with 25 µg total protein loaded for the Coomassie gels and various amounts according to the standard curves prepared for each primary antibody (appendix 2) used in the western blots analysis. Extracts were separated by SDS-PAGE, transferred onto nitrocellulose and probed with antibodies or antisera specific for the proteins of interest, followed by secondary antibodies conjugated to infrared fluorescent dyes. The intensity of the fluorescence signal was detected and quantified using an Odyssey 2.1 Image Analyser as described in sections 2.5.9 and 2.5.17. The results obtained with each tissue are described below. To facilitate interpretation, target proteins were arranged into groups based on function. Thus, those involved in protein biosynthesis (Rpl17, Sec61β, SPC25), protein folding (BiP, calnexin, calreticulin, ERp57, PDI, p5) and ERAD (OS9, Sel1L, Der-1, Der-2, p97) pathways were grouped together and are presented in separate figures. Following retrotranslocation, the ERAD substrates are ubiquitinated in the cytosol and degraded via the proteasome. As BAG6, a member of the BAG family, has recently been found to play a role in degradation of proteins with hydrophobic domains, including ERAD substrates (Claessen & Ploegh 2011; Hessa *et al.* 2011; Wang *et al.* 2011), it was analysed together with the ERAD substrates. Separate blots of the same extracts

gave very similar results to those shown in Fig 3.1 -3.21, validating the reproducibility of the approach taken.

3.2.1 Liver

Initially, extracts prepared from liver were analyzed, since liver is a secretory tissue and therefore has an abundant rER. No major differences in the total protein profile of young versus old mice were observed in the Coomassie stained gels (Fig 3.1A), and confirmed equal loading of each extract. First, three components of key machineries involved in protein biosynthesis at the ER were examined, namely Rpl17, a component of large ribosomal subunit (Taylor *et al.* 2009), SPC25 from the signal peptidase complex (Martoglio 2003), and Sec61β, a core component of the ER translocon (Rapoport 2007). The results of the western blots are shown in Fig 3.1B. A single major immunoreactive band was detected for each of the proteins at the expected molecular weight of 23 kD for Rpl17, 25 kD for SPC25, and 10 kD for Sec61β (appendix 1). In order to obtain a quantitative measurement of the relative abundance of the proteins, the fluorescent signal in each sample was quantified and normalised relative to the corresponding Coomassie signal, and represented graphically (Fig 3.1B). No significant difference was observed between Rpl17, SPC25 or Sec61β in liver from young and old mice, suggesting that expression levels of these components do not change dramatically with age. This is consistent with results obtained by transcriptome analysis of mRNA levels in aged liver (Zahn *et al.* 2007).

The same protocol was used to examine components from the major folding ER folding systems: the chaperones (BiP, calnexin and calreticulin) and oxidoreductases (ERp57, PDI and p5) in the liver of young and old mice (Fig 3.2). For BiP, two immunoreactive species of approximately the molecular weight expected for BiP were detected (Fig 3.2A). Further investigation revealed that the upper band represents BiP, since only this species was present in isolated ER microsomes (appendix 3). All the other antibodies gave a major distinct band at the appropriate molecular weight. No obvious changes in expression level were found for BiP or for the two lectin chaperones calnexin and calreticulin. Similarly, no differences in the expression levels of ERp57 and p5 oxidoreductases were observed between the samples from young and old mice. Of interest, a significant increase of approximately 40% in the level of PDI in liver tissue from old mice was observed. The levels of ERAD components are shown in Fig 3.3, together with BAG6. Two prominent species were observed for OS9. However this is not surprising as 3 different transcript variants of OS9 have been identified (Kimura *et al.* 1998), isoform 2 being the major form in most of the cell types or tissues (Kimura *et al.* 1998; Litovchick *et al.* 2002). The expression level of OS-9, Sel1L, Der-1, p97 and BAG6 was similar in liver from young and old mice. The notable exception was Der-2, the level of which showed a significant increase of approximately 20% in the liver of aged animals.

In summary, in liver, the level of expression of most of the proteins tested was not dramatically affected by age. However, a significant increase was found in the levels of PDI and Der-2.

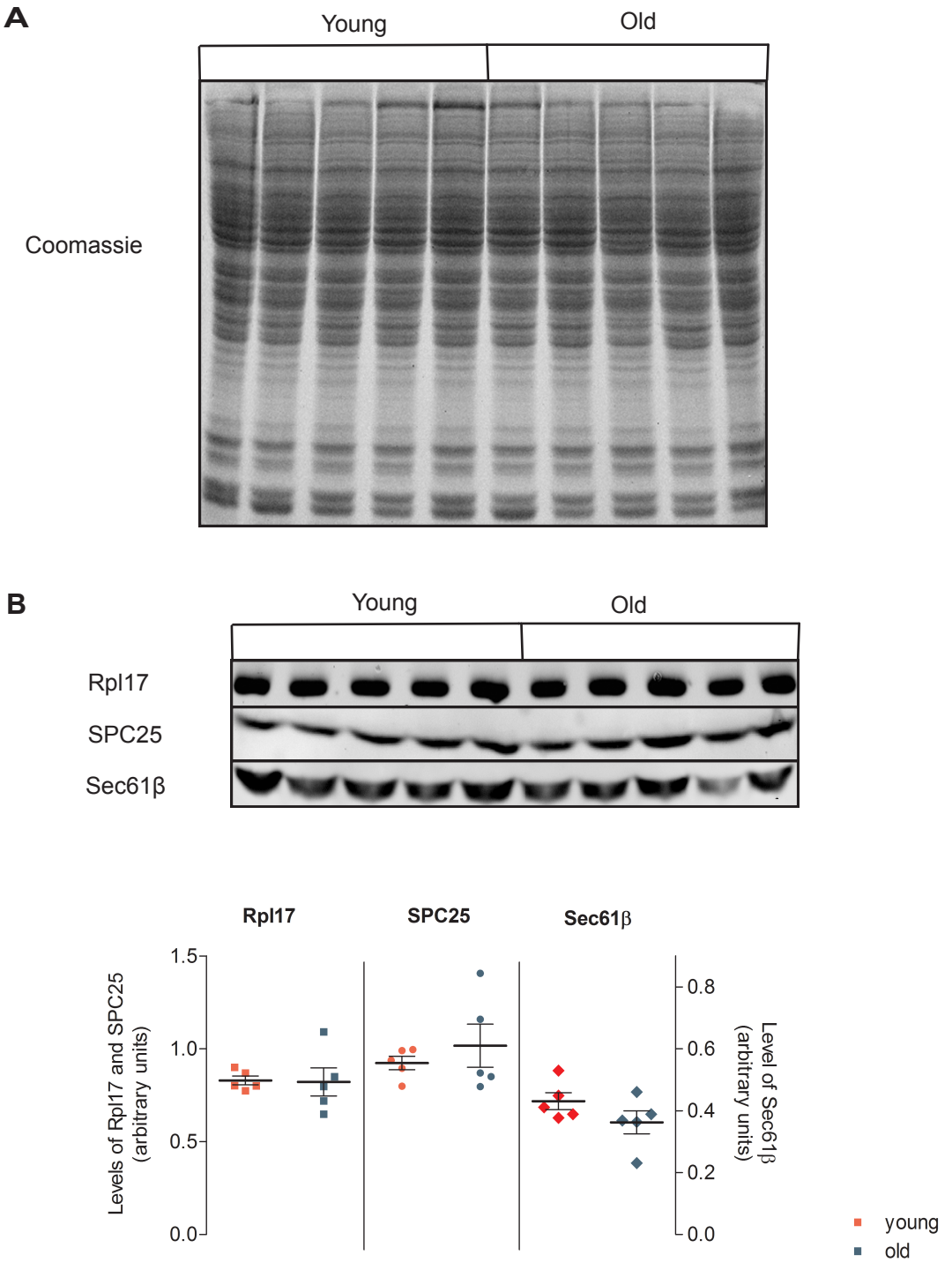

Figure 3.1: Total protein and levels of components of the protein synthesis machinery in mouse liver.
Extracts from young and old livers were prepared in 6 M urea buffer, and equal amounts of total protein were loaded for each sample. Proteins were separated on 12% Tris-glycine gel. **(A)** Total proteins were visualised by Coomassie blue staining. **(B)** Samples were analysed by western blotting using the primary antibodies indicated followed by infrared secondary antibodies. The intensity of the fluorescent signal obtained with each antibody was quantified using the Odyssey software, and normalised relative to the intensity of the Coomassie blue signal. The scatter plots in **(B)** show the normalised signal for each protein (Rpl17, SPC25 and Sec61β), and each point represents data from a single animal. The lines and error bars show the mean ± s.e.m.

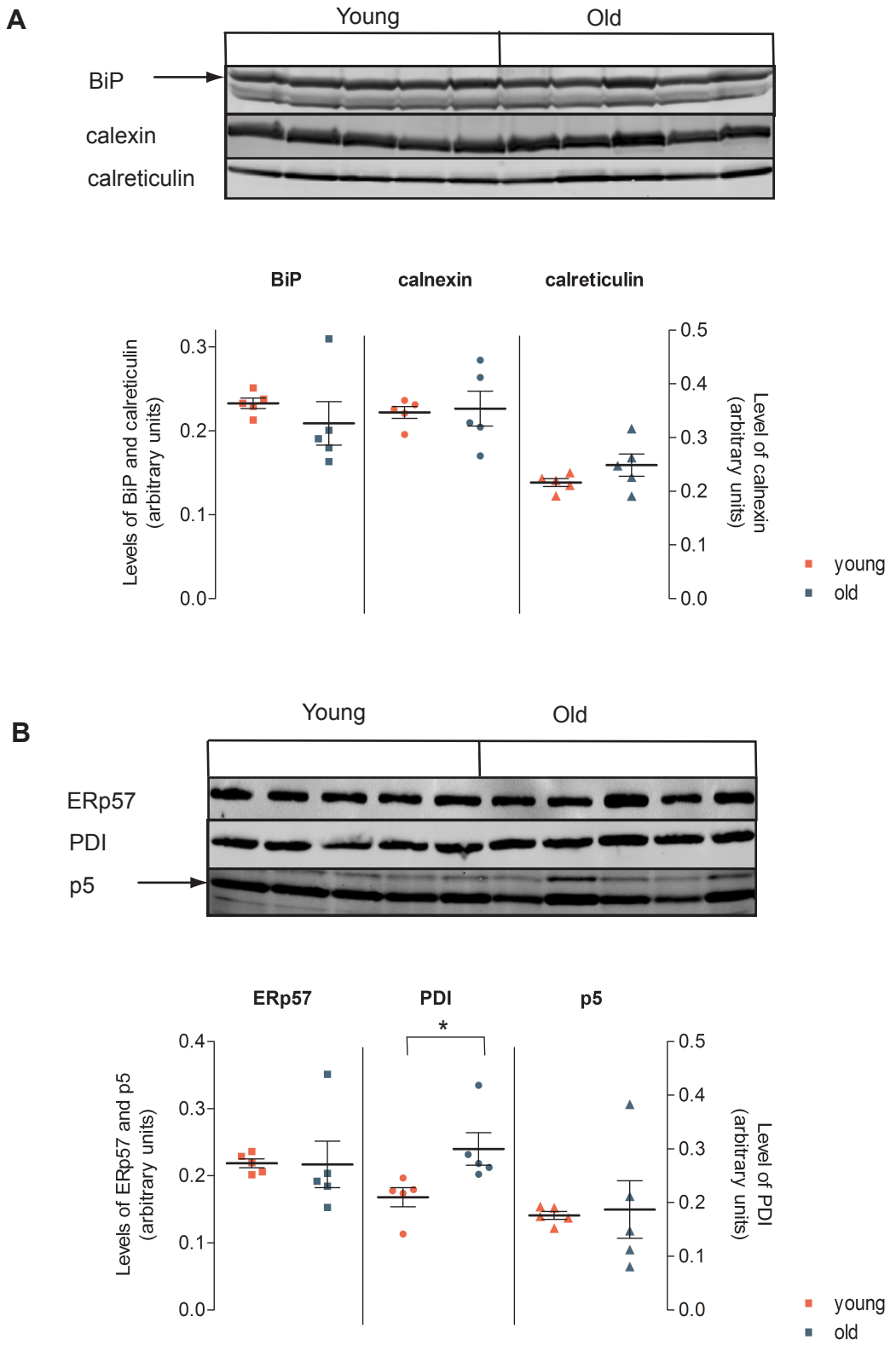

Figure 3.2: Levels of ER chaperones and ER oxidoreductases in mouse liver.
Protein extracts were prepared and analysed as described in Fig. 3.1. Immunoblots showing the level of ER chaperones **(A)** and ER oxidoreductases **(B)** were quantified and the results are shown underneath the respective immunoblot. The results are presented as mean ± s.e.m. The Student's t-test was used to determine significant differences between levels of the proteins in young and aged tissues. Asterisks indicate significant difference (*) denotes $P < 0.05$ and (**) denotes $P < 0.01$.

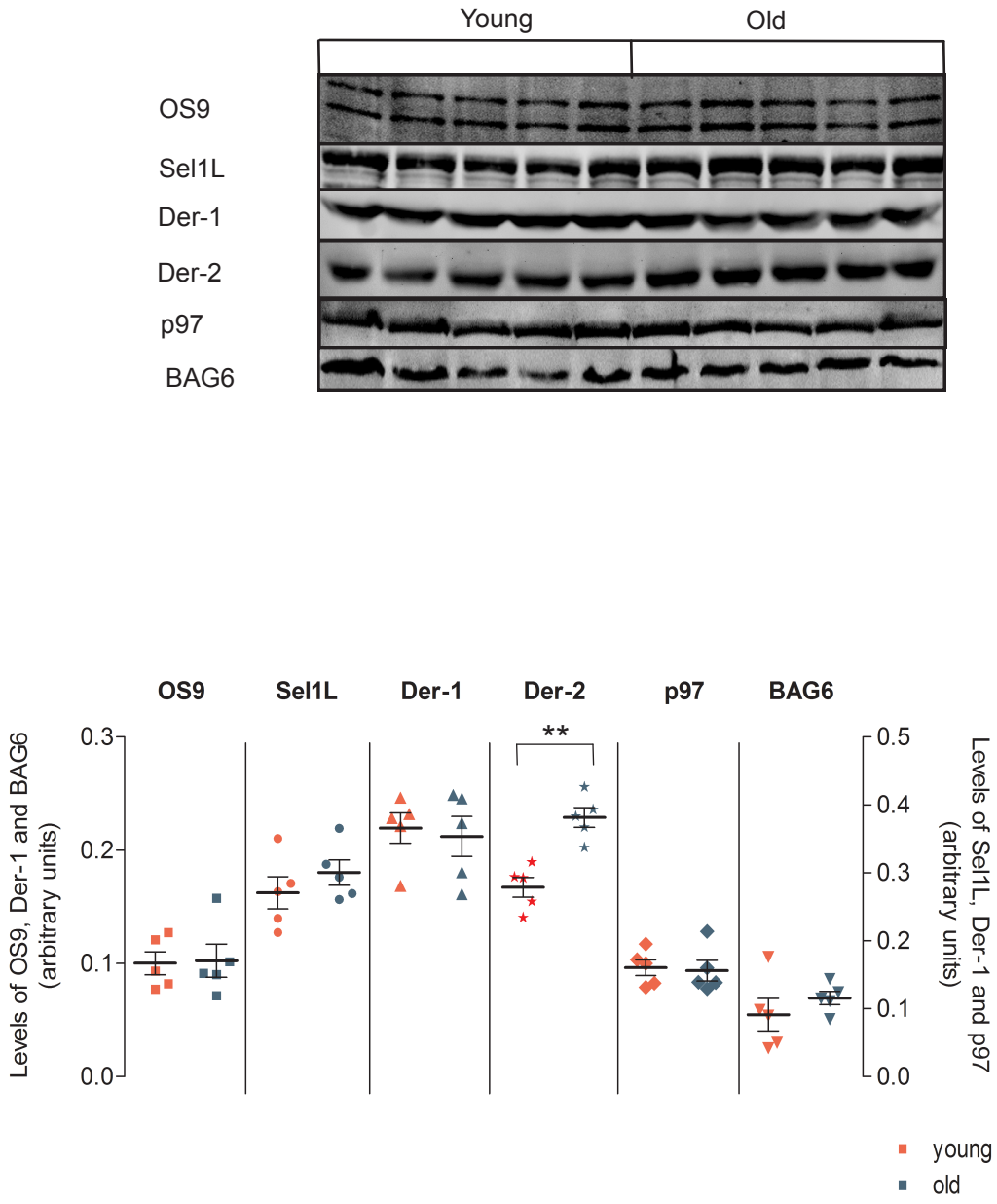

Figure 3.3: Levels of components of the ERAD pathway in mouse liver.
Protein extracts from livers of young and old mice were prepared in 6 M urea buffer, and equal amounts of total proteins were loaded for each sample. Proteins were resolved by 12% SDS-PAGE and analysed by immunoblotting with the indicated primary antibodies followed by infrared secondary antibodies. The results of immunoblots were quantified and plotted as described in the Fig 3.1. A Student's t-test was used for statistical analysis of the levels of ERAD proteins in young and aged tissues. Significant differences are indicated with a single star ($P < 0.05$) or double stars ($P < 0.01$).

3.2.2 Heart

Protein extracts from heart were prepared as for liver, and the same protein components of protein biosynthesis, folding and degradation pathways were analysed by quantitative western blotting. The Coomassie gel confirmed that equal amount of total protein were loaded for each sample (Fig 3.4A). Quantification of components of the protein biosynthetic pathway revealed that levels of SPC25 were not changed in old compared to young heart tissue (Fig 3.4B). By contrast, a significant increase, of over 40%, was observed in the level of Rpl17 in heart tissue from old mice (Fig 3.4B). This result is in agreement with an increase in Rpl17 mRNA in the heart of aged mice (Zahn *et al.* 2007). This suggests that the composition of the large subunit of the ribosome might be altered in the aged heart, a factor which could potentially impact on ribosome function. Sec61β could not be reproducibly detected in heart. This could be due to the fact that major cells in heart are cardiomyocytes which have and increased percentage of sarcoplasmic reticulum, an ER form specialised in calcium storage and release (Michalak & Opas 2009). Compared to the rER, the sarcoplasmic reticulum has no ribosomes attached and its membrane and lumen have a different composition of proteins (e.g. increased amount of calcium pump, or calcium retention proteins) (Michalak & Opas 2009). Thus some of the tested proteins might be expressed at a very low level, under the detection limit of western blotting in heart. Next, the levels of ER chaperones and ER oxidoreductases were tested (Fig 3.5). Although levels of calnexin, ERp57 and p5 were similar in heart tissue from young and old mice, the levels of BiP, calreticulin and PDI were all significantly decreased in samples from old mice. Such changes could potentially have a negative impact upon the ER folding capacity in aged heart tissue. Similarly, when the levels of ERAD components and BAG6 were tested (Fig 3.6) in extracts of young and aged heart tissue, it was found that the expression levels of Sel1L, Der-1 and Der-2 were lower in old heart. Together, the decreased expression of several chaperones and ERAD factors in heart tissue from old mice indicates that ER protein homeostasis in the heart may be impaired with age in mice.

3.2.3 Lung

The lung was analysed as described above. Analysis of components involved in protein biosynthesis showed that the level of SPC25 was significantly increased in the lung tissue of old mice, whereas the level of Rpl17 was not changed (Fig 3.7B). The levels of most ER chaperones and all ER oxidoreductases (Fig 3.8) were not significantly different in the lung tissue from old and young mice. The only exception was BiP, the expression of which was approximately 23% lower in lung from aged mice. This is consistent with the previous measurements of BiP protein in lung extracts (Hussain & Ramaiah 2007), but in contrast to the reported increased BiP mRNA expression in old lung (Zahn *et al.* 2007). None of the ERAD factors or BAG 6 changed significantly, apart from OS9 that showed a dramatic increase in expression level of over 80% in lung tissue from old mice (Fig 3.9). Notably, only one transcript variant was seen in lung – possibly the OS9.2 isoform, since is the most abundant transcript in majority of cells and tissues. This increase might suggest an imbalance of ER proteostasis – presumably because OS9 is UPR target (Okada *et al.* 2002).

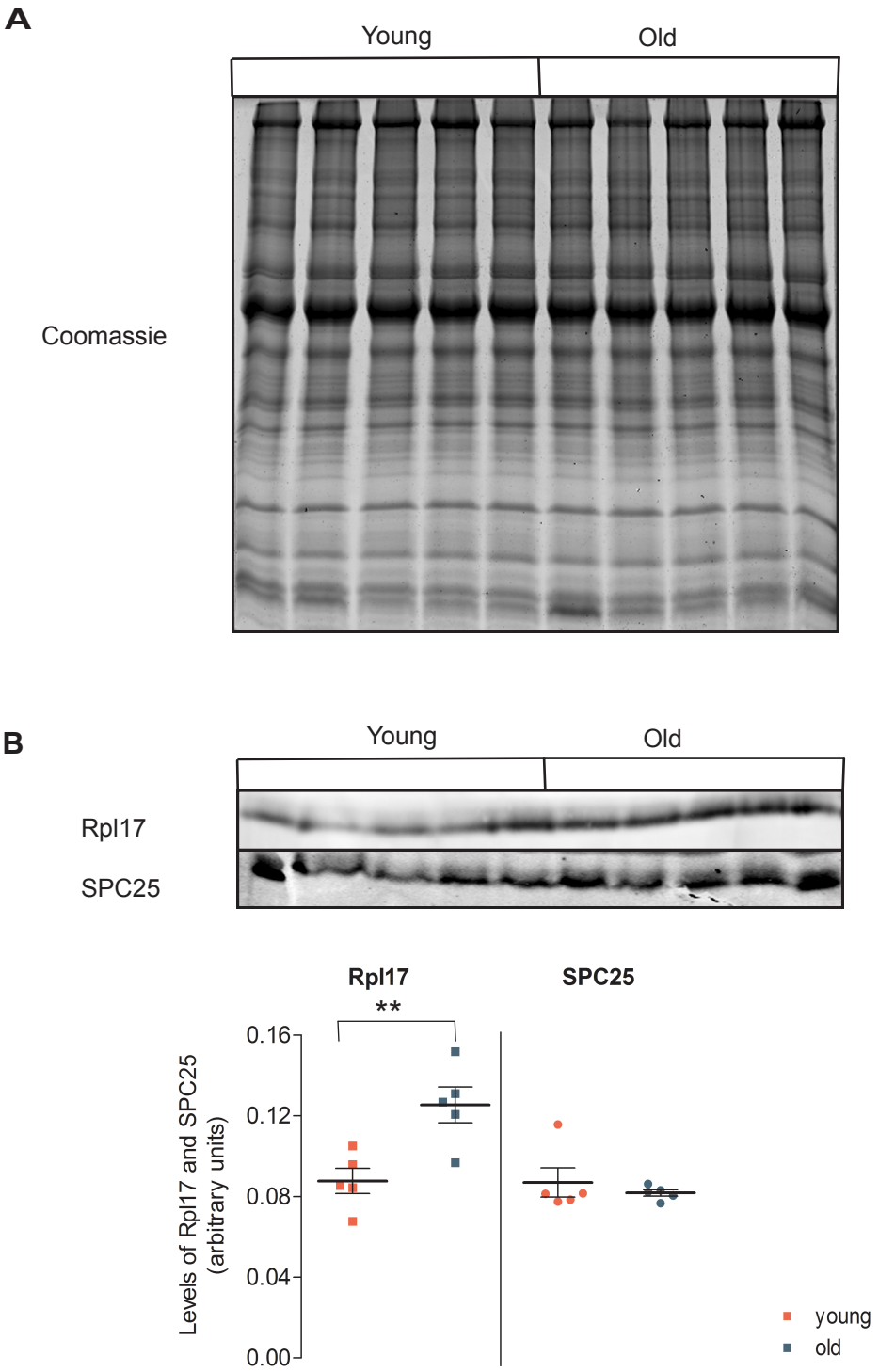

Figure 3.4: Total protein and levels of components of the protein synthesis machinery in mouse heart.
Extracts from young and old hearts were prepared in 6 M urea buffer, and equal amounts of total protein were loaded for each sample. Proteins were separated on 12% Tris-glycine gel. **(A)** Total proteins were visualised by Coomassie blue staining. **(B)** Samples were analysed by western blotting using the primary antibodies indicated followed by infrared secondary antibodies. The intensity of the fluorescent signal obtained with each antibody was quantified using the Odyssey software, and normalised relative to the intensity of the Coomassie blue signal. The scatter plots in **(B)** show the normalised signal for each protein (Rpl17 and SPC25), and each point represents data from a single animal. The lines and error bars show the mean ± s.e.m. respectively. The Student's t-test was used to determine significant differences between levels of the proteins in young and aged tissues. * denotes $P < 0.05$ and ** P denotes < 0.01.

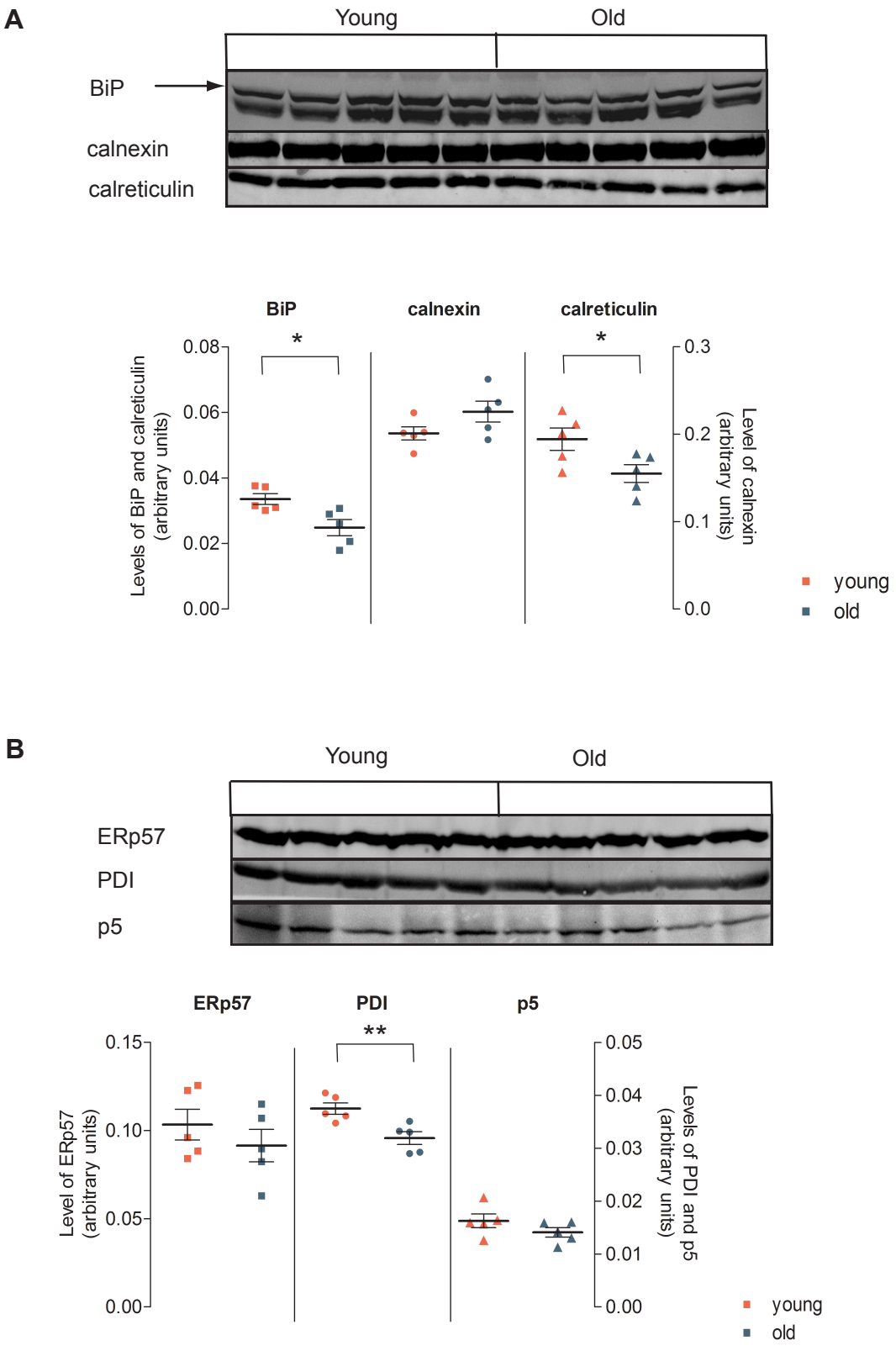

Figure 3.5: Levels of ER chaperones and ER oxidoreductases in young and old heart. Protein extracts were prepared and analysed as described in Fig. 3.4. Immunoblots showing the level of ER chaperones **(A)** and ER oxidoreductases **(B)** were quantified and the results are shown underneath the respective immunoblot. The results are presented as mean ± s.e.m. The Student's t-test was used to compare differences between levels of the proteins in young and aged tissues. Asterisks indicate significant difference (*) $P < 0.05$ and (**) $P < 0.01$.

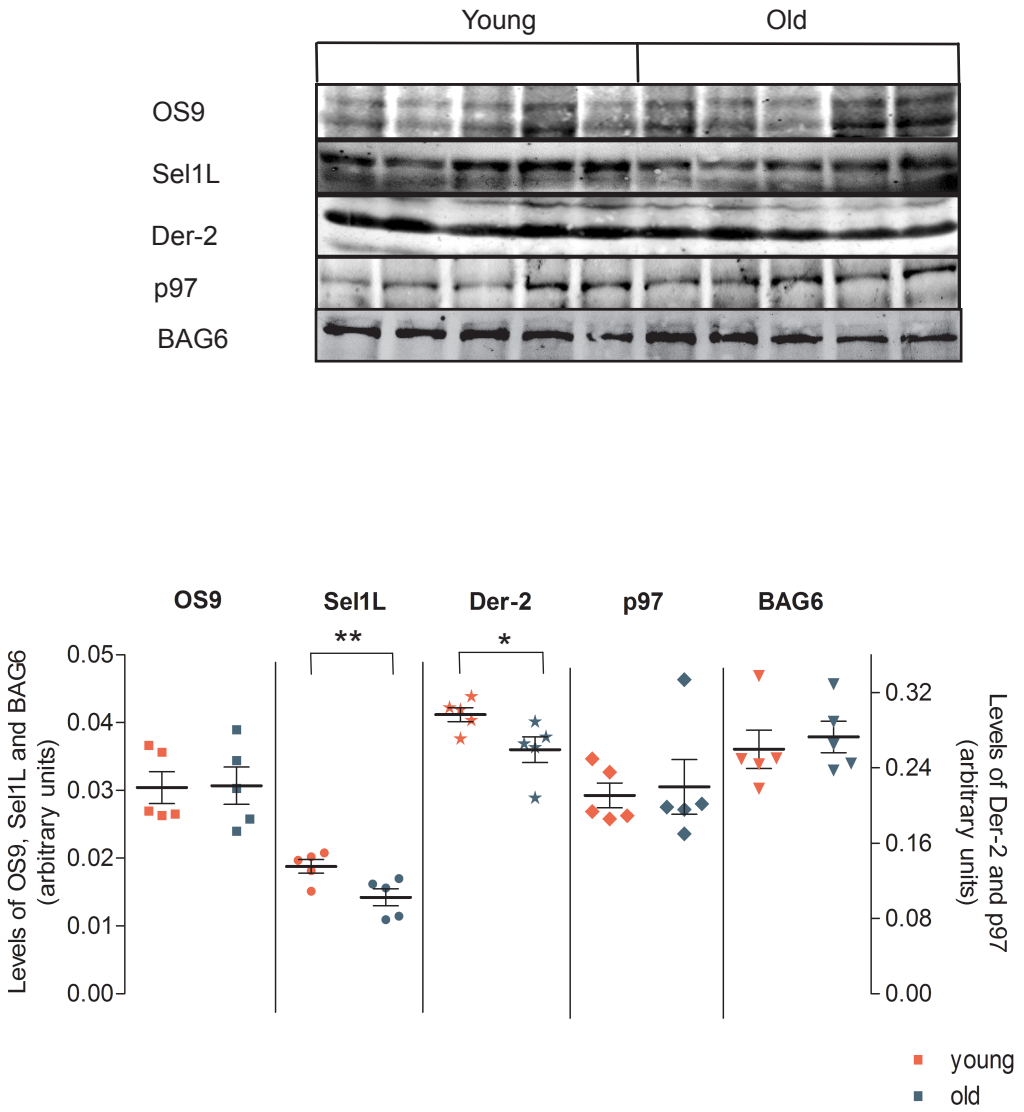

Figure 3.6: Levels of components of the ERAD pathway in mouse heart.
Protein extracts from hearts of young and old mice were prepared in 6 M urea buffer, and equal amounts of total proteins were loaded for each sample. Proteins were resolved by 12% SDS-PAGE and analysed by immunoblotting with the indicated primary antibodies followed by infrared secondary antibodies. The results of immunoblots were quantified and plotted as described in Fig 3.4. A Student's t-test was used for statistical analysis of the levels of ERAD proteins in young and aged tissues. Significant differences are indicated with a single star ($P < 0.05$) or double stars ($P < 0.01$).

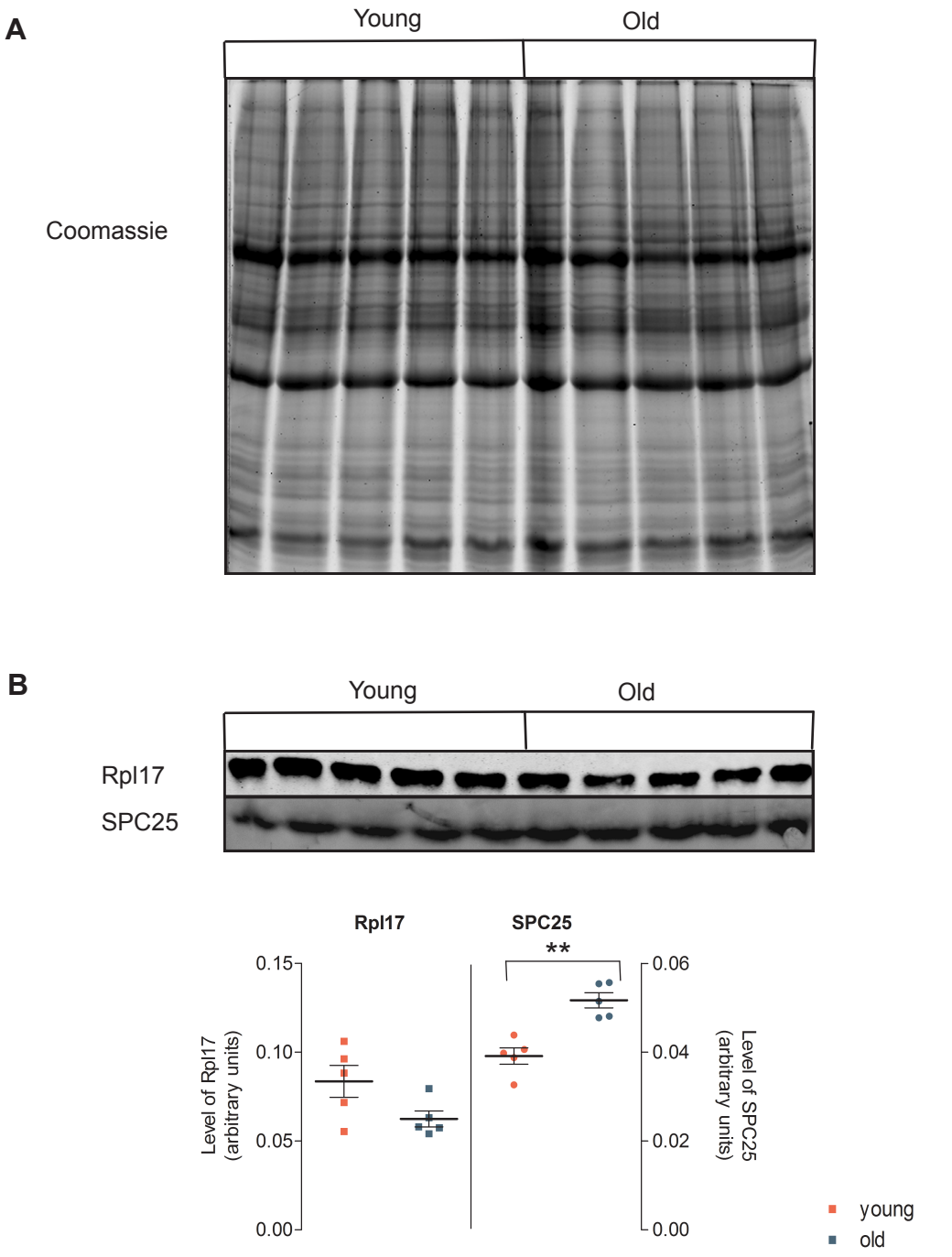

Figure 3.7: Total protein and levels of components of the protein synthesis system in mouse lung.
Extracts from young and old lungs were prepared in 6 M urea buffer, and equal amounts of total protein were loaded for each sample. Proteins were separated on 12% Tris-glycine gel. **(A)** Total proteins were visualised by Coomassie blue staining. **(B)** Samples were analysed by western blotting using the primary antibodies indicated followed by infrared secondary antibodies. The intensity of the infrared signal obtained with each antibody was quantified using the Odyssey software, and normalised relative to the intensity of the Coomassie blue signal. The scatter plots in **(B)** show the normalised signal for each protein (Rpl17 and SPC25), and each point represents data from a single animal. The lines and error bars show the mean ± s.e.m. respectively. The Student's t-test was used to determine significant differences between levels of the proteins in young and aged tissues.
* denotes $P < 0.05$ and ** P denotes < 0.01.

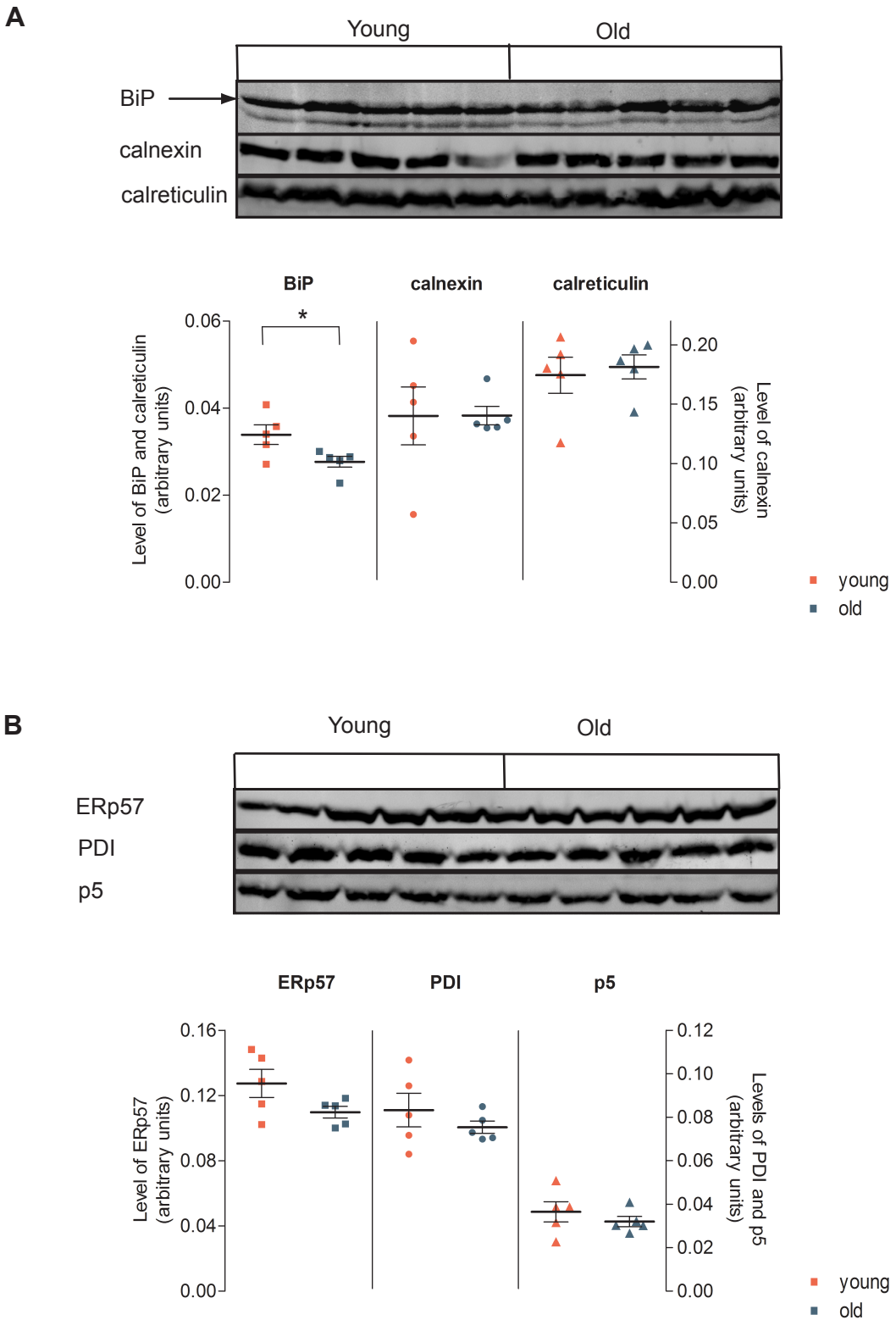

Figure 3.8: Levels of ER chaperones and ER oxidoreductases in lung.
Protein extracts were prepared and analysed as described in Fig. 3.7. Immunoblots showing the level of ER chaperones **(A)** and ER oxidoreductases **(B)** were quantified and the results are shown underneath the respective immunoblot. The results are presented as mean ± s.e.m. The Student's t-test was used to compare differences between levels of the proteins in young and aged tissues. Asterisks indicate significant difference (*) $P < 0.05$ and (**) $P < 0.01$.

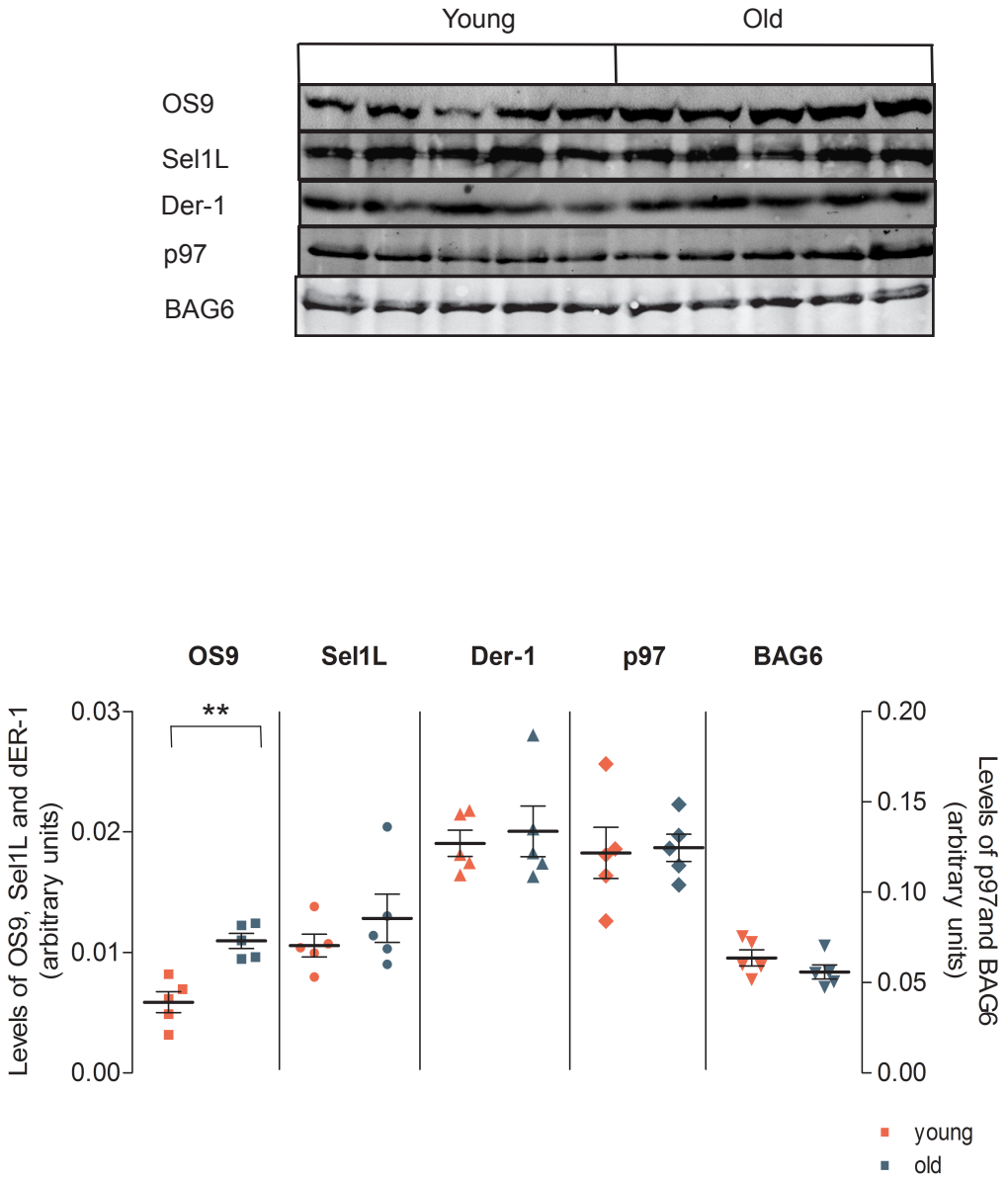

Figure 3.9: Levels of components of the ERAD pathway in mouse lung.
Protein extracts from lungs of young and old mice were prepared in 6 M urea buffer, and equal amounts of total proteins were loaded for each sample. Proteins were resolved by 12% SDS-PAGE and analysed by immunoblotting with the indicated primary antibodies followed by infrared secondary antibodies. The results of immunoblots were quantified and plotted as described in Fig 3.7. A Student's t-test was used for statistical analysis of the levels of ERAD proteins in young and aged tissues. Significant differences are indicated with a single star ($P < 0.05$) or double stars ($P < 0.01$).

3.2.4 Brain

In total brain extracts, the levels of both Rpl17 and SPC25 (Fig 3.10B) was significantly decreased in tissue from old compared to young animals. Decreased levels of these factors may indicate that protein biosynthetic pathways are affected in aged brain. Indeed, previous studies have suggested that protein biosynthesis in brain might be impaired in neurodegenerative diseases (Moreno *et al.* 2012), and also with increasing age (Hayase & Yokogoshi 1994). In contrast, gene-profiling studies have shown an age–related increase in the ribosomal protein gene set (Lee *et al.* 2000; Zahn *et al.* 2007). Of the ER chaperones examined, only the level of BiP was significantly affected by age, being up regulated by around 20% in the brain from old mice (Fig 3.11A). This is in contrast to the three previous tissues, liver, heat and lung, in which BiP levels were decreased significantly. When the ER oxidoreductases were tested (Fig 3.11B), expression of p5 was found to be almost 30% lower in the brain of old animals, whereas ERp57 and PDI had the similar expression levels in old and young mice. Strikingly, expression of each of the ERAD factors examined (OS9, Sel1L, Der-1 and Der-2), with the possible exception of p97, was found to be expressed at a lower level in brain tissue from aged mice compared to young mice (Fig 3.12). Such a widespread decrease in the levels of ERAD factors might well be expected to reduce the overall ERAD capacity, potentially leading to accumulation of misfolded proteins in the ER. Similar to the lung results, again only one major isoform variant was seen for OS9. However, in this case a very faint upper band can be seen, confirming that the lower band is the OS9 isoform 2 (OS9.2) that seems to be the predominant transcript in brain. In addition, the level of BAG6 was 27% lower in brain, supporting the idea that degradation of ERAD substrates might be reduced in aged brain.

3.2.5 Kidney

In the kidney, none of the proteins examined significantly changed in expression level in tissue from aged compared to young mice (Fig 3.13-3.15), with the notable exception of p97 which was significantly lower in kidneys from old mice (Fig 3.15). These observations are in line with a previous transcriptome analysis of young and old mice, which found that the kidney was the organ least affected by age (Zahn *et al.* 2007).

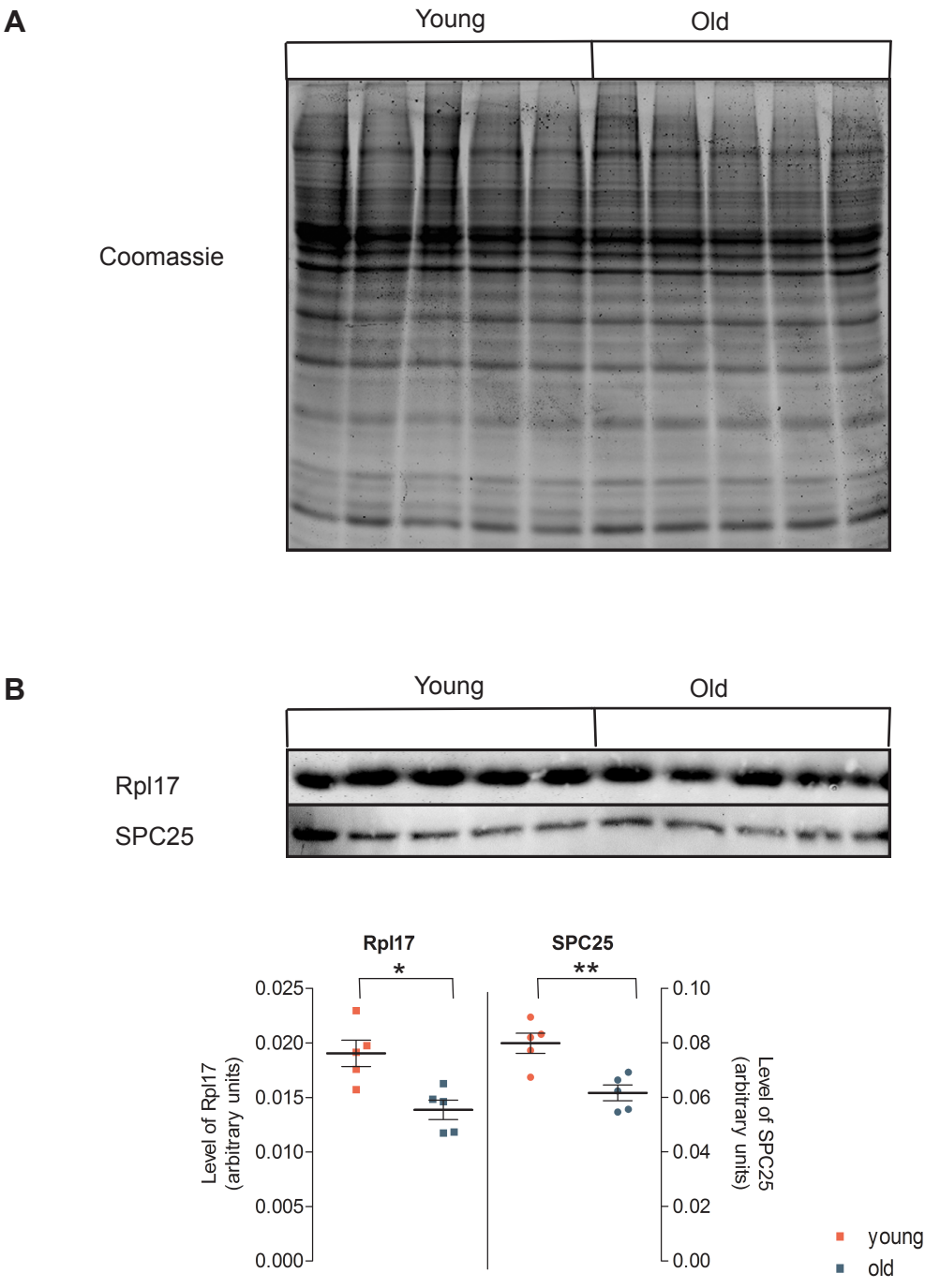

Figure 3.10: Total protein and levels of components of the protein synthesis machinery in mouse brain.
Extracts from young and old brains were prepared in 6 M urea buffer, and equal amounts of total protein were loaded for each sample. Proteins were separated on 12% Tris-glycine gel. **(A)** Total proteins were visualised by Coomassie blue staining. **(B)** Samples were analysed by western blotting using the primary antibodies indicated followed by infrared secondary antibodies. The intensity of the infrared signal obtained with each antibody was quantified using the Odyssey software, and normalised relative to the intensity of the Coomassie blue signal. The scatter plots in **(B)** show the normalised signal for each protein (Rpl17 and SPC25), and each point represents data from a single animal. The lines and error bars show the mean ± s.e.m. respectively. The Student's t-test was used to determine significant differences between levels of the proteins in young and aged tissues. * denotes $P < 0.05$ and ** P denotes < 0.01.

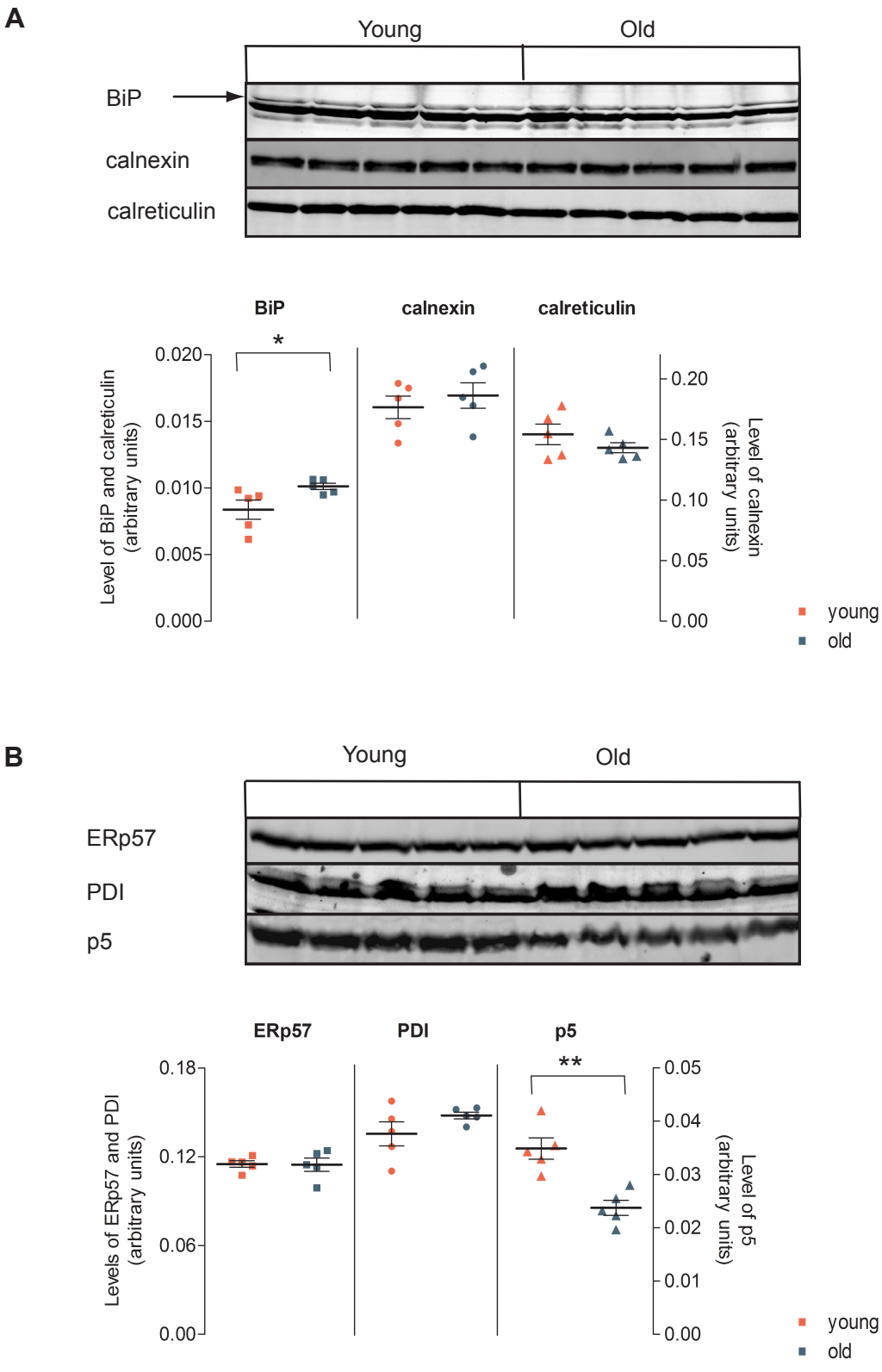

Figure 3.11: Levels of ER chaperones and ER oxidoreductases in young and old brains. Protein extracts were prepared and analysed as described in Fig. 3.10. Immunoblots showing the levels of ER chaperones **(A)** and ER oxidoreductases **(B)** were quantified and the results are shown underneath the respective immunoblot. The results are presented as mean ± s.e.m. The Student's t-test was used to compare differences between levels of the proteins in young and aged tissues. Asterisks indicate significant difference (*) $P < 0.05$ and (**) $P < 0.01$.

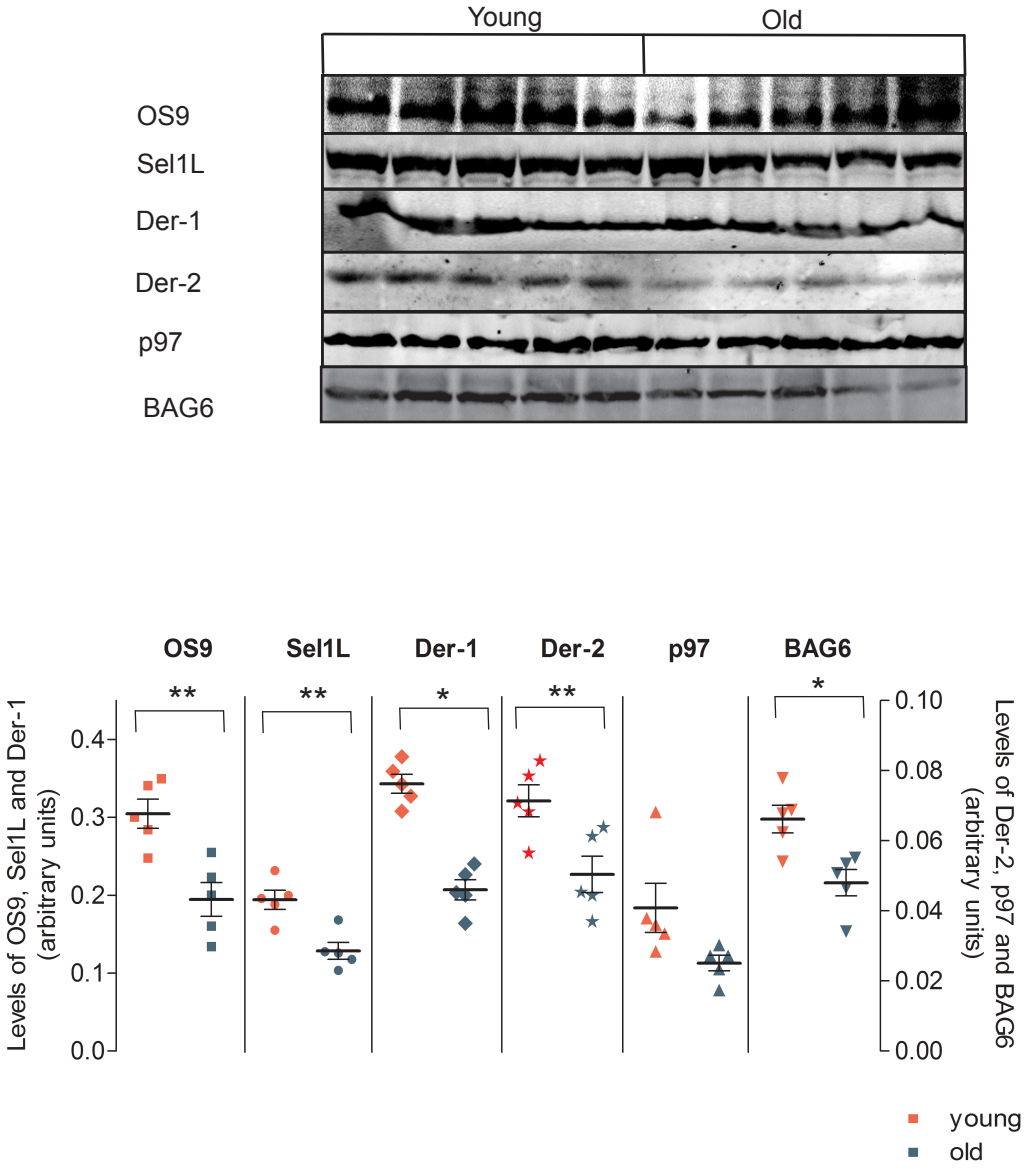

Figure 3.12: Levels of components of the ERAD pathway in mouse brain.
Protein extracts from brains of young and old mice were prepared in 6 M urea buffer, and equal amounts of total proteins were loaded for each sample. Proteins were resolved by 12% SDS-PAGE and analysed by immunoblotting with the indicated primary antibodies followed by infrared secondary antibodies. The results of immunoblots were quantified and plotted as described in Fig 3.10. A Student's t-test was used for statistical analysis of the levels of ERAD proteins in young and aged tissues. Significant differences are indicated with a single star ($P < 0.05$) or double stars ($P < 0.01$).

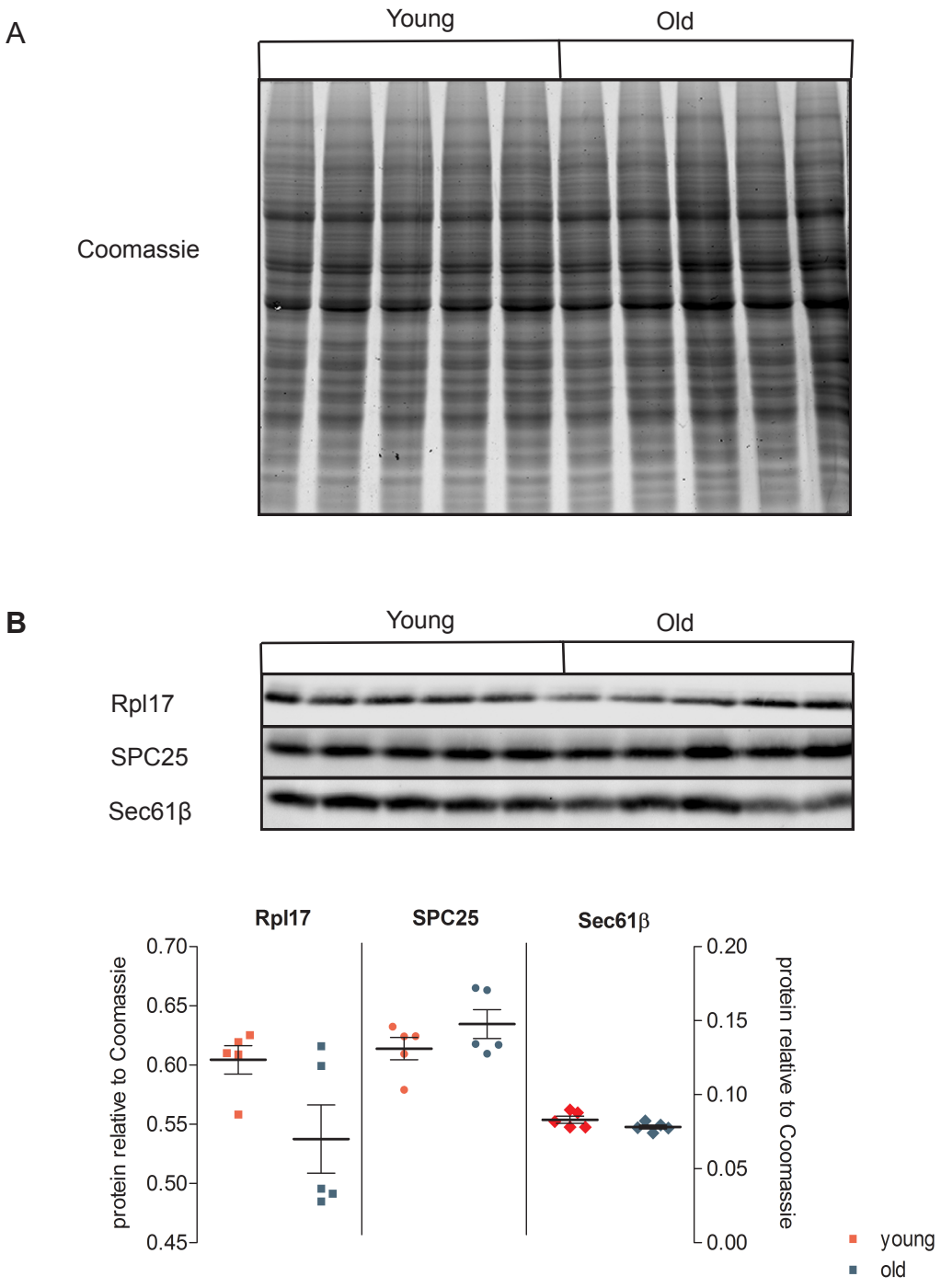

Figure 3.13: Total protein and levels of components of the protein synthesis machinery in mouse kidney.
Extracts from young and old kidneys were prepared in 6 M urea buffer, and equal amounts of total protein were loaded for each sample. Proteins were separated on 12% Tris-glycine gel. **(A)** Total proteins were visualised by Coomassie blue staining. **(B)** Samples were analysed by western blotting using the primary antibodies indicated followed by infrared secondary antibodies. The intensity of the infrared signal obtained with each antibody was quantified using the Odyssey software, and normalised relative to the intensity of the Coomassie blue signal. The scatter plots in **(B)** show the normalised signal for each protein (Rpl17, SPC25 and Sec61β), and each point represents data from a single animal. The lines and error bars show the mean ± s.e.m. respectively.

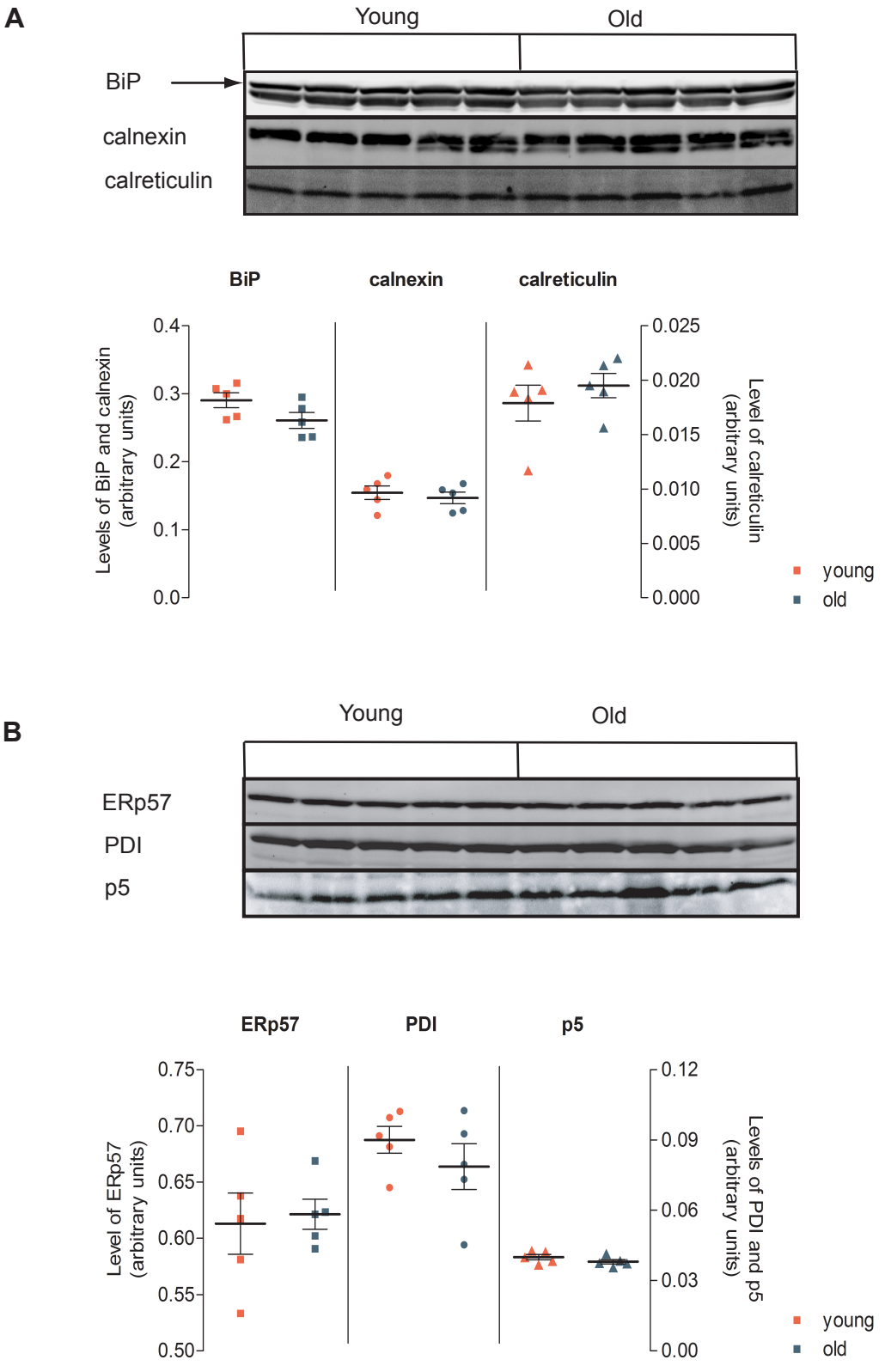

Figure 3.14: Levels of ER chaperones and ER oxidoreductases in kidney.
Protein extracts were prepared and analysed as described in Fig. 3.13. Immunoblots showing the levels of ER chaperones **(A)** and ER oxidoreductases **(B)** were quantified and the results are shown underneath the respective immunoblot. The results are presented as mean ± s.e.m.

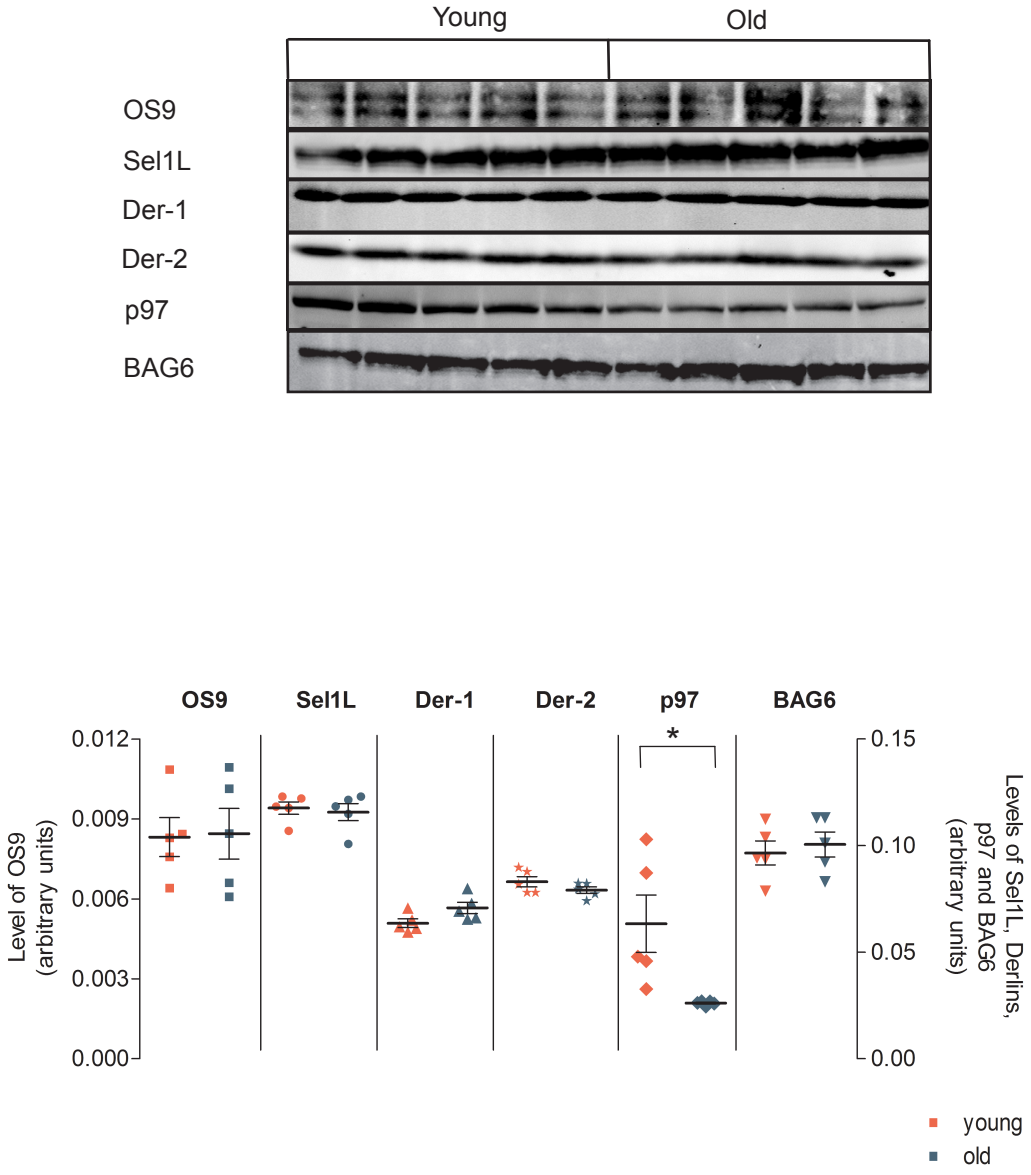

Figure 3.15: Levels of components of the ERAD pathway in mouse kidney.
Protein extracts from kidneys of young and old mice were prepared in 6 M urea buffer, and equal amounts of total proteins were loaded for each sample. Proteins were resolved by 12% SDS-PAGE and analysed by immunoblotting with the indicated primary antibodies followed by infrared secondary antibodies. The results of immunoblots were quantified and plotted as described in Fig 3.13. The Student's t-test was used for statistical analysis of the levels of ERAD proteins in young and aged tissues. Significant differences are indicated with a single star ($P < 0.05$) or double stars ($P < 0.01$).

3.2.6 Spleen

The level of ribosomal (Rpl17), translocon (Sec61β) and peptidase complexes (SPC25) did not change significantly in spleen samples from old mice (Fig 3.16). Of the ER chaperones tested, the expression level of BiP was found to be almost 75% higher in spleen from aged mice (Fig 3.17A). In addition, levels of the oxidoreductases ERp57 and p5 showed a significant increase in the spleen from old mice (Fig 3.17B), with p5 being almost double that in young tissue, and ERp57 increased by nearly 40%. Furthermore, most of the ERAD components (OS9, Sel1L, Der-1, Der-2) were increased by at least 30% in aged spleens (Fig 3.18). Again, from the two detected OS9 isoforms, the smaller one (OS9.2) is the predominant form, similar to the observations from brain and possiblly lung. Similarly, the expression level of BAG6 was also increased by almost 35% in the spleen of old mice. It is possible that this coordinated upregulation of multiple ER factors reflects activation of the UPR in the spleens of old mice. In spleen, UPR is activated during the maturation of B-cells to antibody producing cells (plasma cells) (Iwakoshi *et al.* 2003; Shaffer *et al.* 2004; Ma *et al.* 2009) and the stimulation of specific T-cells (Brunsing *et al.* 2008) as part of normal immune response.

3.2.7 Skeletal muscle

No change in the level of expression of Rpl17 was detected in the skeletal muscle of aged mice (Fig 3.19B). In addition, SPC 25 could not be detected. Nevertheless, in general, the expression levels of the ER proteins in skeletal muscle were quite low and a possible explanation is that skeletal muscle might contain relatively little rER to SR. Of interest was an approximately 2-fold increase in BiP expression in muscle from old mice (Fig 3.20A). This is consistent with an age-related increase in BiP mRNA reported in large scale transcriptome analysis (Edwards *et al.* 2007; Zahn *et al.* 2007). From the tested oxidoreductases (Fig 3.20B), only the ERp57 level was decreased in the muscle of old mice. Similarly, OS9 was decreased by almost 30% (Fig 3.21). Although three bands were observed in the OS9 Western blotting (Fig 3.21A) the top one (marked *) is a non specific band. This band was not seen in other OS9 immunoblots and also is at a higher MW that of any of the OS9 isoforms.

These analyses identified a number of potentially interesting changes in expression of many ER proteins in various tissues. These findings are summarised in the heat map shown in Fig 3.34. Two tissues in particular, the brain and the spleen, showed widespread changes in the expression level of multiple proteins with age. In brain tissue from aged mice significant decreases were observed in the level of a range of components, most strikingly those associated with ERAD (Fig 3.12). Such extensive changes are highly likely to impact upon the capacity of the ERAD pathway, and potentially other pathways of the proteostasis network in brain. In contrast, increased expression of many ER factors was observed in the spleen of aged mice (Fig 3.18). This could potentially be related to role of spleen in generation of plasma cells and activated T-cells. In contrast, the kidney and liver showed relatively few changes in expression of these proteins with age. This might reflect the relative moderate histological

changes in the liver and kidney with age (Yabuki *et al.* 2003; Schmucker & Sanchez 2011). In other tissues, such as heart and lung, some proteins increased, whilst others decreased. Also, there no clear pattern for the effect of age on expression of individual chaperones across different tissues. For instance, BiP was found to increase in some tissues (brain, muscle and spleen), but decrease in others (heart, lung). Similar results, i.e. both increases and decreases in expression in different organs, were obtained for other ER proteins, such as ERAD components (OS9, Sel1L, Derlins). The only ER-resident proteins whose expression levels seem to be relatively unchanged with increased age are calreticulin and calnexin. In conclusion, the results support the hypothesis that ER proteostasis might be negatively affected with age.

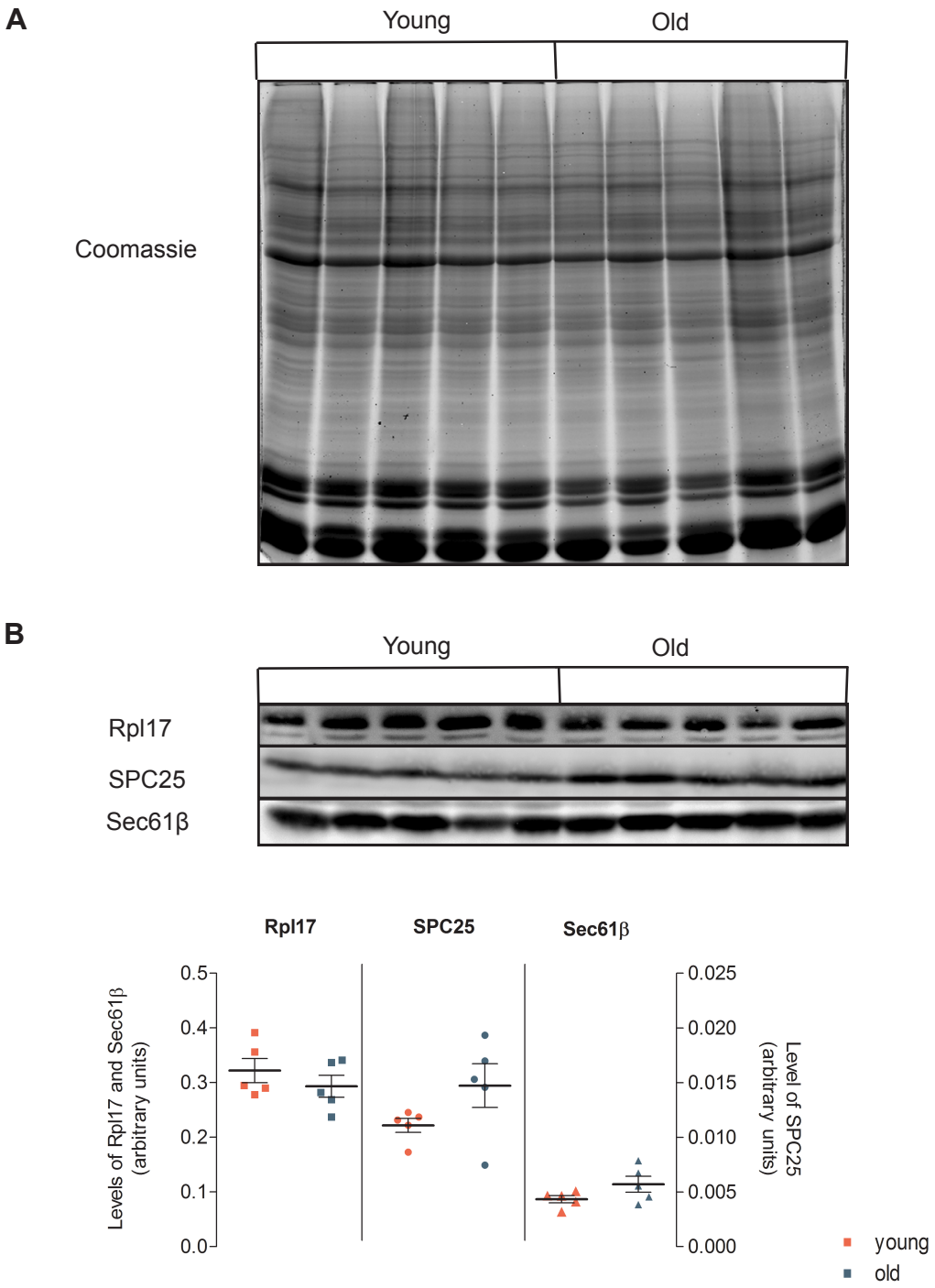

Figure 3.16: Total protein and levels of components of the protein synthesis machinery in mouse spleen.
Extracts from young and old spleens were prepared in 6 M urea buffer, and equal amounts of total protein were loaded for each sample. Proteins were separated on 12% Tris-glycine gel. **(A)** Total proteins were visualised by Coomassie blue staining. **(B)** Samples were analysed by western blotting using the primary antibodies indicated followed by infrared secondary antibodies. The intensity of the fluorescent signal obtained with each antibody was quantified using the Odyssey software, and normalised relative to the intensity of the Coomassie blue signal. The scatter plots in **(B)** show the normalised signal for each protein (Rpl17, SPC25 and Sec61β), and each point represents data from a single animal. The lines and error bars show the mean ± s.e.m. respectively.

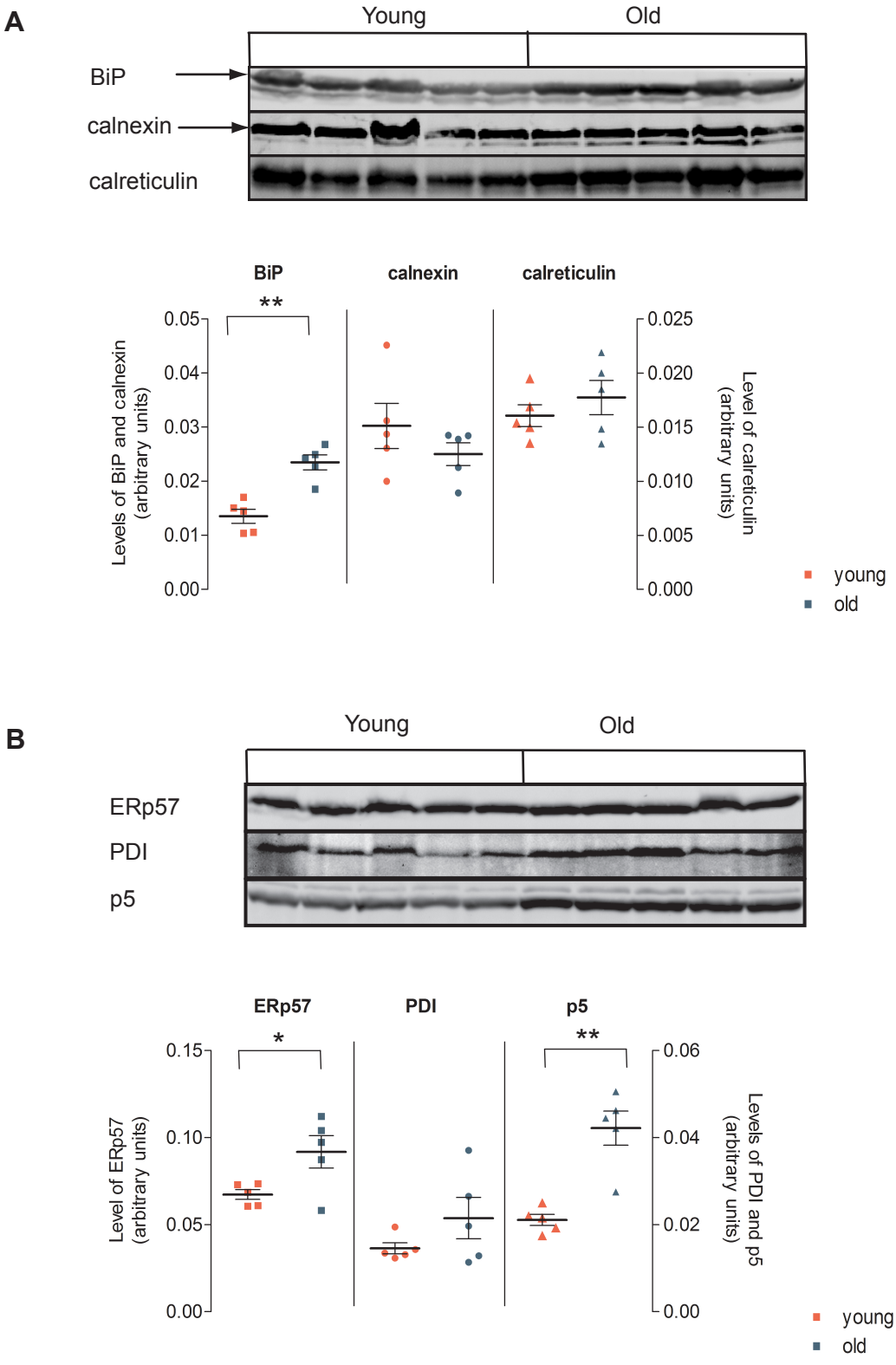

Figure 3.17: Levels of ER chaperones and ER oxidoreductases in young and old spleen. Protein extracts were prepared and analysed as described in Fig. 3.16. Immunoblots showing the levels of ER chaperones **(A)** and ER oxidoreductases **(B)** were quantified and the results are shown underneath the respective immunoblot. The results are presented as mean ± s.e.m. The Student's t-test was used to determine significant differences between levels of the proteins in young and aged tissues. Asterisks indicate significant difference (*) $P < 0.05$ and (**) $P < 0.01$.

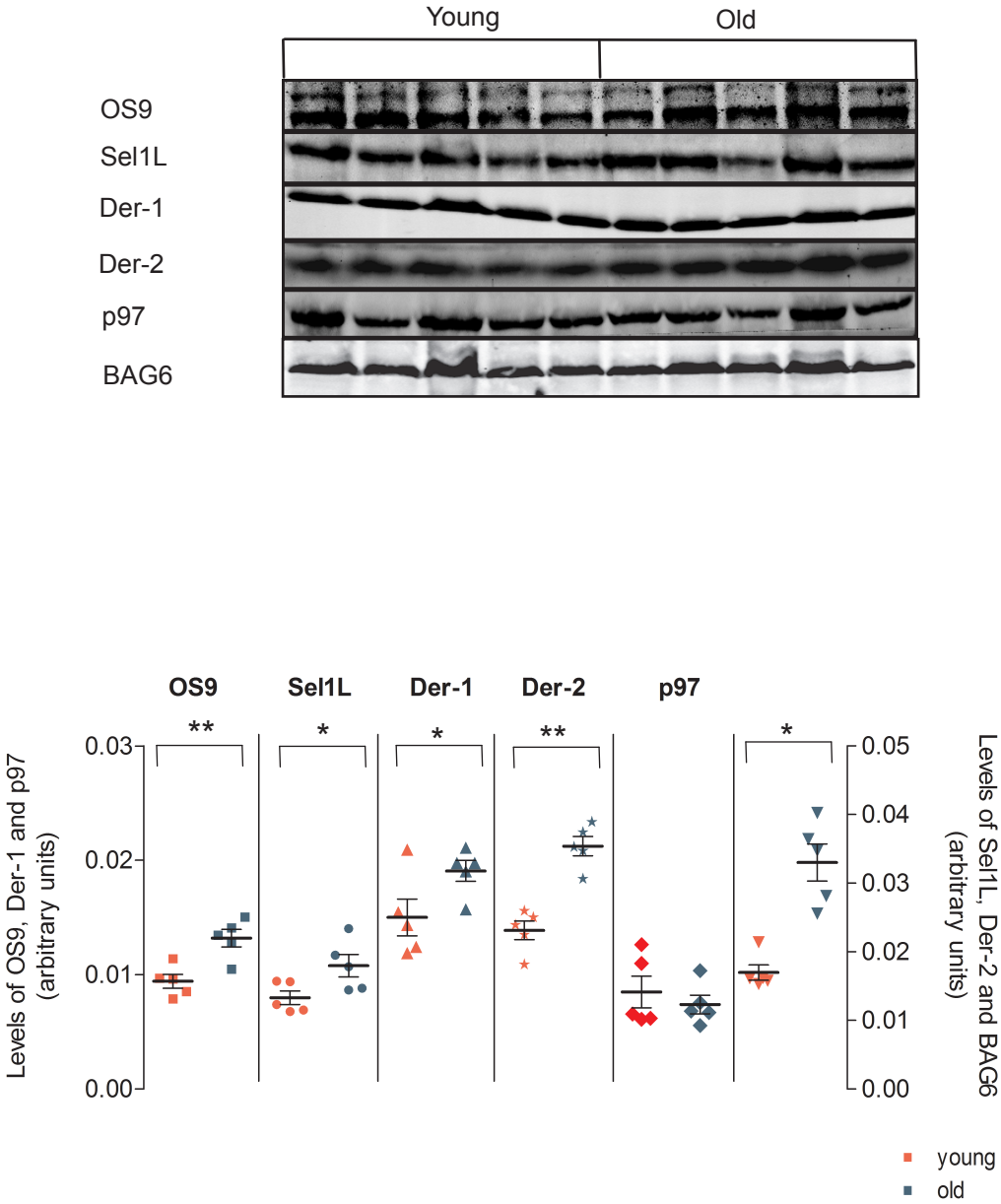

Figure 3.18: Levels of components of the ERAD pathway in mouse spleen.
Protein extracts from spleens of young and old mice were prepared in 6 M urea buffer, and equal amounts of total proteins were loaded for each sample. Proteins were resolved by 12% SDS-PAGE and analysed by immunoblotting with the indicated primary antibodies followed by infrared secondary antibodies. The results of immunoblots were quantified and plotted as described in Fig 3.16. The Student's t-test was used for statistical analysis of the levels of ERAD proteins in young and aged tissues. Significant differences are indicated with a single star for ($P < 0.05$) or double stars for ($P < 0.01$).

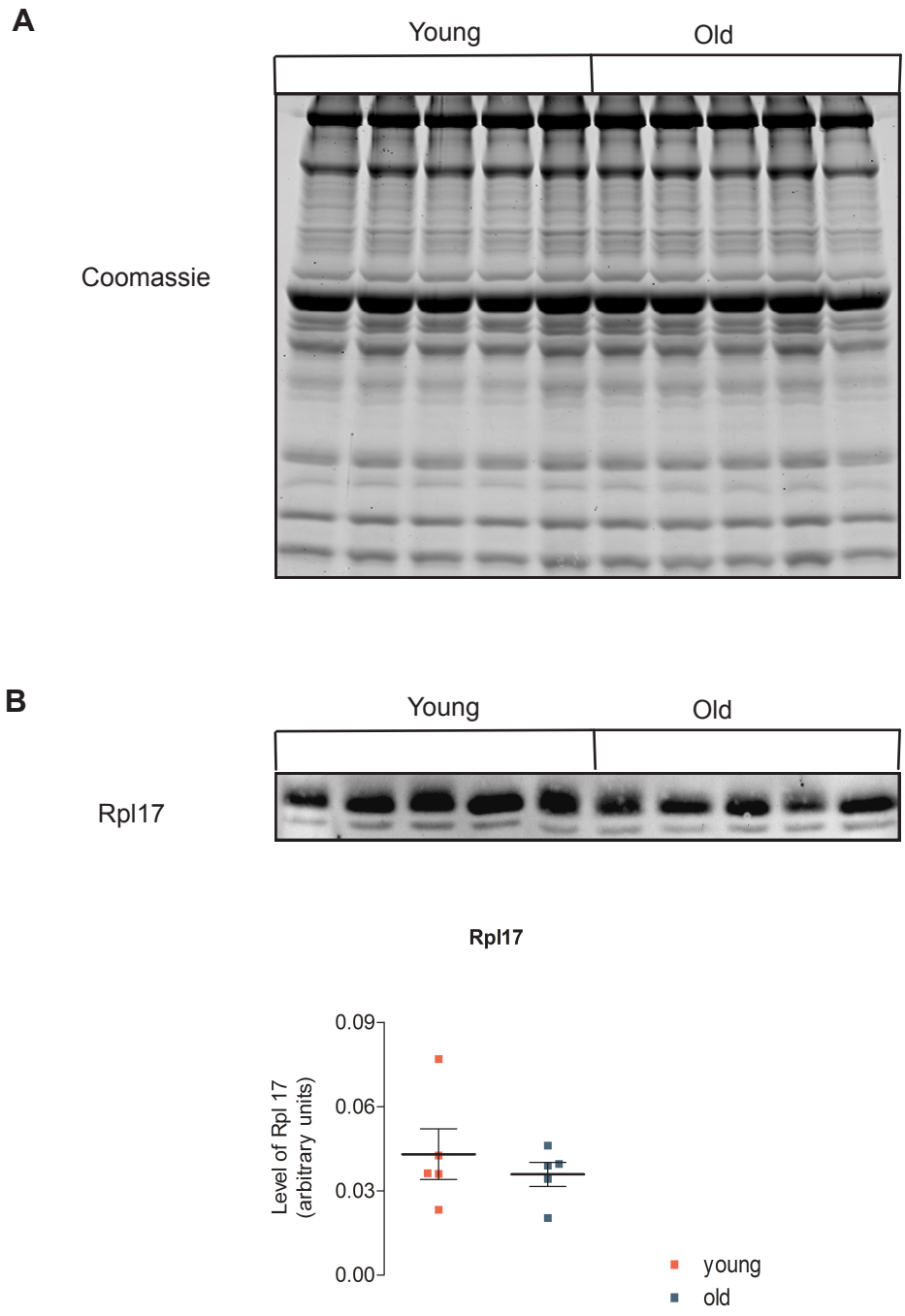

Figure 3.19: Total protein and levels of components of the protein synthesis machinery in mouse muscle.
Extracts from young and old muscles were prepared in 6 M urea buffer, and equal amounts of total protein were loaded for each sample. Proteins were separated on 12% Tris-glycine gel. **(A)** Total proteins were visualised by Coomassie blue staining. **(B)** Samples were analysed by western blotting using the indicated primary antibodies followed by infrared secondary antibodies. The intensity of the fluorescent signal obtained with anti Rpl17antibody was quantified using the Odyssey software, and normalised relative to the intensity of the Coomassie blue signal. The scatter plots in **(B)** show the normalised signal for Rpl17 protein, and each point represents data from a single animal. The lines and error bars show the mean ± s.e.m. respectively.

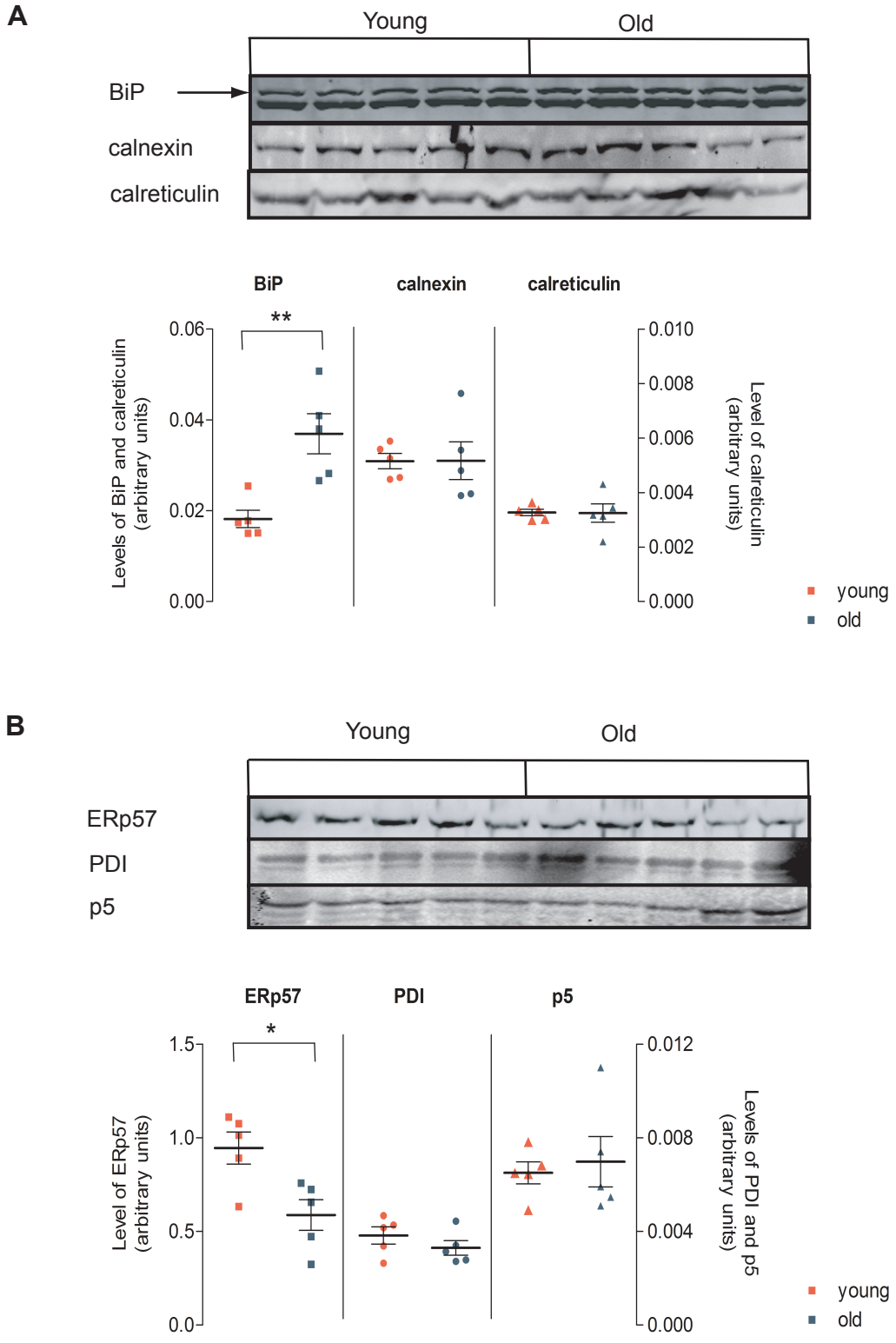

Figure 3.20: Levels of ER chaperones and ER oxidoreductases in muscle.
Protein extracts were prepared and analysed as described in Fig. 3.19. Immunoblots showing the levels of ER chaperones **(A)** and ER oxidoreductases **(B)** were quantified and the results are shown underneath the respective immunoblot. The results are presented as mean ± s.e.m. The Student's t-test was used to determine significant differences between levels of the proteins in young and aged tissues. Asterisks indicate significant difference (*) $P < 0.05$ and (**) $P < 0.01$.

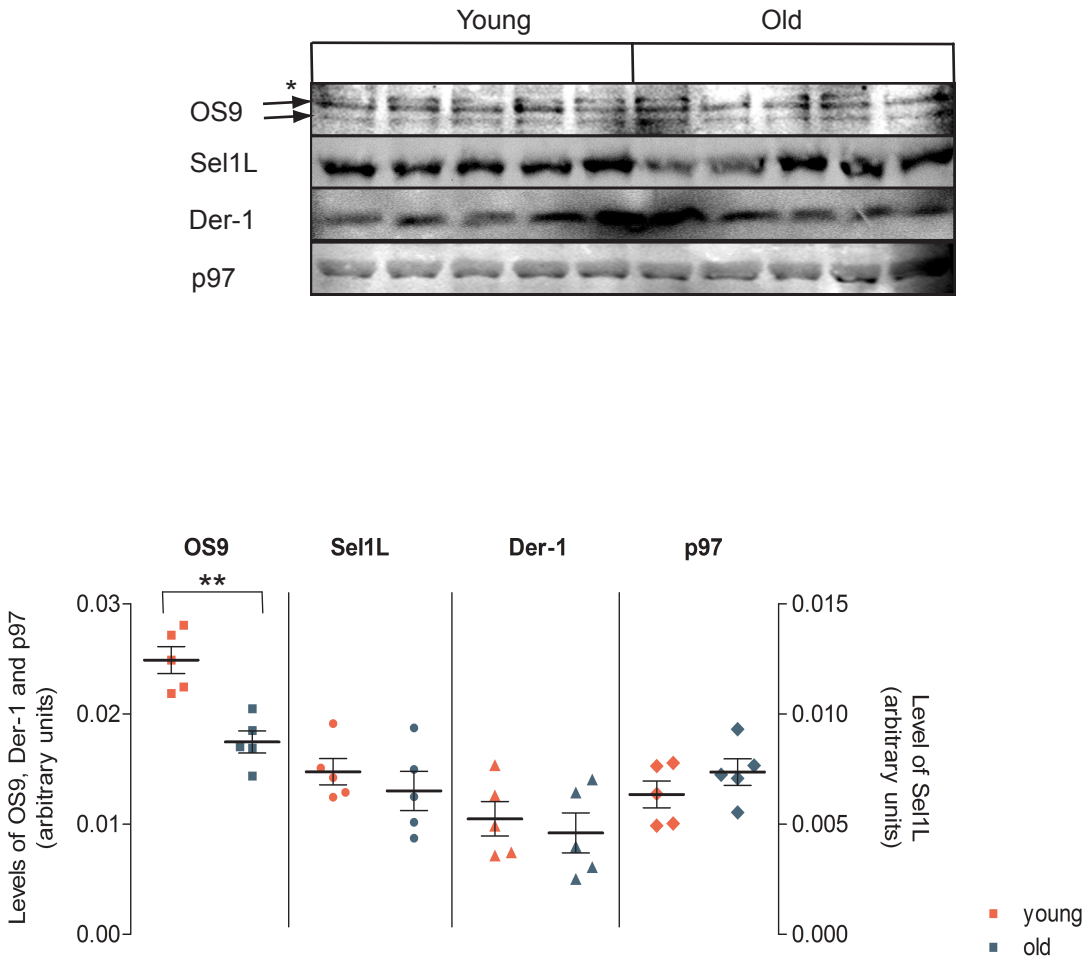

Figure 3.21: Levels of components of the ERAD pathway in mouse muscle.
Protein extracts from muscles of young and old mice were prepared in 6 M urea buffer, and equal amounts of total proteins were loaded for each sample. Proteins were resolved by 12% SDS-PAGE and analysed by immunoblotting with the indicated primary antibodies followed by infrared secondary antibodies. The results of immunoblots were quantified and plotted as described in Fig 3.19. The Student's t-test was used for statistical analysis of the levels of ERAD proteins in young and aged tissues. Significant differences are indicated with a single star for ($P < 0.05$) or double stars for ($P < 0.01$).

3.3 Overall state of the proteome in aged tissues

The major route for removal of abnormal proteins from inside cells is the UPS. Therefore, this system is critical for maintaining cellular protein homeostasis. Misfolded or otherwise defective proteins, including those originating from the ER, are marked for proteasomal degradation by the addition of multiple Ub molecules (Finley 2009). Thus, increased protein misfolding or inhibition of proteasome activity promotes accumulation of polyUb proteins (Chen *et al.* 2011). Such high MW polyUb conjugates can be visualised by Western blotting with anti-Ub antibodies to provide a measure of the ability of the UPS to degrade its substrate proteins (Paz Gavilan *et al.* 2006). Thus, in order to examine whether the efficiency of the UPS and/or production of UPS substrates were affected in aged tissues, the protein extracts were blotted with anti-Ub (Fig. 3.22 - 3.25)

3.3.1 Level of polyUb proteins in the tissues of young and old mice

Western blotting extracts of liver tissue from young and old mice with anti-Ub showed the presence of considerable amounts of immunoreactive material, presumably representing Ub conjugates. Most of these were concentrated in a broad smear near the top of the separating gel (Fig 3.22 – 3.25). PolyUb UPS substrates are typically seen as a high MW smear on SDS-PAGE and western blotting (Paz Gavilan *et al.* 2006), due to the diverse range of UPS substrates that are conjugated to a variable number of Ub units (Huzil *et al.* 2007). Interestingly, the intensity of the high MW polyUb species appeared to be greater in several of the liver samples from old mice (Fig 3.22A). Quantification of this area of the blot in each lane revealed that these polyUb conjugates were significantly more abundant in liver from aged mice compared to the liver of old mice (Figs 3.22A and 3.26). A significant increase in the level of high MW species was observed in most of the other tissues including heart, lung, brain and muscle (Fig 3.26). The intense bands at around 50 kDa and 25 kDa seen in some of the old tissues (most noticeably muscle, lung and spleen, Figs 3.23, 3.24 and 3.25), is due to the presence of cross-reacting IgG heavy and light chains in the tissue extracts. These were distinct from the area representing high MW polyUb proteins and were excluded from the quantification. In contrast, no significant changes were seen in kidney, which also showed little changes in expression of ER proteins, or in the spleen (Figs 3.24 and 3.26). Although the quantification of such large areas of the blot may be less accurate than for discreet bands, the apparently widespread increase in high MW Ub containing material in multiple tissues from aged mice, suggests that the old tissues contain an accumulation of polyUb proteins. This is consistent with previous studies which have also observed higher levels of polyUb conjugates in aged tissues (Ohtsuka *et al.* 1995; Mura *et al.* 1996), and suggests that the UPS as a whole may be perturbed. This could be due to less efficient proteasomal degradation, as has been previously documented (Low 2011), increased production of UPS substrates as would be expected if folding efficiency decreased, or reduced degradation using alternative pathways (Rubinsztein *et al.* 2011), or perhaps most likely, a combination of these. In any case, these results provide further evidence that overall proteostasis declines in multiple mouse tissues during ageing.

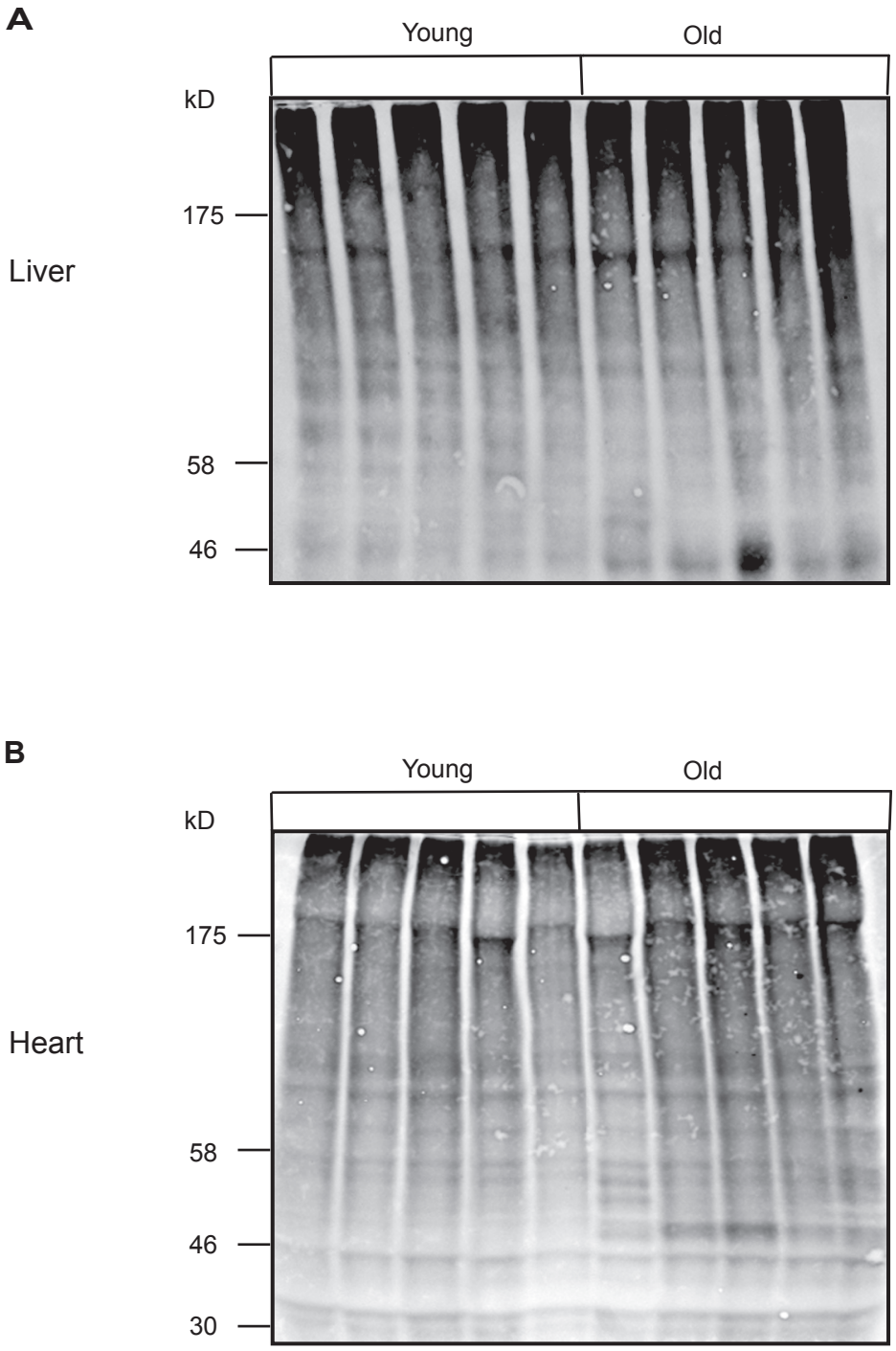

Figure 3.22: Level of polyubiquitinated (polyUb) proteins in mouse hepatic and cardiac mouse tissues.
Extracts from young and old tissues were prepared in 6 M urea buffer, and equal amounts of total protein were loaded for each sample. Proteins were separated on an 8% Tris-glycine gel and analysed by western blotting using the anti-ubiquitin (anti-Ub) primary antibodies followed by infrared secondary antibodies. The results for liver and heart are shown in **A**, and **B**.

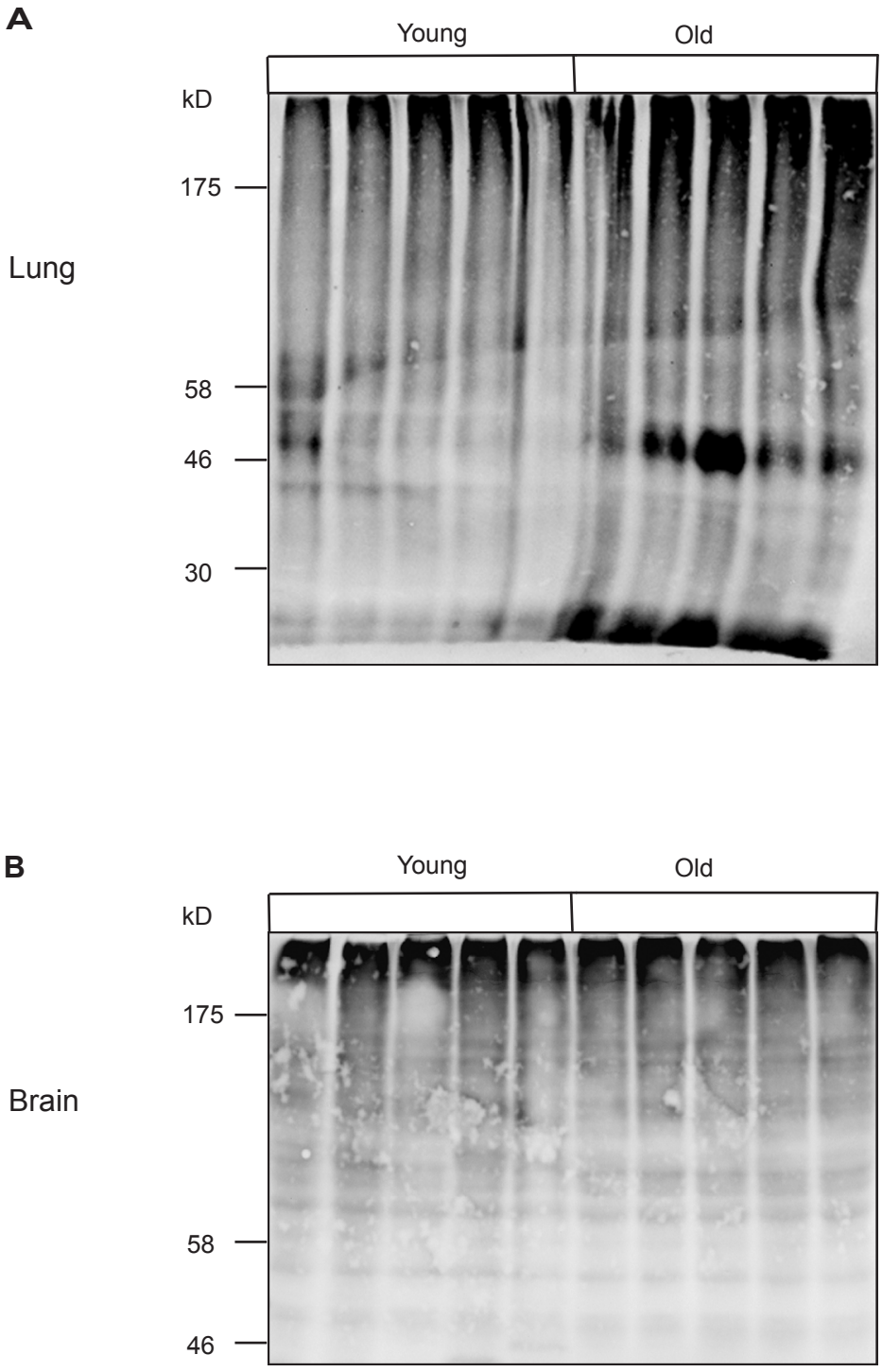

Figure 3.23: Level of polyUb proteins in mouse lung and brain.
Protein extracts from young and old tissues were prepared as described in Fig 3.22. Proteins were separated on an 8% Tris-glycine gel and analysed by western blotting using the anti-Ub primary antibodies followed by infrared secondary antibodies. The results for lung and brain are shown above in **A**, and **B**.

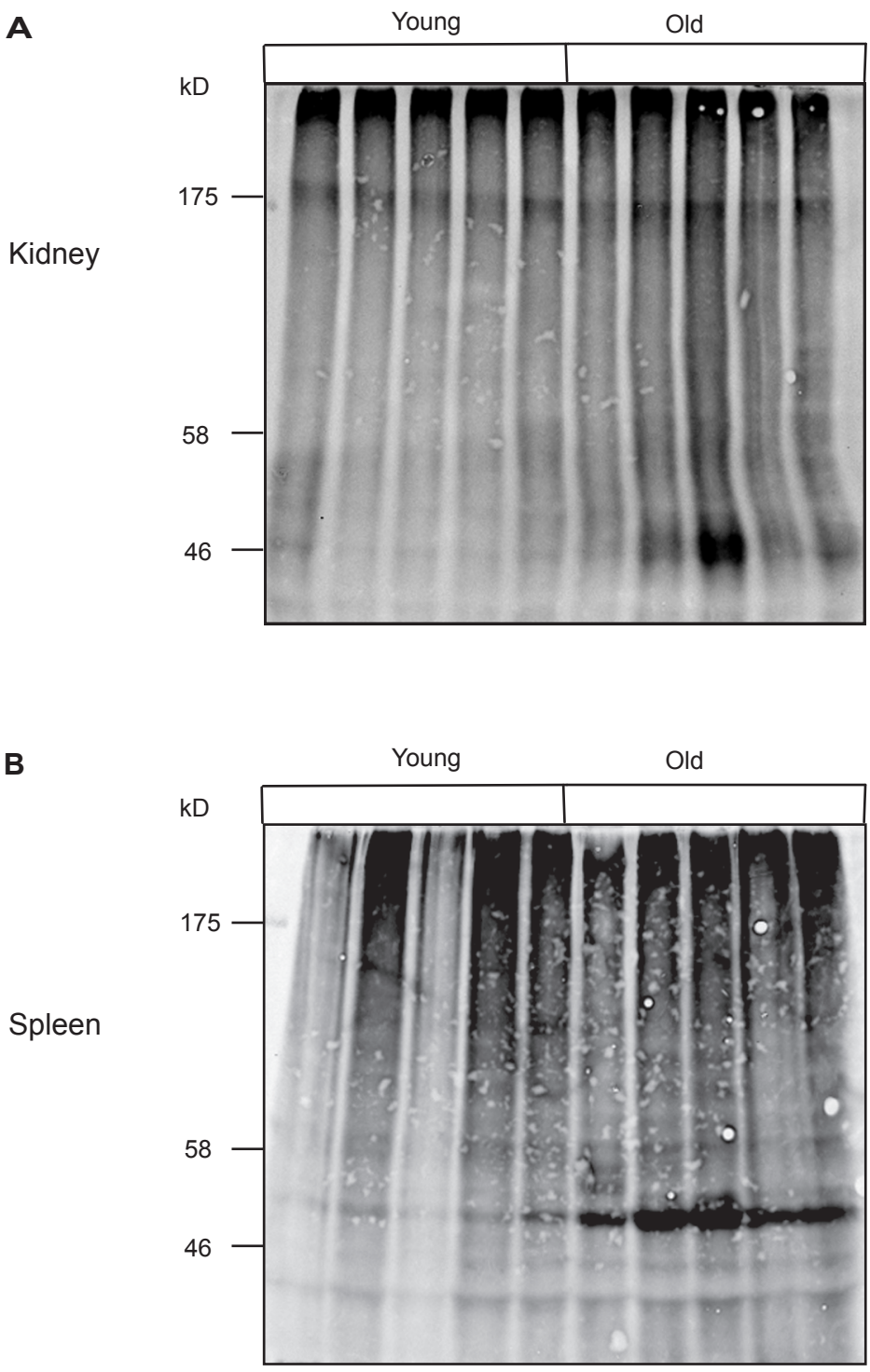

Figure 3.24: Level of polyUb proteins in mouse kidney and spleen.
Extracts from young and old tissues were prepared in 6 M urea buffer, and equal amounts of total protein were loaded for each sample. Proteins were separated on an 8% Tris-glycine gel. Samples were analysed by western blotting using the anti-Ub primary antibodies followed by infrared secondary antibodies. The results for kidney and spleen are shown above in **A**, and **B**.

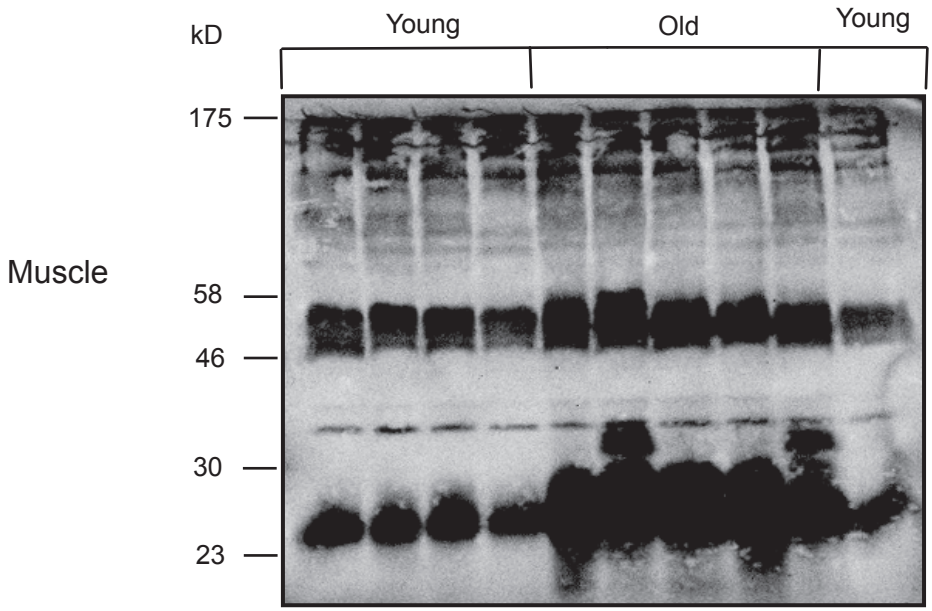

Figure 3.25: Level of polyUb proteins in mouse skeletal muscle.
Protein extracts from young and old muscles were prepared and analysed by western blotting as described in Fig 3.24.

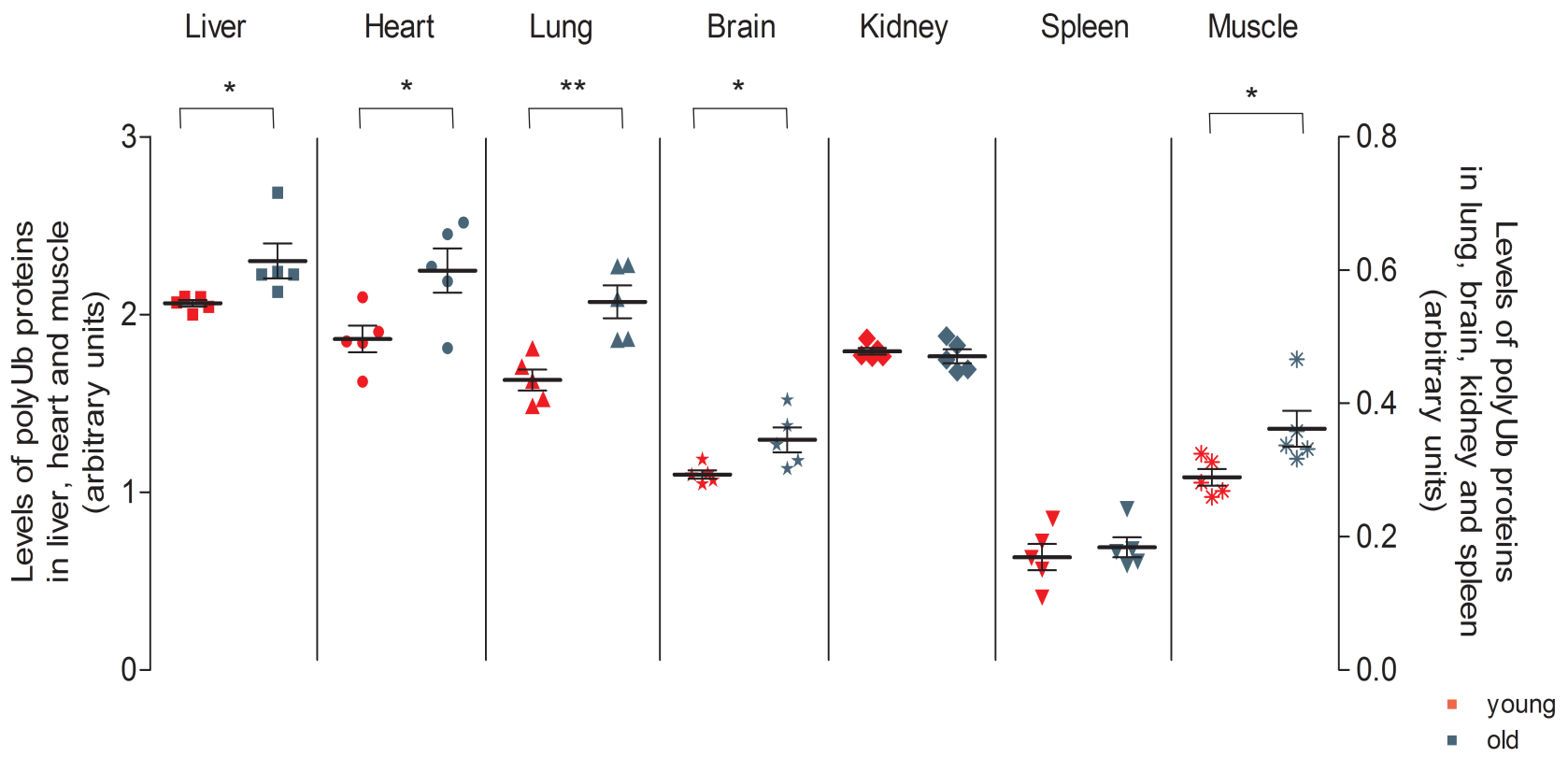

Figure 3.26: The level of polyUb proteins in mouse tissues.
Tissues were harvested from young and old mice and analysed by quantitative Western blot (Fig 3.22 - 3.25). The intensity of the high molecular weight complexes (> 80 kD) - representing the polyUb proteins - were quantified using the Odyssey software, and normalised relative to the intensity of the Coomassie blue signal. The above scatter plots show the normalised signal for each tissue, and each point represents data from a single animal. The lines and error bars show the mean ± s.e.m. respectively. The Student's t-test was used to determine significant differences between levels of the proteins in young and aged tissues. * denotes $P < 0.05$ and ** P denotes < 0.01, n = 5.

3.3.2 Accumulation of aggregated proteins in the tissues of old mice

Aberrant proteins such as those that are damaged or misfolded, are a major class of UPS substrates. These proteins by their nature will expose non-native determinants such as hydrophobic regions that make them prone to aggregation. Failure to effectively degrade such proteins therefore would therefore increase the risk of their aggregation. Various age-related diseases, including the neurodegenerative diseases, are characterized by the accumulation of insoluble aggregates formed by aberrant forms of a protein (e.g. tau in AD, α-synuclein in PD), suggesting that protein aggregation may occur in aged neurons (Yao 2010). In addition, recent work in *C. elegans* has provided evidence that numerous proteins become insoluble and aggregate during ageing (David *et al.* 2010). However, whether such widespread protein aggregation is also a feature of higher eukaryotes is still unknown. In order to begin to address this, a preliminary investigation of protein aggregation in young and old mouse muscle was carried out. An assay based on the detergent insolubility of aggregated proteins was developed based on that established to examine aggregation in *C. elegans* (David *et al.* 2010). Although it did not exhibit the most age-related changes in the expression level of ER proteostasis components, skeletal muscle was chosen for this assay since it presented a few advantages. First, the skeletal muscle was considered to be the closest match to whole *C. elegans* in terms of protein to lipid ratio (Klapper *et al.* 2011), which would impact on tissue solubility in the detergent containing buffer. In addition, a fair amount of polyUb proteins seem to accumulate in aged skeletal muscle (Fig 3.26), indicating that the level of aggregation-prone proteins in this tissue might be appreciable. Finally, and not trivially, skeletal muscle provided sufficient material for such analyses.

Samples of skeletal muscle from young and old mice were resuspended in RIPA buffer containing 1% SDS, and subjected to centrifugation at increasing speeds in order to pellet detergent-insoluble aggregates (see section 2.5.3). The pellets were resuspended in urea buffer, and samples of the total RIPA buffer extract, each pellet and the supernatant were analysed by SDS-PAGE followed by Coomassie blue staining to show total proteins (Fig 3.27A). The gels were scanned using the Odyssey scanner and the intensity of the Coomassie stained bands was quantified. For the total sample the whole lane was quantified, while for all the other samples the abundant bands over 60 kD and between 50-30 kD were considered, as previously reported by David et. al. (David *et al.* 2010). The amount of proteins recovered in each pellet and from the supernatant was normalised relative to the total protein in the starting material (i.e. total sample) (Fig 3.27B). Different pairs of young and old mice were used for this assay, and the gel shows a representative image, whilst the quantification is of 3 independent experiments using different mice. The intensity of the Coomassie stained bands in the total extracts of muscle from young and old muscle was very similar (Fig 3.27A, lanes 9 and 10), confirming equal amounts of protein in the starting extracts. However, there was a clear increase in the quantity of SDS-insoluble proteins that were isolated in the pellets 2 and 3 obtained from muscle of old mice compared to muscle from young mice (Fig 3.27A, compare lanes 5 and 7

with lanes 6 and 8). It is worth noting that the amount of protein remaining in the high speed supernatant, representing the SDS-soluble fraction, is clearly lower in samples from aged mice, consistent with increased recovery in pellets. These results are very interesting as they suggest that there is a general increase in the amount of SDS-insoluble, aggregated proteins in muscle from aged mice.

In order to explore the nature of proteins in the detergent insoluble fractions, the levels of polyUb proteins were assessed by western blotting (Figs 3.28). As previously observed, the amount of the polyUb proteins in the total extracts was higher in aged muscle (Fig 3.28A, lanes 9 and 10). An even more striking increase in polyUb protein was seen in the detergent insoluble fractions, especially in the pellets 2 and 3 (Fig 3.28A, lanes 3, 4 and 5, 6). The intensity of polyUb species with MW higher than 80 kD was quantified in each lane and the fluorescent signal obtained with anti-Ub was normalised relative to the Coomassie blue stained total protein in the starting material (refer to Fig 3.27A, lanes 9 and 10) and graphically represented in Fig 3.28B. As previously observed (Fig 3.26) aged muscle contains a higher amount of polyUb proteins (Fig 3.28A, lanes 9 and 10, Fig 3.28B - total). The amount of SDS-insoluble protein was also considerably higher in all the pellets from aged mice (Fig 3.28A compare lanes 1, 3, 5 with 2, 4, 6, Fig 3.28B – P1 to P4). Thus, the aggregated proteins present in the SDS-insoluble pellets might contain polyUb species. This might be expected given that many polyUb proteins are en route to being degraded and may therefore be abnormally folded exposing aggregation-protein regions. Molecular chaperones bind to misfolded proteins and can potentially become trapped in aggregates (Duennwald & Lindquist 2008). Thus western blotting was used to examine whether BiP was present in the pellets containing aggregated proteins (Fig 3.29). When muscle tissue from young mice was analysed, only very faint bands corresponding to BiP were detected in the SDS-insoluble pellets (Fig 3.29A, upper of the two bands). Most of the BiP remained in the detergent soluble supernatant (Fig 3.29A lanes 11 and 12). The fluorescent signal for obtained with anti-BiP was quantified and normalised relative to the total amount of protein from the starting material (Fig 3.27A, lanes 9 and 10), and the obtained ratio was represented in Fig 3.29B. In the aged muscle, the total level of BiP in the RIPA buffer extracts was increased as seen in the analysis of ER chaperones (Fig 3.29A, lane 10, Fig 3.29B - Total). Although the intensity may look similar, this may be due spread of the signal over a larger area. The amount of detergent insoluble BiP in each of the pellets was markedly increased (Fig 3.29A, compare lanes 1, 3, 5, with 2, 4, 6, and Fig 3.29B – P1 to P3). Moreover, a greater proportion of the chaperone was associated with the detergent-insoluble pellets in muscle from old mice compared to young animals, especially in the pellets 2 and 3 (Fig 3.29A, lanes 4 and 6, and Fig 3.29B). Also it can be seen that the cross-reacting band appears to pellet more in aged tissue (Fig 3.29A, lower band). This could indicate that the SDS-insoluble aggregates sequester numerous unrelated proteins. This is consistent with a previous study showing that amyloid aggregates sequester various metastable proteins (Olzscha *et al.* 2011).

Together these results suggest that in mouse muscle, a number of proteins become insoluble during ageing. The previous study in *C. elegans* found that those proteins that become SDS-insoluble and aggregate with age include numerous components of the proteostasis network, such as proteasome subunits, ribosomal proteins, and chaperones (David *et al.* 2010).. Although the identity of the aggregated proteins detected in the aged muscle is not known, they included polyUb species, most likely representing misfolded UPS substrates. The aggregation of polyUb proteins suggests that in the muscle of old mice, the degradation capacity of proteasome is exceeded by the generation of aberrant polyUb proteins, leading to accumulation and aggregation. In addition, the detergent-insoluble fractions include the chaperone BiP, which is consistent with the data from *C. elegans* reporting increased insolubility of the worm BiP homolog (Heat shock 70 kDa protein D) with age. The association with aggregated proteins or aggregation of BiP itself would be likely to impair its function. Therefore, it is possible that despite the overall increase in BiP levels in skeletal muscle with age, that the functional activity of the chaperone is decreased.

3.3.4 Increased expression of BAG3 in tissues form aged mice

Autophagy is a proteolytic pathway implicated in clearance of aggregated proteins, both from cytosol and from the ER (Bernales *et al.* 2007; Yao 2010; Gamerdinger *et al.* 2011). A recent study showed that BAG3 which is known to play a role in targeting of misfolded proteins to autophagic degradation was upregulated in aged cells. The authors suggested that as adaptation to the presence of aggregated proteins, aged cells switched from proteasomal to lysosomal degradation (Gamerdinger *et al.* 2009). The levels of BAG3 were analysed by western blotting in tissues of young and old mice (Fig 3.30A). An obvious increase in the expression level of BAG3 was apparent in almost all the aged tissues, especially in the liver and lung (Fig 3.29A). When the level of BAG relative to Coomassie was quantified (Fig 3.30B), significantly higher expression level was confirmed for all tissues from aged mice, apart from spleen and kidney. Interestingly, a decreased level of expression of BAG3 was observed only in the spleen of old mice. These data suggest that the changes observed in BAG3 in using cellular models (Gamerdinger *et al.* 2009) also occur in tissues from aged organisms. Thus the functional implication is that macroautophagy may increase with age.

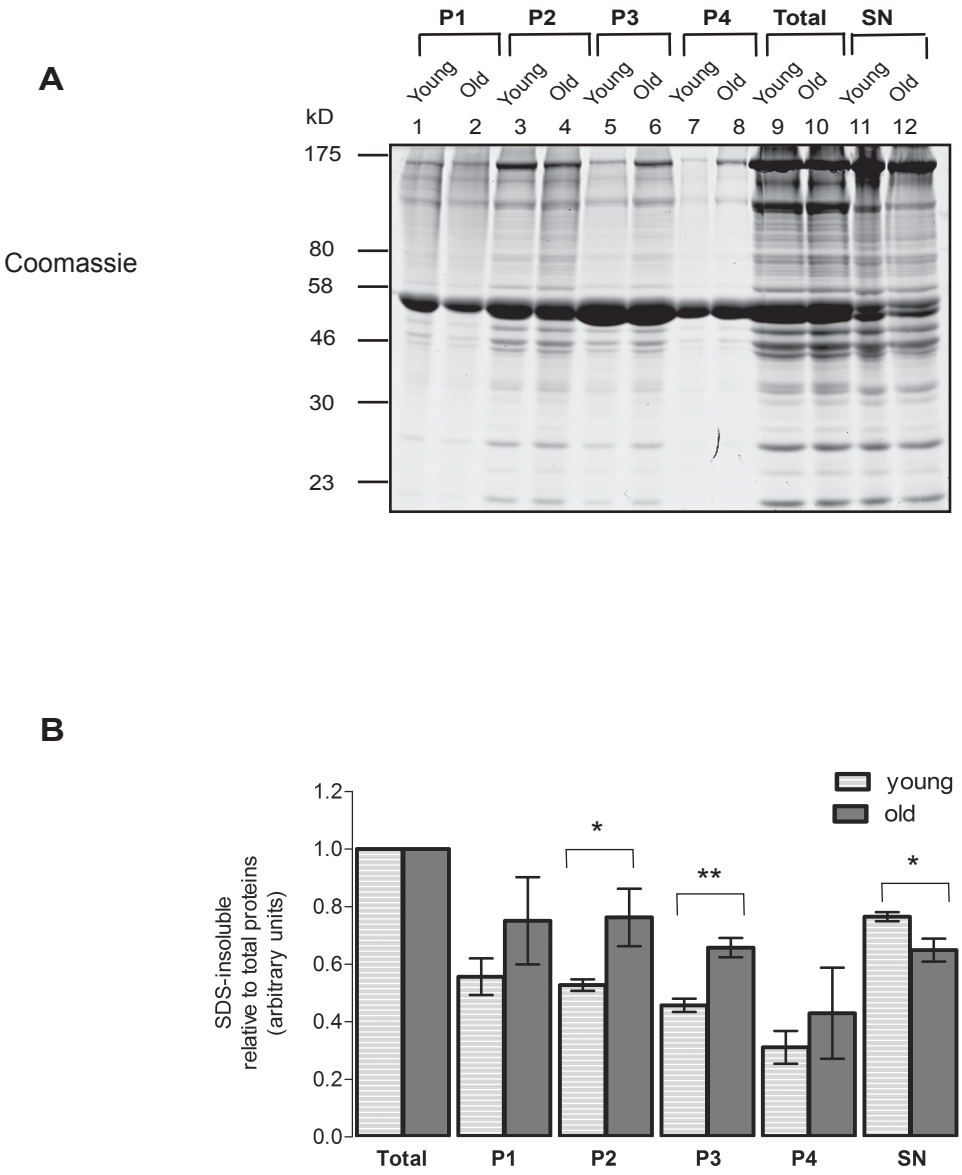

Figure 3.27: Level of aggregated proteins in mouse muscle.
Extracts from young and old muscles were prepared in 1% SDS RIPA buffer, and sequentially centrifuged at increased speed to obtain the pellets (P1-P4). Equal amounts of total protein were loaded for each sample and were separated on an 10% Tris-glycine gel.
(A) Total proteins were visualised by Coomassie blue staining.
(B) The intensity of the infrared signal obtained was quantified using the Odyssey software. The graph shows the signal for each sample normalised to the total amount of protein (i.e. Total). The error bars show the mean ± s.e.m. The Student's t-test was used to determine significant differences between levels of the proteins in young and aged muscle.
* denotes $P < 0.05$ and ** P denotes < 0.01, n=3.
SN = supernatant.

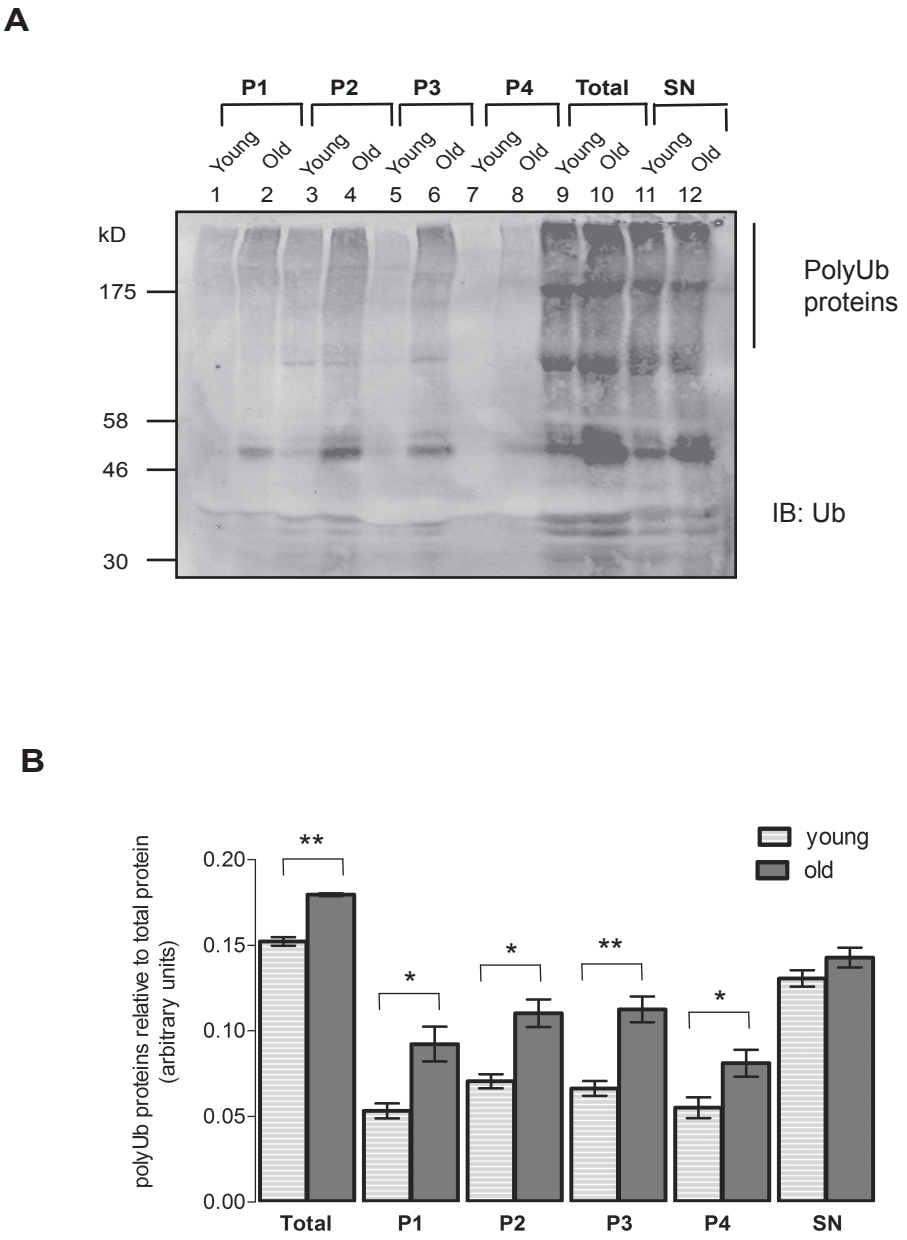

Figure 3.28: Level of polyUb proteins in aggregated compexes in mouse muscle.
(A) Samples were obtained as described in Fig 3.27 and analysed by immunoblotting with the anti-Ub antibodies followed by infrared secondary antibodies. The intensity of the infrared signal obtained was quantified using the Odyssey software.
(B) The graph shows the signal for each protein pellet and total sample, normalised to Coomassie blue stained total protein in the starting material. The error bars show the mean ± s.e.m. The Student's t-test was used to determine significant differences between levels of the proteins in young and aged tissues.
* denotes $P < 0.05$ and ** P denotes < 0.01, $n = 3$.

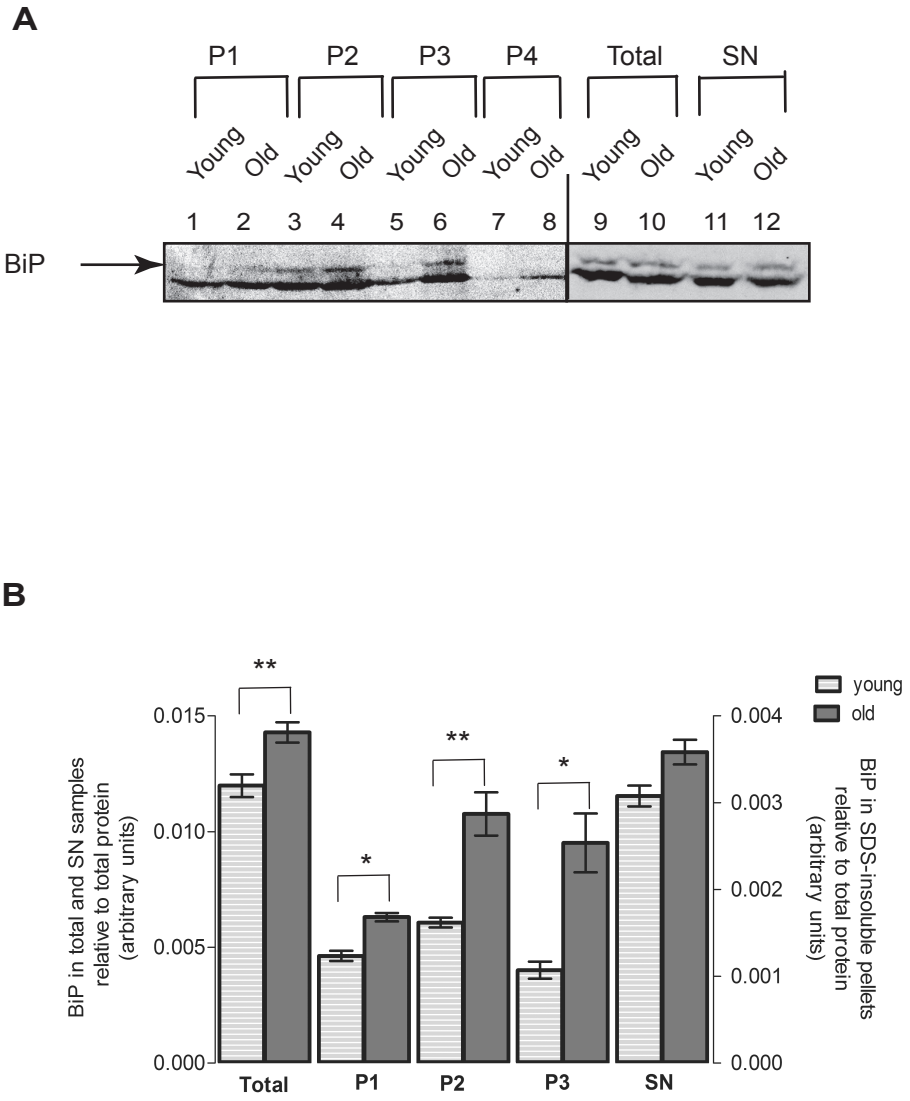

Figure 3.29: Levels of BiP in aggregated compexes in mouse muscle
(A) Samples were analysed and quantified as described in Fig 3.28.
(B) The graph shows the signal for BiP in each protein pellet and in total samples, normalised to Coomassie blue stained total protein in the starting material. The error bars show the mean ± s.e.m respectively.
The Student's t-test was used to determine significant differences between levels of the proteins in young and aged tissues. * denotes $P < 0.05$ and ** P denotes < 0.01, $n = 3$.

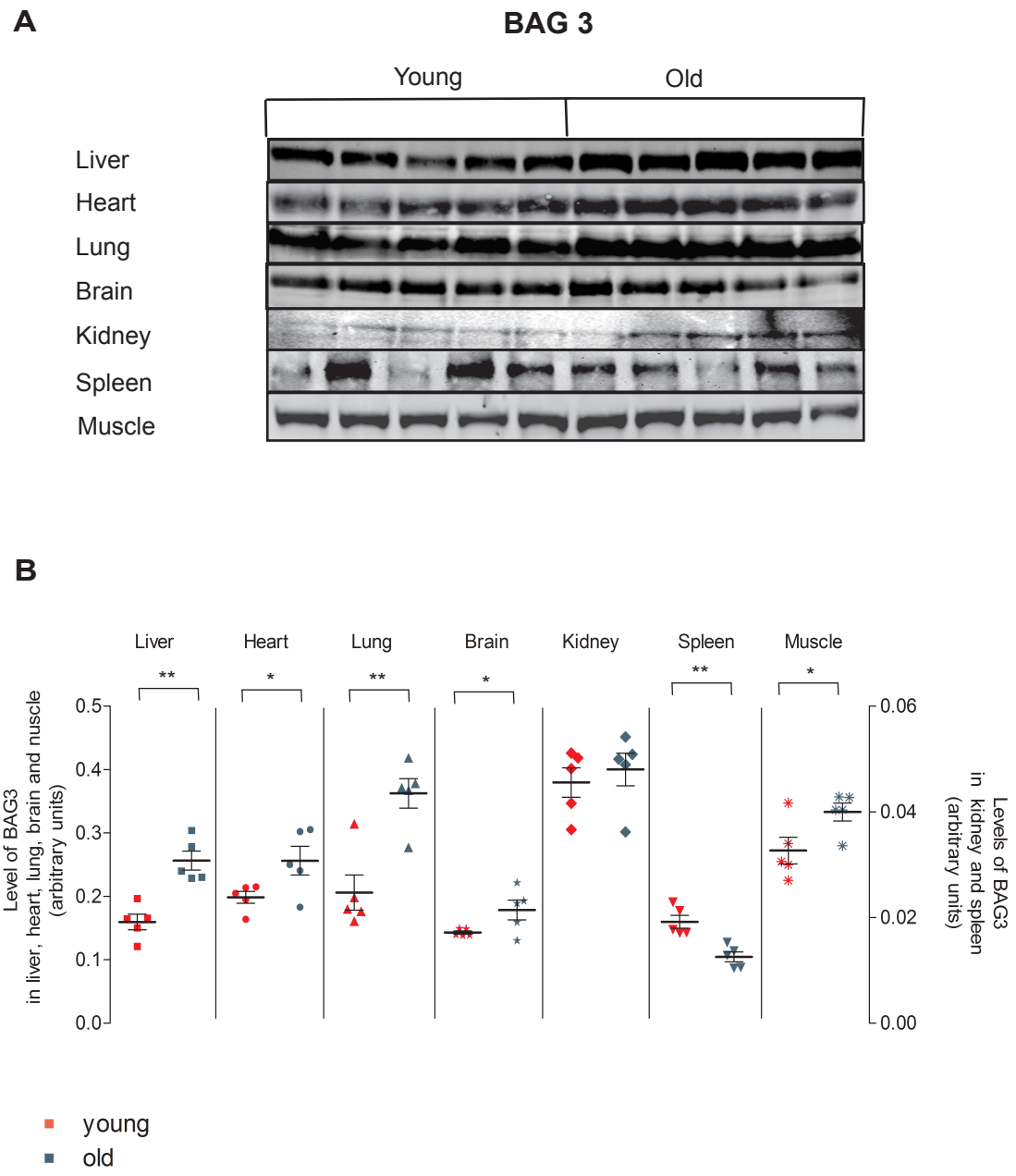

Figure 3.30: Levels of BAG 3 in mouse tissues.
(A) Extracts from young and old tissues were prepared in 6 M urea buffer, and equal amounts of total protein were loaded for each sample. Proteins were separated on an 12% Tris-glycine gel. Samples were analysed by western blotting using the anti-BAG3 primary antibodies followed by infrared secondary antibodies. The intensity of the infrared signal obtained for each sample was quantified using the Odyssey software, and normalised relative to the intensity of the Coomassie blue signal.
(B) The scatter plots in show the normalised signal for each tissue and each point represents data from a single animal. The lines and error bars show the mean ± s.e.m. respectively.
The Student's t-test was used to determine significant differences between levels of the proteins in young and aged tissues. * denotes $P < 0.05$ and ** P denotes < 0.01, $n = 5$.

3.4 Increased phosphorylation of eIF2α in aged tissues

In order to try and address whether ER homeostasis overall was indeed affected with age, the phosphorylation state of eIF2α was measured in the different tissues. Conditions of perturbed ER homeostasis lead to activation of the UPR sensors, including PERK, which subsequently phosphorylates eIF2α, leading to inhibition of translation initiation. Thus, the level of phospho-eIF2α is commonly used as a measure of UPR activation, and can provide a readout of ER proteostasis. Thus, antibodies that recognise only the Ser 51 phosphorylated eIF2α were used together with antibodies recognising total eIF2α, to assess the relative phosphorylation state of eIF2α in tissues from young and old mice (Fig 3.31). The bands corresponding to phosphorylated and total eIF2α were quantified and the level of phospho-eIF2α expressed relative to total eIF2α in each sample (Fig 3.32). Strikingly, the ratio of phosphorylated to total eIF2α was significantly higher in all of the aged tissues compared to those harvested from young mice (Fig 3.32). This increase in the amount of phospho-eIF2α ranged from 18% in the heart, to 40% in brain, kidney and liver, and more that 80% in lung (Fig 3.32). Thus in aged mice, there appears to be a widespread increase in the phosphorylation state of eIF2α. Although PERK is one of the major kinases controlling eIF2α phosphorylation, several other stress-related kinases, including GCN2 which is activated by amino acid starvation, also phosphorylates Ser51 of eIF2α (Harding *et al.* 2003). Hence, although increased phospho-eIF2α is consistent with ER stress in these tissues, it is important to note that it does not only report on UPR activation. This analysis also suggested that the phosphorylation state of eIF2α varies between tissues, in both young and old animals. Hence, a greater proportion eIF2α was phosphorylated in muscle, whilst a much lower proportion was phosphorylated in liver (Fig 3.32). The widespread increase in eIF2α phosphorylation in the aged tissues provides further support for the hypothesis that ER protein homeostasis may be perturbed in aged tissues, leading to activation of the UPR.

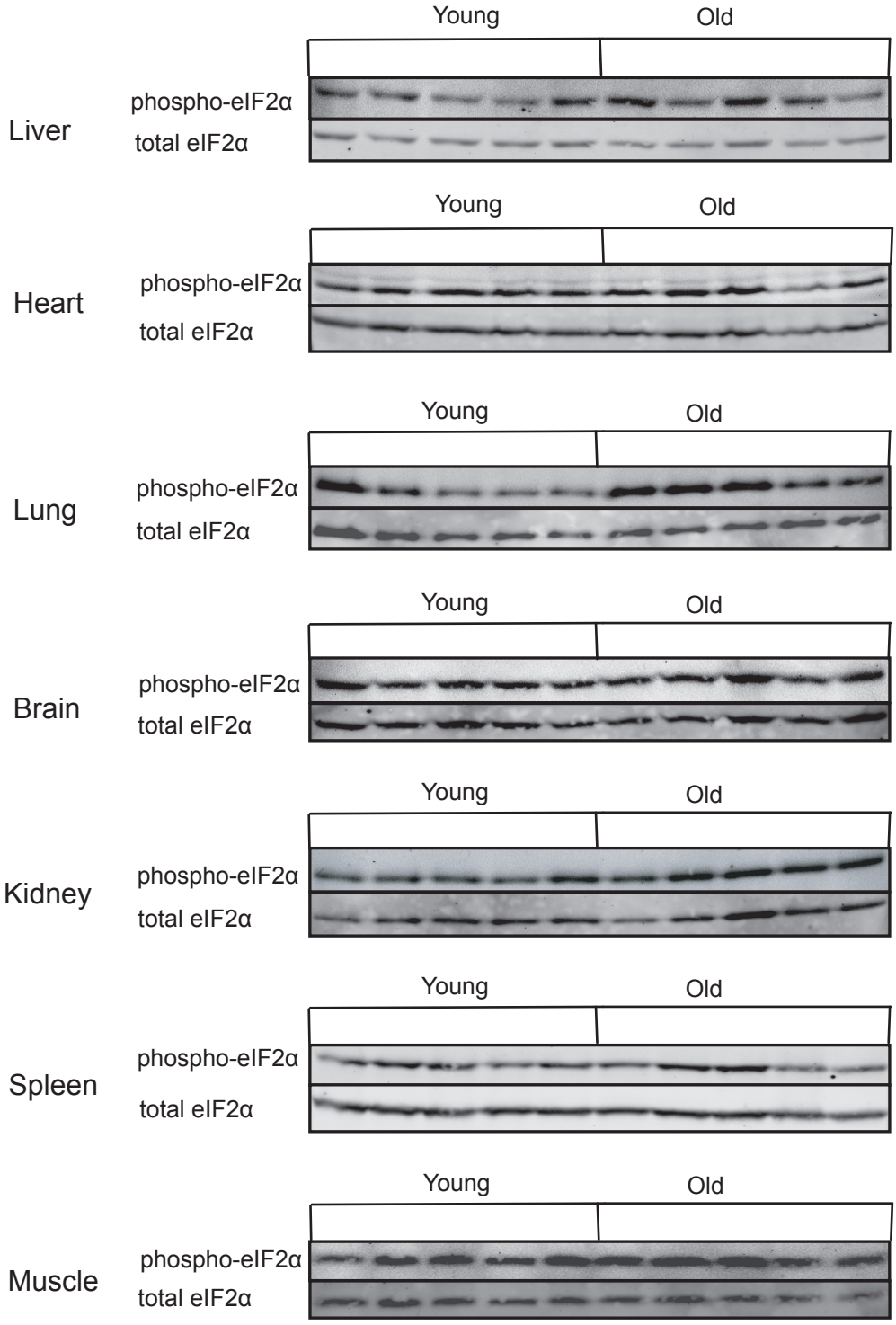

Figure 3.31: Level of phosphorylated and total eIF2α in mouse tissues.
Extracts from young and old tissues were prepared in 6 M urea buffer, and equal amounts of total protein were loaded for each sample. Proteins were separated on 12% Tris-glycine gels. Samples were analysed by western blotting using the indicated primary antibodies followed by infrared secondary antibodies.

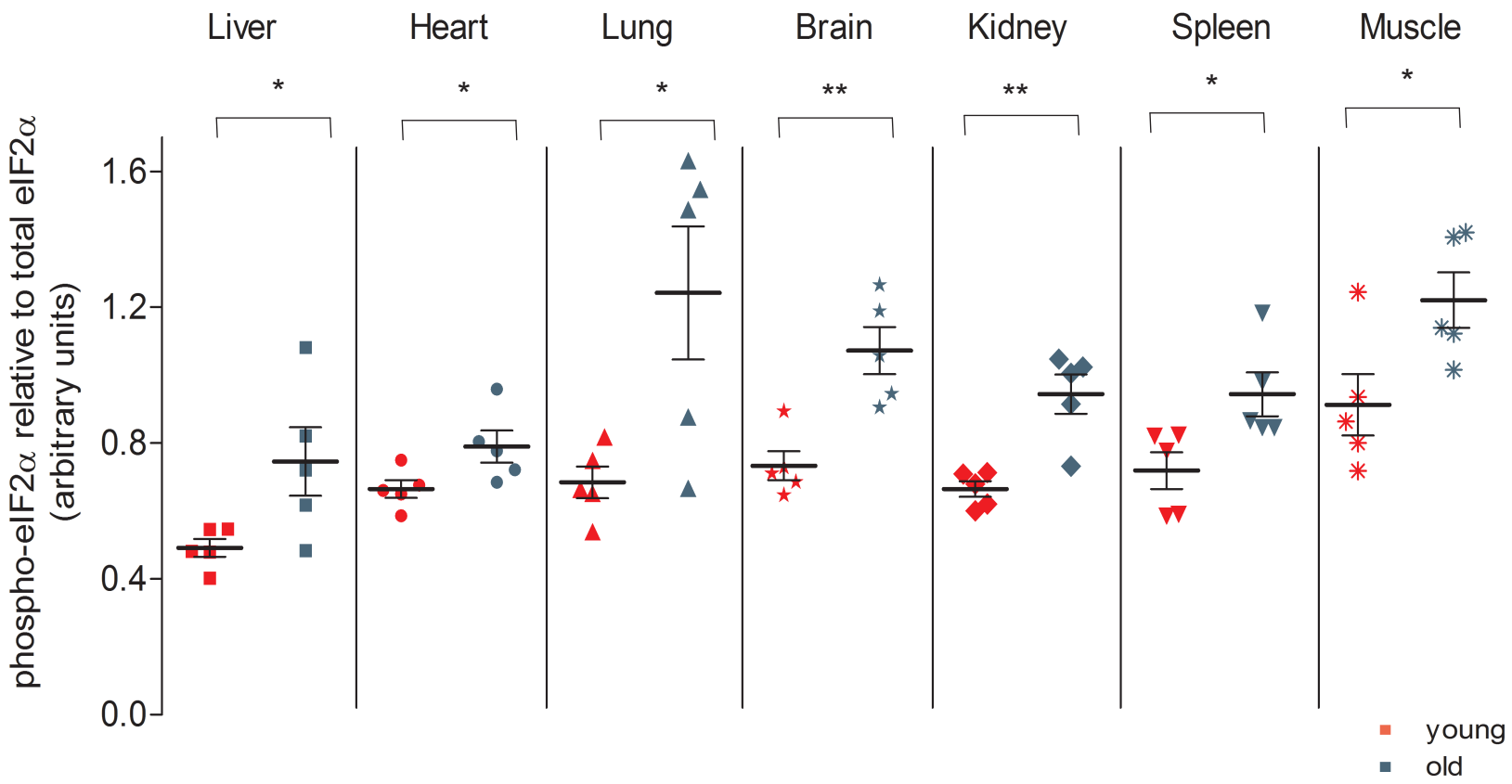

Figure 3.32: Levels of phosphorylated eIF2α in mouse tissues.
Tissues from five young and five old mice were harvested and analysed by quantitative Western blotting (Fig 3.31). The fluorescent intensity of each band was quantified using the Odyssey software. The intensity of phospho-eIF2α was normalized to the intensity of the corespondent total eIF2α band. The above scatter plots show the normalised signal for each tissue, and each point represents data from a single animal. The lines and error bars show the mean ± s.e.m. respectively. The Student's t-test was used to determine significant differences between levels of the proteins in young and aged tissues. * denotes $P < 0.05$ and ** P denotes < 0.01.

3.5 Discussion

In this chapter, the effect of ageing on components of ER proteostasis pathways, and the solubility and ubiquitination state of the overall proteome were investigated in a range of tissues isolated from young (3 month) and aged (22-24 month) mice. The findings are summarised in the heat map presented in section 3.3 (Fig 3.33). Many age-associated changes in expression levels of ER-resident or ER-linked proteins were observed, and a lot of heterogeneity in terms of the extent and direction of change for most of the proteins was noticed. Although each tissue exhibited a unique profile of changes in expression level of components of ER proteostasis, some trends were apparent. In particular, brain showed decreased levels of components of protein biosynthesis and degradation pathways, suggesting that incorrectly folded proteins might accumulate in the ER lumen. In contrast, spleen had increased levels of proteins from ERAD machinery. Overall, the changes observed indicate that ER proteostasis pathways may be affected by age, but in distinct ways in different tissues. Consistent with this conclusion, increased phosphorylation of eIF2α was observed in all tissues from aged mice. In addition, a widespread accumulation of polyUb proteins was seen in aged tissues, and this correlated with general increase in levels of BAG3 a protein involved in degradation of protein aggregates via autophagy. Altogether, these results indicate that aged tissues experience low levels of stress, possible due to accumulation of misfolded proteins.

It is important to appreciate that different organs are exposed to different forms of age–related stress, and this is likely to be reflected in any changes in protein expression during ageing. Therefore, it is not surprising that each tissue had a unique profile of age-related changes in the expression level expression of the proteins examined. The spleen for example exhibited higher expression levels of a range of many chaperones and ERAD factors. Most of these proteins are targets of UPR effectors, suggesting a possible UPR activation. The spleen is a lymphatic organ involved in immune response. Here the B-cells are matured to antibody secreting B cells and naive T cells are stimulated to become cytokine producing cells (Mebius & Kraal 2005). The UPR plays an important role in the development of these immune cells (Iwakoshi *et al.* 2003; Brunsing *et al.* 2008; Ma *et al.* 2009). However, prolonged ER stress can result in increased number of cytokine secreting cells, thus activation of inflammatory response. This can create a vicious cycle, with the inflammatory response inducing ER perturbations (e.g. misfolding) thus maintaining UPR signalling, which would further increase the amount of inflammatory stimuli (Hasnain *et al.* 2012). Therefore perturbation of ER homeostasis in the spleen with age could potentially generate a proinflammatory environment, which might in turn promote heightened levels of ER stress and upregulation of multiple UPR targets. This is consistent with the observation that a chronic inflammatory state develops during in the ageing process (Iwakoshi *et al.* 2003; Boren & Gershwin 2004).

Ageing is also associated with increased incidence of neurodegenerative diseases. Studies on models of neurodegenerative diseases, showed chronic activation of UPR suggesting that the ER homeostasis might be perturbed in the diseased brain (Cohen *et al.* 2006; Hoozemans *et al.* 2009; Seidel *et al.* 2011; Moreno *et al.* 2012). The study of the expression levels of ER proteins revealed significantly lower levels of multiple ERAD components in the aged brain (Fig 3.33). Such a widespread decline in key ERAD factors would be predicted to reduce the capacity for clearing misfolded proteins, thus leading to accumulation of misfolded proteins and perturbation of ER proteostasis. Indeed, brain showed a clear increase in levels of BiP, a key UPR target gene and enhanced phosphorylation of eIF2α, consistent with elevated levels of UPR signalling. UPR activation might also be expected to result in upregulation of factors involved in ERAD and folding/QC pathways, which is clearly not the case. The reduced levels of Rpl17 and SPC25 may indicate that general decline in many protein constituents is linked to a decrease in protein biosynthesis, though increased levels of BiP and BAG3 argue against this. Another possibility is that despite perturbation in ER proteostasis, in the aged brain the UPR signalling pathways can be affected, thus the upregulation of downstream targets might be suboptimal.

A recent study has shown that old mice are more susceptible to lung fibrosis (Torres-Gonzalez *et al.* 2012). An important role in the pathogenesis of this disease is the prolonged activation of UPR (Lawson *et al.* 2011). It has therefore been suggested that the aged lung may have a reduced capacity to maintain the homeostasis in the ER, which may predispose the lung to greater injury following an environmental insult. Interestingly, in support of this theory, increased eIF2α phosphorylation, together with increased levels of polyUb proteins and BAG3 are consistent with perturbed ER proteostasis in aged lung (Fig 3.33). From all the tested tissues, liver and kidney had relatively little change in ER protein levels. This is similar with the results form transcriptomic studies, showing that these two tissues had also exhibited reduced age-related changes in genes expression (Zahn *et al.* 2007). Also, kidney and spleen are the only tissues that not to show accumulation of polyUb proteins, nor increased BAG3. This is further support the idea that kidney is the least affected organ during ageing, at least regarding the ER homeostasis. It is also important to note that the whole tissues (excluding fat, obvious connective tissue and vasculature) were collected, and therefore a mixture of different cells were analysed in each case, including blood cells/formed elements from the organ blood vessels. This could potentially mask more (or less) dramatic changes in the tissue specific cell type.

The most consistent change observed in all tissues was increased eIF2α phosphorylation. When misfolded proteins accumulate in the ER, the UPR is activated and the rates of protein synthesis, folding and degradation are altered in a coordinated way to restore ER proteostasis. A small number of studies have suggested that age might impair these UPR responses. For instance, the eIF2α phosphorylation was shown to decrease in aged mice, suggesting diminished capacity to adapt ER proteostasis to stress. (Hussain & Ramaiah 2007; Naidoo *et al.*

2008). In these studies, the level of phospho-eIF2α was measured relative to actin, or total protein, not relative to total eIF2α. Another study that has used the same way of measuring phospho-eIF2α has indicated an increase of phosphorylation of eIF2α in old hepatocytes (Li & Holbrook 2004). On the other hand, various age-related diseases are correlated with activation of chronic UPR (Hoozemans *et al.* 2009). Moreover, a direct link between constitutive activation of the UPR and reduced lifespan has been demonstrated in nematodes (Viswanathan *et al.* 2005), pointing to the importance of maintaining ER homeostasis. More recently one study had linked the elevated levels of phospho-eIF2α with reduced survival of prion-diseases mice (Moreno *et al.* 2012). In this chapter, a higher level of phosphorylated eIF2α was detected in all the aged tissues, similar to the data generated by the hepatocytes of old mice (Li & Holbrook 2004). This increase in the amount of phospho-eIF2α provides further support for the hypothesis that ER protein homeostasis is perturbed in aged tissues.

As the ER and cytosol use the same machineries to eliminate misfolded proteins, the protein homeostasis of these two compartments is intimately linked (Ben-Gedalya & Cohen 2012). Therefore, misfolded protein that accumulates in the cytosol may impact upon ER proteostasis and vice versa. Increased levels of high MW Ub proteins were observed in all the aged tissues, except kidney and spleen (Fig 3.33). This was especially clear in the brain and lung (Fig 3.33), suggesting decreased efficiency of protein folding pathways, and/or the degradation pathways that would normally eliminate damaged proteins, namely the proteasome and autophagy. Other studies have also observed accumulation of polyUb material in various aged tissues, such as brain and liver (Ohtsuka *et al.* 1995; Mura *et al.* 1996). A vast amount of data shows that with age the amount of oxidised proteins increased, indicating that proteome is accumulating damage during ageing (Rabek *et al.* 2003; Papaconstantinou *et al.* 2005). In addition, it has been shown that proteasome activity declines with age (Low 2011). Moreover a recent study showed a link between lifespan and efficient proteasomal degradation (Vilchez *et al.* 2012). This is important as declining proteasomal degradation would exacerbate accumulation of polyUb. An alternative degradation pathway is autophagy that removes polyUb and aggregated proteins, and ubiquitination is important for recognition of proteins for autophagy. BAG3 is a key mediator of the macroautophagy pathway that removes protein aggregates (Gamerdinger *et al.* 2011). Interestingly, BAG3 levels were significantly higher in all aged tissues apart from the kidney and spleen (Fig 3.30B). These were the only tissues not to have increased amounts of polyUb proteins (Fig 3.26), suggesting a direct correlation between accumulation of polyub proteins and BAG3 levels. A previous study identified an increase in BAG3 expression in *in vitro* aged lung fibroblasts (Gamerdinger *et al.* 2009), and provided evidence that aged cells shifted from proteasomal degradation to lysosomal - autophagic degradation in an attempt to prevent the accumulation of misfolded proteins (Gamerdinger *et al.* 2009). However, the efficiency of autophagy is also affected by age (Hubbard *et al.* 2011), therefore upregulation of macroautophagic degradation may be insufficient to prevent the accumulation of polyUb proteins in the cell. Such reduced capacity for clearing aberrant proteins may increase protein

aggregation. Indeed, the accumulation of aggregated proteins has been shown to occur in many age–related pathologies (e.g. neurodegenerative diseases, stroke), and recently even during normal ageing in *C. elegans* (David *et al.* 2010). Similar to the results of this latter study, an increase in SDS-insoluble protein aggregates was observed in the muscle of aged mice. These insoluble aggregates included polyUb proteins, and also contained BiP, which could potentially reduce the amount of the available BiP, perturbing the ER homeostasis.

All together, the results in this chapter point to a change in ER capacity in aged tissues. However, post mortem tissues do not allow ER function to be examined in detail. Thus, a more tractable system was needed in order to investigate how age affects the ability to activate UPR following exposure to a stress or to assess the extent of which ER folding and degradation capacities are affected by age.

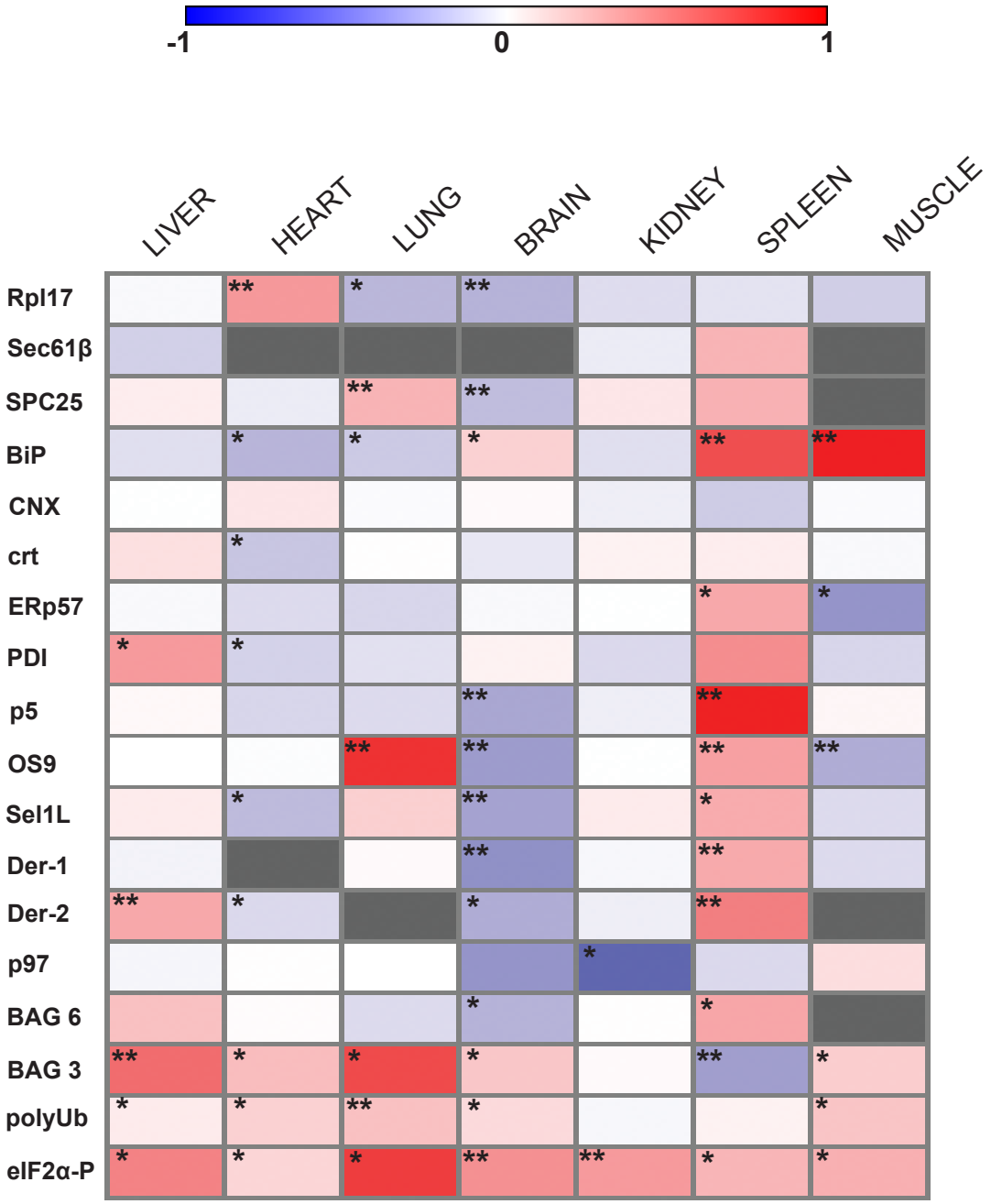

Figure 3.33: Heat map of protein expression in old mouse tissues relative to young mouse tissues.
The heat map visualizes the variance of the protein expression across all mouse tissues studied. Blue indicates a decreased level of expression and red shows an increased level of expression of a protein in the aged tissues. Dark gray indicate the samples which could not be detected by western blotting. The stastistical significance, previously calculated for each sample by using Student's t-test is indicated in the figure (* $P < 0.05$, ** $P < 0.01$).

CHAPTER 4

Analysis of age-related changes in ER proteostasis using *in vitro* aged human fibroblasts

4.1 Introduction

The analysis of tissues from old and young mice described in the previous chapter identified a number of age-related changes in the level of components of ER protein folding, quality control and degradation machineries. Prominent among these were an accumulation of polyUb proteins and increased phosphorylation of eIF2α, which together suggest that ER proteostasis may be perturbed in aged tissues, leading to a low level of UPR activation. In order to examine of the function of ER protestasis pathways and the ER stress response, post-mortem tissues cannot be used, and is very difficult to study these pathways in live animals. A relatively simple and tractable system for investigating ER function are isolated cells growing in culture. Two potential cellular models have been used in previous studies of ageing: primary cells aged *in vitro* by serial passage, and primary cells isolated from tissues of young and old organisms, inclusive humans. Human lung fibroblast cells (IMR90) have been used for a number of studies of cellular ageing (Kil *et al.* 2004; Kern *et al.* 2006; Gamerdinger *et al.* 2009). In such studies, IMR90 cells at low population doublings (LPD) of 15-17 are usually considered young, whilst cells at high population doublings (HPD) of over 50 PD are considered old. Importantly, many of the changes observed in the *in vitro* aged cells are also apparent in cells isolated from old organisms, including rodents and human (Campisi *et al.* 2011).

First, a basic characterisation of the IMR90 fibroblasts was performed. The subcellular morphology of LPD and HPD cells was examined by immunofluorescence microscopy (Fig 4.1A). The HPD cells were wider and more spread out than LPD fibroblasts, which had a more elongated morphology (Fig 4.1A), as previously reported (Gamerdinger *et al.* 2009). Also, the organization of vimentin filaments was less parallel and more disorganised in HDP cells, suggesting that the cytoskeleton may be altered in these cells. This is consistent with data of other studies, which showed that senescent fibroblasts, regardless of their tissues of origin present disorganised filaments of vimentin and actin (Nishio & Inoue 2005). The level of expression of the senescence marker caveolin-1 was also tested (Fig 4.1B), and as observed previously (Gamerdinger *et al.* 2009), found to increase by more than two-fold in the HPD cells. The immunofluorescence analysis of ER, using calnexin as subcellular marker, showed that the shape and size of ER relative to the cell size was similar in LPD and HPD cells.

4.2 Level of ER folding and quality control factors in IMR90 fibroblasts

Two of the most widespread changes observed in tissues from aged mice were an accumulation of high MW polyUb proteins and an increase in the phosphorylation state of eIF2α. Therefore, it was important to determine whether these features were also observed the IMR90 model of cellular ageing. Extracts of IMR90 cells at LPD and HPD were analysed by infrared Western blotting (Fig 4.2A).

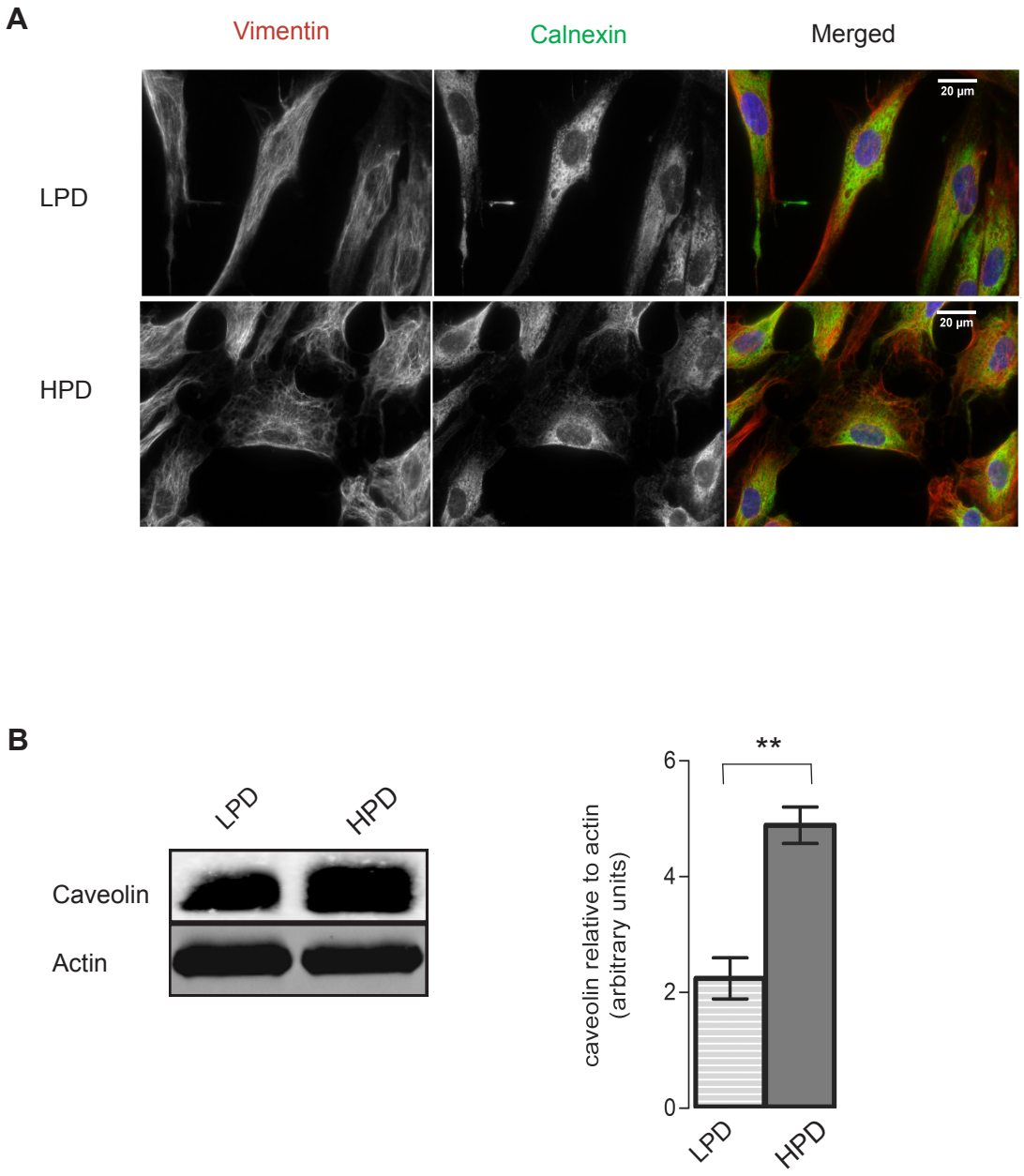

Figure 4.1: Characterisation of LDP and HPD cells.
(**A**) Immunofluorescence labelling of intermediate filaments (vimentin) and ER (calnexin). Cells were grown on glass coverslip. After methanol fixation and permeabilization the cells were incubated with the specific antibodies.
(**B**) Protein extracts were prepared in SDS buffer and analysed by western blotting using the primary antibodies indicated followed by infrared secondary antibodies. The intensity of the infrared signal obtained with anti-caveolin antibody was quantified using the Odyssey software, and normalised relative to the intensity of the signal of actin. The graph shows the normalised signal. The lines and error bars show the mean ± s.e.m. respectively. The Student's t-test was used to determine significant differences between levels of the proteins in LPD and HPD cells. ** P denotes < 0.01, n = 3.

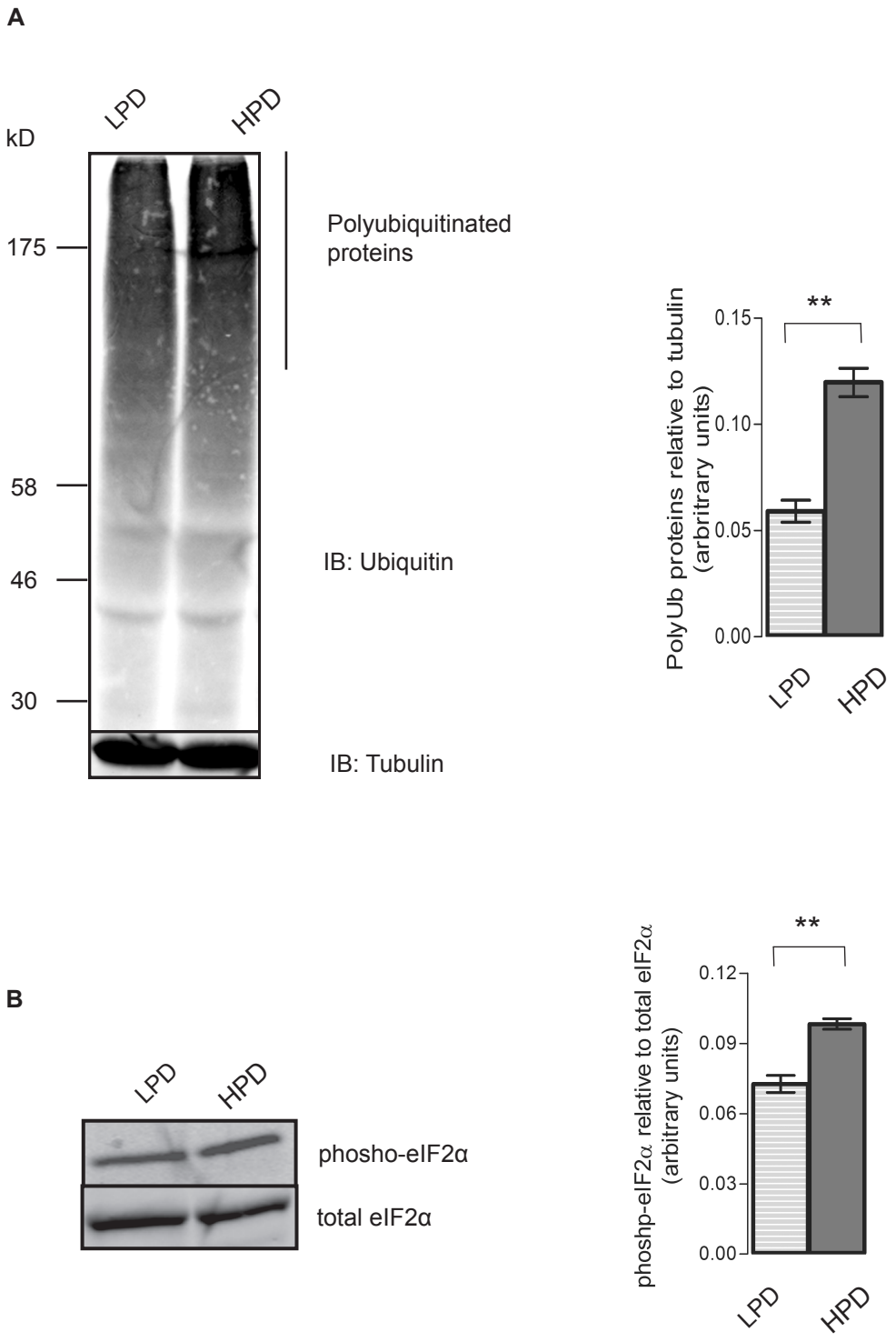

Figure 4.2: Immunoblot analysis of polyUb proteins and of basal levels of phosho-eIF2α in LPD and HPD cells.
LPD and HPD IMR90 cells were extracted in SDS loading buffer. The same amount of total protein (50 µg) was analysed by SDS - PAGE and western blotting using the indicated primary antibodies followed by infrared secondary antibodies. The intensity of the infrared signal obtained with each antibody was quantified using the Odyssey software, and normalised relative to the intensity of control protein signal (actin or total eIF2α). The graph shows the normalised signal for each protein. The lines and error bars show the mean ± s.e.m. The Student's t-test was used to determine significant differences between levels of the proteins in LPD and HPD cells. ** P denotes < 0.01, n = 3.

.

Quantification of the total polyUb proteins from 3 separate cultures showed that the level of Ub tagged proteins in the HPD cells was approximately two-fold higher than in LDP cells (Fig 4.2A). In addition, levels of phospho-eIF2α were also increased in the aged HPD cells compared to cells at LPD (Fig 4.2B). Quantification of the ratio of phospho-eIF2α to total eIF2α revealed that a significantly higher proportion of the total eIF2α was phosphorylated in HPD cells, suggesting that in older cells, the UPR may be activated (Walter & Ron 2011). Thus, *in vitro* ageing of IMR90 fibroblasts is accompanied by an accumulation of polyUb proteins and increased phosphorylation of eIF2α. Both these features were observed in multiple tissues of aged mice (sections 3.3 and 3.4), and these results provide support for the use of these cells as a model to study the effect of cellular ageing on ER proteostasis.

The analysis of ER function in these cells began by examining the expression level of factors involved in protein biosynthesis and QC. Extracts of cultures of LDP and HPD cells were analysed by SDS-PAGE and infrared western blot with a range of antibodies specific for components of protein biosynthesis, folding and QC pathways (see table 2.1). In addition, actin and tubulin were validated as loading control by testing that the levels of actin and tubulin relative to total protein do not vary between LPD and HPD cells (appendix 4). Most of these factors (Rpl17, SPC25, calnexin, calreticulin, ERp57 and p5) were not significantly different between cells at LDP and HPD (Fig 4.3), suggesting that this form of cellular ageing is not accompanied by global changes in the expression level of ER components. However, the expression level of PDI decreased in the HPD cells (Fig 4.3), indicating that oxidative folding pathways may be perturbed in the aged cells. In contrast, the level of BiP together with the ERAD factors Sel1L and Der-1 were markedly increased in the HPD cells (Figs 4.3 and 4.4). Interestingly, each of these proteins is known to be upregulated in response to ER stress (Kaneko & Nomura 2003; Oda *et al.* 2006). Together with the increased basal level of phospho-eIF2α (Fig 4.2), these results indicate that the *in vitro* aged HPD cells may have elevated levels ER stress. The levels of several components of different proteolytic pathways were also found to change in HPD compared to LDP cells. Expression of the 19S proteasome subunit Rpt6 was almost 50% lower in HDP cells compared to LPD cells (Fig 4.4). Similarly, levels of BAG6 were decreased to approximately half in HPD cells (Fig 4.4). BAG6 plays a role in posttranslational targeting to ER (Wang *et al.* 2011), thus decreased levels might potentially impact upon efficiency of translocation. Also BAG6 has a role in QC/ERAD of mislocalised polypeptides (Claessen & Ploegh 2011), so this system could also be affected by reduced levels of BAG6 in HPD cells. The reduced expression level of Rpt6 in HPD (Fig 4.4) is consistent with the results of numerous previous studies reporting altered composition of proteasome (Koga *et al.* 2010). By contrast, BAG3 levels were significantly higher in the HPD cells (Fig 4.4). BAG6 and Rpt6 are involved in proteasomal degradation, whilst BAG3 functions in the autophagic pathway (Carra *et al.* 2008; Gamerdinger *et al.* 2011), thus the results indicate that in the aged cells, the proteasomal pathway may be less efficient, whilst an alternative autophagy pathway may be enhanced.

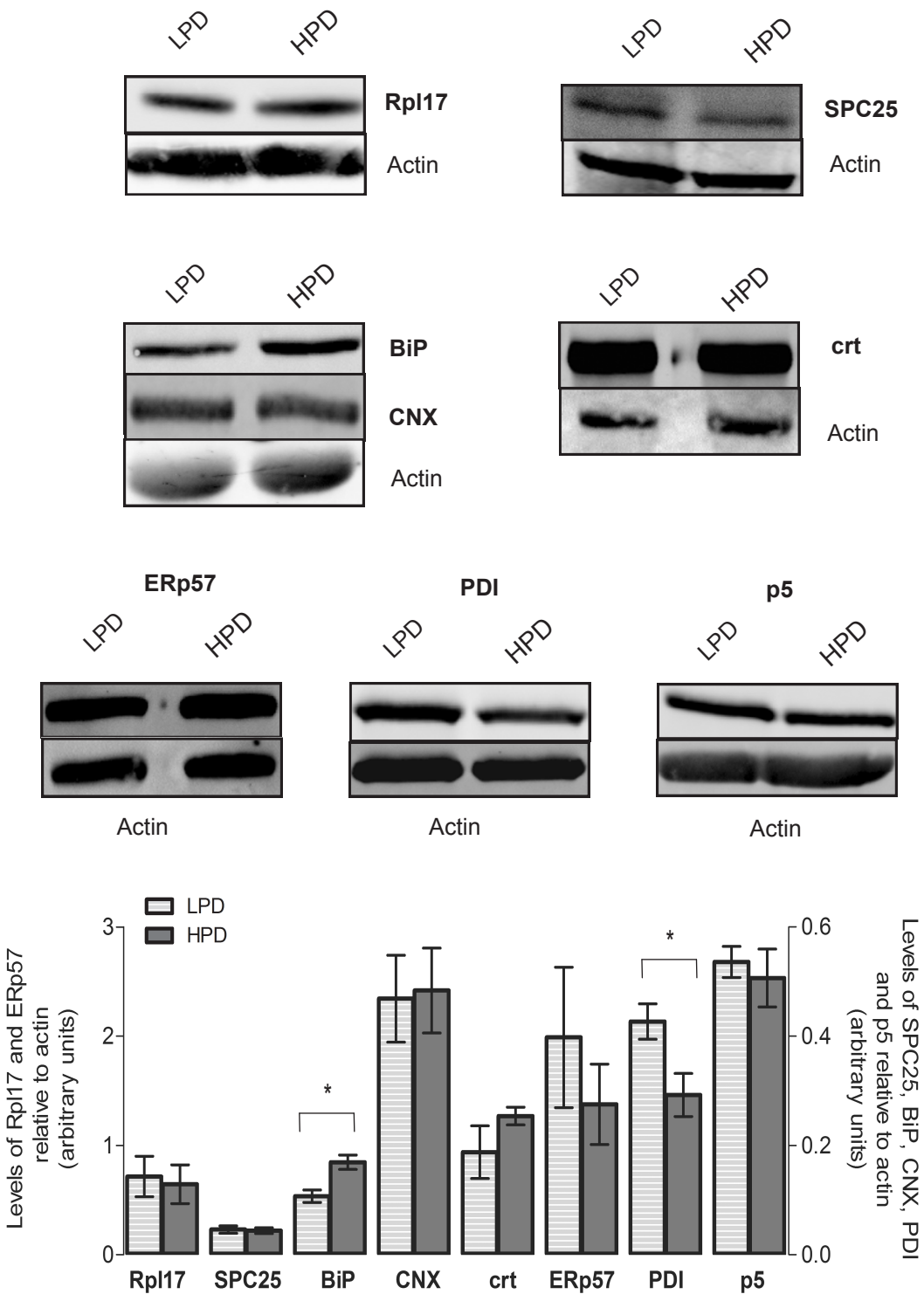

Figure 4.3: Expression levels of of factors involved in protein biosynthesis and ER folding in LPD and HPD cells.
Cells were lysed in SDS loading buffer to obtain the protein extracts and equal amounts of total protein were loaded for each sample. Proteins were separated on 12%Tris-glycine gels and analysed by Western blotting using the indicated primary antibodies followed by infrared secondary antibodies. The intensity of the fluorescent signal obtained with each antibody was quantified using the Odyssey software, and normalised relative to the intensity of the actin signal. The graph shows the normalised signal for each protein. The lines and error bars show the mean ± s.e.m. The Student's t-test was used to determine significant differences between levels of the proteins in LPD and HPD cells. * denotes $P < 0.05$, $n = 3$.

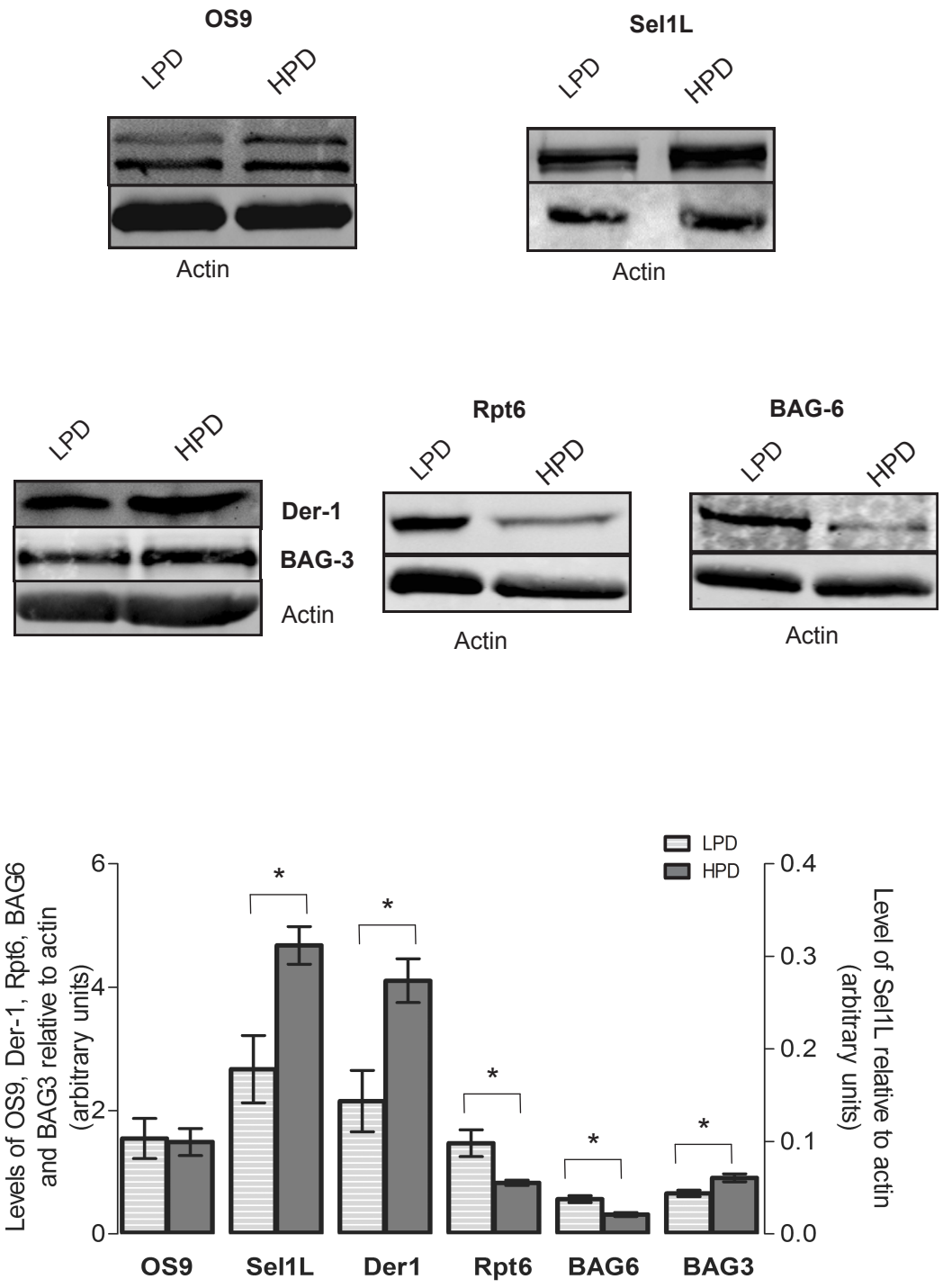

Figure 4.4: Levels of components of the ERAD machinery and of proteolytic pathways in LPD and HPD cells.
Protein extracts from LPD and HPD cells were prepared and analysed as described in Fig 4.3. The intensity of the infrared signal obtained with each antibody was quantified using the Odyssey software, and normalised relative to the intensity of actin signal. The graph shows the normalised signal for each protein. The lines and error bars show the mean ± s.e.m. The Student's t-test was used to determine significant differences between levels of the proteins in LPD and HPD cells * denotes $P < 0.05$ and ** P denotes < 0.01, n = 3.

This is similar with a previous report demonstrating that aged cells switch from proteasomal to the autophagic pathway as an adaptation to the presence of misfolded proteins (Gamerdinger *et al.* 2009).

In conclusion, ageing of IMR90 fibroblasts is associated with changes in expression of components of ER proteostasis pathways. The accumulation of polyUb and changes in expression of BAGs and Rpt6 indicate that globally the machineries that mediate protein degradation are altered. Increased levels of BiP, phospho- eIF2α and of various UPR-regulated ERAD factors suggest that aged cells may be experiencing elevated levels of ER stress. Analysis of expression level of ER resident and ER associated proteins, and of UPS and autophagic pathways suggests that in HPD cells the capacity to degrade misfolded proteins is affected, which correlated with increased levels of polyUb proteins. Accumulation of high MW Ub conjugated proteins correlate activation of UPR if they include non-degraded ERAD substrates (Kelly *et al.* 2007).

4.3 Protein biosynthesis and translocation into the ER

Several studies have shown that the efficiency of co-translational translocation of at least some ER targeted proteins is reduced during ER stress (Kang *et al.* 2006; Shang *et al.* 2007; Merksamer *et al.* 2008; Miesbauer *et al.* 2009). This has been termed pre-emptive quality control, and is proposed to help prevent the overload of the ER under conditions of reduced folding capacity (Kang et al, 2006). Therefore, it was of interest to determine whether cellular ageing was associated with any changes in the efficiency of protein translocation at the ER. 'Global' ER protein translocation efficiency in LPD and HPD cells was assessed using a modification of the assay established by the Hegde laboratory (Kang *et al.* 2006), in which N-glycosylation is used as a surrogate marker of protein import into the ER. In addition, the translocation of a range of model ER targeted proteins was examined in vitro using a cell-free assay (Wilson *et al.* 1995) in which semi-permeabilised HDP and LPD fibroblasts provided the source of ER membrane for translocation.

The previously established protocol to measure changes in global translocation efficiency (Kang *et al.* 2006) was adapted as schematically presented in Fig 4.5A. Briefly, cells were pulse-labelled with [^{35}S] Met/Cys to radiolabel newly synthesised proteins, then treated with a low concentration of digitonin to selectively permeabilised the plasma membrane and extract cytosolic proteins (Fig 4.5A). The semi-permeabilised cells were then extracted with 1% Triton X-100 to extract proteins from the ER and other intracellular compartments and membranes. The N-glycoproteins were isolated from the TX-100 extract by binding to the lectin concanavalin A (conA). An equal proportion of each fraction was analysed by SDS-PAGE and phosphorimaging (Fig 4.5B). The radioactive signal in each lane was quantified using AIDA software, and the conA bound fraction was expressed as a percentage of the cytosolic proteins

or the unbound proteins (Fig 4.5D), to provide an estimative of what proportion of the newly synthesised proteins were translocated into the ER and subjected to N-glycosylation. In fact, the ratio of N-glycoproteins to cytosolic (conA or unbound) proteins was similar in the two cell populations (Fig 4.5D). Similar results were obtained when the conA bound proteins were expressed as a percentage of total radiolabelled proteins detected when pulse-labelled cells were extracted in 1% SDS (Fig 4.5C), further suggesting that the proportion of nascent proteins imported into the ER and modified with N-glycans, was not significantly different in LDP and HPD cells. These results indicate that cellular ageing is not associated with a global decrease in the efficiency of translocation at the ER. In addition, the results of this assay provide evidence that the overall load of client proteins entering the ER is similar in LPD and HPD cells.

Next, it was tested whether the young and old cells differed in their ability to downregulate translocation in response to ER stress – i.e. the efficiency of pre-emptive QC. Briefly, the cells were left untreated or treated with 2 mM DTT during the pulse-labelling to induce acute ER stress. These conditions were previously shown to result in attenuation of ER translocation in cultured cells (Kang *et al.* 2006), The cytosolic and N-glycosylated proteins isolated as previously described (Fig 4.5A). Samples of the cytosolic and conA bound fractions were analysed by SDS-PAGE and phoshorimaging (Fig 4.6). In both HPD and LPD cells, treatment with DTT resulted in a decrease in the amount of radiolabelled proteins in the cytosolic and conA-bound N-glycosylated fractions (Fig 4.6A), as expected following activation of the UPR and phosphorylation of eIF2α. However, when the conA bound proteins were expressed as a proportion of the cytosolic proteins, it was clear that the effect of DTT treatment reduced the amount of conA bound N-glycoproteins (Fig 4.6A, lanes 5, 8) more dramatically than the cytosolic proteins (Fig 4.6A lanes 2, 4). Thus, the ratio of conA bound N-glycoproteins to cytosolic proteins decreased significantly following DTT treatment (Fig 4.6B). This is consistent with translocation attenuation in response to ER stress (Kang *et al.* 2006; Wang & Kaufman 2012), and provides evidence that the overall efficiency of protein entry into the ER was reduced following DTT-induced ER stress. As observed in the previous set of experiments (Fig 4.5), in the untreated samples, the ratio of N-glycoproteins to cytosolic proteins was similar in both LPD and HPD cells (Fig 4.6 B). Interestingly however, the ratio of N-glycoproteins to cytosolic proteins decreased significantly more in HPD than LDP (Fig 4.6B, compare LPD and HPD + DTT). Thus, inducing ER stress appears to inhibit protein import into the ER (as measured by N-glycosylation) in HPD cells to a greater extent compared to LDP. This indicates that in vitro ageing of IMR90 fibroblasts may be associated with changes in ER homeostasis.

Several studies indicated that the extent to which translocation can be regulated by ER stress depends upon the precise nature of the ER targeting signal sequence (Hegde & Kang 2008). Hence, some proteins appear to have less efficient and more ‘regulatable’ signal sequences that may be more severely affected by conditions of ER stress (Rane *et al.* 2008), such as might potentially occur with cellular ageing.

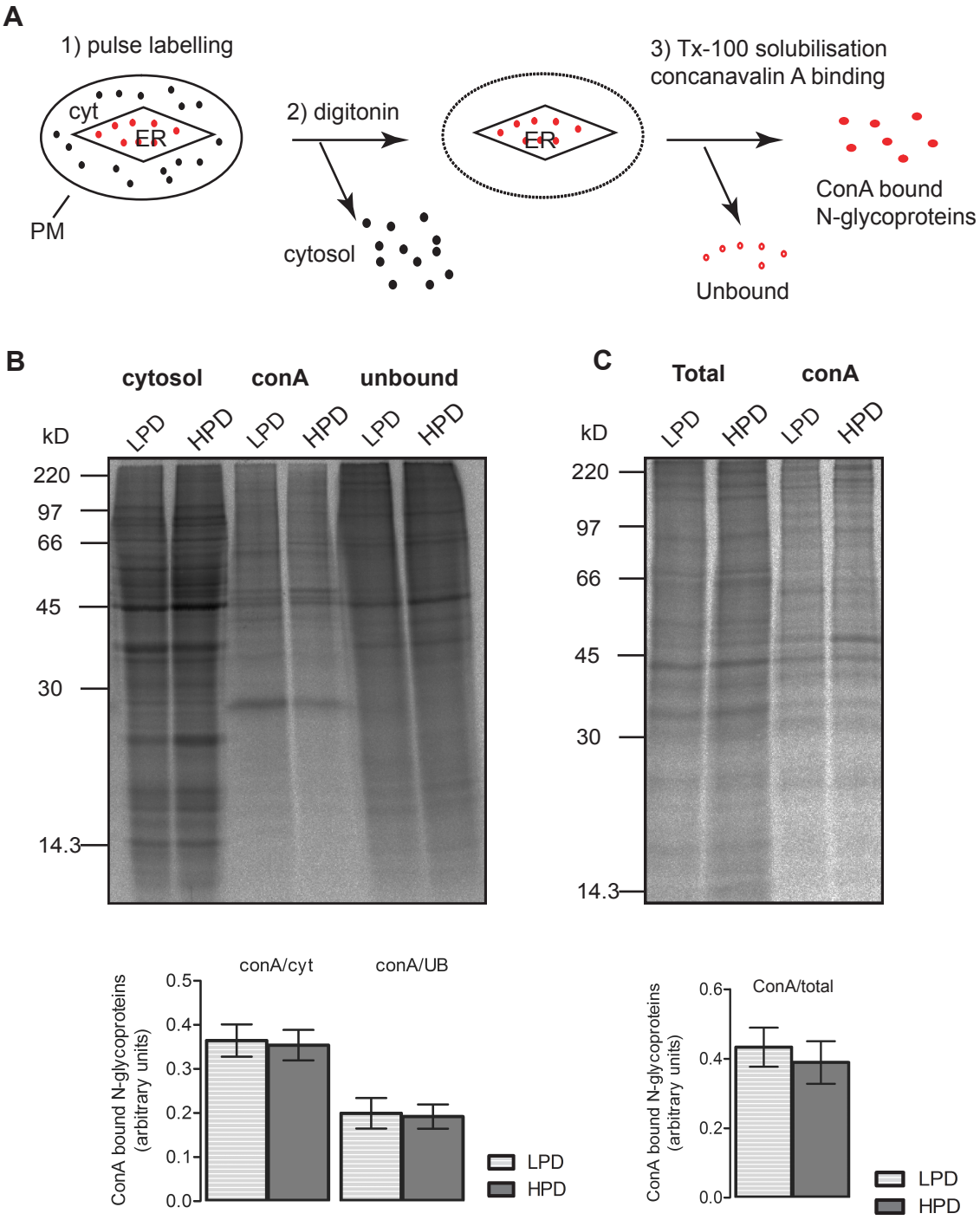

Figure 4.5: General glycoprotein biosynthesis in LPD and HPD cells.
(A) Schematic representation of the protocol. Cells were pulse labelled (step1), followed by digitonin treatment on ice and the cytosolic fraction was extracted (step 2). Then cells were lysed in buffer containing 1% Triton X-100 and the lysate was incubated with conA -sepharose (step 3). The conA bound glycoproteins were eluted with 0.25 M α-methylmannosidase.
(B) Radiolabelled proteins from cytosol, conA-bound, and conA-unbound fractions. The cytosol and unbound fractions were subject to TCA precipitation and 1/10th of cytosol and unbound and 1/3rd of conA bound fraction were analysed by SDS-PAGE and phosphorimaging. Each lane was quantified using AIDA software and the conA bound fraction was expressed relative to cytosol, or to unbound fraction and plotted as mean ± s.e.m., n = 6.
(C) Total radiolabelled cell lysate (total) and glycoproteins (conA). Cells were pulse-labelled and lysed in 1% Triton X-100 buffer. A tenth of the lysate was kept as total. The remaining lysate was incubated with conA and the glycoproteins were eluted with α-methylmannosidase.
The lanes were quantified and the con A bound fraction was expressed relative to total cell lysate and plotted as mean ± s.e.m., n = 6.

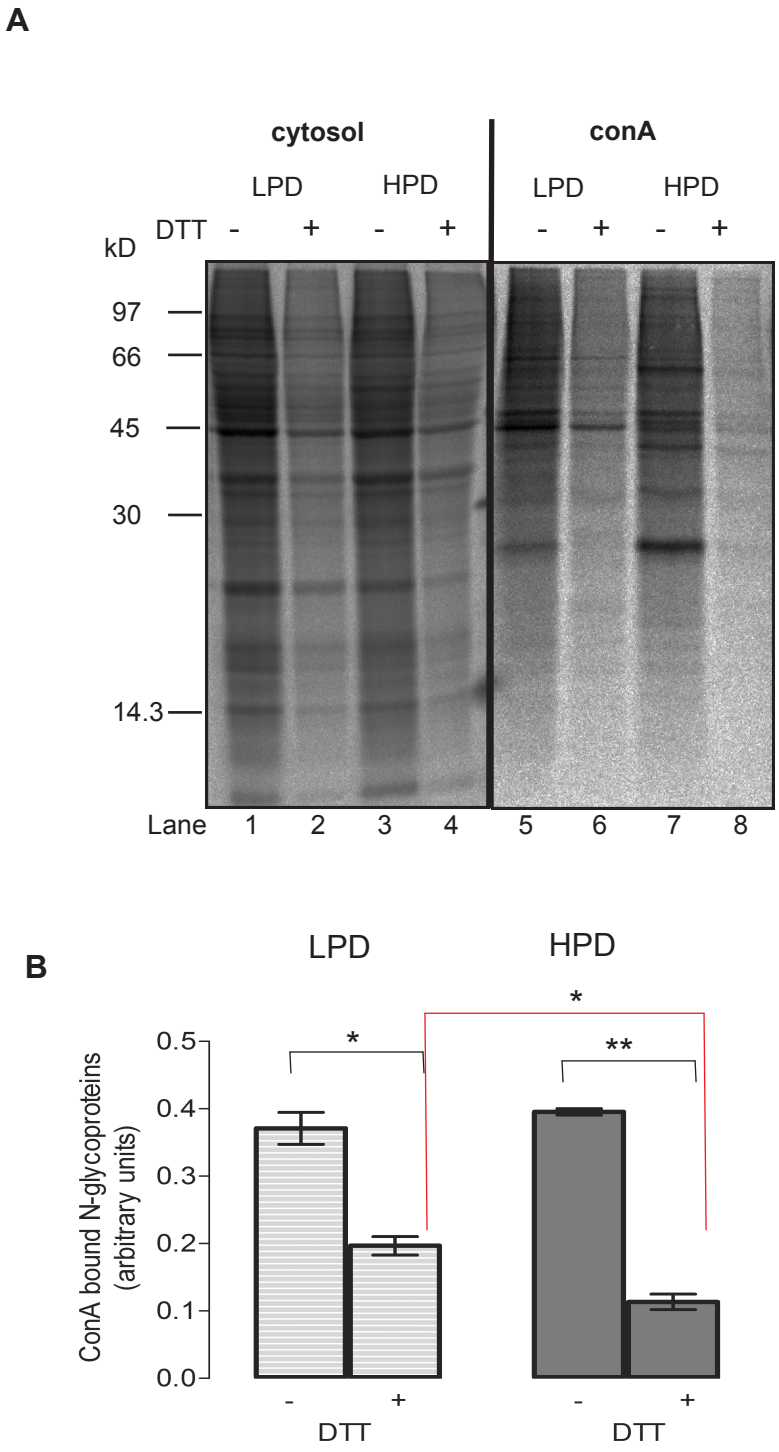

Figure 4.6: General glycoprotein biosynthesis in LPD and HPD cells following DTT treatment. (A) Cells were pulse labelled in the presence (+) or absence (-) of 2 mM DTT, followed by digitonin treatment on ice, to extract the cytosol. Then cells were lysed in buffer containing 1% Triton X-100 and the lysate was incubated with con A. The conA bound glycoproteins were eluated by incubating the resin with 0.25 M α-methylmannosidase. The radiolabelled samples from cytosol and conA-bound fractions were separated on a12% SDS gel and the gel was dried and exposed to PhosphorImager plates. **(B)** The lanes were quantified and the conA-bound fraction was normalised to the cytosol fraction and plotted as mean ± s.e.m. The statistical significance was determined by using a two way ANOVA test with a slice test (* $P < 0.05$, ** $P < 0.01$), n = 3. The red lines show the statistical significance for the DTT treated samples.

Therefore, the translocation efficiency of several membrane and secretory proteins was examined individually using an *in vitro* translation/translocation system (Fig 4.7B). Two proteins with 'low' efficiency signal sequences were chosen, namely gamma interferon (γ-INF) and the viral protein US2 (Kim *et al.* 2002; Drori *et al.* 2010). In contrast, pre-prolactin (pPL) was chosen as it has a highly efficient signal sequence (Kim *et al.* 2002). In addition, two proteins with multiple transmembrane domains, signal peptide peptidase (SPP) and opsin (ops), which require multiple interactions with the translocon, were selected together with haemagglutinin (HA), a single spanning type I protein with multiple glycosylation sites and disulphide bonds, as more challenging substrates for translocation apparatus. mRNA encoding each substrate was translated using an in vitro translation system (rabbit reticulocyte lysate) in the presence of [^{35}S] Met/Cys and semi-permeabilised LPD or HPD cells to provide ER membranes for translocation (Wilson *et al.* 1995). The advantage of this *in vitro* technique is that it allows examination of the ER processing capacity of individual ER targeted model proteins. Since the cytosolic components required for translation are provided by the reticulocyte lysate, any age-related changes in these factors can be ruled out. The radiolabelled translation products were analysed by SDS-PAGE and phosphorimaging (Fig 4.7Ai-vii). Five of the substrates are N-glycosylated, and therefore this modification was again used as a marker for entry into the ER, allowing the efficiency of translocation to be estimated based on percent of the total translation product that was N-glycosylated (Cross *et al.* 2009a). Endoglycosidase H (EndoH), which removes high-mannose structures, was used to confirm the identity of the N-glycosylated product in each case. The EndoH treatment leads to disappearance of the higher MW translation products that represent the N-glycosylated proteins which have been translocated across the ER membrane. Two major radiolabelled γ-IFN translation products were observed in both LDP and HPD cells (Fig 4.7Ai, lanes 1 and 3, Fig 4.7Avii lane 1). Following EndoH treatment, the higher MW form was lost (Fig 4.7Aii, lanes 2 and 4, Fig 4.7Avii lane 2), showing that it represented a N-glycosylated species. In contrast, the lower MW band was not affected by EndoH treatment (Fig 4.7Ai, lanes 2 and 4), showing that this was a non-glycosylated form. When the in vitro translated γ-INF was treated with proteinase K, which digests the polypeptide chains unprotected by membranes, this lower MW species disappeared (Fig 4.7Avii lane 3), showing that it was not protected within the lumen of the ER and therefore represents an untranslocated form of the protein. The higher MW glycosylated form(s) however was not degraded by proteinase K in the absence of detergent (Fig 4.7Avii lane 3) demonstrating that this band represents γ-INF that had been translocated into the lumen of the ER and was thus protected from the protease. Following EndoH treatment, an additional lower MW species which migrated just below the non-glycosylated form, was generated (Fig 4.7Ai and vii lane 1). This form was not degraded by proteinase K (Fig 4.7 Avii lane 4), therefore this specie represents the signal sequence cleaved, de-glycosylated form of γ-IFN.

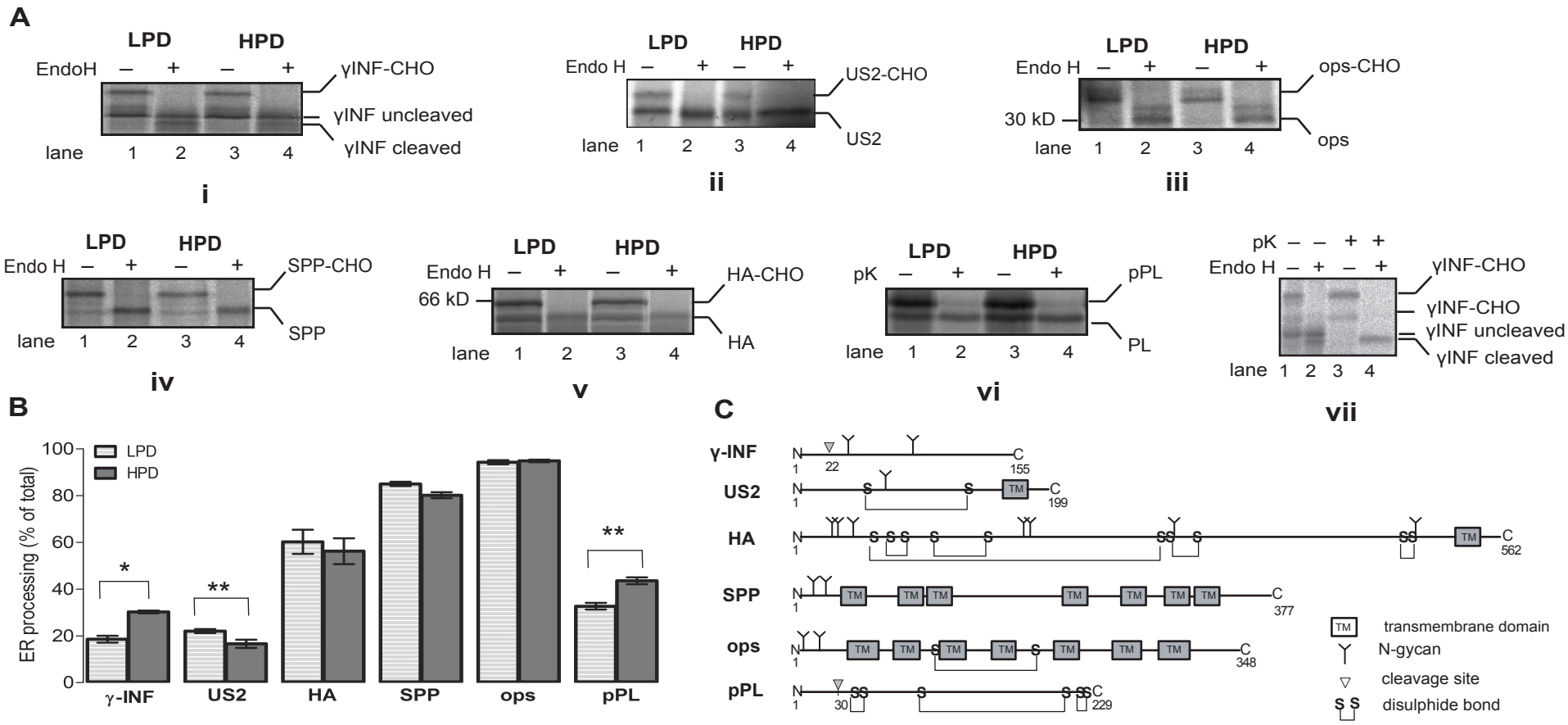

Figure 4.7: Analysis of translocation in LPD and HPD cells.
(A) mRNA were in vitro translated in the presence of [35S] Met/Cys and LDP and HPD semi-permeabilised cells, and the products were proteinase K or Endo H treated, as indicated. The samples were loaded onto 10% (HA) and 12% Tris-glycine gels and following drying, the gel was exposed to a Phosphoimager plate. **(B)** Each band was quantified using the AIDA software. The glycosylated form representing the translocated substrate was plotted as a percentage of total. In the case of pPL, protease K protection was used for monitoring translocation and the signal sequence cleaved pPL was plotted as percentage of total radiolabelled product. The Student's t-test was used to determine significant differences between levels of the proteins translocation in LPD and HPD cells. * denotes $P < 0.05$ and ** P denotes < 0.01, $n = 3$. **(C)** Scheme showing the topology of each protein used, indicating the glycosylation and cleavage sites.

Altogether, these experiments show that the high MW form of γ-IFN represents N-glycosylated ER translocated protein, whilst the lower MW form represents a non-translocated, signal sequence uncleaved form. Thus, the amount of the glycosylated γ-INF was quantified and expressed as percentage of the total translated product to provide a measure of the γ-IFN translocation efficiency (Fig 4.7B). The mean data from 3 experiments showed that a significantly greater proportion of γ-INF was translocated across the ER of semi-permeabilised HPD cells and N-glycosylated (30%) compared to LPD cells (19%). However, this difference was not observed for the other ER targeted proteins. The other glycosylated proteins (US2, SPP, HA and opsin) lacked cleavable signal sequences, and just two translation products were generated for each of these proteins (Fig 4.7Aii-v lanes 1 and 3). In each case, the upper band was lost upon EndoH treatment, demonstrating that these represented the ER translocated N-glycosylated form of the proteins. The lower MW forms were not sensitive to EndoH showing these were unglycosylated non-translocated forms (fig 4.7Aii-v lanes 2 and 4). The N-glycosylated form was quantified and expressed as percentage of total translated product and was represented graphically in each case (Fig 4.7B). Similar to γ-IFN, the efficiency of US2 translocation was quite low, as judged by N-glycosylation, and, consistent with having a 'weak' signal sequence (Fons *et al.* 2003), In contrast to γ-INF however, US2 was less efficiently translocated in HPD than LPD (Fig 4.7B). The polytopic membrane proteins (SPP, ops) were translocated very efficiently (more than 80% N-glycosylated) and showed no difference between LPD and HPD cells. Similarly, the single spanning HA protein appeared to be translocated and N-glycosylated with equal efficiency in LPD and HPD cells.

Translation of the last substrate (pPL) generated two products (fig 4.7). Because pPL is not glycosylated but has cleavable signal sequence, these most likely represent the uncleaved and cleaved forms of the protein (Cross *et al.* 2009a). Proteinase K treatment was used to discriminate between the translocated and non-translocated forms of pPL. The disappearance of the upper band after the proteinase K treatment showed that this form was not translocated into ER lumen. The resistance of the lower band to the proteinase K treatment demonstrates that this was the translocated form of pPL, also called prolactin (PL), consistent with its signal peptide having been cleaved leading to more rapid migration (Fig 4.7Avi, lanes 2 and 4). Slightly surprisingly, quantification of the cleaved PL as percentage of total revealed that the proportion of this translocated form of PL was very low (35-40%) despite it supposedly having a 'strong' signal sequence (Kim *et al.* 2002). However, when the efficiency of translocation (as indicated by ER processing – N-glycosylation or signal sequence cleavage) was compared between LPD and HPD cells, PL appeared to be more efficient translocated into the ER of semi-permeable HPD cells than LPD cells, as observed for γ-IFN.

From these functional analyses of ER, it seems that overall rate of protein synthesis and the load of client proteins entering ER are similar in LDP and HPD cells. Also, the global translocation efficiency, as measured by proportion of proteins receiving N-glycosylation is

similar in LPD and HPD cells. However, in response to ER stress, it seems that HPD cells downregulate translocation to a greater extent than LPD cells, indicating that ER homeostasis in HPD cells may already be slightly perturbed. Analysis of the translocation of individual substrates did not give a consistent picture (Kim *et al.* 2002), but some differences were seen with translocation of two ER targeted proteins (γ-INF and pPL) increasing, and another one (US2) decreasing. The differences seemed to be observed in those substrates that were less efficiently processed by ER, possible indicating that translocation machinery could be organised or regulated differently.

4.4 Folding and trafficking in the secretory pathway

Next, the capacity of HPD and LPD fibroblasts to fold and export cargo protein was examined. To address this issue, a temperature sensitive mutant of the vesicular stomatitis virus glycoprotein (tsO45 VSV-G), was used. VSV-G is a type I membrane viral glycoprotein, and the tsO45 variant harbours a mutation that causes a single amino acid substitution and makes the folding of the mutant protein temperature dependent (Gallione & Rose 1985). Thus, at lower temperatures, tsO45 VSV-G is able to achieve its native structure and is transported along the secretory pathway to plasma membrane, but at higher temperatures becomes misfolded and is therefore retained by the ER QC system and prevented from moving along the secretory pathway (Mezzacasa & Helenius 2002). This means that a pool of misfolded tsO45 VSV-G can be synthesised in the ER at the non-permissive temperature. Subsequently, reducing the temperature allows the protein to fold correctly, and the export of a synchronous wave of the cargo protein can be monitored. The tsO45 VSV-G is a glycoprotein, and in its misfolded ER localised state, the N-glycans remain sensitive to EndoH digestion. However, when it reaches the medial Golgi apparatus, the N-glycans undergo further modifications (e.g additional trimming of the mannose residues) and tsO45 VSV-G becomes resistant to EndoH. Therefore, the folding state can be assessed biochemically by resistance of the N-glycans to EndoH, and microscopically by visualising its subcellular localization. Thus at restrictive temperatures (above 39.5^{o}C) tsO45 VSV-G is retained in the ER and is EndoH sensitive, whereas at permissive temperature (32^{o}C), it acquires the native conformation, is exported to the Golgi apparatus and becomes EndoH resistant (Mezzacasa & Helenius 2002; Vasserman *et al.* 2006). As such, tsO45 VSV-G represents a metastable protein, in that it is folded under permissive conditions (e.g. permissive temperature), but misfolds under suboptimal conditions (e.g. restrictive temperature). Therefore it can be used as 'folding sensor' to monitor the folding landscape or folding efficiency within the in ER.

First, the biochemical assay was tested by growing cells infected with adenovirus encoding VSV-G overnight at restrictive (40^{o}C) and permissive (32^{o}C) temperatures. Following lysis, the samples were EndoH treated and analysed by infrared western blotting (Fig 4.8A) As predicted, EndoH treatment caused a decrease in the MW of protein obtained from cells at restrictive temperature, showing that the N-glycans remained in an EndoH sensitive state at this

temperature, and allowing the N-glycosylated (Fig 4.8A, lane 1) and de-glycosylated (Fig 4.8A, lane 2) forms of VSV-G to be identified. When cells were grown at the permissive temperature, VSV-G became resistant to EndoH and no shift in MW was observed (Fig 4.8A, lanes 3 and 4), showing that under these conditions the protein had reached the medial Golgi apparatus. The kinetics of VSV-G folding and transport to the Golgi apparatus was analysed using a temperature shift and cycloheximide chase approach, followed by western blotting to monitor the acquisition of EndoH resistant N-glycans (Fig 4.8B). Cells were infected with adenovirus encoding tsO45 VSV-G, and were incubated overnight at 40^{o}C to allow synthesis of VSV-G, then shifted to 32^{o}C and treated with cycloheximide to inhibit further VSV-G synthesis, and incubated for 0-240 min at 32^{o}C. At each time point, the cells were harvested and treated with EndoH prior to SDS-PAGE and western blotting with anti-VGV-G. At time zero (i.e. before shifting to the lower temperature), all the VSV-G in LPD and HPD cells was converted to the lower MW form following EndoH treatment (Fig 4.8B, lanes 1 and 7). This shows that at the start of the chase, only the EndoH sensitive from of VSV-G was present in both LPD and HPD cells, consistent with the protein being in an ER retained misfolded state. Upon incubation at 32^{o}C, this lower MW form decreased in intensity, whilst the higher MW EndoH resistant form of VSV-G began to appear (Fig 4.8B, lanes 3-6 and 9-12). The conversion of the EndoH sensitive form to the EndoH resistant form reflects folding of the previously misfolded VSV-G and transport from the ER to the medial Golgi apparatus. In the LPD cells, the EndoH resistant form was clearly visible after 40 minutes of chase (Fig 4.8B, lane 3), and the intensity of this band increased with the incubation time, as more of the protein was folded and transported to the Golgi apparatus (Fig 4.8B, lanes 4-6). After 60 minutes, the EndoH resistant form was the major species (Fig 4.8B, lanes 4-6). Interestingly, the VSGV-G expressed in HPD cells appeared to acquire Golgi apparatus modification more slowly than HPD cells (Fig 4.8B, lanes 7-12). This is most obvious at 60 and 90 min chase when only a small proportion of the VSV-G was in the EndoH sensitive form in LPD cells, whilst much more of this form was seen in the HPD cells (Fig 4.8B, lanes 10 and 11). The signal intensity of the two forms of VSV-G at each time point was quantified, and the ratio of EndoH resistant to EndoH sensitive VSV-G was plotted against time (Fig 4.8C). Comparison of the results obtained with LPD and HPD showed a significant delay in the aquisition of EndoH resistant form in HPD cells (Fig 4.8C). This difference was statistically significant at each time point after 20 min, (Fig 4.8B, compare lane 4 and 10, 5 and 11), These results are very interesting because they suggest that the in vitro aged HPD cells may have a reduced ability to fold and VSV-G in the ER and export it to the Golgi apparatus.

Delayed acquisition of VSGV-G EndoH resistance in HPD cells could be explained by differences in the capacity of the ER to properly fold the misfolded VSV-G upon shifting to 32^{o}C, or by changes in the efficiency of vesicular transport from the ER to the Golgi apparatus, or both. In order to address this, the rate of VSV-G traffic from the ER to Golgi apparatus was measured in LPD and HPD cells. To do this, the temperature shift assay was adapted based on a protocol described by Mezzacasa and Helenius (Mezzacasa & Helenius 2002), presented

schematically in Fig 4.10A. After the accumulation of misfolded tsO45 VSV-G by growing cells at the restrictive temperature overnight, the cells were treated with cycloheximide and incubated at 10^{o}C for 2 hours.

At this temperature VSV-G acquires the correct conformation and accumulates in ER exit sites, but does not leave ER since vesicular transport from the ER is restricted at this low temperature (Mezzacasa & Helenius 2002). Then cells were shifted to 32^{o}C, releasing inhibition of vesicular traffic and allowing the VSV-G that had accumulated in the ER exit sites to be transported to the Golgi apparatus. Since the VSV-G protein that entered the ER exit sites at 10^{o}C will have been properly folded (Mezzacasa & Helenius 2002), the appearance of the EndoH resistant form should reflect the rate of vesicular transport from the ER to the medial Golgi apparatus. First, immunofluorescence microscopy was used to confirm the sub-cellular localization of VSV-G at the different temperatures (Fig 4.9). At 40^{o}C VSV-G was distributed throughout cell and visible as a ring around the nucleus (Fig 4.9, panels 1 and 4). In both HPD and LPD, the protein showed a high level of co-localisation with calnexin (Fig 4.9, panels 1 and 4). This is consistent with biochemical analysis showing that the N-glycans were EndoH sensitive this temp (Fig 4.8A), and confirms the ER localization of VSV-G at 40^{o}C. After the incubation at 10^{o}C, the distribution of VSV-G was changed and it was seen in punctate structures (Fig 4.9, panels 2 and 5). These structures were positive for the COPII subunit Sec24, providing evidence that following 2 hours at 10^{o}C, the VSV-G was accumulated in ER exit sites. The Golgi apparatus localization after 40 minutes pulse at 32^{o}C was confirmed by the co-localization with the Golgi apparatus marker GM130 (Fig 4.9, panels 3 and 6).

Having confirmed that the 40^{o}C-10^{o}C-32^{o}C temperature shifts produced the expected distribution of VSV-G, the kinetics of delivery of VSV-G to the medial Golgi apparatus was analysed by monitoring the acquisition of EndoH resistant N-glycans when the temperature was shifted from 10 to 32 (Fig 4.10B). Consistent with the previous experiments and ER localisation seen in the microscopy, at 40^{o}C no EndoH resistant form of VSV-G was detected (Fig 4.10B, lanes1 and 8), confirming that the protein had not reached the Golgi apparatus. Similarly, at the end of the two hour incubation at 10^{o}C, VSV-G remained completely EndoH sensitive (Fig 4.10B, lanes 2 and 9), showing that despite entering ER exit sites, the protein was not delivered to the Golgi apparatus. When the cells were shifted to 32^{o}C, Endo H resistant VSV-G began to appear (Fig 4.10B). Starting after 40 minutes at 32^{o}C, the upper EndoH resistant band became visible and its intensity increased with time, whilst the intensity of the lower EndoH sensitive form decreased, showing that the VGV-G was being delivered to the medial Golgi apparatus. There is not a perfect match with the data obtained from immunofluorescence microscopy which suggests that by 40 minutes of chase almost all the VSV-G is in Golgi apparatus, whereas less than 50% had obtained EndoH resistance at this time (Fig 4.10B, lanes 4 and 11). This might be explained if a proportion of VSV-G detected by co-localization with GM130 was in the cis Golgi apparatus/ERGIC at this point, as this would still be expected to be EndoH sensitive.

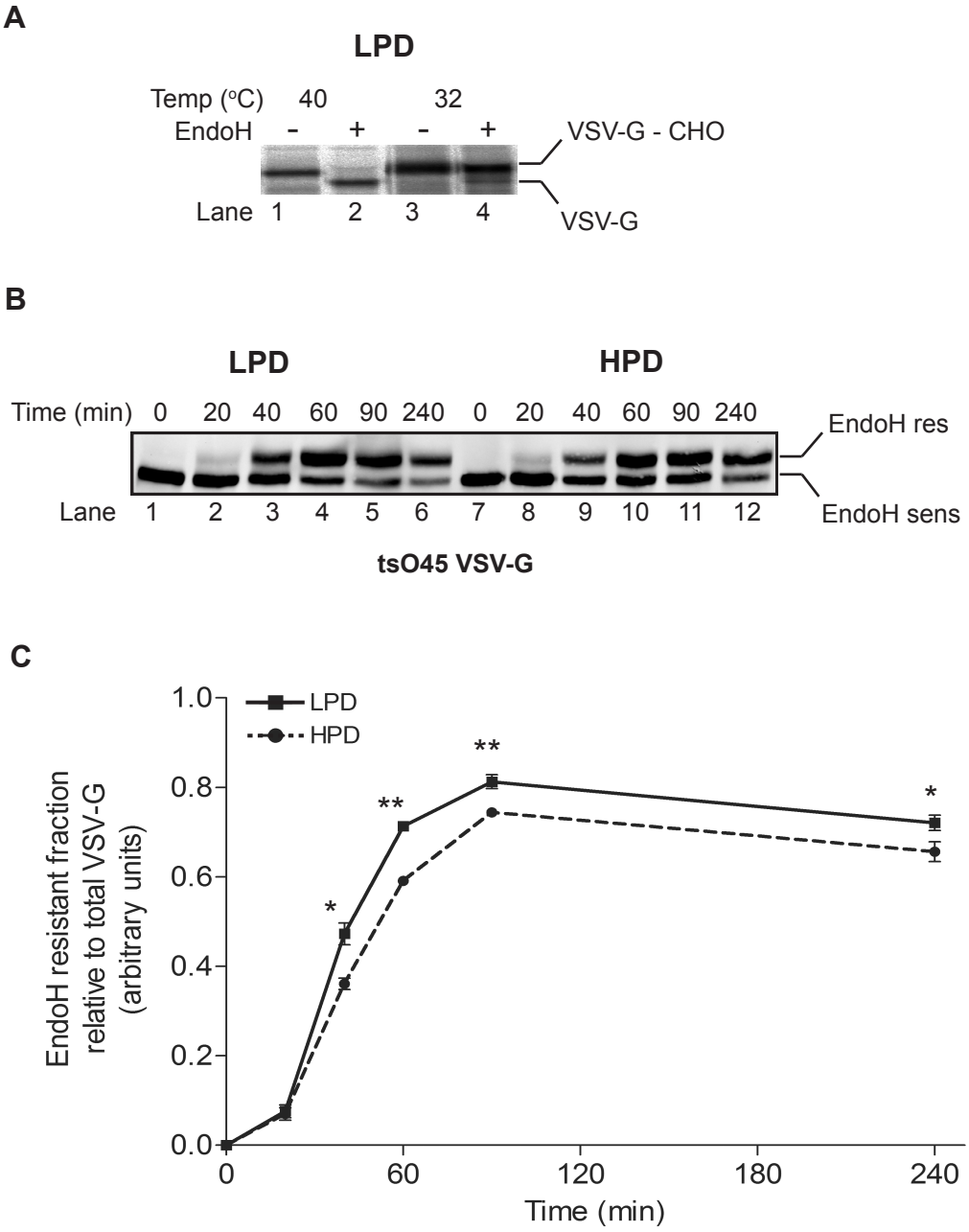

Figure 4.8: Analysis of folding and traffic of ts VSV-G in LPD and HPD cells.
(A) VSV-G infected cells were incubated at 40°C and respectively at 32°C overnight. The next day cells were lysed, EndoH treated and analysed by Western blotting with anti-VSV-G primary antibody, followed by incubation with infrared secondary antibodies.
(B) VSV-G infected cells were incubated overnight at 40°C. The next day cycloheximide was added and the cells were shifted at 32°C. Cells were then incubated at 32°C for the indicated time points, lysed and EndoH treated. Equal amounts of sample were separated by 8% SDS-PAGE and then analysed by Western blotting with the anti-VSV-G antibodies. The EndoH resistant form and the EndoH sensitive form are indicated.
(C) The signal intensity of both bands as quantified and the EndoH resistant fraction relative to total VSV-G was plotted against time as mean ± s.e.m. The statistical significance was determined by two way ANOVA completed with a slice test for each time point and it is shown on the graph (* $P < 0.05$, ** $P < 0.01$), n = 3.

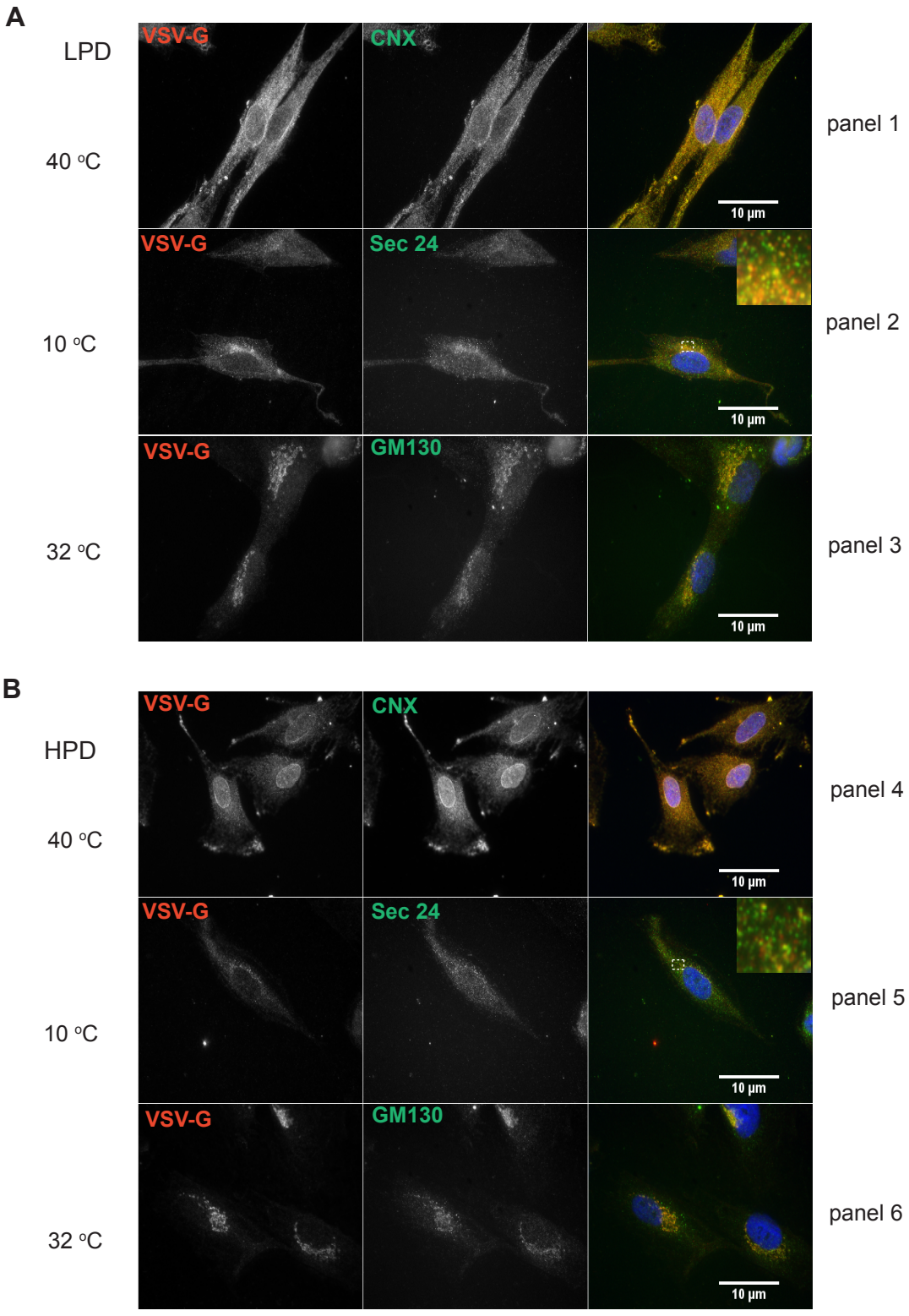

Figure 4.9: The ER to Golgi traffic of ts VSV-G in LPD and HPD cells.
VSV-G infected cells were incubated overnight at 40°C. Next day the cells were shifted to 10°C for 2 hours, then chased for 40 minutes at 32°C. The cells were methanol fixed and permeabilised and analysed by indirect fluorescence. The nuclei were stained with DAPI (blue). Colocalization of VSV-G (stained in red) with calnexin, Sec24 or GM130 (green) appears as yellow (right colum). Inserts (cf dashed boxes) are the magnified images showing the co-localization of VSV-G with ER exit sites marker Sec24.
LPD **(A)** and HPD **(B)** cells.

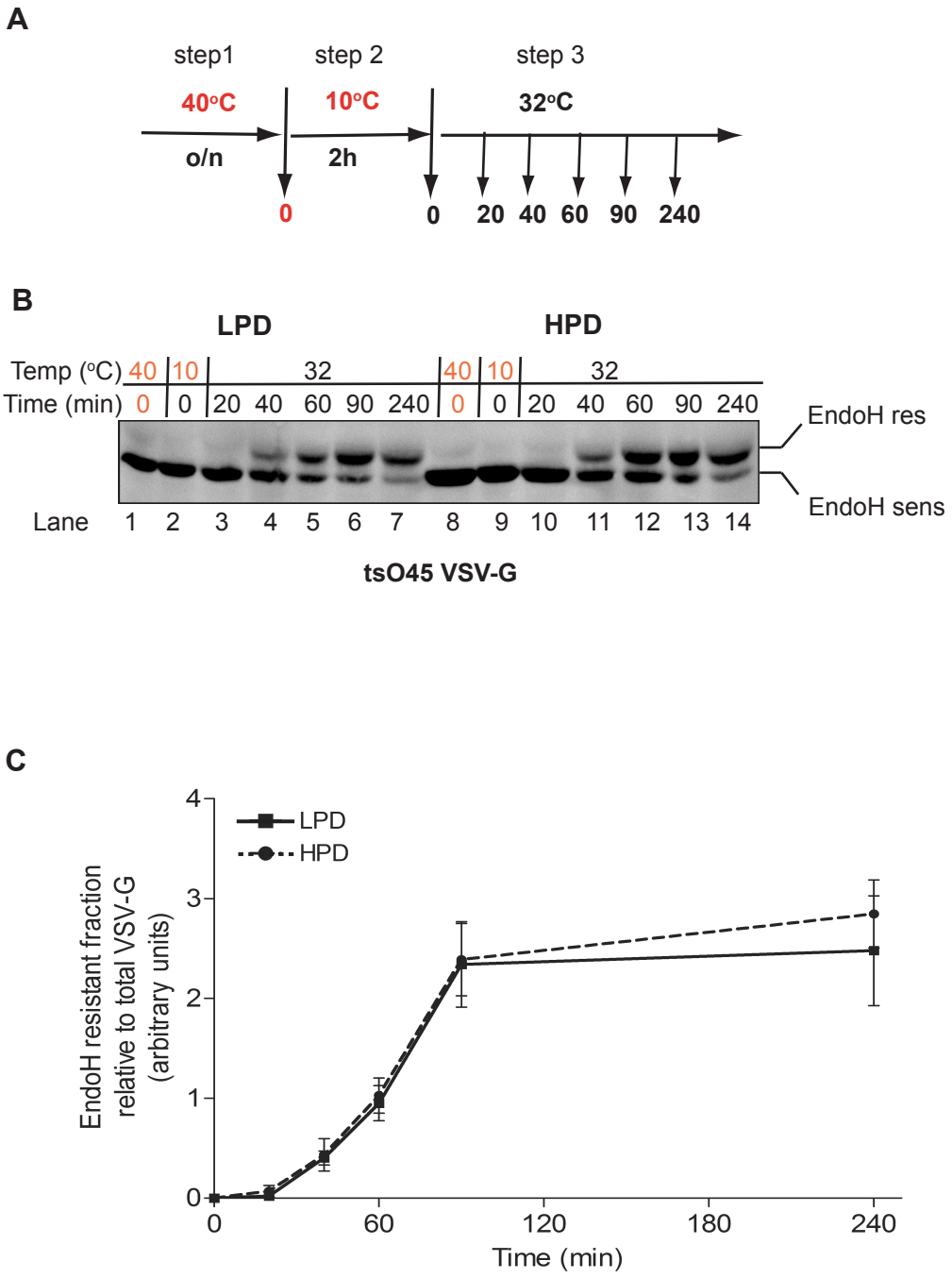

Figure 4.10: The ER to Golgi traffic of ts VSV-G in LPD and HPD cells.
(A) Scheme of the assay. VSV-G infected cells were incubated overnight at 40°C (step1). The next day cycloheximide was added and the cells were shifted to 10°C for 2 hours (step2), then chased for the indicated times at 32°C (step3).
(B) Cells were lysed, EndoH treated and analysed by SDS-PAGE and Western blotting. The EndoH resistant form and the EndoH sensitive form are indicated.
(C) The EndoH resistant fraction relative to total amount of VSV-G was plotted against time as mean ± s.e.m.

The signal intensity of each form was quantified and the ratio of EndoH resistant to EndoH sensitive VSV-G was plotted against time to provide a measure of the rate of delivery to the medial Golgi apparatus (Fig 4.10C). This showed the rate at which EndoH resistance was acquired was the same in both LPD and HPD cells. No differences in the ratio of EndoH resistant to EndoH sensitive VSV-G was seen between LPD and HPD cells at any time point (Fig 4.10C). These results are interesting because they provide evidence that the rate of vesicular traffic from the ER to the medial Golgi apparatus in LPD and HPD cells is similar. Thus, the effect of ER – Golgi apparatus traffic on the previous experiment regarding the kinetics of VSV-G folding (Fig 4.8B) could be considered minimal. This suggests that the delay in delivery of VGV-G to the medial Golgi apparatus upon shifting directly from 40^{o}C to 32^{o}C observed in the previous experiment (Fig 4.8B, C) was more likely due to differences in the ability of HDP and LPD cells to mediate folding of VSV-G and/or incorporate protein into ER exit sites. In order to try and examine the folding capacity of LPD and HPD more directly, cells expressing tsO45 VSV-G were grown at a range of different temperatures between 32^{o}C and 40^{o}C. The following day, the proportion of the total VSV-G that was resistant to EndoH at each temperature was determined in order to provide a readout of the proportion of the protein that had successfully achieved the correct conformation and been transported through the Golgi apparatus at each temperature. Metastable proteins such as temperature sensitive mutant proteins (e.g. ts myosin, ts VSV-G) are highly dependent on molecular chaperones for acquiring the correct folded, active conformation, thus can be useful sensors of folding status (Ben-Zvi *et al.* 2009). In contrast to the previous assays, this experiment observed the total pool of protein at steady state in order to gain information about the folding capacity of the ER. As seen previously, at 40^{o}C the VSV-G was completely EndoH sensitive in both LPD and HPD cells (Fig 4.11A lanes 1 and 7). As the temperature that the cells were grown at was reduced, an increasing proportion of the protein was in the EndoH resistant form (Fig 4.11A lanes 2-6 and 8-12), suggesting that with decreasing temperature a greater fraction of the VSV-G was able to fold correctly and proceed through the Golgi apparatus. The signal intensity of each form was quantified, and the EndoH resistant protein was expressed as a percentage of the total VSV-G to provide a readout of the relative amount of properly folded protein at each temperature (Fig 4.11B). This revealed a clear difference in the temperature sensitivity of VSV-G folding in the HPD and LPD cells. Even at the permissive temperature, 32^{o}C, a greater proportion of the VSV-G protein in HPD cells was in a form that was resistant to EndoH (Fig 4.11B), suggesting that more of the protein misfolds in HPD compared to LPD. This was also seen at temperatures up to 38^{o}C, when essentially all the protein was in the EndoH sensitive form in both HPD and LPD cells (Fig 4.11, lanes 3-4 and 9-11). These results suggest that VSV-G misfolds more extensively in HPD, providing further evidence that the folding capacity in the ER of these in vitro aged cells is lower than in the LPD cells. Altogether, the results using the metastable tsO45 VSV-G are consistent with a reduced folding capacity in the ER in HPD cells compared to LPD cells. This indicates that cellular ageing may be associated with a decline in ability of ER to properly fold proteins.

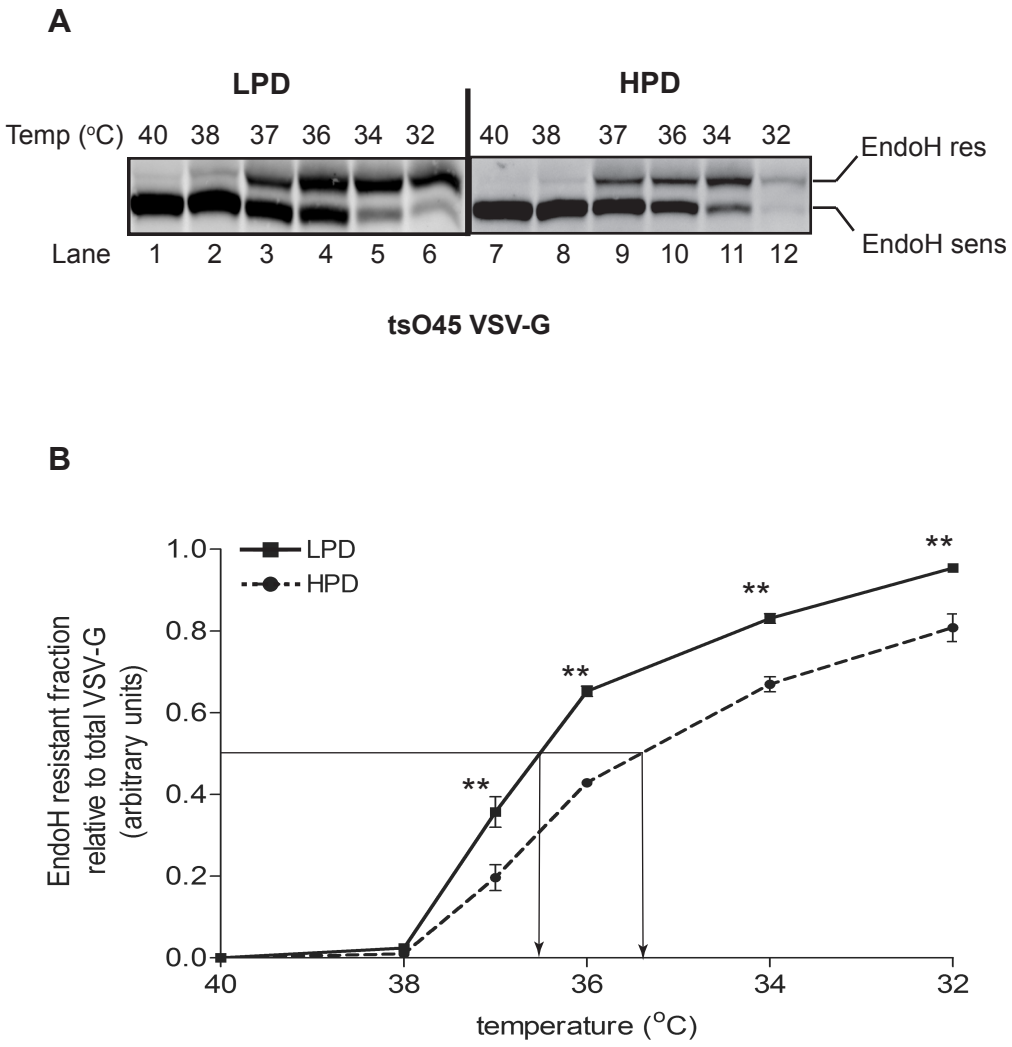

Figure 4.11: Analysis of folding capacity in LPD and HPD cells.
(A) VSV-G infected cells were incubated overnight at the indicated temperature. The next day the cells were lysated and samples were EndoH treated. Equal amounts of sample were loaded onto an 8% SDS gel and then analysed by immunoblot. with anti-VSV-G antibodies. The EndoH resistant and the EndoH sensitive forms are indicated above.
(B) The EndoH resistant fraction was expressed as proportion of total VSV-G at each temperature. The statistical significance was determined by two way ANOVA completed with a slice test for each temperature point and is shown on the graph (* $P < 0.05$, ** $P < 0.01$), n = 3. The estimated temperature at which 50% of VSV-G is EndoH resistent is shown on the graph.

4.5 Assessing ER - associated degradation

As well as folding pathways, protein degradation pathways are key components in maintaining ER homeostasis. To investigate whether the efficiency of ERAD to eliminate misfolded proteins was decreased in the cellular model of ageing, the stability of two well characterised ERAD substrates was examined. The null Hong - Kong variant of α1 antitrypsin (NHK α1AT) is a C-terminally truncated form of the soluble glycoprotein α1 antitrypsin, which is folding defective and is degraded via ERAD (Sifers *et al.* 1988). The alpha subunit of the T-cell receptor complex (TCRα) is a type I membrane glycoprotein, and when expressed in the absence of partner subunits, unassembled TCRα is rapidly degraded by the ERAD machinery (Lippincott-Schwartz *et al.* 1988). To determine the rate of degradation of both NHK α1AT and TCRα, HDP and LPD cells were transiently transfected with plasmids encoding these proteins, then treated with the protein synthesis inhibitor cycloheximide (CHX) to prevent further protein synthesis. The loss of TCRα or NHK α1AT over time was then monitored by harvesting cells at different time points following addition of CHX, followed by western blotting cell lysates in order to determine the amount of each protein remaining. A single band, representing the NHK α1AT was observed at ~46 kDa as expected (Fig 4.12A). Similarly, the immunoblot analysis of TCRα (Fig 4.12B) showed only a single major reactive band higher at a MW slightly higher than 46 kDa. The intensity of the signal obtained with TCRα and α1AT was normalised relative to actin. In order to determine rate of degradation, the amount of each protein remaining at each time point was expressed as percentage of that present at start of chase (Fig. 4.12A and Fig 4.12B). In LDP cells, levels of NHK α1AT decreased rapidly following addition of CHX, with only 30% remaining after 4 hours of chase, consistent with the rapid degradation of this protein via ERAD (Liu *et al.* 1997; Oda *et al.* 2003; Christianson *et al.* 2008). In HPD cells however, the rate of NHK α1AT degradation was considerably slower, with significantly more of the protein remaining at each time point. Similarly, TCRα was rapidly lost following addition of CHX in LPD cells, with only 35% of protein remaining at 2 hours (Fig 4.12B), showing that it was efficiently degraded in these cells. Again, the loss of TCRa cells was also significantly slower in HPD cells. These data suggest that degraded both ERAD substrates were degraded more slowly in HPD cells.

These two ERAD substrates have different requirements for various ERAD components (Huppa & Ploegh 1997; Nowis *et al.* 2006; Christianson *et al.* 2008; Soetandyo *et al.* 2010), suggesting that the efficiency of multiple pathways of ERAD may be less efficient in HPD than in LPD cells.

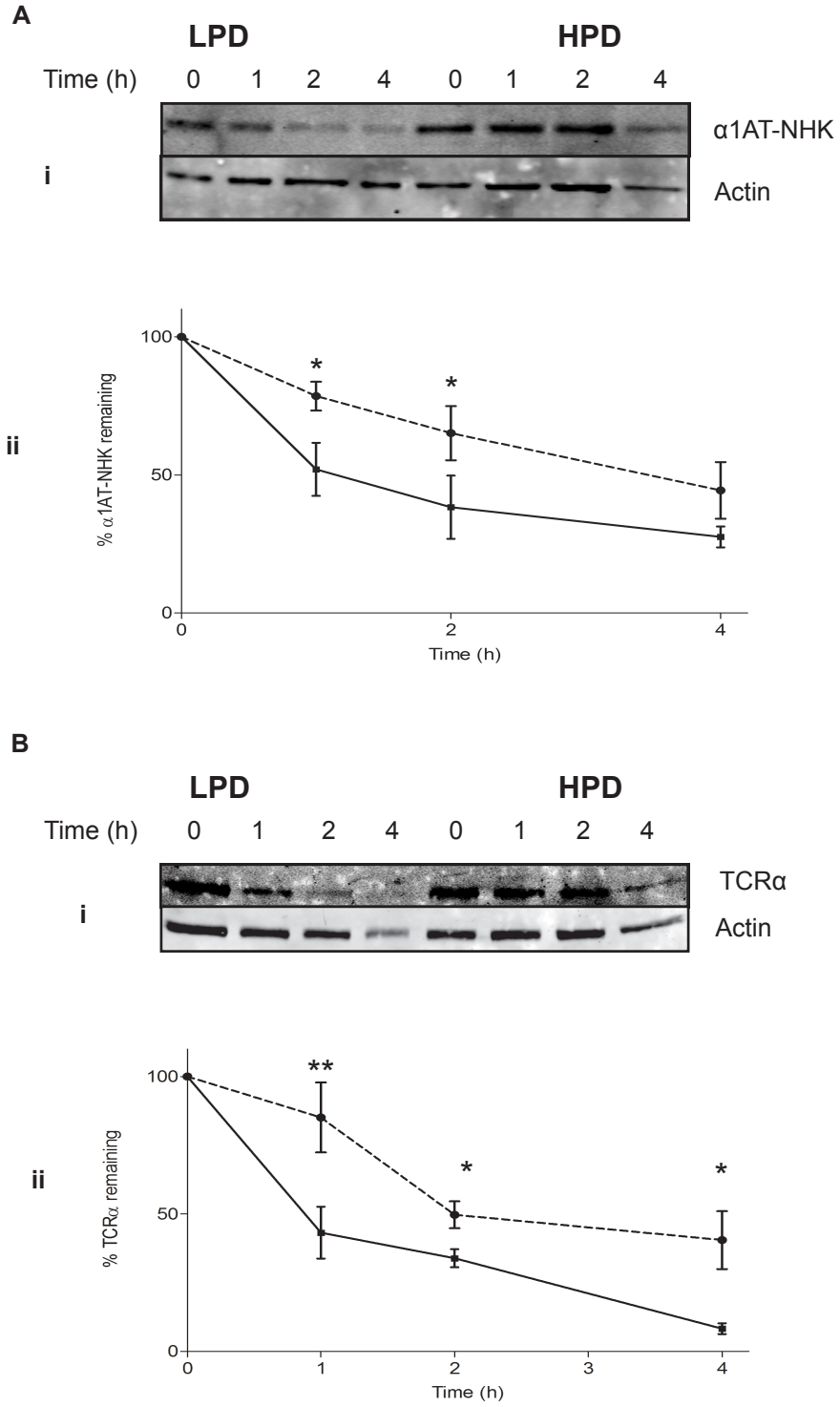

Figure 4.12: Cycloheximide pulse analysis of α1A-NHK and TCRα degradation in LPD and HPD cells.

Two days after transfection the cells were treated with cycloheximide and harvested immediately (t=0) or after above mentioned time. The proteins were resolved by 12% SDS-PAGE and analysed by quantitative immunoblotting using the specified antibodies. Actin was used as loading control.

Each band was quantified using the the Odyssey software, and normalised relative to the intensity of the actin signal and represented as percentage of the value at chase time 0 that was set as 100%. The graph shows the mean ± s.e.m from three independent experiments. The two way ANOVA followed by slice test was used to determine significant differences between LPD and HPD cells. * denotes $P < 0.05$ and ** P denotes < 0.01.

The results for α1A-NHK are presented in **(A)** panel and for TCRα are shown in panel **(B).**

4.6 ER stress and the unfolded protein response

The experiments described above suggested that the ability of the ER to fold cargo and degrade misfolded proteins is impaired in the *in vitro* aged cells. This might be expected to perturb ER homeostasis, leading to low level accumulation of misfolded/unfolded proteins and an increased basal level of phospho-eIF2α. Several studies have highlighted that the ability to successfully deal with stress declines with age (Kourtis & Tavernarakis 2011). This may be due to defects in the signalling pathways as seen for the HSR which is reduced in aged animals (e.g. attenuated transcriptional upregulation of Hsps – see section 1.2). A similarly defective UPR could potentially explain the observed defects in ER proteostasis pathways. Therefore, the effect of *in vitro* ageing on the response to stress was tested.

In order to examine the response of LPD and HPD cells to ER stress and their ability to initiate the UPR, cells were treated with the stress inducter tunicamycin (Tn). Tn inhibits glycosylation by blocking the transfer of N-acetyl-d-glucosamine-1-phosphate (GlcNAc-1-P) from diphosphoryl-N-acetylglucosamine (UDP-GlcNAc) to dolichyl phosphate (Varki A 1999), therefore inhibiting synthesis of the precursor oligosaccharide. Because N-glycosylation occurs only in the lumen of the ER, the use of Tn leads to accumulation of misfolded proteins specifically in the ER lumen.

Activation of the IRE1 branch of the UPR was investigated first, by monitoring the production of spliced of *XBP1* mRNA, which is an early event in activation of the UPR (section 1.3.4) and can be measured by reverse transcription PCR (RT PCR). Initially, cells were treated with increasing concentrations of Tn for 8 hours in order to determine whether there was any difference in the sensitivity of LPD and HPD cells to this ER stressor. In untreated cells, only a single PCR product, corresponding to unspliced *XBP1*, was visible (Fig 4.13A lanes 1 and 6, *XBP1*u). In cells treated with Tn, an additional faster migrating PCR product was also observed (Fig 4.13A lanes 2-5 and 7-10), representing the spliced *XBP1*. Some of the spliced *XBP1* product was detected in both LPD and HPD cells after treatment with the lowest concentration of Tn (0.25 µg/ml), suggesting that even at this concentration of inhibitor the UPR was activated, as previous shown by experiments with MEF cells (Rutkowski *et al.* 2006). However the amount of spliced relative to unspliced *XBP1* was similar in both young and aged cells. With increased concentrations of Tn, an increasing proportion of the PCR products represented the spliced form of *XBP*1, and a striking difference between LPD and HPD cells became apparent. This difference was very clear at a concentration of 10 µg/ml Tn, when a spliced *XBP1* was only a minor product in LPD cells, but the main product in HPD cells (Fig 4.13A lanes 5 and 10), suggesting that HPD cells are more sensitive to ER stress. Since the overall biosynthesis of ER targeted N-glycoproteins was similar in LPD and HPD cells (Fig 4.7B), the differences in sensitivity to Tn-induced ER stress are unlikely to be due to differences in the load of client proteins entering the ER in the two types of cells. Another explanation for the difference in the ability of Tn to induce UPR in HPD and LPD cells could be differences in the ability of Tn to

inhibit glycosylation in HPD and LPD cells e.g. through differences in the absorbance rates of the drug. Indeed, modifications of extracellular matrix and plasma membrane composition have been suggested to occur with age (Schroeder *et al.* 1984; Bartling *et al.* 2009) and might potentially affect Tn uptake. Therefore the ability of different concentrations of Tn to inhibit N-glycosylation in LPD and HPD cells was tested (Fig 4.13B). An experiment that combined the Tn treatment with the in *vitro* translation of a glycosylated substrate (SPP) was designed, and the effect of Tn on the production of glycosylated SPP was measured in both LPD and HPD cells. When untreated semi-permeabilised cells were included in the in vitro translation reactions, two forms of SPP were generated, representing the unglycosylated SPP which migrated at a lower MW and the glycosylated protein at a higher MW (Fig 4.13B lanes 1 and 6). When cells were treated with Tn prior to semi-permeabilisation, the amount of glycosylated SPP decreased with the increased concentration of Tn (Fig 4.13B). The signal of each form was quantified using AIDA software, and the relative SPP glycosylation calculated from the ratio of glycosylated SPP to non–glycosylated SPP expressed as percentage of the ratio in untreated cells. These data are presented under the corresponding lane in Fig 4.13B. No difference was observed between the ability of Tn to inhibit N-glycosylation of SPP in LPD and HPD was observed at any of the Tn concentrations used (Fig 4.13B). Therefore, it is unlikely that the increased sensitivity of HPD cells to Tn in terms of *XBP1* splicing was due to differences in the absorption of the inhibitor. This suggests that the increase in splicing of *XBP1* observed in HPD cells most likely reflects increased sensitivity of HPD cells to ER stress.

To investigate this possibility further, the kinetics of IRE-1/*XBP1* activation in LPD and HPD cells was investigated, by treating cells with a fixed concentrations of Tn (10 µg/ml) for increasing amounts of time (Fig 4.14A), and monitoring *XBP1* splicing. As previously seen in untreated cells, no spliced *XBP1* product was detected after 0 min treatment with Tn (Fig 4.14A lanes 1 and 7), but with increasing time, the appearance of the product corresponding to the spliced form of *XBP1* was observed (Fig 4.14A lanes 2-4 and 8-11). This kinetic analysis also highlighted a clear difference between the response of HPD and LPD cells to Tn-induced ER stress (Fig 4.13A), and both the extent and timing of *XBP1* splicing appeared to be different. In LDP cells, the extent of *XBP1* splicing increased up to 8h at which point the abundance of the spliced and unspliced products were approximately equal (Fig 4.14A, lane 4). In HPD cells, the spliced *XBP1* PCR product increased more dramatically, and between 4 and 8h was the dominant form (Fig 4.14A compare lanes 3 and 4 with 8 and 9). After 16 hours, the spliced product was no longer visible in the LPD cells, suggesting that the IRE1 response had been inactivated, whereas *XBP1* splicing was still evident in HPD cells, although at a reduced level (Fig 4.14A, lanes 5 and 11). By 24 hours only the higher MW band of unspliced *XBP1* was detected in both LPD and HPD suggesting that the cells had adapted to the conditions and the UPR was completely switched off (Li *et al.* 2010; Pincus *et al.* 2010).

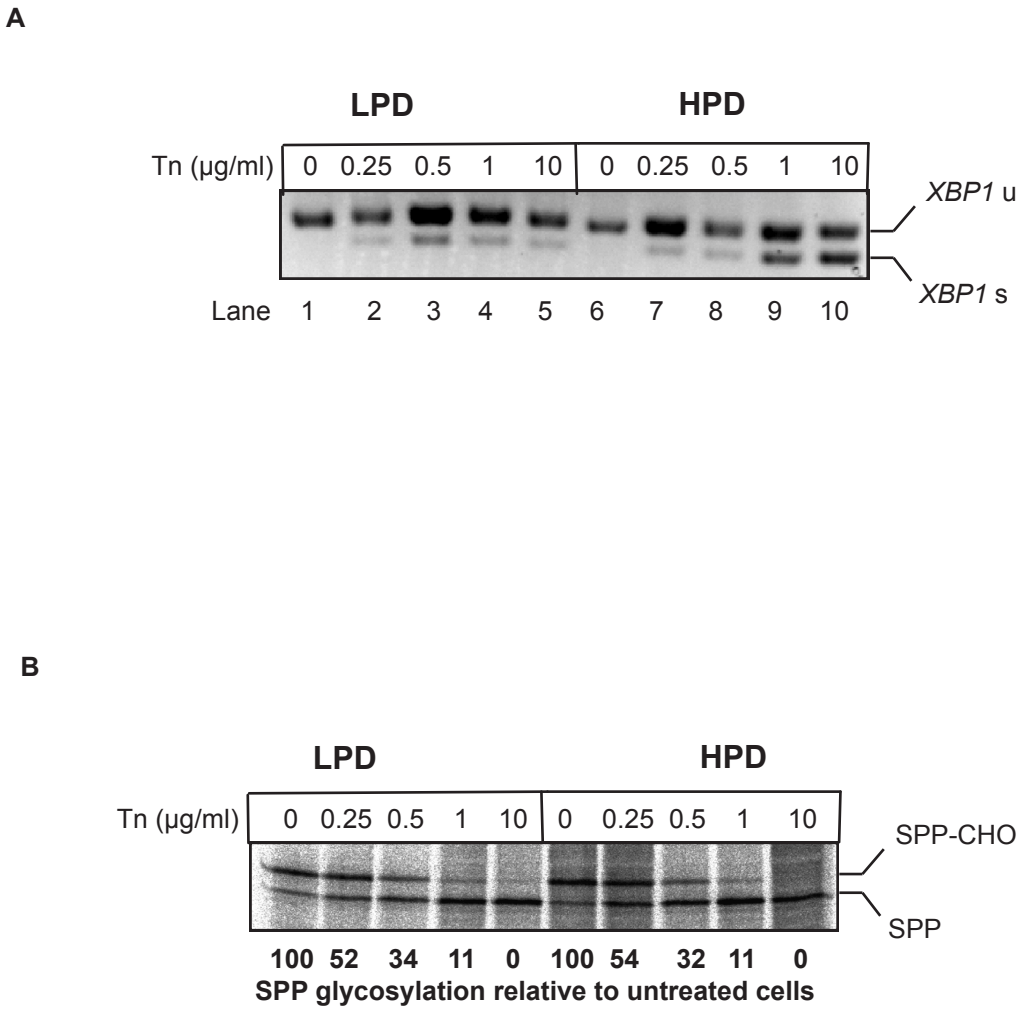

Figure 4.13: Evaluation of IRE-1 arm activation in LPD and HPD cells, after tunicamycin treatment.
(A) Cells were treated with the indicated concentration of tunicamycin (Tn) for 8 hours and *XBP1* mRNA splicing was determined by RT-PCR. The spliced (*XBP1*s) and unspliced (*XBP1*u) forms are indicated in the figure.
(B) Tn treated cells were treated with digitonin to produce semi-permeable cells. SPP mRNA was translated for one hour and products were resolved by 12% SDS-PAGE and analysed by phosphorimaging. The bands were quantified and the glycosylated form to non-glyosylated ratio was expressed as percentage of the untreated sample. The figure shows data from one of two independent experiments with similar results.

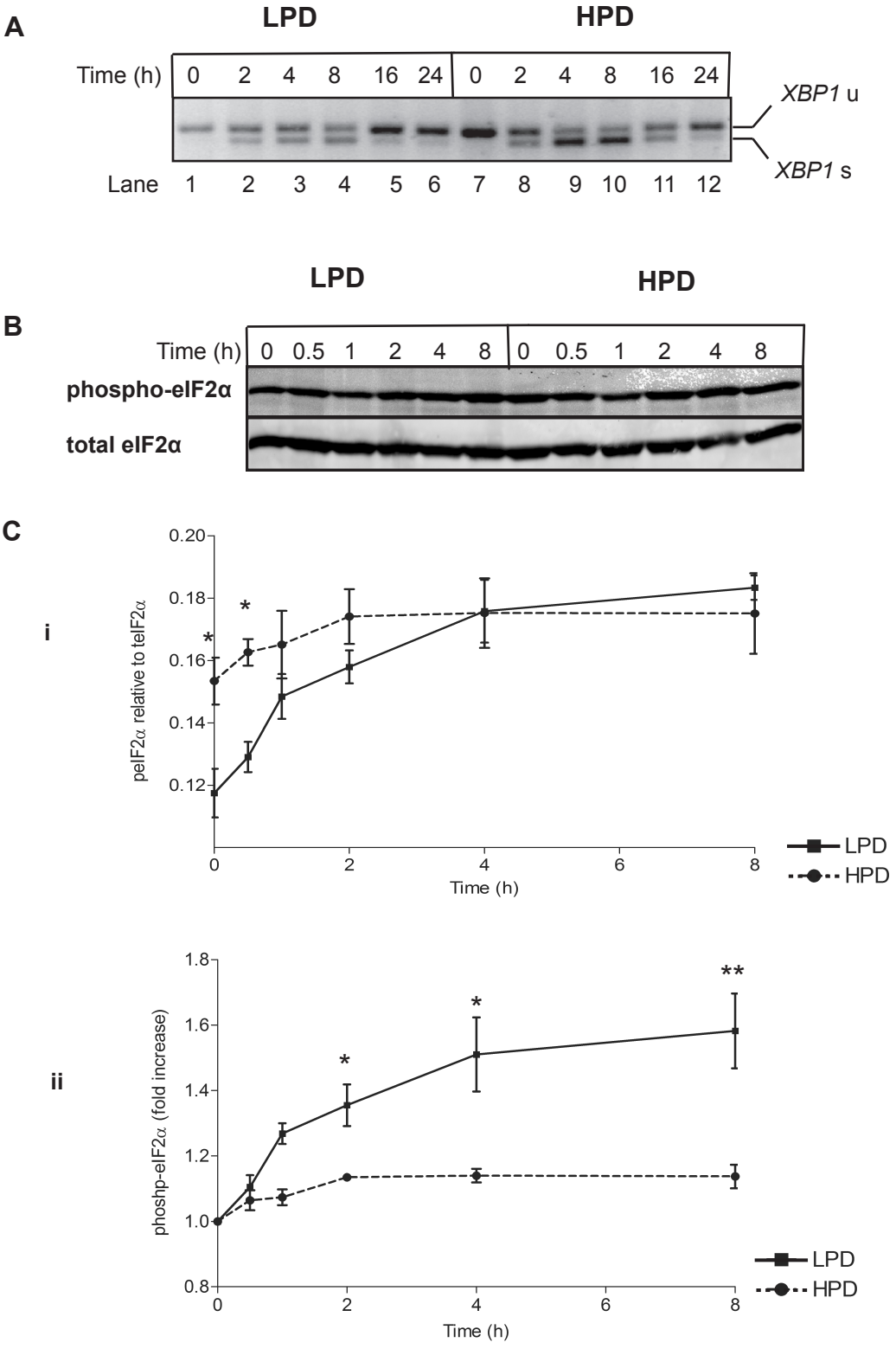

Figure 4.14: *XPB1* splicing and eIF2α phosphorylation in LPD and HPD following Tn induced UPR.
(A) Cells were treated with 10 µg/ml Tn for the indicated times and the splicing of *XBP1* was analysed as in Fig 4.13A.
(B) Tn treated cells were harvested immediately (t=0) or after the indicated time. The proteins were resolved by 12% SDS-PAGE and analysed by quantitative immunoblotting.
(C) The bands were quantified and normalized to total eIF2α (**i**) and plotted against time. The phospho- to total eIF2α values were expressed as proportion of untreated cells and plotted against time (**ii**). The graphs shows the mean ± s.e.m from five independent experiments (* $P < 0.05$, ** $P < 0.01$, two way ANOVA and Student's t-test).

These results are very interesting because they further suggest that HPD cells are more sensitive to Tn induced misfolding, so that the UPR is more rapidly activated by inhibition of N-glycosylation, and are less able to recover and therefore switch off IRE1 signalling more slowly. Next, activation of the PERK arm of the UPR was investigated. In this case, phosphorylation of eIF2α was used as a readout of PERK activity. HDP and LPD cells were treated with 10 µg/ml Tn for increasing time periods, then lysed and analysed by quantitative immunoblotting using the phospho-specific antibody to phospho-eIF2α (Fig 4.14B). The intensity of the signal obtained with the anti-phospho eIF2α and the anti-total eIF2α was quantified, and the ratio of phospho-eIF2α to total eIF2α was plotted against time (Fig 4.14Ci). To address the fold-increase in eIF2α phosphorylation following ER stress induction, the phospho- to total eIF2α values were expressed as proportion of untreated cells and plotted against time (Fig 4.14Cii). As previously seen (Fig 4.2), the basal level of phospho-eIF2α without Tn treatment was higher in the HPD cells than LDP cells (Fig 4.14Ci). In the LPD cells, the relative amount of phospho-eIF2α increased with time following addition of Tn, reaching a maximum after 4 hours treatment at which point the reached the same level as in the HPD cells (Fig 4.14Ci), however at this time point the phosphorylation level of eIF2α was 1.5 fold higher than in the untreated LPD cells (Fig 4.14Cii). By contrast, in HDP cells, which started with a higher basal level of phospho-eIF2α, Tn treatment did not show a significant increase in eIF2α phosphorylation (Fig 4.14Ci). Even after 8 h in the presence of Tn, no increase in the phosphorylation state of eIF2α was observed (Fig 4.14Ci, ii). These results are consistent with HPD cells having less efficient ER protein homeostasis pathways, and thus having low level UPR, reflected in higher basal phospho-eIF2α. Also the data suggests that these cells are unable to induce further phosphorylation of eIF2α in the face of acute Tn-induced misfolding – this could be potentially harmful, since the ability to downregulate protein synthesis is important for surviving ER stress (Lin *et al.* 2009).

Because Tn induces misfolding in the ER in a very specific way, i.e. inhibition of N-glycosylation, other ER stressors were examined in order to test whether similar differences in UPR activation were seen with distinct challenges to ER folding homeostasis. Therefore, two methods that perturb folding in different ways were selected. L-azetidine-2-carboxylic acid (AzC), is a proline analogue that is incorporated into nascent proteins and induces misfolding by altering protein structure (Zagari *et al.* 1990; Metzger & Michaelis 2009), whilst dithiothreitol (DTT), is a reducing agent that inhibits the formation of disulphide bonds thereby preventing oxidative folding (DuRose *et al.* 2006). Cells were grown in media containing AzC for up to 16 hours, then harvested and the activation of IRE1 was assessed by RT-PCR detection of spliced *XBP1* mRNA. Consistent with previous experiments (Fig 4.14A), no spliced *XBP1* was detected in either LPD or HPD cells in the absence of AzC (Fig 4.15A lanes 1 and 6). However, growth in AzC containing media activated IRE1 in both cell types, as shown by the appearance of the faster migrating PCR product representing spliced *XBP1* (Fig 4.15A, lanes 2 and 7). As seen with Tn treatment, *XBP1* splicing was induced to a greater extent in HPD cells than LPD cells.

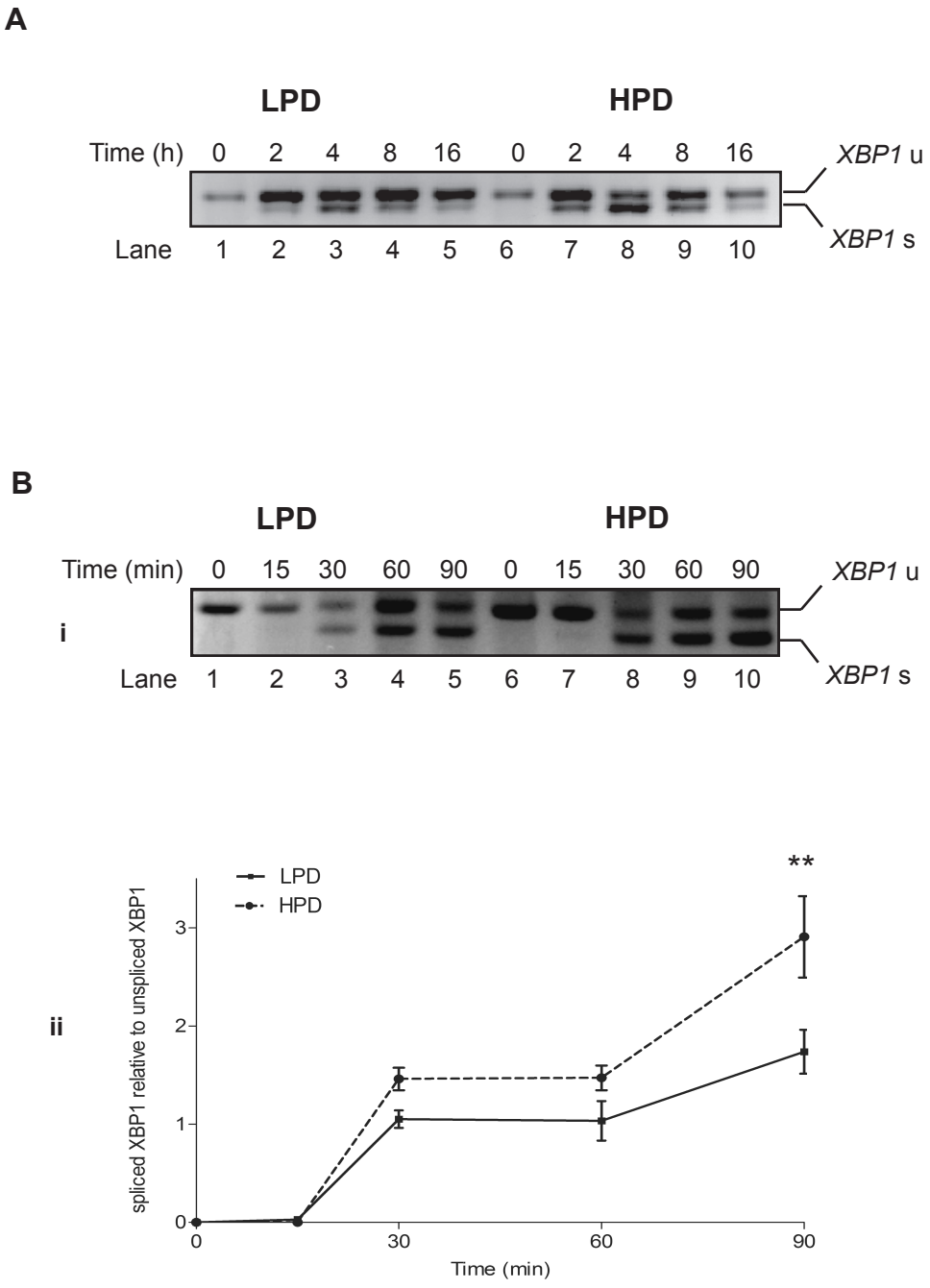

Figure 4.15: Evaluation of UPR activation in LPD and HPD cells, after treatment with AzC and DTT.
Cells were treated with 20 mM L-azetidine-2-carboxylic acid **(A)** or with 0.5 mM DTT **(B)** for the indicated times and *XBP1* mRNA splicing was determined by RT-PCR. The spliced *XBP1* relative to unspliced form was plotted against time and the error bars show the mean ± s.e.m. The significance of the difference between the spliced *XBP1* levels in LPD and HPD cells was determined by two way ANOVA, completed with a slice test. * denotes $P < 0.05$ and ** denotes $P < 0.01$, $n = 3$.

This was most evident between 2 and 4 h of growth in the presence of AzC (Fig 4.15A, compare lanes 2 and 3 with lanes and 7 and 8). After 8 h, very little spliced *XBP1* product was seen in LPD cells (Fig 4.15A lane 5), while splicing was still apparent in HPD cells (Fig 4.15A lane 9). This is similar to the results obtained with Tn, and suggests that the ability to recover from misfolding stress and/or switch off IRE1 signalling may be perturbed in these aged cells. When DTT was used to induce ER stress in LPD and HPD cells, the treatment times were shorter, since disruption of disulphide bonds produces a very severe and acute activation of the UPR (DuRose *et al.* 2006). Indeed, after 30 minutes of DTT treatment, the spliced *XBP1* product was clearly visible in both LPD and HPD cells (Fig 4.15Bi lanes 3 and 8), and was present at all further time points (Fig 4.15Bi lanes 3-5 and 8-10). The intensity of each band was quantified and the ratio of spliced to unspliced *XBP1* was plotted against time to estimate what proportion of XBP1 was spliced at each time point in LPD and HPD cells (Fig 4.15Bii). No significant differences in the ratio of spliced to unspliced *XBP1* PCR product was seen between LPD and HPD up to 60 minutes of treatment, However, after 90 minutes treatment with DTT, the relative amount of spliced *XBP1* product was significant higher in HPD than in LPD cells (Fig 4.15Bii), providing further support for the idea that the ER folding homeostasis is perturbed in HPD cells, leading to greater activation of the UPR upon further challenge. These results are also consistent with the previous observation that DTT treatment resulted in greater attenuation of translocation in HPD cells than in LDP cells (Fig 4.6A, B).

The previous experiments monitoring the kinetics of IRE1/*XBP1* activation indicated that there may be a delay in the recovery of homeostasis, so a two step assay was performed in which ER stress was induced by treatment with DTT, followed by washing and chasing in the absence of DTT to allow recovery. Using DTT as the stressor in this type of assay has two major advantages, namely that it rapidly induces the UPR and it is easily washed out, allowing the recovery phase of the UPR to be monitored without the need for long incubations that could compromise cell viability and/or lead to adaptation (Pincus *et al.* 2010). The appearance of spliced *XBP1* was monitored as a reporter of activation of IRE1. A 30 minutes treatment with DTT was chosen as it induced a robust response, with the faster migrating spliced *XBP1* product clearly apparent (Fig 4.16A lanes 2 and 6). After DTT was wash out, the extent of *XBP1* splicing in LPD cells decreased rapidly, and only the unspliced *XBP1* product was visible band after 60 minutes (Fig 4.16A lanes 3-5), demonstrating that IRE1 signalling had been switched off and ER homeostasis was restored. By contrast, this re-establishment of homeostasis appeared to be slower in HPD cells (Fig 4.16A). During the first 15 minutes following DTT washout, the extent of *XBP1* splicing did not decrease, and the spliced *XBP1* product remained the predominant form (Fig 4.16A, lane 8, Fig 4.16B) and was more abundant than in LPD cells. After 30 minutes of recovery, the relative amount of spliced *XBP1* had declined, but was still higher than in LPD cells after just 15 min recovery (Fig 4.16A lanes 3 and 9, Fig 4.16B). By 60 minutes, unspliced *XBP1* did become the major form (Fig 4.16A lanes 8-10), suggesting that homeostasis had been restored sufficiently for IRE1 signalling to be switched off.

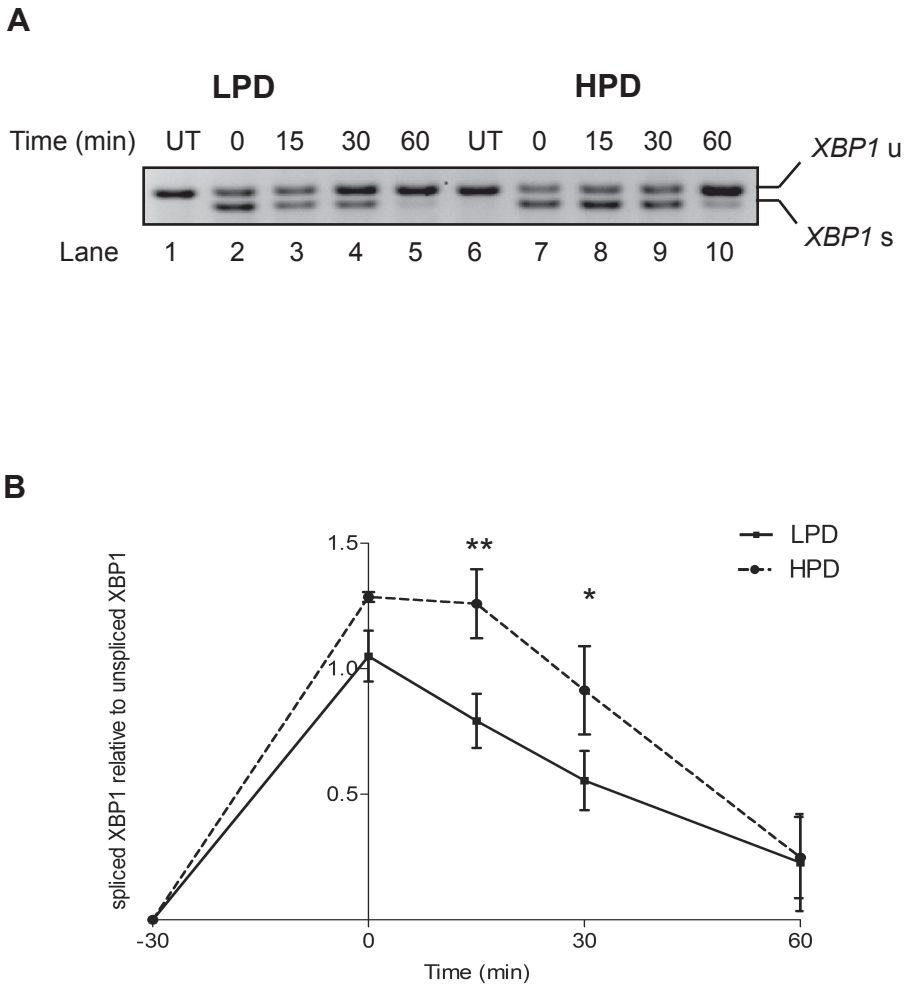

Figure 4.16: Recovery of LPD and HPD cells after DTT-induced ER stress.
Cells were treated with 0.5 mM DTT for 30 minutes then the washed with fresh media and harvested at the indicated time points. The *XBP1* mRNA splicing was determined by RT-PCR and the spliced and the unspliced products are indicated in the figure. The bands were quantified and the spliced form was expressed relative to the unspliced form. The values were expressed as percent of the untreated cells (set as 100%) and plotted against time. A two way ANOVA, combined with a slice test, was used to calculate the significant differences between levels of spliced *XBP1* for each time point.
* denotes $P < 0.05$, and ** denotes $P < 0.01$, n = 3.

These results show that the amplitude and timing of IRE1/*XBP1* activation in response several distinct challenges to ER folding homeostasis was different in HPD than in LPD cells. Specifically, the HPD appeared sensitised to activation of this branch of the UPR, with splicing of *XBP1* being induced more strongly and/or rapidly upon induction of ER stress. IRE1/*XBP1* activation also persisted for longer in HPD cells following removal of the stress inducer, suggesting that restoration of homeostasis was slower in these cells. In contrast, HPD cells were less able to increase phosphorylation of eIF2α following Tn treatment. All these data together suggest a model where cellular ageing *in vitro* is associated with a low constitutive level of ER misfolding stress, leading to higher basal phosphorylation of eIF2α and increased sensitivity to further challenge to folding pathways. The observation that HPD cells were unable to induce further phosphorylation of eIF2α is important, since this response has been shown to be important for the ability of cells to survive (Harding *et al.* 2000b; Teske *et al.* 2011). In conclusion, the *in vitro* ageing is associated with disturbed UPR signalling. The data altogether show that kinetics of IRE1 and PERK are affected in HPD cells

4.7 Consequences of ER stress and UPR activation

The UPR is a homeostatic mechanism, and initially induces the upregulation of chaperones, folding factors and ERAD components which together help re-establish ER homeostasis (Wang & Kaufman 2012). In order to monitor the effect of UPR activation in HPD and LPD cells, cells were treated with Tn for increasing amounts of time, and the levels of BiP (Fig 4.17A), were analysed by quantitative western blotting. The level of actin was unchanged over the time course of Tn treatment (Fig 4.17A), and was therefore used as a loading control. The intensity of the BiP signal was normalised relative to the actin signal and plotted against time (Fig 4.17Bi). In addition, to visualise the fold-increase in BiP levels following ER stress inducing, BiP normalised to actin was expressed as proportion of untreated cells and plotted against time (Fig 4.17Bii). In the untreated cells, i.e. time zero, a higher level of BiP was detected in HPD cells, as observed previously (Fig 4.3). Following treatment of LPD cells with Tn, BiP expression increased significantly, and after 4 h treatment, the level of BiP was approximately 2-fold higher than in untreated cells (Fig 4.17Bi, ii). By contrast, although the HPD cells started with a higher level of BiP (Fig 4.17Bi), Tn treatment did not result in upregulation of BiP expression (Fig 4.17Bii). Even after 8 h treatment, the level of BiP was not significant different to that in untreated cells (Fig 4.17B). Thus, HPD cells were unable to upregulate levels of this chaperone protein in response to Tn induced ER stress. The result was unexpected given the heightened sensitivity of the IRE1/*XBP1* axis to activation by multiple ER stressors in HPD cells. However, they do correlate with the lack of increased eIF2α phosphorylation in HPD cells. These results are potentially important because they indicate that cellular ageing is associated with a defective response to ER stress.

BiP upregulation is important to allow cells to survive ER stress, therefore is possible that the lower level of BiP might make cells more vulnerable to ER stress induced cell death. In order to test how the differences in UPR signalling between HPD and LPD cells impacted on cell fate, Therefore, cell survival after 16 hours treatment with different concentration of Tn was measured using the MTT assay (Fig 4.18). After Tn treatment, cells were incubated for 2 hours with MTT, which is reduced by a mitochondrial enzyme only in viable cells (Mosmann 1983). The metabolised MTT generates purple formazan crystals, which can be quantified to provide a measure of the number of viable cells. The cell number after treatment with each concentration of Tn was expressed as a percentage of the untreated cells (Fig 4.18). The number of viable cells that survived the treatment decreased with increasing concentration of Tn (Fig 4.18). At the lowest concentration of Tn (0.25 µg/ml) only a very small loss of viability was observed for both HPD and LPD cells, whilst at the highest concentration (10 µg/ml) less than 25% of the cells remained viable (Fig 4.18). At these extremes, there was no obvious difference in viability between LPD and HPD cells. However, at the intermediate concentrations of Tn, HPD cells exhibited a significantly greater loss of viability (Fig 4.18). Thus, when treated with 0.5 µg/ml Tn, only 30 % of the HPD cells were still viable compared to almost 70% of the LPD cells.

These results suggest that the alterations in UPR signalling observed in HPD cells result in a reduced ability of these *in vitro* aged cells to survive Tn-induced challenge to ER folding homeostasis.

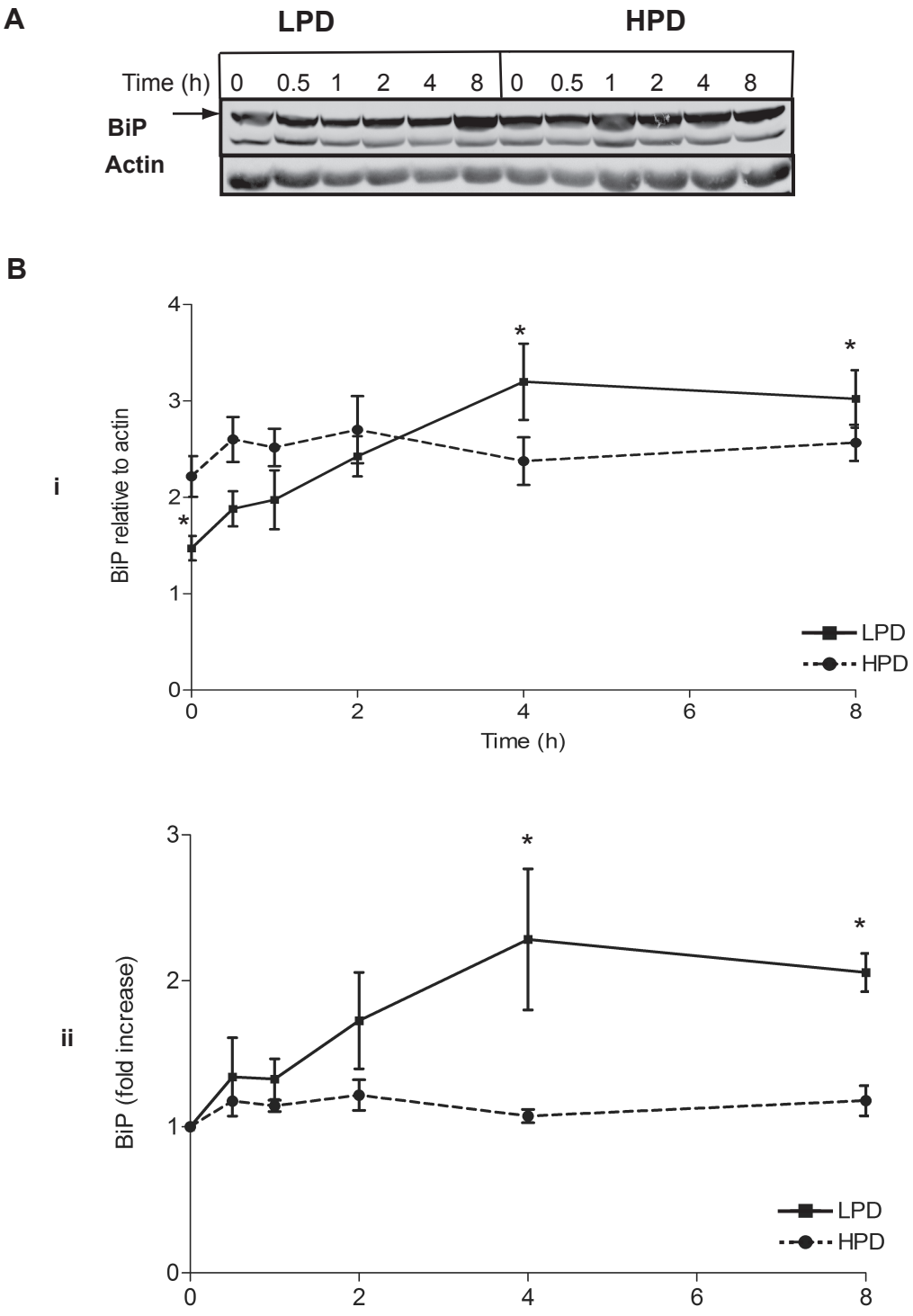

Figure 4.17: Immunoblot analysis of BiP levels in LPD and HPD cells, following Tn treatment.

(A) Cells were treated with Tn and harvested immediately (t=0) or after the indicated time points. The samples were resolved by 12% SDS-PAGE and analysed by quantitative immunoblot with anti-BiP antibodies. The bands were quantified and normalized to actin and plotted against time (**i**). The BiP to actin values were expressed as proportion of untreated cells and plotted against time (**ii**). The graphs show the mean ± s.e.m from five independent experiments. * $P < 0.05$, ** $P < 0.01$, two way ANOVA with slice test.

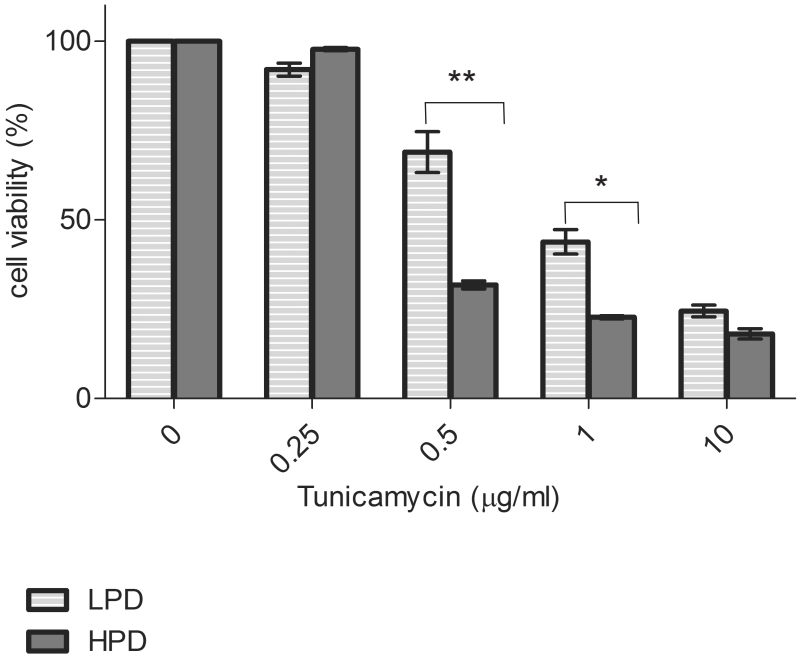

Figure 4.18: LPD and HPD cell viability after Tn treatment.
LPD and HPD cells were seeded in 96 well plates and the following day were treated with the indicated concentrations of Tn. Cell viability was measured using the MTT assay. The cell number at each Tn concentration was expressed as percent of the untreated culture. The statistical significance was determined by two way ANOVA with a slice test.
(* $P < 0.05$, ** $P < 0.01$), n = 3.

4.8 Discussion

In this chapter, human lung fibroblasts aged *in vitro* by serial passage were used as a model of cellular ageing to integrate the expression levels of ER proteins with the analysis of ER function.

Similar to the results from the previous chapter, and in agreement with other studies (Erickson *et al.* 2006; Paz Gavilan *et al.* 2006; Gamerdinger *et al.* 2009), it was found that the expression levels of key components of ER folding and ERAD systems, as well as levels of components of autophagic and proteasomal degradation pathways, were affected in the HPD cells. These results indicated that ER function might be affected with cellular age. To address this, a variety of approaches and assays were used to examine different aspects of ER function. Together the results provide evidence that cellular ageing is associated with a decline in the function of ER protein homeostasis pathways, alterations in UPR signalling, resulting in decreased resistance to ER stress. Specifically, HPD cells were less able to support folding of a metastable ER cargo protein, and had a reduced capacity to promote degradation of misfolded ERAD substrates. In addition, the response to ER stress and UPR signalling were altered in HPD cells – specifically IRE1/*XBP1* axis was more sensitive to activation by several stressors. HPD cells also exhibited higher basal levels of phospho- eIF2α, but no increase in eIF2α phosphorylation was observed in response to ER stress, suggesting that PERK was not (further) activated in HPD cells. Similarly, no upregulation of the key UPR target BiP was detected in HDP cells subjected to ER stress, and HPD cells were found to be significantly more sensitive to Tn-induced cell death. Altogether, these results provide evidence that ER protesostasis and stress signalling pathways are perturbed with age, resulting in a decline in resistance to ER stress.

Folding experiments, using ts O45 VSV-G and Golgi apparatus modification as a measure of ER exit and correct folding, showed that this metastable protein misfolds more extensively in HPD cells at a range of temperatures. In addition, the folding of VSV-G is slower in HPD cells than in LPD, indicating that HPD cells have a reduced ER folding capacity. Previous work has provided strong evidence that ageing is associated with a general loss of protein homeostasis in *C. elegans* (Cohen *et al.* 2006; Yun *et al.* 2008; David *et al.* 2010). In particular, the study from (Ben-Zvi *et al.* 2009) showed that metastable proteins bearing temperature sensitive mutations exhibited progressive misfolding with increasing age. The results described above are important because they provide evidence that ageing of mammalian cells is also associated with a decline in the folding capacity, specifically at the level of the ER. It is important to note that these assays did not look at VSV-G folding directly, but used the appearance of Golgi apparatus modified N-glycans as marker of ER exit and thus correct folding. Therefore, the potential contribution of changes in the Golgi apparatus glycosylation machinery and/or vesicular traffic to Golgi apparatus cannot be ruled out completely. Still, the experiments looking at biosynthesis of N-glycoproteins (conA) and ER-Golgi apparatus traffic showed no significant difference between LPD and HPD cells, suggesting that any such differences may be relatively small. Therefore, it seems reasonable to conclude that the higher level of VSV-G lacking Golgi apparatus

modifications (i.e. EndoH sensitive) in HPD cells is due to an increased amount of the protein being misfolded and thus retained in the ER. Further experiments using other model proteins to more directly assess the protein folding landscape in the ER of HPD cells will be important to test this hypothesis.

It is interesting to consider what underlies the apparent decline in ER folding capacity of HPD cells. This could be a direct effect of changes in the ER chaperone/oxidoreductase expression level, such as observed in HPD cells in this study (PDI and ERp57) and tissues from aged organisms documented in chapter 3 and in other previous reports (see table 1.5). In addition, some modifications (e.g. oxidation) of ER chaperones and oxidoreductases (BiP, PDI, calreticulin) that inhibit their function have been observed in liver of aged mice (Rabek *et al.* 2003; Morley & Morimoto 2004; Nuss *et al.* 2008). Such changes could be induced by altered redox conditions in ER lumen (Starke-Reed & Oliver 1989; van der Vlies *et al.* 2003) which could also inhibit oxidative folding. Another possibility is that sequestration of chaperones by misfolded proteins may reduce folding efficiency. A similar scenario has been suggested following assessment of protein aggregation in muscle of old mice and as seen in the old worms (David *et al.* 2010). In support of this hypothesis, a decreased capacity to degrade ERAD substrates was observed in HPD cells, suggesting that these cells may well have increased levels of misfolded proteins in the ER. The cause of the decline in ERAD efficiency could be due to a reduced capacity to target and/or dislocate the misfolded proteins from the ER lumen, and/or by reduced degradation at proteasome. The latter is likely to make a contribution since deficiencies in proteasomal degradation with age have been previously reported in various tissues and models of ageing (Low 2011). A study using the same IMR90 cells as used in this chapter has shown that HPD cells have decreased proteasomal degradation, and thus use the macroautophagic pathway to degrade polyUb substrates (Gamerdinger *et al.* 2009). This is also consistent with the results presented here showing that HPD cells have increased levels of polyUb proteins and increased levels of BAG3. Although the capacity of autophagic-lysosomal degradation was not assessed in this study, numerous data indicate that it also declines with age (Rubinsztein *et al.* 2011). In addition, the experiments examining 'global' translocation efficiency indicate that the ability to attenuate translocation in response to ER stress may be compromised in HDP cells, which could potentially increase production of misfolded proteins under conditions of stress (Kang *et al.* 2006). Furthermore, the apparent failure to upregulate BiP and other chaperone expression in response to ER stress would also have a negative impact on folding capacity under conditions of stress. Together, these factors could lead to the creation of a vicious cycle, whereby misfolded proteins disrupt folding and lead to further accumulation of misfolded proteins. Indeed, such a situation has been proposed as an initiating factor in neurodegenerative diseases. In addition, this idea is supported by a previous study that showed that low level ER stress (e.g. accumulation of misfolded proteins in ER) can result in reduced folding efficiency in ER (Eriksson *et al.* 2004). Thus deficiency in one of the pathway involved in ER proteostasis (e.g. upregulation of ERAD) impaired the activity of another

pathway component of ER protein homeostasis (e.g. folding). Indeed, studies in *C. elegans* (Gidalevitz *et al.* 2006) and in mammalian cells (Ren *et al.* 2009; Olzscha *et al.* 2011; Hipp *et al.* 2012) have shown that the presence of aggregation prone polyQ proteins negatively affects the folding of other metastable proteins, thus suggesting a collapse of proteostasis can be initiated by a single misfolding species.

.

The HPD cells also exhibited higher basal levels of phospho-eIF2α and BiP, indicating that these cells may be experiencing heightened conditions of ER stress compared to LPD cells. This would be consistent with the increased sensitivity of HPD cells to activation of the IRE1/*XBP1* arm of the UPR observed. In addition, increased levels of phospho-eIF2α have been reported in cultured hepatocytes of old mice (Li & Holbrook 2004). In contrast, previous studies that analysed the level of eIF2α phosphorylation in tissues from young and old rats (Hussain & Ramaiah 2007; Naidoo *et al.* 2008) found that aged animals had a lower basal level of phosho-eIF2α that the young counterpart. This inconsistency could be due to differences in system type e.g. tissues (brain, heart, lung, liver, kidney, spleen) versus primary lung fibroblast and/or organism (e.g. rat versus human). Despite the higher phospho-eIF2α, no sign of IRE1 activation/XBP1 splicing was observed in HPD under basal conditions. It is possible that the increased basal eIF2α phosphorylation is not mediated by PERK but by some other eIF2α kinase. Indeed, in mouse fibroblasts proteasome inhibition induces phosphorylation of eIF2α via activation of GCN2, not via ER stress and PERK (Jiang & Wek 2005; Mazroui *et al.* 2007). Since HDP cells may have a reduced proteasome capacity, it is possible that GCN2 may contribute to the higher basal phospho-eIF2α observed. Another possible explanation for the lack of *XBP1* splicing in HPD despite higher eIF2α phosphorylation could be the regulation or reprogramming of the UPR under conditions of low level ER stress. For example, increased levels of an IRE-1 inhibitor could be present in HDP cells. In support of such an idea, BI-1 also functions as an inhibitor of IRE-1 and is normally subjected to proteasomal degradation, but is stabilised by reduced proteasome activity, and therefore IRE1 activity is negatively regulated at low levels of stress that affect proteasome function (Lisbona *et al.* 2009; Rong *et al.* 2011).

Following treatment with various ER stress inductors, HPD cells exhibited increased sensitivity of IRE1/*XBP1* to activation suggesting that HDP cells are less able to cope with perturbation of ER folding. This could be related to decreased folding and ERAD capacity which may increase the levels of unfolded/misfolded proteins in lumen of HPD cells, so that any further perturbation of folding tips the balance and IRE1 is activated. In other words, HPD could be sensitised to UPR activation by low level misfolding stress. Interestingly, a *C. elegans* study, found that the ire1/*xbp1* set point or activity is lowered by mutations that increase lifespan, suggesting that ER proteostasis may contribute to lifespan extension in these animals (Henis-Korenblit *et al.* 2010). In addition, cross talk may occur between UPR signalling pathways and this could contribute to enhanced sensitivity of the IRE1/*XBP1* arm to activation in HPD cells. A recently described adaptation to stress involves the stabilisation of spliced *XBP1* mRNA by phospho-eIF2α during

the initial stages of UPR induction, resulting in higher levels of spliced *XBP1* mRNA (Majumder *et al.* 2012). Thus it was suggested that higher levels of phospho-eIF2α can enhance *XBP1* splicing. This would appear to mirror the situation in HPD cells, indicating that the enhanced basal phospho-eIF2α in HDP cells facilitates activation of IRE1/*XBP1* by conditions of stress. In addition, the increased level of spliced *XBP1* might be correlated with the lack of BiP upregulation (see below). This might impact on ER folding capacity under stress, therefore increasing the amount of misfolded proteins within lumen could favour further XBP1 activation.

In contrast to the enhanced sensitivity of the IRE1/*XBP1* arm of the UPR to activation in HPD cells, no increase in eIF2α phosphorylation was observed in response to Tn. It is not immediately clear how conditions of ER stress that activate *XBP1* in HPD cells fail to induce PERK and increase phosphorylation of eIF2α. It is possible that activation of PERK did occur, but eIF2α was almost maximally phosphorylated under basal conditions (see above), so that no major increase was further detected. Another possibility is suggested by the observation that *PERK* mRNA was lower in hippocampus of aged rats (Paz Gavilan *et al.* 2006), and if a similar situation exists in HPD cells, this could contribute to the lack of increased phospho-eIF2α. Furthermore, the same study found that the level of GADD34 was increased in aged rats (Paz Gavilan *et al.* 2006). Since GADD34 is a component of the phosphatase that dephosphorylates eIF2α (Novoa *et al.* 2001), this could limit the extent of eIF2α phosphorylation. Indeed, only a very transient increase in phospho-eIF2 α was observed in hepatocytes of aged rats after 1 and 2 hours of treatment with low concentrations of Tn (Li & Holbrook 2004). In fact, a very slight, but statistically significant increase in level of phospho-eIF2α was observed in HPD cells after 30 minutes of treatment with Tn. Thus it is possible that levels of the phosphatase were higher in HPD cells which could possibly limit the extent of phoshorylation that can be achieved. Indeed, the level of the transcription factor ATF4 which induces GADD34 would be predicted to be higher in HPD cells under basal conditions due to the enhanced eIF2α phosphorylation (Brush *et al.* 2003). Similar, a negative feedback of PERK is controlled via P58(IPK), an Hsp40 family member, that is upregulated downstream of IRE/XBP1 arm (Yan *et al.* 2002). Thus, the increased IRE/*XBP1* activation observed in HPD cells could be responsible for the reduced level of phosho-eIF2α. In contrast, previous studies reported that following treatment with lactacystin (a proteasome inhibitor), higher level of phospho-eIF2α and less spliced *XBP1* were observed in hippocampus of old rats compared with young animals (Paz Gavilan *et al.* 2006; Paz Gavilán *et al.* 2009). The reason for this difference is not clear, but may be related to differences in the forms of stress used and the experimental systems used.

In line with the lack of increased eIF2α phosphorylation, no upregulation of the key UPR target BiP was detected in HDP cells subjected to ER stress. This makes an interesting parallel with data from various models showing that aged organisms, in spite of higher basal levels of Hsps, are less able to increase the level of cytosolic chaperones after the HSR is induced (Nardai *et al.* 2002). This failure is due to dysfunctions in the HSR signalling pathway, including increased

degradation of the master regulator transcription factor Hsf1 and inactivation of HSF1 due to association with Hsp70 (Heydari *et al.* 2000; Morimoto 2002). The inability of HPD cells to upregulate BiP levels following stress induction could be a consequence of lack of increased eIF2α phosphorylation, resulting in lack of ATF4. In this sense, a recent study showed that upregulation of ATF6 targets, including BiP, depends on phosphorylation of eIF2α (Teske *et al.* 2011). However, BiP expression is also controlled by the IRE arm (Lee *et al.* 2003), thus expression of BiP would be expected to increase given heightened activation of XBP1 in HPD cells. However, it could be possible that a combination of transcription factors downstream of both IRE1 and ATF6, might be required to induce optimal levels of BiP (Lee *et al.* 2003; Wang *et al.* 2009b). More speculatively, it is possible that the stability of BiP mRNA may be altered in aged cells (Rutkowski *et al.* 2006), or that high levels of IRE1/*XBP1* activation might play a role via RNase activity of IRE1 (Han *et al.* 2009). It could also be speculated that epigenetic modifications, such as histone modification, could reduce UPR-induced transcriptional activation of BiP (Wang *et al.* 2009b). It is possible that the lack of BiP upregulation at the protein level might be related to an effect on transcript export from the nucleus (Bonelli *et al.* 1999) or translation efficiency This seems unlikely since it would have to be a selective failure to translate a particular subset of mRNAs, since the global rate of protein synthesis seems to be same in both cells. Thus, to address these possibilities, it will be important to examine mRNA levels of BiP and other targets in HDP and LPD cells following stress.

Since pathways that modulate protein homeostasis are interconnected (Roth & Balch 2010), a defect in any of the pathways will have an impact on whole network. Moreover, if the stress response pathways that should rebalance the system do not work properly, then the result is a collapse of the system and accumulation of misfolded protein, leaving the cell sensitive to additional stress (intrinsic or environmental). In line with this, HPD cells were also found to be significantly more sensitive to Tn-induced cell death, suggesting that resistance to ER stress may decline with age. This could be related to the failure of HPD cell to upregulate the expression level of BiP, therefore being less capable to adapt the ER proteostasis to Tn-induced stress. On the other hand, the increased death of HPD cells in face of Tn-induced ER stress could be due to the increased IRE1 activation. There is evidence that IRE1 can promote cell death via non-specific RNA degradation (Han *et al.* 2009) or interaction with proapoptotic molecules (Urano *et al.* 2000; Klee *et al.* 2009).

Altogether, these results suggest that decreased folding and degradation capacities could promote accumulation of misfolded proteins into the ER of HPD cells, further perturbing the ER homeostatsis and inducing the UPR. Indeed, evidence such as higher levels of BiP and phospho-eIF2α in aged cells, suggest that HPD cells are exposed to high levels of stress even in the absence of any external inductor. At this point a model of HPD cells can be envisaged in which they rely on the UPR as a survival mechanism to cope with decreased folding capacity, by upregulating expression of chaperones such as BiP and of ERAD components (Sel1L, Der1).

This could maintain a rather fragile homeostatic state within ER. Although by setting a higher stress threshold, the adaptive UPR can offer an initial cytoprotection to HPD cells against mild stress (Rutkowski *et al.* 2006; Lewerenz & Maher 2009), it can be hypothesised that aged cells might still be vulnerable to the action of a strong ER stressor. The decreased survival of the HPD cells following ER stress also supports the idea that ageing makes cells less able to cope with folding stress in the ER. These data are in agreement with observations that aged organism are more susceptible to a large range of stressors, leading to increased sensitivity to diseases. However, this model of cellular ageing has the limitation that it selects for cells that are able to survive prolonged time in culture, in the absence of a typical tissue environment (e.g. interaction with other cell type, exposure to various stimuli such as inflammatory mediators), therefore clearly is not the same as *in vivo* ageing.

CHAPTER 5

Analysis of age-related changes in ER proteostasis using *in vivo* aged human fibroblasts

5.1 Introduction

Data from the previous chapter suggest that replicative ageing of cells is associated with the diminished function of ER proteostasis pathways and alterations in the response to ER stress. In addition, several age-related changes observed in tissues were also seen in the *in vitro* aged cells, notably an increased level of polyUb proteins and increased phosphorylation of eIF2α, suggesting that these cells may provide one potential model for studying the impact of age on ER proteostasis. Although the identification of senescent cells in various aged tissues (Herbig *et al.* 2006; Panda *et al.* 2008; Wang *et al.* 2009a), as well as the evidences that senescent cells contribute to age-related pathologies (Martin & Buckwalter 2002), pointed out to the involvement of cellular ageing in organismal ageing, it is still under debate whether the *vitro* cellular senescence correlates with cell ageing *in vivo*. An additional cellular model that has been used in several studies (Gamerdinger *et al.* 2009) are skin fibroblasts harvested from young and old donors. The Coriell Institute supplies a range of human skin fibroblasts that have been isolated from young and old donors. In order to reduce variation in genetic background, which could potentially impact upon ER protesostasis, cells from related donors were identified. An additional selection criterion was identification of cells at a relatively low PD in order to avoid changes associated with replicative ageing (seen in previous chapter) and also to minimise loss of 'aged' cells that might have reduced capacity to proliferate. The cells that met all these conditions were chosen and the young and old cells were analysed at similar PDs, and PD kept below 15. The morphological features of the subcellular compartments were investigated by immunofluorescence microscopy (Fig 5.1A). Similar to the *in vitro* aged cells, the fibroblasts from old donors exhibited an enlarged size (Fig 5.1A). However, no difference could be seen in the organization of the vimentin network (Fig 5.1A) or ER structure (Fig 5.1A, calnexin) in cells from young and old donors. In addition, similar levels of caveolin-1 were observed in the young and old cells (Fig 5.1B), which could explain why no changes in the organisation of vimentin filaments were seen since downregulation of caveolin-1 in *in vitro* aged skin fibroblasts resulted in shift to 'young' type morphology and actin filaments organization (Cho *et al.* 2004).

5.2 Level of various ER proteins detected in young and old cells

First, the level of polyUb proteins and eIF2α phosphorylation were examined in cells from young and old donors. Lysates were prepared from cultures of cells from young and old cell donors and analysed by infrared Western blotting as previously described. Quantification revealed an increase in the level of polyUb proteins (relative to tubulin) (Fig5.2A) and phosphorylated eIF2α (relative to total eIF2) (Fig 5.2B), as seen in tissues from aged mice and in the HPD cells. Although statistically significant, the changes observed in these in vivo aged cells were smaller than observed in the other model systems. However, the fact that changes in eIF2α phosphorylation status and levels of polyUb proteins are consistently observed in multiple models of ageing suggest that they are widespread and fundamental features of ageing.

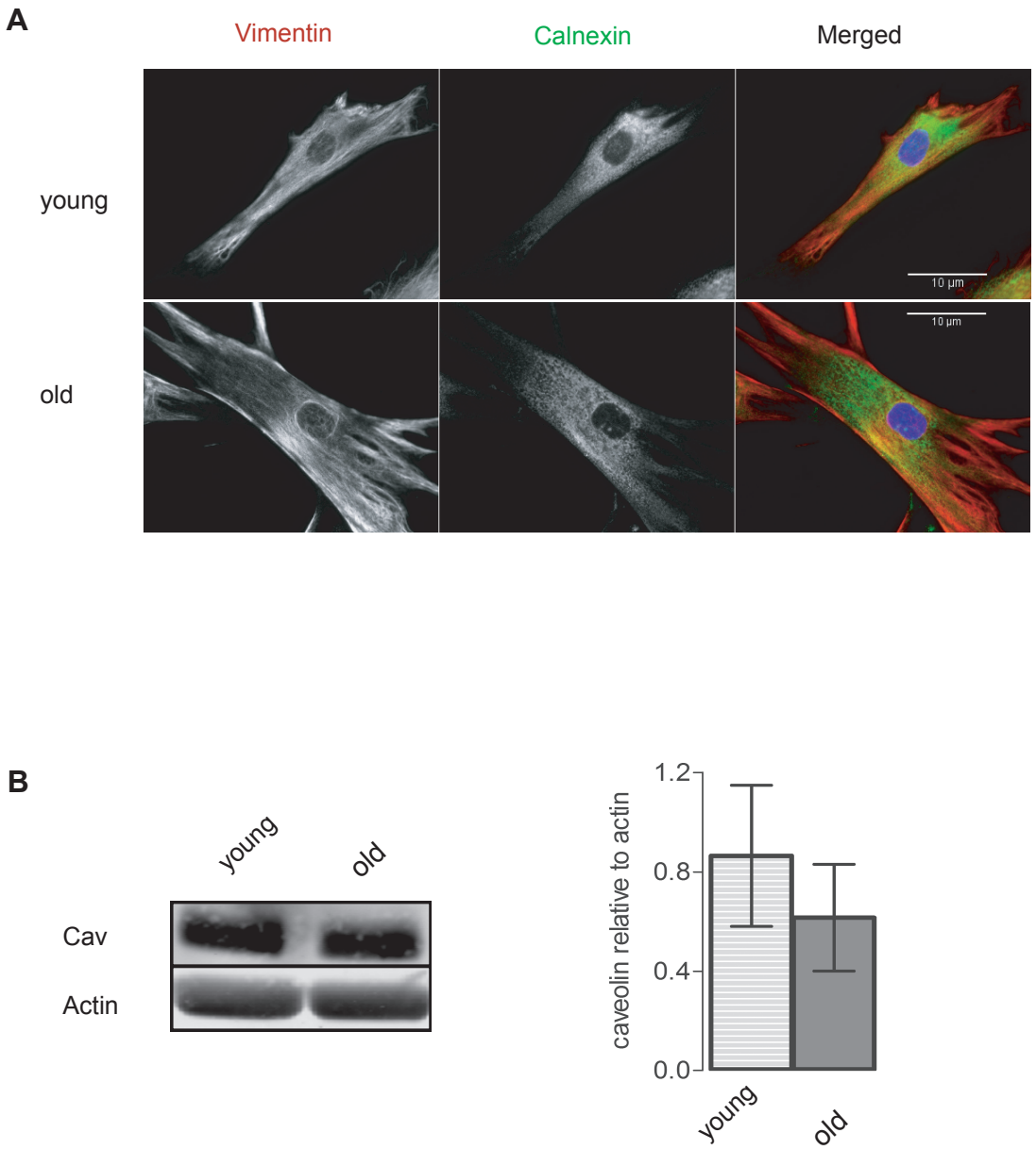

Figure 5.1: Characterisation of skin fibroblasts from young and old donors.
A) Immunofluorescence of intermediate filaments (vimentin) and the ER (calnexin). Cells were grown on glass coverslips. After methanol fixation and permeabilisation the cells were incubated with the indicated antibodies.
(**B**) Protein extracts were prepared in SDS buffer and analysed by Western blotting using the indicated primary antibodies followed by infrared secondary antibodies. The intensity of the infrared signal obtained with anti-caveolin antibody was quantified using the Odyssey software, and normalised relative to the intensity of the signal of actin. The graph shows the normalised signal. The lines and error bars show the mean ± s.e.m.of three independent experiments.

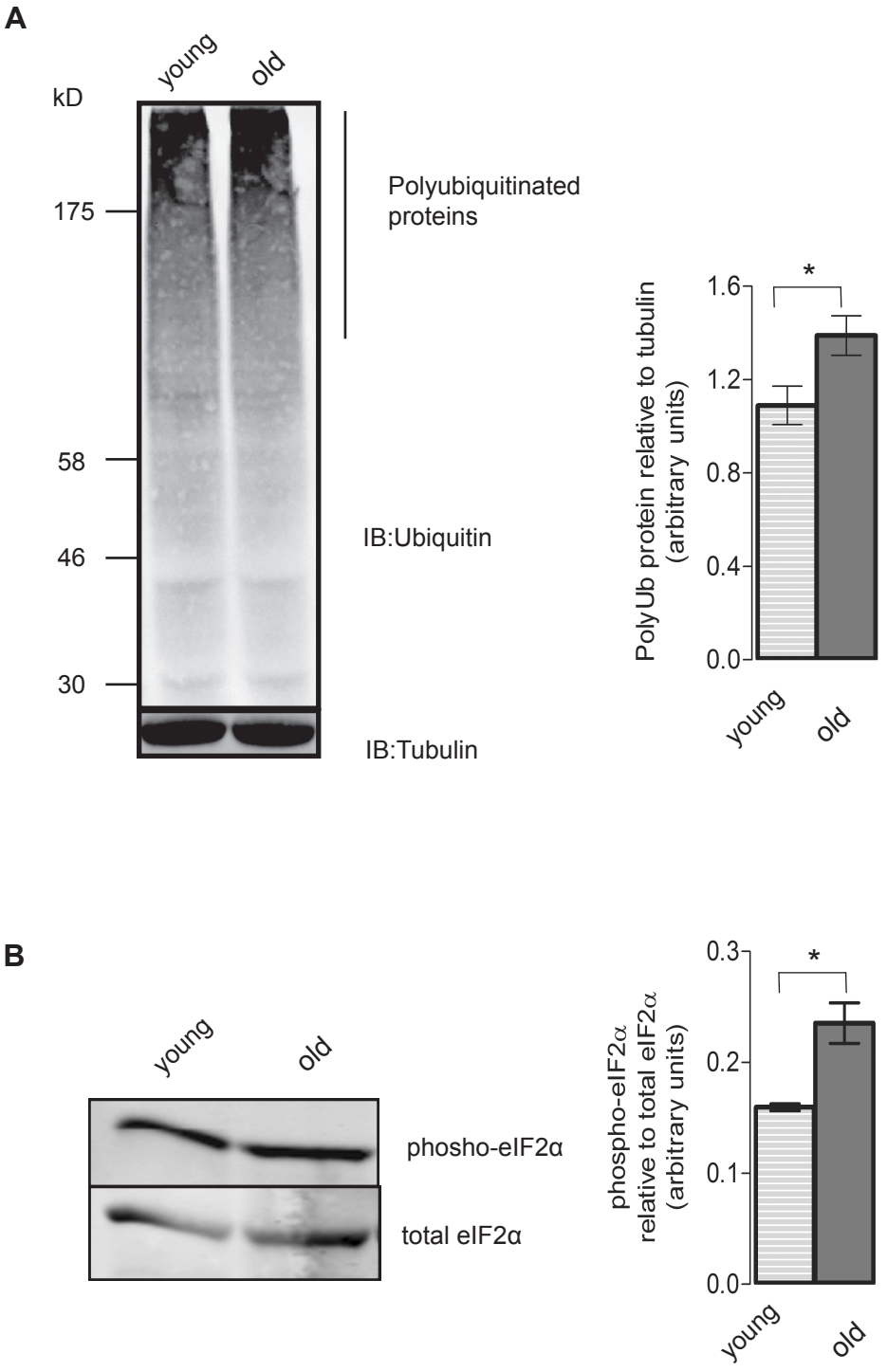

Figure 5.2: Immunoblot analysis of polyUb proteins and of basal level of phospho-eIF2α in fibroblasts from young and old donors.
Cells were extracted in SDS loading buffer and 50 µg of total protein was analysed by SDS-PAGE and western blotting using the specified primary antibodies followed by infrared secondary antibodies. The intensity of the infrared signal obtained with each antibody was quantified using the Odyssey software, and normalised relative to the intensity of control protein (e.g. tubulin and total eIF2α). The graph shows the normalised signal for each protein. The lines and error bars show the mean ± s.e.m. respectively. The Student's t-test was used to determine significant differences between levels of the proteins in the cells from young and old donors. * P denotes < 0.05, n=3

The next step was to analyse the expression levels of ER resident proteins or of proteins that are key components of ER-associated processes. Cellular extracts were prepared from 3 different cultures of young and old cells and analysed by SDS-PAGE and infrared western blotting as described previously. The level of expression of many of the tested proteins (Rpl17, SPC25, calnexin, ERp57, PDI, p5, OS9, Der-1 and p97) did not change in cells from old donors (Fig 5.3 and Fig 5.4), suggesting that ageing of skin fibroblasts is not accompanied by global changes in the expression level of these ER components. However, the expression level of BiP was increased in the *in vivo* aged cells (Fig 5.3), as observed previously in the HPD in vitro aged cells (Fig 5.3). In contrast, the expression levels of calreticulin and Sel1L were decreased by almost 25% in the old cells (Fig 5.3 and Fig 5.4).

Again, as seen in the *in vitro* aged cells, a significant decline of approximately 40% in the level of Rpt6 was observed in cells from old donors (Fig 5.4B). Consistent with studies indicating altered composition of proteasome with age (Koga *et al.* 2010), the function of the proteasome may also be compromised in these cells. This could explain the increased levels of polyUb proteins in the cells from the old donor. In addition, the expression levels of BAG3 (a component of the autophagic pathway) was slightly increased in fibroblasts from old donors (Fig 5.4B), similar to the results from aged tissues and the *in vitro* aged cells, indicating that the autophagic pathway is upregulated in these cells as well. Thus the upregulation of an alternative proteolytic pathway (e.g. BAG3-mediated macroautophagy) seems to be another common feature of ageing.

In summary, some but not all, of the changes in proteostasis components observed in cells aged *in vitro* were also seen fibroblasts obtained from old donors, namely decreased levels of Rpt6, increased levels of BiP and phospho-eIF2α

5.3 Protein biosynthesis and translocation into the ER

Next, the same assays described for the IMR90 fibroblasts (section 4.3) were used to determine whether the efficiency of ER protein translocation was different in fibroblasts isolated from young and old donors. First, the 'global' efficiency of ER protein translocation was examined by pulse-labelling cells, followed by digitonin extraction of cytosolic components and isolation of N-glycoproteins by conA binding. The conA-bound fraction, representing ER translocated proteins, was expressed as a percentage of the total proteins, cytosolic proteins or the unbound proteins (Fig 5.5B). In each case, a similar ratio of N-glycoprotein to non-glycoprotein was observed in cells from young and old donors, suggesting that the proportion of nascent proteins transported into the ER and subject to N-glycosylation, was similar in both cell populations. Thus the overall load of client proteins entering the ER is not significantly different in the young and old cells. Similar results were obtained in the LDP and HPD fibroblasts (section 4.3). The translocation of individual ER-targeted model proteins was tested using an *in vitro* translation system in the presence of [^{35}S] Met/Cys and semi-permeabilised young or old cells (Wilson *et al.* 1995). The

same substrates (i.e. γ-INF, US2, HA, SPP, ops and pPL) described for IMR90 fibroblasts were used here (see section 4.3 and Fig 4.7) and N-glycosylation was used as a surrogate marker of protein import into the ER. As observed previously, *in vitro* translation of γ-INF generated two products (Fig 5.6 Ai lanes 1 and 3) and EndoH treatment (Fig 5.6 Ai lanes 2 and 4) showed that the high MW band represents N-glycosylated, and thus ER-translocated γ-IFN. The lower MW band was not affected by EndoH treatment and had a slightly higher MW than the EndoH cleaved protein, suggesting it represents a non-glycosylated form of γ-IFN that still possesses the N-terminal signal sequence. The amount of the glycosylated γ-INF was quantified and expressed as percentage of the total translation product in order to provide measure of translocation efficiency (Fig 5.6B). A slight increase in the proportion of N-glycosylated γ-IFN was observed in old cells (27%) compared to the young cells (20%). Although small, this change is interesting as a similar effect on γ-IFN translocation was observed in *in vitro aged* cells (section 4.3). For each of the other N-glycosylated proteins, only two translation products were observed (Fig 5.6Ai – vi, lanes 1 and 3), the larger of which disappeared after EndoH treatment (Fig 5.6Ai – vi, lanes 2 and 4), and only low MW form could be seen. Thus the upper band represents the N-glycosylated form, whilst the lower band is the non-glycosylated and likely non-translocated form (section 4.3). In the case of HA, a significant loss of protein was observed upon EndoH treatment (Fig 5.6 Aiii) potentially as result of proteolysis during the 16 hour EndoH treatment. Translation of the unglycosylated substrate (pPL) also generated two species. As described previously, these were identified as the signal cleaved, ER translocated protein (Fig 5.6 Avi lanes 2 and 4, resistant to proteinase K). and the non-translocated signal uncleaved protein following protease protection (Fig 5.6 Avi lanes 1 and 3, sensitive to proteinase K). The low MW band represents the cleaved, translocated form (resistant to proteinase K treatment) and the high MW band is the uncleaved, non-translocated form (proteinase K sensitive) of the protein. Hence, the amount of translocated pPL was calculated as proportion of total translated product and plotted (Fig 5.6B). Following quantification, the glycosylated form, or signal cleaved form in the case of pPL, was again expressed as a percentage of the total translation product (Fig 5.6B). However, these assays were only performed once, and would therefore need to be repeated in order to perform statistical analysis. Nonetheless, it is striking that each of the changes in translocation efficiency of the various substrates observed in HPD cells were also seen in fibroblasts isolated from old donors. Thus US2 appears to be less efficiently translocated in old fibroblasts versus young fibroblasts, while HA, SPP and opsin look similar in both young and old cells.

These results indicate that the efficiency of global translocation, measured by the proportion of proteins undergoing N-glycosylation is similar in skin fibroblasts isolated from young and old cells. The similar intensity of radiolabelling in both young and old cells, indicating that the load of client proteins imported in the ER is similar in cells isolated from young and old individuals. In addition, the analysis of individual substrates showed some minor differences in terms of the efficiency of translocation, mirroring those observed in the HPD IMR90 lung fibroblasts.

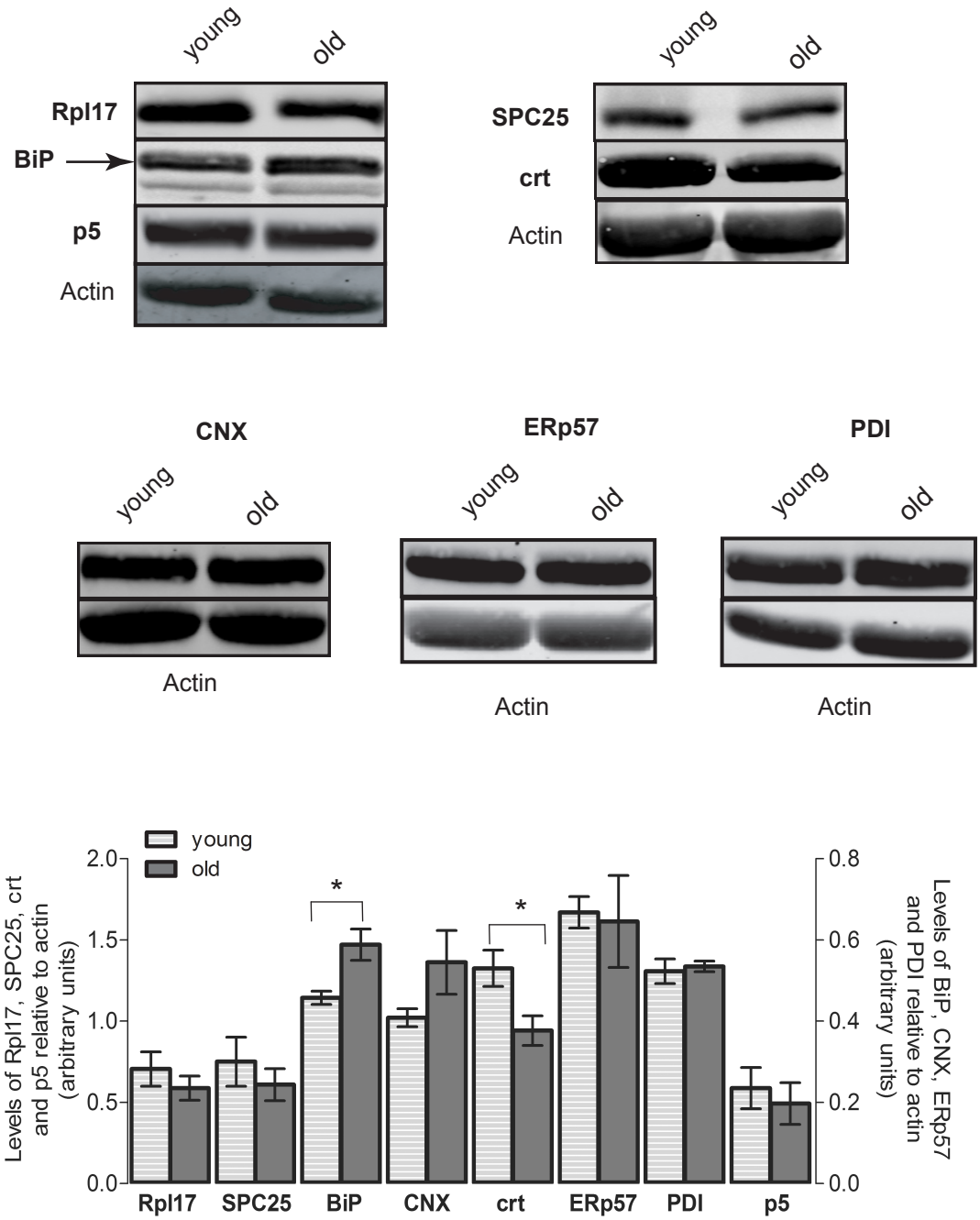

Figure 5.3: Expression level of factors involved in protein biosynthesis and ER folding in fibroblasts from young and old donors.
Cells were lysed in SDS loading buffer to obtain protein extracts and equal amounts of total protein were loaded for each sample. Proteins were separated on 12% Tris-glycine gels and analysed by western blotting using the primary antibodies indicated followed by infrared secondary antibodies. The intensity of the fluorescent signal obtained with each antibody was quantified using the Odyssey software, and normalised relative to the intensity of the actin signal. The graph shows the normalised signal for each protein. The lines and error bars show the mean ± s.e.m. The Student's t-test was used to determine significant differences between levels of the proteins in young and old cells. * denotes $P < 0.05$, $n = 3$.

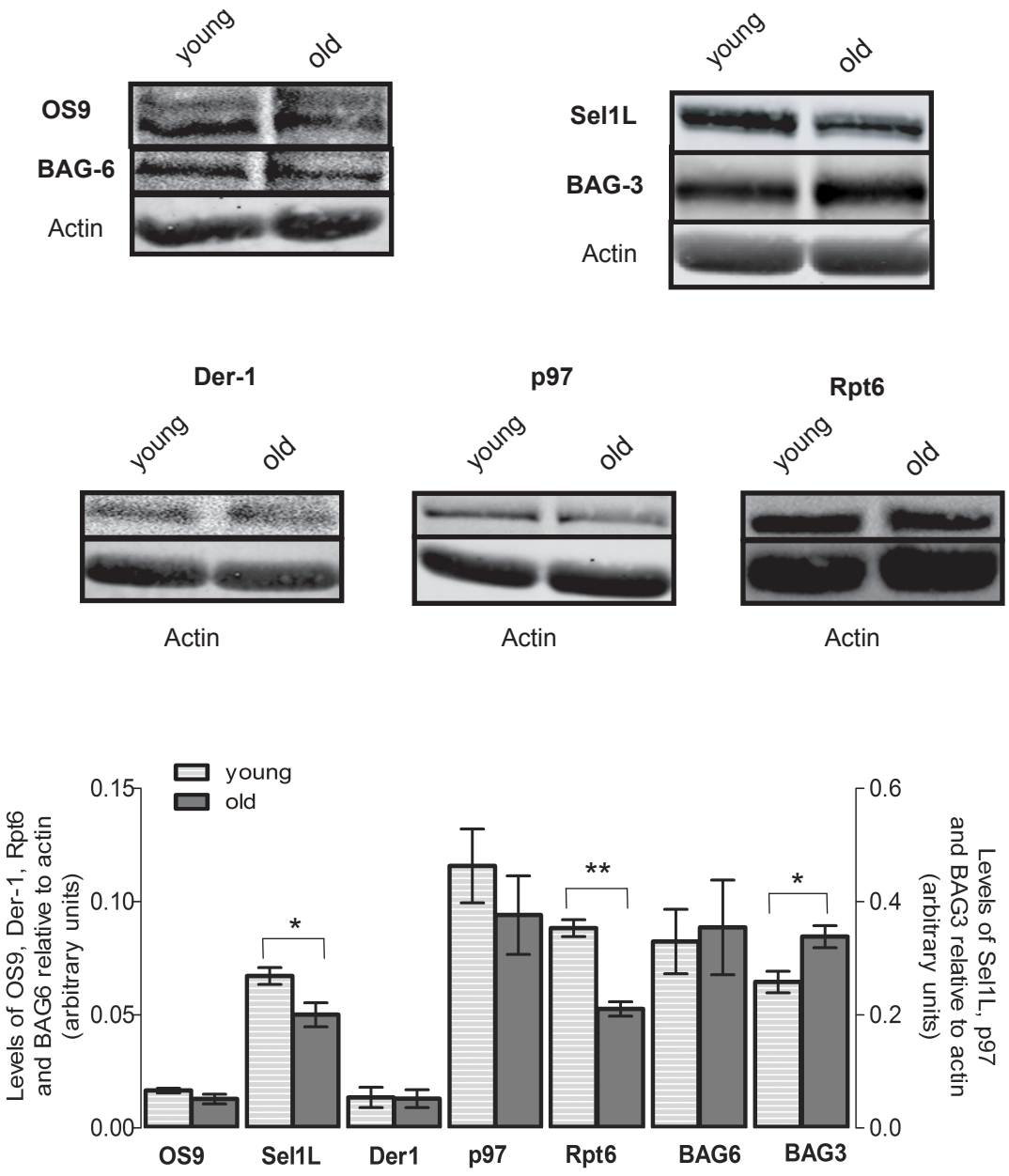

Figure 5.4: Levels of components of the ERAD machinery and of proteolytic pathways in skin fibroblasts from young and old donors.
Protein extracts from young and old cells were prepared and analysed as described in Fig 5.3. The intensity of the infrared signal obtained with each antibody was quantified using the Odyssey software, and normalised relative to the intensity of actin signal. The graph shows the normalised signal for each protein. The lines and error bars show the mean ± s.e.m. respectively. The Student's t-test was used to determine significant differences between levels of the proteins in cells from young and old donors.
* denotes $P < 0.05$ and ** denotes $P < 0.01$, n = 3.

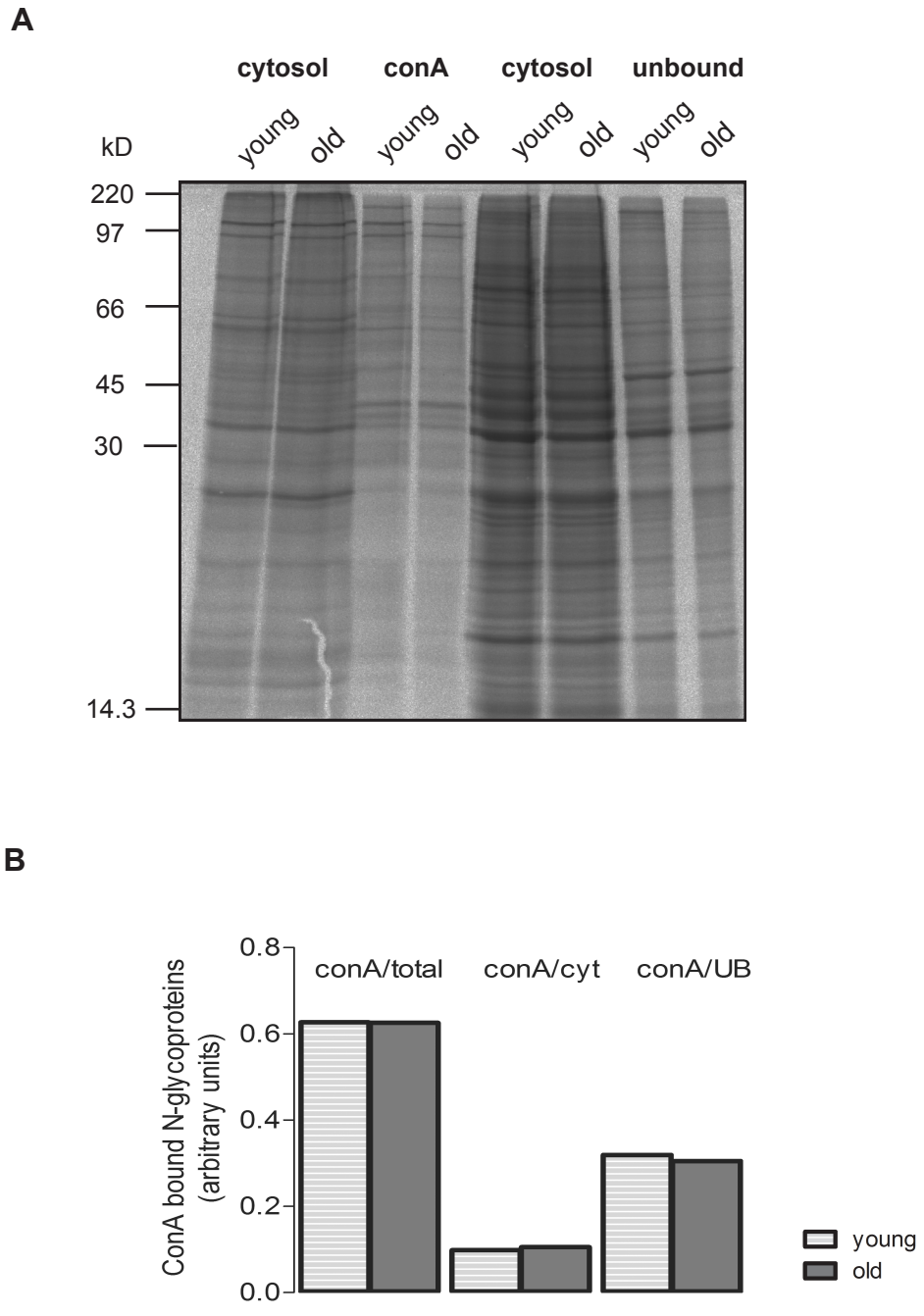

Figure 5.5: General glycoprotein biosynthesis in fibroblsast from young and old donors.
(A) Cells were pulse labelled and digitonin treated to extract the cytosol, then lysed in buffer containing 1% Triton X-100. The cell lysate was incubated with conA-sepharose and the bound glycoproteins were eluted with α-methylmannosidase. The cytosol and unbound (UB) fraction were subject to TCA precipitation and 1/10th of cytosol and unbound and 1/3rd of conA bound fraction were analysed by SDS-PAGE and phosphorimaging.
(B) The lanes were quantified using the AIDA software and the glycoproteins (conA-bound fraction) was normalised to the cytosol (cyt), UB or total cell lysate (total) and graphically represented.

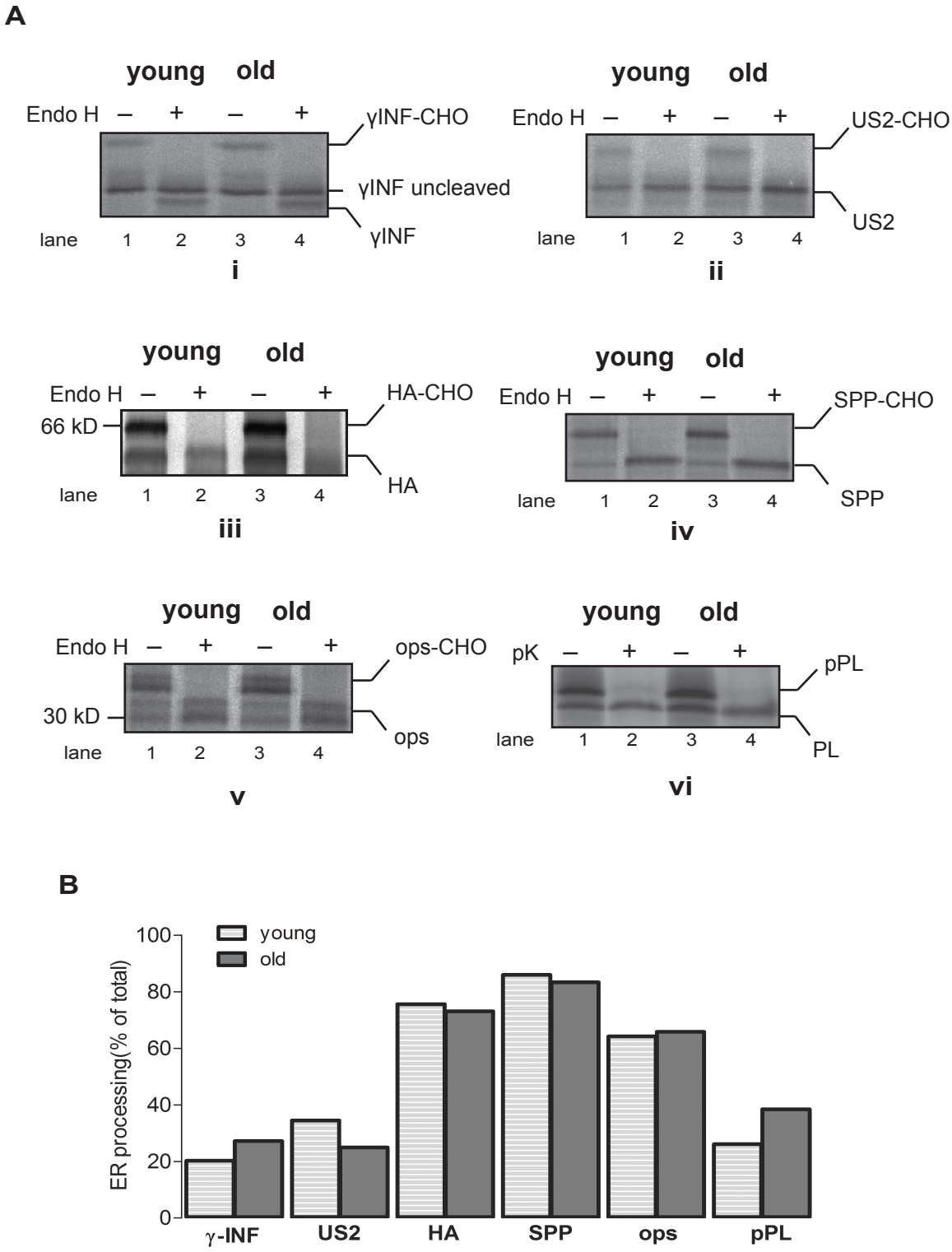

Figure 5.6: Analysis of translocation in young and old cells.
The indicated mRNA were in *vitro* translated in the presence of [^{35}S] Met/Cys and semi-intact young and old cells and the products were EndoH or proteinase K treated as indicated. The samples were loaded onto 10% (HA) and 12% Tris-glycine gels and following drying, the gel was exposed to a Phosphoimager plate. Each band was quantified using the AIDA software. The glycosylated form representing the translocated substrate was plotted as percentage of the total. In the case of pPL, protease K protection was used for monitoring translocation and the cleaved pPL was plotted as percentage of the total.

5.4 Folding and trafficking in the secretory pathway

The capacity to fold and export cargo proteins of young and old cells was examined using the metastable, temperature sensitive mutant tsO45VSV-G as a folding sensor. First, the kinetics of VSV-G folding was analyzed using the temperature shift assay described previously. Cells expressing VSV-G were grown overnight at the restrictive (40^{o}C) temperature, at which temperature VSV-G is synthesised but fails to fold correctly and is retained in the ER. Cells were then shifted to the permissive (32^{o}C) temperature and incubated with cycloheximide, in order to allow the misfolded VSV-G to fold and progress along the secretory pathway. Cells were harvested at different time points following the shift to 32^{o}C, the samples were treated with EndoH, and the acquisition of EndoH resistant N-glycans was monitored by increased migration upon SDS-PAGE and Western blotting (Fig 5.7A). At the 0 time point all the VSV-G shifted to the lower MW form upon Endo H treatment, (Fig 5.7A, lanes 1 and 7), consistent with the protein being retained in the ER of both cell populations at restrictive temperatures. After 20 minutes at the permissive temperature, a proportion of the VSV-G was resistant to EndoH and remained in the higher MW form following treatment (Fig 5.7A, lanes 2 and 8), indicating that this pool VSV-G had been properly folded and transported to the medial Golgi apparatus. With increasing incubation time, the amount of the EndoH resistant form increased with a parallel decline in the intensity of the lower EndoH sensitive form, showing that the VSV-G was being folded and exported to the Golgi apparatus (Fig 5.7 lanes 3-6 and 9-12). Each band was quantified and the ratio of EndoH resistant to EndoH sensitive VSV-G was plotted against time (Fig 5.7B). No differences were observed in either the speed with which EndoH resistance was achieved, or the extent of EndoH resistance at any of the time points in the young and old cells (Fig 5.7B). This suggests that there is no difference in the ability of cells obtained from young and old donors to support the folding and trafficking of this metastable protein. This is in contrast to the IMR90 fibroblasts, where EndoH resistance was acquired significantly more slowly and to a lesser extent in HPD cells.

The ability of the skin fibroblasts from young and old donors to support the folding of VSV-G was then examined at different temperatures, again using EndoH resistance as a measure of correct folding, in order to determine whether any folding defects became apparent at higher temperatures. To this end, cells expressing VSV-G were grown overnight at 32, 37 or 40 ^{o}C and the relative proportion of EndoH-sensitive and EndoH-resistant protein was determined to provide a readout of the folding capacity of young and old cells (Fig 5.7C). The advantage of this method over the kinetic assay is that it allows measurement of steady state pool of protein at a range of different temperatures, which could potentially reveal more subtle changes in folding capacity. In the absence of EndoH treatment, a single form of VSV-G was observed (Fig 5.7C lanes 1, 3, 5, 7, 9, 11). In cells that had been incubated at 40^{o}C, EndoH treatment resulted in this band disappearing and being replaced by a lower MW form, consistent with the VSV-G being misfolded and retained in the ER at 40^{o}C (Fig 5.7C, lanes 6 and 12). In contrast, when

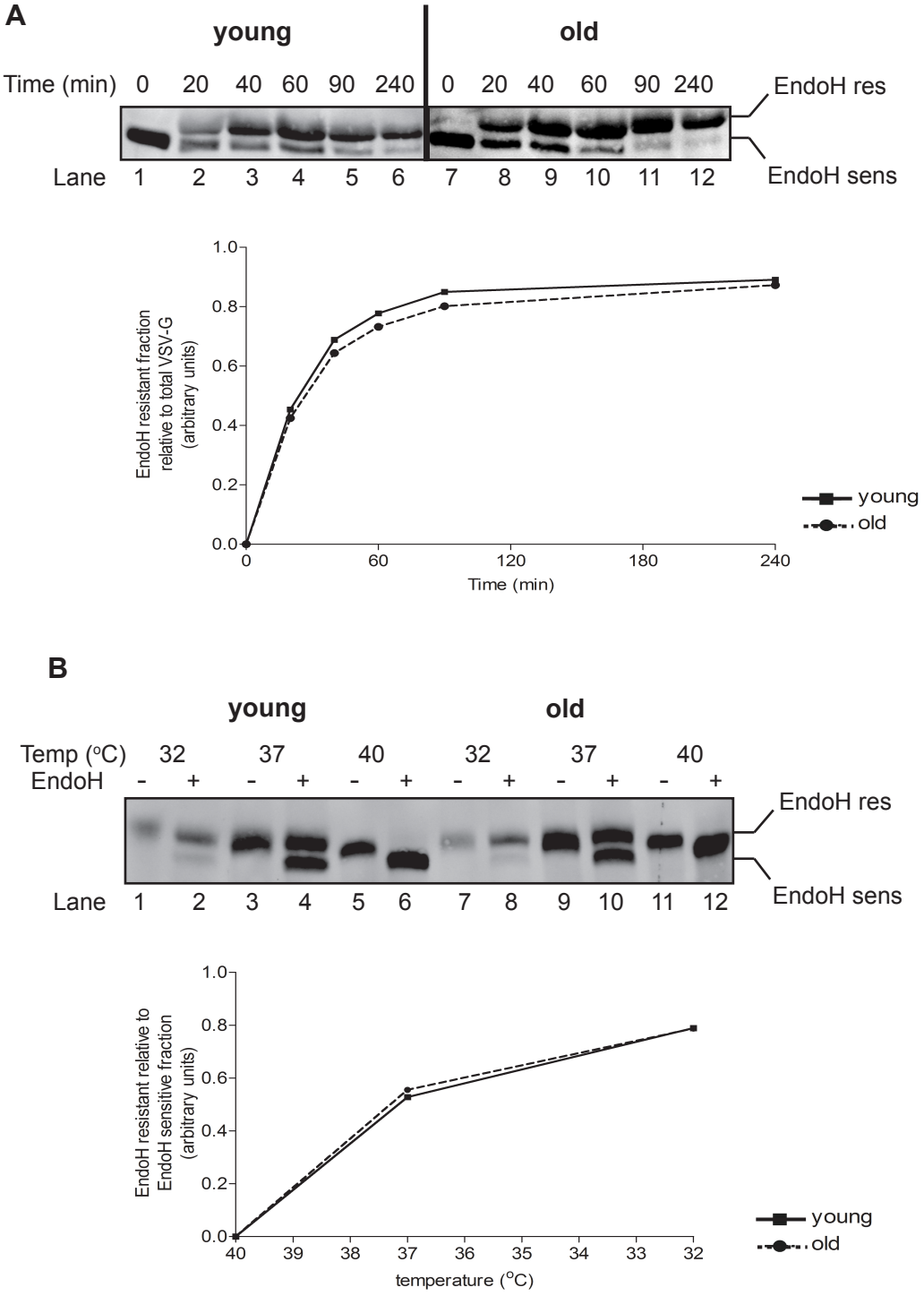

Figure 5.7: Analysis of folding capacity in fibroblasts from young and old donors.
(A) VSV-G infected cells were incubated overnight at 40°C. The next day the cells were treated with cycloheximide and chased for the indicated time points. Following lysis, the samples were EndoH treated, separated by 8% SDS-PAGE and analysed by immunoblotting with anti-VSV-G antibodies. **(B)** VSV-G infected cells were incubated overnight at the indicated temperature. In the next day the cells were lysed, EndoH treated and analysed by SDS-PAGE and immunoblotting.
(A, B) The intensity of fluorescence for each band was quantified using the Odyssey software and the ratio of EndoH resistant to total VSV-G was plotted against time **(A)** or temperature **(B)**.

cells were grown at 32^{o}C, the VSVG was almost completely resistant to EndoH treatment, with only a very faint band detected at a lower MW upon EndoH treatment (Fig 5.7C lanes 2 and 8), showing that at this temperature, the protein had been correctly folded and transported through the Golgi apparatus. Cells grown at 37^{o}C contained a mixture of both EndoH-resistant and EndoH-sensitive VSV-G (Fig 5.7C lanes 4 and 10), suggesting that at this intermediate temperature, a proportion of the protein was correctly folded whilst some failed to attain the correct conformation and was retained in the ER. In HPD IMR90, significantly less VSV-G was able to fold correctly at 37^{o}C than in LPD cells, suggesting that the in vitro aged cells were less able to support folding of this metastable protein. However, when the ratio of EndoH-resistant to EndoH-sensitive VSV-G was calculated, no differences were seen between *in vivo* young and old cells.

Thus, no loss of ER folding capacity was detected the skin fibroblasts obtained from the aged donor compared to those from the young donor.

5.5 Assessing ER-associated degradation

The efficiency of the ERAD process was investigated in young and old cells using the same two ERAD substrates, NHK-α1AT and TCRα, as for IMR90 cells. Cells transiently expressing the ERAD substrates were treated with cycloheximide to stop synthesis of additional protein, then chased for the indicated times, and the amount of the ERAD substrate remaining at each time point determined by quantitative western blotting. A single immunoreactive species was observed at the predicted MW for each of the model substrates NHK-α1AT (Fig 5.8A > 46kD) and TCRα (Fig 5.8B, <46kD). In the cells from young donors, both ERAD substrates were rapidly lost following addition of cycloheximide (Fig 5.8A and B), suggesting both proteins were efficiently degraded. In contrast, the loss of TCRα (Fig 5.8B) and to a lesser extent NHK-α1AT, was slower (Fig 5.8A.). In the case of TCRa, very little of the protein was degraded within the 2 h chase in old cells, whilst over 50% had been eliminated in young cells (Fig 5.8B). These preliminary results indicate that the ERAD pathway may be less efficient in cells obtained from the old donor. Similarly, the *in vitro* aged IMR90 cells exhibited a marked defect in ERAD of these two substrates, suggesting that a decline in ERAD capacity may be a feature of both forms of cellular ageing.

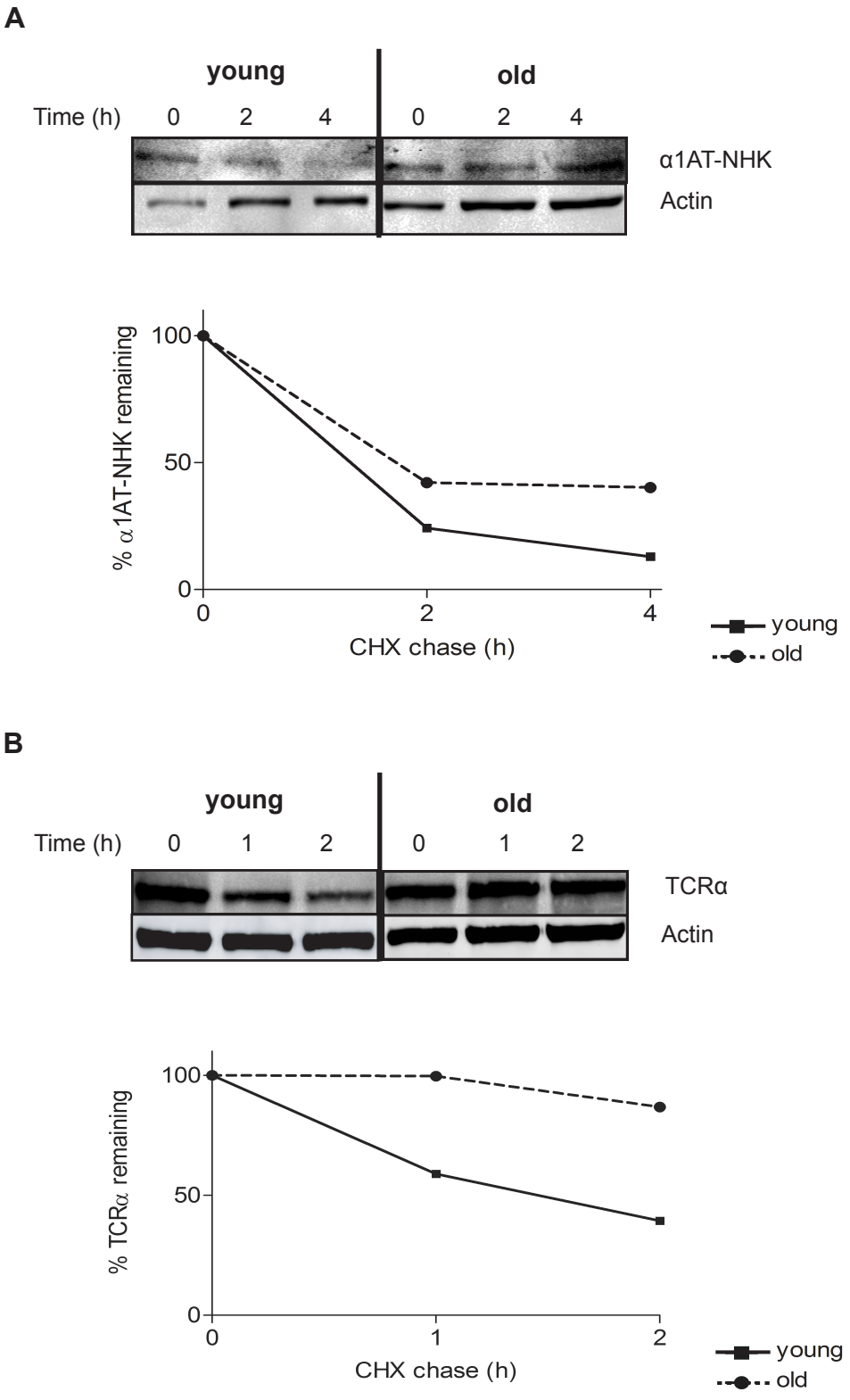

Figure 5.8: Degradation assay of α1A-NHK and of TCRα in fibroblast from young and old donors.
Two days after transfection the cells were treated with cycloheximide and harvested immediately (t=0) or after the indicated times. Lysates were resolved by 12% SDS-PAGE and analysed by quantitative immunoblot using the specific antibodies. Actin was used as loading control. The bands were quantified, normalized to actin and plotted as percentage of the value at chase time 0. The results for α1A-NHK are presented in **(A)** and for TCRα are shown in **(B)**

5.6 UPR signalling in the young and old cells

One of the most striking observations in the previous chapter was the increased sensitivity of HPD fibroblasts to activation of the IRE1/*XBP1* arm of the UPR upon perturbation of ER folding. Therefore, it was of interest to examine whether the cells obtained from the old donor exhibited a similarly heightened sensitivity to ER stress induction.

First, the activation of IRE1 in response to treatment with two ER stressors, Tn or DTT, for increasing lengths of time, was measured using RT-PCR to monitor splicing of *XBP1* mRNA (Fig 5.9A). In the untreated cells, only a single PCR product was observed, corresponding to the unspliced Xbp1 mRNA (Fig 5.9A lanes 1 and 7). When cells were treated with Tn, splicing of *XBP1* was first observed in both young and old cells at 2 hours after treatment. In both young and old cells, the spliced *XBP1* mRNA became the predominant form after 4 hours and the major form at 8 hours of treatment (Fig 5.9A lanes 3-4 and 9-10). By 16 hours, a decrease in the *XBP1* splicing was observed in young cells, suggesting they had begun to recover and attenuate IRE1 signalling (Fig 5.9A lane 5), In contrast, the spliced *XBP1* was still the major form in the old cells at this time, suggesting a delay in recovery and/or attenuation of IRE1. A difference between the two cell populations was still just about visible after 24 hours of treatment, with the unspliced *XBP1* mRNA product being the predominant form in the young cells (Fig 5.9A lane 6), while in the old cells the spliced product was slightly more abundant (Fig 5.9A, lane 12). These data suggest that although the activation of UPR seems to be similar in both young and old cells, the recovery and/or attenuation of IRE1 signalling may be delayed in fibroblasts isolated from the aged donor.

It was important to rule out that the differences in IRE1/*XBP1* splicing seen after the Tn treatment were caused by differences in the effect of Tn to inhibit N-glycosylation in the two different cell populations. Therefore cells were treated with different concentrations of Tn, semi-permeabilised and their ability to mediate N-glycosylation of the model glycoprotein SPP examined using the *in vitro* translation/translocation assay (Fig 5.9B). As observed previously, both N-glycosylated and non-glycosylated forms of SPP were observed in the untreated cells (Fig 5.9B, lanes 1 and 6). With the increasing concentration of Tn the intensity of the upper form representing glycosylated SPP band decreased in intensity, and completely disappeared at 10 µg/ml (Fig 5.9B lanes 2-5 and 7-10). The intensity of each form was quantified and the ratio of glycosylated to non-glycosylated SPP was calculated and expressed as percentage of the untreated samples. The effect of Tn on this ratio was almost identical in the young and old cells, suggesting that the ability of Tn to inhibit glycosylation was the same in young and old cells

Next, the ability of a second ER stressor to activate IRE1/*XBP1* was examined (Fig 5.10A). As seen with Tn, there was no clear difference in the ability of DTT to induce *XBP1* mRNA splicing in the cells from young and old donors (Fig 5.10A). In order to assess recovery from DTT-induced misfolding and the subsequent attenuation of UPR signalling, cells were treated with

DTT for 30 min, then washed to remove DTT and incubated at 37^{o}C in the continued absence of DTT to allow recovery (Fig 5.10B). As observed in the previous experiment, after 30 minutes of DTT treatment, most of the *XBP1* mRNA product was the spliced form in both cell populations (Fig 5.10B, lanes 2 and 7). Following DTT removal, the level of spliced *XBP1* mRNA product started to decrease whilst the unspliced product increased and became the major form after 60 minutes of chase (Fig 5.10B, lanes 4-5 and 9-10). A similar profile was observed for young and old cells. Quantification of the ratio of spliced to unspliced *XBP1* at each time point indicated there may be a slight lag period in the recovery from DTT induced stress in the cells from the old donor (Fig 5.10B). Hence, the level of spliced X *XBP1* increased slightly in the 15 min following DTT washout, but declined slightly in cells from young donors (Fig 5.10B). Whilst this experiment clearly needs to be repeated before firm conclusions can be drawn, the result are consistent with the delay in recovery from Tn induced stress (Fig 5.9A), and imply that the cells from the old donor recover more slower from ER stress.

In conclusion, activation of the IRE1/*XBP1* branch of the UPR following treatment with Tn or DTT seems to be similar in both young and old cells. However, the cells from the aged donor may have a reduced capacity to recover from ER stress and switch off IRE1 signalling.

A

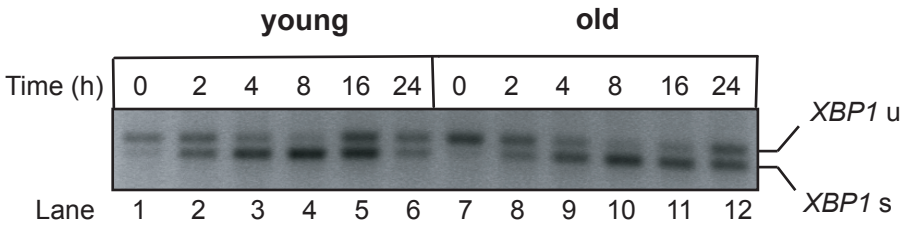

B

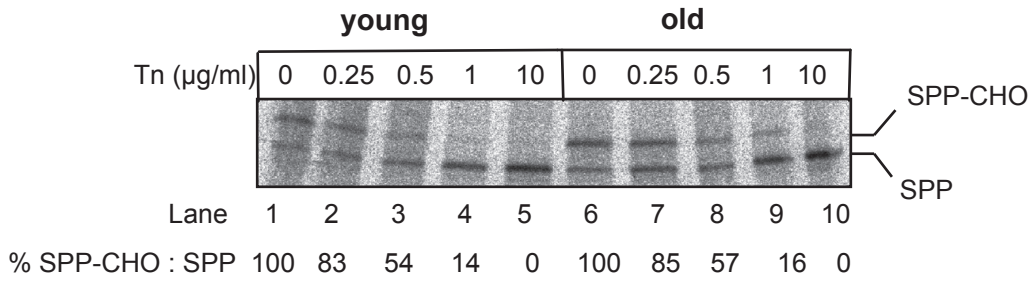

Figure 5.9: Evaluation of IRE-1 arm activation in fibroblasts from young and old donors, after treatment with tunicamycin.
(A) Cells were treated with Tn for the indicated time points and *XBP1* mRNA splicing was determined by RT-PCR. The spliced and unspliced forms are indicated in the figure.
(B) Cells treated with the indicated concentration of Tn for 8 hours were used to obtain the semi-permeable cells. SPP mRNA was translated for 1 hour and products were resolved by SDS-PAGE and analysed by phosphorimaging. The bands were quantified and the ratio of glycosylated to the non-glycosylated form was expressed as percentage of the untreated sample.

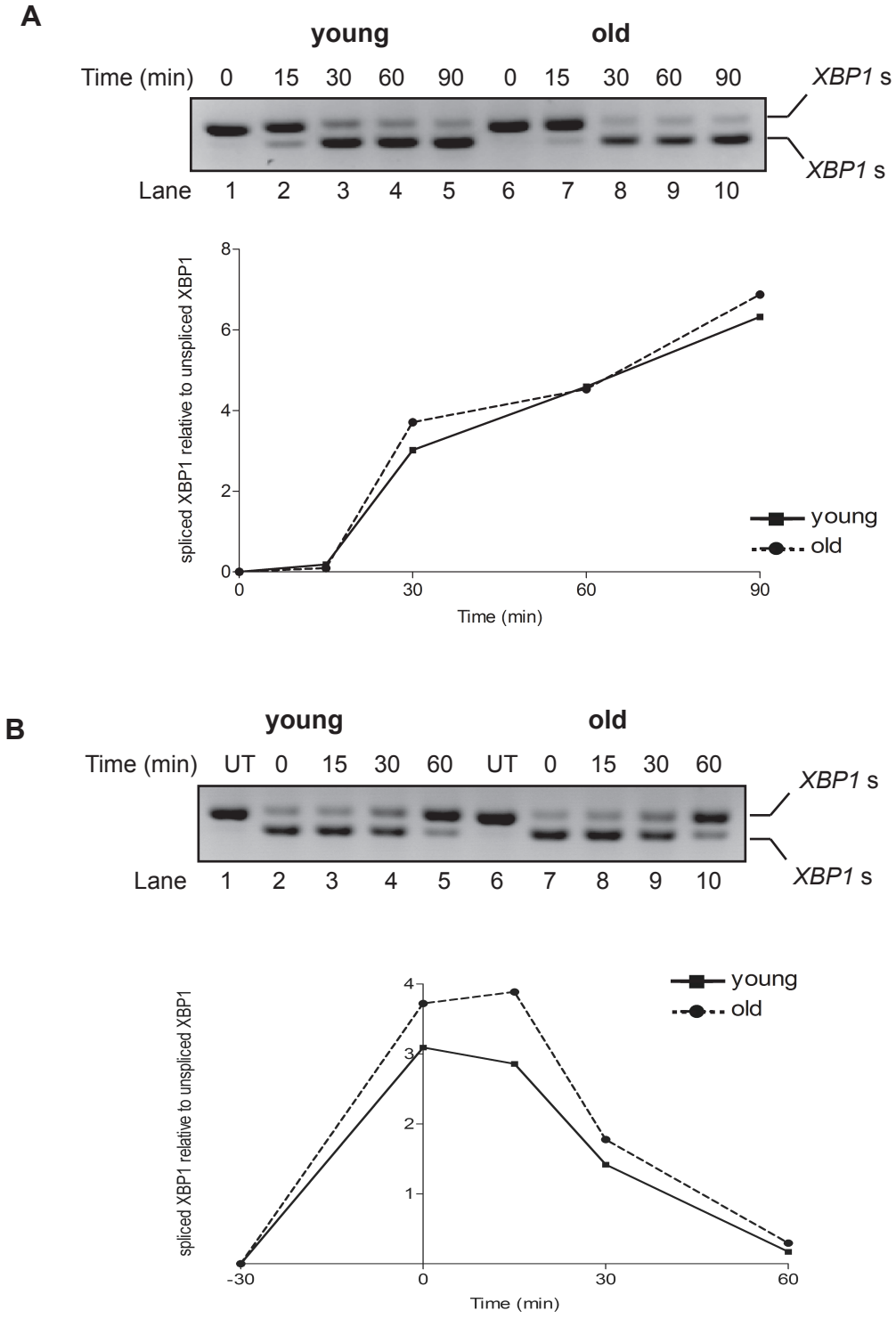

Figure 5.10: Evaluation of IRE1 branch in fibroblasts from young and old donors, after DTT treatment.
(A) Cells were treated with 0.5 mM DTT for the indicated time and *XBP1* splicing was determined by RT-PCR.
(B) After a 30 minute treatment with 0.5 mM DTT, cells were washed, then harvested at the indicated time points and analysed by RT-PCR for *XBP1* splicing.
The bands were quantified using AIDA sofware and the spliced form relative to the unspliced form was plotted against time.

5.7 Discussion

Skin fibroblasts harvested from young and old donors were used as an additional model to test whether ER protein homeostasis is affected with age. The *in vivo* aged cells are clearly different to the IMR90 mode of replicative ageing. Both accumulate age-related changes, but in different ways. Although the skin fibroblasts from young and old donors may have been aged in a more physiological manner, i.e. in situ, there are potential problems with these as an experimental model for ageing. First, the cultures were obtained from separate donors and may have been established at different times under different conditions. This means that genetic variation and differences in initial culture conditions may make detection of age-related changes in biological pathways, particularly subtle effects, very difficult to detect. In addition, expansion of the cultures in vitro may select against 'aged' cells if they are less able to replicate. Thus, it was important to analyse these cells at as low PD as possible. Unfortunately, this limits the numbers of cells that are available for analysis. Furthermore, once they are removed from the donor and cultured in vitro, they will no longer be exposed to the extrinsic influences of the 'aged' environment. These latter two factors may also be relevant for the IMR90s and any cell culture model. On balance, the IMR90s have the advantage that they are genetically identical and therefore can rule out differences in genetic background. However, it must be appreciated that there are differences between this form of replicative ageing *in vitro* and normal *in vivo* cellular ageing in situ. Other possibilite models might include cells from premature ageing syndromes which are available from the Coriell Institute.

The study of expression level of proteostasis components revealed that the expression level of various proteins were different in cells from young and aged donors. The pattern of age-related changes was different to those observed in the *in vitro* aged cells. However, some similarities were noted, namely the decreased level of expression of the proteasomal subunit Rpt6, the accumulation of polyUb proteins, the increased levels of BiP and phospho-eIF2α were observed in both HPD IMR90 fibroblasts and skin fibroblasts from the old donor, compared to their young counterparts. Some of these changes (e.g. increased levels of polyUb proteins, and phospho-eIF2α), were also observed in the tissues from aged mice, indicating that they may represent fundamental features of ageing.

When the function of ER was investigated using the fibroblast from young and old donors, some of the same trends were observed as noted in the LPD/HPD IMR90 fibroblasts, however the differences between the young and the old cells were much less clear . The overall efficiency of glycoprotein biosynthesis seemed to be unchanged in old cells, but the translocation efficiency of several individual model proteins was affected. Interestingly, these changes appeared to mirror those seen in the IMR90 cells. For instance, the translocation of US2 was reduced in old fibroblasts and HPD cells, while the translocation of pPL was increased, as previously seen for HPD cells. In addition, the degradation of two ERAD substrates, NHK-α1AT and TCRα, appeared to be compromised in the old fibroblasts, similar to the data obtained for HPD cells. In

addition, examination of IRE1/*XBP1* activation showed some similarities with the data from *in vitro* aged IMR90 cells. Although no difference in the initial activation of IRE1 was observed, the cells from the old donor appeared to exhibit a delay in recovery and switching off *XBP1* splicing. This could indicate that the old cells were less capable of coping with the changes in ER homeostasis than young cells. In contrast, no differences could be seen between the ability of young and old cells to support folding and trafficking of the metastable folding sensor ts VSV-G. This may be due to the inability of this assay to detect subtle changes in folding capacity, which would be consistent with the lower magnitude of age-associated changes in the other assays. Equally, it is possible that the folding capacity of the old cells and young cells is similar.

.

Altogether, these preliminary results are intriguing and suggest that at least some of the changes in ER proteostasis pathways observed in the *in vitro* aged cells may also be a feature of cells isolated from aged individuals. However, these changes are very subtle and not all those observed in the LDP/HPD IMR90 cells were seen. Despite the use of cells obtained from related donors (father and son), the confounding influence of genetic variation cannot be ruled out. In the future, it would be important to repeat these experiments with cells obtained from several old and young donors.

CHAPTER 6

Discussion

6.1 General discussion

Ageing is accompanied by decline in immune function and multiple endocrine changes, loss of adaptability and increased susceptibility to diseases. As life expectancy has increased, the incidence of age-associated disorders, such as neurodegenerative diseases, diabetes, cardiovascular diseases, has also risen. Thus, a key goal of ageing research is ultimately to increase the effective 'healthspan.' Ageing is not a random decay of function as once believed, but is now known to be influenced by genetic and environmental factors. Thus there is a real possibility of intervention in such pathways to improve health in old age (Kenyon 2010a). Increasing evidence indicates that protein misfolding contributes both to normal ageing and many age-associated diseases (Douglas & Dillin 2010). The network of pathways responsible for maintaining the proteome in a functional state are thought to decline with increasing age, at least in lower animals such as *C. elegans* (Kourtis & Tavernarakis 2011). Recent studies performed in *C. elegans* have provided evidence of a collapse of the proteostasis network with age (Morley *et al.* 2002; Ben-Zvi *et al.* 2009). This progressive inability to maintain proteins in their correctly folded state leads to widespread aggregation of numerous cellular proteins into insoluble aggregates (David *et al.* 2010). Environmental and genetic manipulations that increase longevity have been shown to modulate proteostasis pathways and delay protein aggregation and proteotoxicity (Morley & Morimoto 2004; David *et al.* 2010; Henis-Korenblit *et al.* 2010), strongly arguing for a role of these pathways in determining healthy lifespan (Kenyon 2010a).

The ER is an essential subcellular compartment, which represents the site of synthesis of approximately 30% of the proteome. The subset of proteins synthesised at the ER includes membrane proteins such as ion channels, receptors and also secretory proteins such as hormones, and signalling molecules. Therefore perturbations in the protein folding function of the ER can induce a broad range of cellular defects. Situations that disrupt protein folding in the ER lead to activation of a stress response pathway, the UPR, which aims to restore proper ER function (Walter & Ron 2011). Prolonged UPR signalling however can disrupt cellular function and has been implicated in the pathology of many diseases, including age-associated neurodegenerative diseases (Wang & Kaufman 2012). There is some evidence that ER proteostasis pathways may be affected with age (Hussain & Ramaiah 2007; Naidoo *et al.* 2008; Paz Gavilán *et al.* 2009). In addition, studies in *C. elegans* have provided evidence that UPR signalling may have a direct impact on lifespan (Viswanathan *et al.* 2005; Henis-Korenblit *et al.* 2010). However, few studies have examined the impact of age on ER proteostasis pathways in higher animals or directly examined the functional capacity of these pathways. To this end, the aim of this project was to investigate how ageing impacts on ER folding/QC, ERAD and UPR pathways. Using tissues from young and old mice, widespread changes in expression of many components of ER proteostasis network were observed. In addition changes in the global proteome consistent with increased incidence of misfolding (e.g. accumulation of polyUb

proteins, increased levels of insoluble, aggregated proteins in muscle, increased levels of BAG3), and evidence of UPR activation (increased phosphorylation of eIF2α) were found. Using an *in vitro* model of cellular ageing provided evidence that increased replicative age is associated with a decline in the protein folding and degradation capacity of the ER, leading to increased sensitivity to ER stress. Intriguingly, the results also indicated that upregulation of chaperone expression in response to ER stress was inefficient in the *in vitro* aged cells. These results are interesting because they indicate that ageing is associated with alterations in components of ER proteostasis pathways, and also the signalling pathways that control the ER homeostasis network in response to intrinsic or environmental challenges. These factors could potentially contribute to an overall decline in protein homeostasis with age.

Chaperone proteins are essential components of the protein homoeostasis machinery, which interact with the polypeptide chain to protect against aggregation and to promote folding, and also recognise misfolded proteins and target them for degradation. The importance of chaperones in maintaining proteostasis has been highlighted by the correlation between reduced chaperone function and conformational diseases, such as Alzheimer's disease (Wilhelmus *et al.* 2006) and longevity (Walker & Lithgow 2003; Morley & Morimoto 2004; Morrow *et al.* 2004). Several previous studies showed that the level of various ER oxidoreductases and ER chaperones decreased with age in rodents. For example, the level of BiP, was assessed in a range of tissues (cortex, hippocampus, cerebellum, heart, lung, liver, kidney and spleen) of young and old rats, and was found to decrease with age (Erickson *et al.* 2006; Paz Gavilan *et al.* 2006; Hussain & Ramaiah 2007). In addition, there are lower levels of ERp57 and calnexin in the liver of aged rats (Erickson *et al.* 2006), and decreased levels of PDI and calnexin in the hippocampus of old rats (Paz Gavilan *et al.* 2006). However, no systematic study of age-associated changes in expression levels of components of the ER proteostasis network has yet been published. To determine the effect of age on the expression of various ER-resident and ER-linked proteins, the level of proteins of interest were analysed using quantitative western blotting in tissues from young and old mice. These experiments generated an extensive set of data regarding the age-related changes in the expression levels of components of ER protein homeostasis. The expression levels of the tested ER proteins were affected in various degrees in the different aged tissues. These changes were heterogeneous, with individual proteins being increased in some tissues but decreased in others. For example, BiP was decreased in some tissues but increased in others. Heterogeneity was also observed at the level of individual tissues, with levels of some proteins being increased whilst others decreased. These data are consistent with the previous observations from transcriptional analysis (Zahn *et al.* 2007) showing that each tissue presents a different pattern of age-related changes. Tissues are exposed to different types of stress therefore it is likely that protein homeostasis will be affected in different ways. The most consistent changes in the expression levels of ER proteostasis components were observed in the aged brain and spleen, with multiple proteins decreased in brain but increased in spleen. Neurons are post-mitotic cells therefore they might be particularly susceptible to accumulation of misfolded proteins with age.

A progressive decline in ERAD capacity with age would increase the burden of misfolded proteins in the ER, thereby destabilising the proteostasis network. This is consistent with the observation that susceptibility to neurodegenerative diseases increases with age (Morley *et al.* 2002). In addition several studies using models of neurodegenerative diseases have showed that presence of misfolded, aggregated proteins can entrap other components of the proteostasis network (Ben-Zvi *et al.* 2009; Olzscha *et al.* 2011), including components of the ERAD pathway (Duennwald & Lindquist 2008; Nishitoh *et al.* 2008). This is interesting since decreased levels of various ERAD chaperones were detected in aged mouse brain (e.g. Der-1, Sel-1, OS9). Thus it is possible that the formation of high MW complexes between ERAD components and aggregated proteins could further compromise elimination of aberrant proteins from the ER lumen. In either case, decreased ERAD capacity might be expected to promote accumulation of misfolded protein in the ER lumen and UPR activation. Indeed, two other features of the aged brain revealed in this study were the accumulation of polyUb proteins, indicating perturbation in the proteasomal degradation pathway, and increased levels of phospho-eIF2α and BiP, consistent with elevated levels of UPR. In addition to the direct effects of increased eIF2α phosphorylation discussed in section 3.5, prolonged UPR has been shown to promote synthesis of pro-inflammatory cytokines as part of the cell-death programme (Bergsbaken *et al.* 2009) and the presence of a neuroinflammatory response has been shown to contribute to the pathology of various neurodegenerative diseases (Frank-Cannon *et al.* 2009). Thus a local inflammatory response can perturb the ER homeostasis in the adjacent cells contributing to the spread of protein homeostasis imbalance and leading to a global perturbation within the organ/ tissues.

Another tissue that presents numerous age-associated changes in the level of expression of ER-resident and ER-linked proteins is the spleen. The spleen is the site of B and T lymphocyte maturation to antibody secreting cells and cytokine secreting T cell clones, processes that involve UPR activation (Brunsing *et al.* 2008). In addition, in the spleen the antigen presenting cells can process 'foreign' proteins. Therefore any perturbations in ER proteostasis which result in the chronic activation of UPR might impact on the function of the immune system. The upregulation of most of the tested ER proteins in the spleen of old mice suggests that the UPR is activated compared with the young counterpart, therefore ER protein homeostasis might be affected in aged spleen. In addition, the increased phosphorylation of eIF2α in aged spleen also indicates a possible perturbation in ER protein homeostasis, since during activation of B-cells this branch is not normally activated (Ma *et al.* 2009). Interestingly, ageing is associated with diminished fidelity and capacity of the immune system, which leads to chronic inflammatory status and secretion of abnormal antibodies - including against self-proteins (autoreactivity), responsible for increased susceptibility to infections or occurrence of age-related diseases such as Alzheimer's disease and cardiovascular diseases (Wordsworth & Dunn-Walters 2011).

Compared to other tissues such as the brain or spleen, a reduced number of changes in the expression level of ER proteins were observed in the aged liver (Fig 3.33). Thus it might be hypothesised that the liver could maintain relative stable ER proteostasis throughout life. However, increased oxidation of components of the folding/QC system (e.g. BiP, PDI, calnexin) was documented in the liver of aged mice (Rabek *et al.* 2003) and correlated with a decline in chaperone function (Nuss *et al.* 2008). The aged kidney exhibits a smaller number of age-related changes, suggesting that it might be relatively unaffected by age. This was also indicated by the data from transcriptomics studies showing that the expression level of most genes is not changed in aged kidney (Rodwell *et al.* 2004; Zahn *et al.* 2007).

These multiple changes in the expression level of ER chaperones, ER oxidoreductases and ERAD factors that occurred in aged tissues indicate a dysregulation of ER proteostasis. Consistent with this interpretation, the level of phospho-eIF2α was increased in all the aged tissues and also in both cellular models of ageing, suggesting that these cells/organs do experience heightened levels of of ER stress. Although eIF2α phosphorylation can be initiated by other kinases (Harding *et al.* 2003), association with the upregulation of UPR targets (e.g. BiP) was observed in some of the aged tissues and both cellular models. In these cases, the increased levels of phospho- eIF2α may well be in response to changes in ER proteostasis.

Interestingly, an increase in the content of high MW polyUb species was observed in multiple aged tissues and in the both cellular models indicating that the Ub-protesome pathway might be affected. Similar results were previously reported for aged brain (Ohtsuka *et al.* 1995) and liver (Perez *et al.* 2009). Reduced degradation capacity of the proteasomal pathway with age is documented by a vast amount of literature (Koga *et al.* 2010; Low 2011), thus indicating that accumulation of misfolded proteins is favoured in aged tissues/cells. However, selective autophagy pathways (e.g. HDAC6–LC3-II, BAG3 mediated autophagosome formation) can function as an alternative for the degradation of polyUb substrates (Lamark & Johansen 2012). A relatively recent study (Gamerdinger *et al.* 2009) has shown that in pre-senescent cells (IMR90, HPD) the level of BAG3 is increased as cells upregulate the lysosomal-autophagic pathways to compensate for the reduced proteasomal degradation. Notably, in many of the aged tissues (liver, heart, brain, lung, muscle) that presented increased levels of polyUb proteins, the level of BAG3, a protein involved in the autophagic pathways, was also increased suggesting a direct correlation between accumulation of polyUb proteins and BAG3 expression. This correlation was also observed in both cellular models of ageing, which also showed increased levels of polyUb conjugates and BAG3. However, reduced autophagy was reported to occur with age, due to diminished lysosomal proteolytic activity, or a decrease in the level of proteins involved in autophagosome formation (e.g. ATG proteins) (Koga *et al.* 2010; Lamark & Johansen 2012). Therefore although channelling of proteins to the autophagic pathway by BAG3 might be upregulated as a protective mechanism, the accumulation of misfolded proteins

might not be prevented in aged tissues/cells. This could be a potential threat for the cells/organisms as such non-native proteins are aggregation-prone.

Protein aggregation was shown to be promoted by the existence of a pool of unstructured proteins, exhibiting hydrophobic regions (David *et al.* 2010; Olzscha *et al.* 2011). Recently accumulation of aggregated proteins was shown to occur during normal ageing in *C. elegans* (David *et al.* 2010), indicating an overall disruption of protein homeostasis. However, it is not known whether protein aggregation occurs with age in higher animals. What is known is that accumulation of aggregated proteins occurs in various human neurodegenerative diseases and increases with age (Douglas & Dillin 2010). Interestingly, in the present study, increased protein aggregation was detected in the skeletal muscle of old mice, suggesting that age-dependent protein aggregation can also occur in mammalian systems. The toxicity of protein aggregates may be linked to their capacity to sequester essential cellular proteins, including components of proteostasis pathways (Duennwald & Lindquist 2008; Nishitoh *et al.* 2008; Olzscha *et al.* 2011). Indeed, BiP was found in the insoluble fraction of skeletal muscle from old mice. Therefore is possible that in this aged tissues, less BiP is available to promote de novo protein folding. However, further analysis on other tissues has to be done to test this idea.

To conclude, many changes in the levels of proteostasis pathway components were observed in aged tissues and cellular models of ageing. The most widespread of these were increased eIF2α phosphorylation, accumulation of polyUb proteins and increased levels of BAG3, suggesting that these may represent general features of ageing cells and tissues

6.2 Effect of cellular ageing on the function of ER protein homeostasis pathways

Two cellular models of ageing were used to examine the functional capacity of ER protein homeostasis pathways. The first were human lung fibroblasts aged in vitro by serial passage, and the second human skin fibroblast isolated from young and old donors. The relative advantages and disadvantages of these models is discussed in section 5.7.

The HPD lung fibroblasts are likely to be approaching senescence, since they were still capable of cell division. However, they also exhibited some of the features of senescence e. g increased size, increased amount of caveolin, decreased replicative capacity. The analysis of ER function performed in this cellular model revealed that HPD cells have a decreased capacity to promote folding of a metastable cargo protein, and diminished efficiency of degradation of two ERAD substrates. Consistent with these observations, HPD cells also had higher basal eIF2α phosphorylation and increased BiP levels, indicating heightened ER stress. In addition, the IRE1/*XBP1* arm of the UPR was more sensitive to activation in HPD cells. However, these cells apparently failed to increase the phosphorylation of eIF2α or upregulate the expression level of

BiP following ER stress induction, suggesting that the UPR signalling is dysfunctional. Studies using aged *C. elegans* showed a progressive decrease in their ability to maintain metastable proteins in the correctly folded state (Ben-Zvi *et al.* 2009). A similar approach was used here and the folding of a metastable protein (ts VSV-G) was examined in HPD fibroblasts. These experiments suggested a marked decrease in the capacity to fold VSV-G in the HPD cells. The folding capacity was indirectly assessed by acquisition of Golgi apparatus modified N-glycans and showing that ER to Golgi apparatus traffic was similar in both cell populations. Although only one model protein was used in this study, it does suggest that the ability to maintain at least a subset of proteins in properly folded state may be compromised in HPD cells. Differences in VSV-G folding were not detected in cells from young and old donors, suggesting that the ER folding capacity in these two cell populations was not significantly different. It is also possible that small differences do exist, but were too subtle to be detected by this assay. This is supported by the observation that other changes observed in HPD cells, such as increased activation of IRE1/*XBP1,* were reproduced in the *in vivo* aged cells but to a lower extent.

One potential cause of the decline in folding capacity could be a decreased function of chaperones due to decreased chaperone and oxidoreductase expression level. Only PDI expression was seen to decrease in HPD cells, but increased oxidation has also been shown to affect in the function of ER folding components aged liver (Papaconstantinou *et al.* 2005; Nuss *et al.* 2008), thus diminishing folding capacity. Another possibility for decreased folding capacity is decreased ERAD capacity, leading to accumulation of misfolded proteins. Indeed, analysis of degradation of two model ERAD substrates, TCRα and α1AT-NHK, was significantly slower in HPD cells. Preliminary results indicate that ERAD capacity might also be diminished in the cells from the old donor. The reason for reduced ERAD may well be related to reduced proteasome function as suggested by a number of studies (Koga *et al.* 2010; Low 2011). This would also be consistent with the decrease in the expression of the 19S proteasomal subunit Rpt6 observed in HPD and fibroblasts from old donors. In addition, several studies using models of neurodegenerative diseases have suggested that essential ERAD components are entrapped by the aggregated disease proteins superoxide dismutase (SOD1) and polyQ containing proteins (Duennwald & Lindquist 2008; Nishitoh *et al.* 2008; Olzscha *et al.* 2011). This was found to promote the accumulation of ERAD substrates within the ER lumen, sensitising cells to activation of the UPR (Zhong & Pittman 2006; Duennwald & Lindquist 2008; Nishitoh *et al.* 2008; Yang *et al.* 2008). UPR activation is linked to the pathology of age-related neurodegenerative diseases (Guerriero & Brodsky 2012), and it is possible that dysfunction of the ERAD system as a result of protein aggregation in the cytosol and/or compromised proteasome function are contributing factors.

No difference in the overall rate of N-glycoprotein biosynthesis was observed between the LDP and HPD cells. This is important as it suggests that the overall load of client proteins entering the ER was similar. However, the translocation of specific substrates into the ER did appear to be different in young and aged cells, possibly pointing to a dysregulation of translocation with

age. Notably, each of the changes observed in the HPD cells (increased translocation of γ-INF and pPL, decreased translocation of US2), were also observed in fibroblasts from old donors, relative to their young counterparts. This is interesting, since translocation appears to be regulated at the level of individual substrates and this feature becomes more evident in response to stress (Kang *et al.* 2006). The implications of this are not currently understood. However, there is evidence that the ability to downregulate translocation in response to stress is an important protective mechanism, preventing proteins that might aggregate entering in the secretory pathway (Kang *et al.* 2006; Rane *et al.* 2010). An inability to regulate translocation could have a detrimental impact on the ER during times of stress, and could also potentially result in production of mis-translocated proteins, which can have adverse effects on cell function (Hessa *et al.* 2011; McKibbin *et al.* 2012). Interestingly, levels of BAG6, which promotes degradation of proteins that fail to translocate, were found to decrease in HPD cells, so it could be speculated that mis-localised proteins could accumulate in these cells. In addition, reduced translocation of US2 due to ER stress was reported previously (Drori *et al.* 2010), and a similar effect has been seen in aged cells here, which would be consistent with the presence of a ER stress stimulus in aged cells (e. g. misfolded/aggregated proteins).

6.3 Response to ER stress

Diminished capacities of ER folding and degradation pathways in aged cells would be envisaged to result in an increasing burden of misfolded proteins in the lumen of the ER, leading ultimately activation of the UPR. Indeed, the basal level of phosphorylated eIF2α was increased in all the aged cells and tissues, similar to previous studies of hepatocytes of aged liver (Li & Holbrook 2004).

A compromised ER stress response is linked to many age-related pathologies, including neurodegenerative diseases, diabetes, and cardiovascular disease (Colla *et al.* 2012; Moreno *et al.* 2012; Wang & Kaufman 2012; Zuleta *et al.* 2012), suggesting that perturbations in UPR signalling could also play an important role in ageing. Studies of aged hippocampus have shown that upon sleep deprivation the activation of PERK branch of UPR does not occur in old animals (Naidoo *et al.* 2008). Similarly, inducing the accumulation of polyUb proteins by lactacystin treatment, in young and old rats led to the improper activation of the IRE1 and ATF6 branches of the UPR (Paz Gavilán *et al.* 2009). This is consistent with the results presented here, showing that the kinetics of IRE1 and PERK branches of UPR were different in young and old cells, and more importantly that the levels of UPR targets (e.g. BiP) were lower in aged than in young cells, suggesting the inability to cope with ER stress. In addition, aged cells are less able to switch off the UPR signalling, presenting prolonged activation of IRE1 signalling. Interestingly, these findings correlate with a recent study in long lived *C. elegans* showing that a low setting of ire/*xbp1* contributes to longevity (Henis-Korenblit *et al.* 2010) through enhancing ER proteostasis which then acts as a negative feed-back loop in the absence of stress thus

highlighting that actually the dysfunctional UPR signalling/homeostasis may contribute to ageing. In this regard, a series of reports have pointed out the link between activation of the ER stress response and longevity (Viswanathan *et al.* 2005). Thus, the lower rate of survival after ER stress induction observed for the HPD cells may indicate that their inability to resolve the ER stress induced by misfolding promotes the activation of the pro-apoptotic phase of the UPR, resulting in cell death. Another recent study using fibroblasts from mice with increased lifespan found that these cells have also low *Xbp1* signalling, but in contrast with *C. elegans* exhibited increased sensibility to ER stress, possibly due to the reduced activation of IRE1 (Sadighi Akha *et al.* 2011). However, in contrast with the above mentioned study, both *in vivo* and *in vitro* aged cells had a higher activation of IRE1, but could not upregulate downstream target genes (e.g. BiP) all indicating a perturbation in UPR signalling, with the increased sensitivity to cell death possibly being mediated by the prolonged IRE1 activation.

6.4 Concluding remarks and future work

Several studies using *C. elegans* mutants and cells from long lived organisms suggest that ER homeostasis and the UPR may contribute to lifespan determination (Viswanathan *et al.* 2005; Henis-Korenblit *et al.* 2010; Vilchez *et al.* 2012; Volovik *et al.* 2012). These studies are important because they open up the possibility of these pathways as targets for intervention to reduce age-associated dysfunction. However, further studies to characterise the age-associated changes in ER proteostasis pathways at a molecular level are required. The work described in this thesis aims to address these issues, but there are clearly many areas that warrant further investigation. Some of these are discussed below.

Protein aggregation as a normal consequence of ageing

Analysis of the level of SDS-insoluble protein aggregates in tissue from young and old mice suggested that ageing is associated with general protein aggregation in skeletal muscle. However, no evidence of increased aggregation was observed in liver. Therefore, it is possible that some tissues are more susceptible to age-associated defects in protein homeostasis, such as those with high numbers of postmitotic cells (e.g. brain, heart, skeletal muscle). It would be interesting to examine whether protein aggregation is a widespread phenomenon in mice, by assessing the level of protein aggregation in other tissues, particularly the brain. In addition, it would be interesting to examine what other components of the ER proteostasis pathways could be associated with protein aggregates. In the longer term, it would be important to test whether manipulations that extend lifespan in mice (e.g. mutation in IGF signalling) modulate protein aggregation in any affected tissues. If protein aggregation does contribute to lifespan, the prediction would be that such interventions would delay or reduce aggregation. .

Investigation of ER folding and degradation capacities

The assay for ER folding using the ts VSV-G suggested that the aged cells have a diminished capacity to maintain metastable proteins in the properly folded state. This indicates that the

folding machinery is less efficient at folding newly synthesized proteins. However, since the methods used to examine VSV-G folding cannot precisely discriminate between folding and traffic, it would be important to examine folding more directly, for example through the use of conformation-specific antibodies. Another priority to test the generality of the findings with VSV-G would be to examine the folding of other model proteins for which such reagents are readily available, such as HA. Ideally, folding of endogenous proteins would also be measured, but the expression levels of ER cargo proteins and lack of reagents such as antibodies make this analysis problematic.

The analyses of the stability of two model ERAD substrates indicated that this pathway (or more accurately pathways) is compromised in both models of cellular ageing. This could be due to reduced capacity of the ERAD machinery itself, and/or reduced proteasomal activity. To measure the ability of the proteasome to degrade other substrates in the aged cells, Ub-GFP reporter constructs could be used (Dantuma *et al.* 2000). It would also be interesting to measure whether autophagic pathways contribute to degradation of ERAD substrates in aged cells.

Examination of UPR signalling

In this study, the activation and attenuation of the IRE1 branch of the UPR was studied, using the production of spliced *XBP1* mRNA as a readout, and the results obtained showed that the amplitude of the stress response is higher and the signalling is prolonged in aged cells. However, a more in-depth analysis of the other branches of the URP will be required. The ATF6 branch can be monitored by antibodies, although a number were tried in this work without success. A critical thing to do will be to look at UPR targets at the mRNA level – since it was showed that IRE1 mediates an ER-stress induced mRNA decay, which also was hypothesised to degrade the mRNA of encoding essential proteins during prolonged UPR. It will also be important to determine whether the enhanced IRE1 activation results in a different output. In addition, such analysis would help to shed light on the apparent failure to upregulate chaperone expression in response to perturbation of ER folding.

Other systems to examine ER proteostasis

Although the cellular systems used in this work provide a useful starting point to examine the impact of age on ER proteostasis, they are clearly far removed from aged tissues in vivo. Therefore, a priority would be to examine to what extent the observations made using the LPD/HPD cells are also observed in aged organisms. One possibility would be the use of acutely isolated cells (e.g. neurons) or organ slices from young and old mice to test the activation of UPR.

Altogether such studies would help to provide a more complete picture of age-associated changes in ER proteostasis, ultimately paving the way for interventions aimed at reducing such age-associated defects in cellular function.

CHAPTER 7

References

Adachi H, Waza M, Tokui K, Katsuno M, Minamiyama M, Tanaka F, Doyu M, Sobue G (2007). CHIP overexpression reduces mutant androgen receptor protein and ameliorates phenotypes of the spinal and bulbar muscular atrophy transgenic mouse model. *J. Neurosci.* **27**, 5115-5126.

Aebi M, Bernasconi R, Clerc S, Molinari M (2010). N-glycan structures: Recognition and processing in the ER. *Trends Biochem. Sci.* **35**, 74-82.

Ahner A, Nakatsukasa K, Zhang H, Frizzell RA, Brodsky JL (2007). Small heat-shock proteins select deltaF508-CFTR for endoplasmic reticulum-associated degradation. *Mol. Biol. Cell* **18**, 806-814.

Akerfelt M, Morimoto RI, Sistonen L (2010). Heat shock factors: integrators of cell stress, development and lifespan. *Nat. Rev. Mol. Cell Biol.* **11**, 545-555.

Appenzeller C, Andersson H, Kappeler F, Hauri HP (1999). The lectin ERGIC-53 is a cargo transport receptor for glycoproteins. *Nat. Cell Biol.* **1**, 330-334.

Arias E, Cuervo AM (2010). Chaperone-mediated autophagy in protein quality control. *Curr. Opin. Cell Biol.* **23**, 184-189.

Axe EL, Walker SA, Manifava M, Chandra P, Roderick HL, Habermann A, Griffiths G, Ktistakis NT (2008). Autophagosome formation from membrane compartments enriched in phosphatidylinositol 3-phosphate and dynamically connected to the endoplasmic reticulum. *J. Cell Biol.* **182**, 685-701.

Bagola K, Mehnert M, Jarosch E, Sommer T (2011). Protein dislocation from the ER. *Biochim. Biophys. Acta* **1808**, 925-936.

Balch WE, Morimoto RI, Dillin A, Kelly JW (2008). Adapting proteostasis for disease intervention. *Science* **319**, 916-919.

Ballar P, Shen Y, Yang H, Fang S (2006). The role of a novel p97/valosin-containing protein-interacting motif of gp78 in endoplasmic reticulum-associated degradation. *J. Biol. Chem.* **281**, 35359-35368.

Barlowe C, Orci L, Yeung T, Hosobuchi M, Hamamoto S, Salama N, Rexach MF, Ravazzola M, Amherdt M, Schekman R (1994). COPII: a membrane coat formed by Sec proteins that drive vesicle budding from the endoplasmic reticulum. *Cell* **77**, 895-907.

Bartke A, Brown-Borg H (2004). Life extension in the dwarf mouse. *Curr. Top. Dev. Biol.* **63**, 189-225.

Bartling B, Desole M, Rohrbach S, Silber RE, Simm A (2009). Age-associated changes of extracellular matrix collagen impair lung cancer cell migration. *FASEB J.* **23**, 1510-1520.

Bass TM, Weinkove D, Houthoofd K, Gems D, Partridge L (2007). Effects of resveratrol on lifespan in Drosophila melanogaster and Caenorhabditis elegans. *Mech. Ageing Dev.* **128**, 546-552.

Beggs ML, Nagarajan R, Taylor-Jones JM, Nolen G, Macnicol M, Peterson CA (2004). Alterations in the TGFbeta signaling pathway in myogenic progenitors with age. *Aging Cell* **3**, 353-361.

Bejarano E, Cuervo AM (2010). Chaperone-mediated autophagy. *Proc. Am. Thorac. Soc.* **7**, 29-39.

Ben-Gedalya T, Cohen E (2012). Quality control compartments coming of age. *Traffic* **13**, 635-642.

Ben-Zvi A, Miller EA, Morimoto RI (2009). Collapse of proteostasis represents an early molecular event in *Caenorhabditis elegans* aging. *Proc. Natl. Acad. Sci. USA*. 106, 14914-14919.

Benham AM (2012). Protein secretion and the endoplasmic reticulum. *Cold Spring Harb. Perspect. Biol.* **4**, a012872.

Bergsbaken T, Fink SL, Cookson BT (2009). Pyroptosis: Host cell death and inflammation. *Nat. Rev. Microbiol.* **7**, 99-109.

Bernales S, McDonald KL, Walter P (2006). Autophagy counterbalances endoplasmic reticulum expansion during the unfolded protein response. *PLoS Biol.* **4**, e423.

Bernales S, S. M, A. M, McCullagh E (2012). Unfolded protein stress in the endoplasmic reticulum and mitochondria: a role in neurodegeneration. *Front. Aging Neurosci.* **4**, 5.

Bernales S, Schuck S, Walter P (2007). ER-phagy: Selective autophagy of the endoplasmic reticulum. *Autophagy* **3**, 285-287.

Bernasconi R, Galli C, Calanca V, Nakajima T, Molinari M (2010). Stringent requirement for HRD1, SEL1L, and OS-9/XTP3-B for disposal of ERAD-LS substrates. *J. Cell Biol.* **188**, 223-235.

Bertolotti A, Zhang Y, Hendershot L, Harding HP, Ron D (2000). Dynamic interaction of BiP and ER stress transducers in the unfolded-protein response. *Nat. Cell Biol.* **2**, 326-332.

Bi X, Corpina RA, Goldberg J (2002). Structure of the Sec23/24-Sar1 pre-budding complex of the COPII vesicle coat. *Nature* **419**, 271-277.

Bonelli MA, Alfieri RR, Petronini PG, Brigotti M, Campanini C, Borghetti AF (1999). Attenuated expression of 70-kDa heat shock protein in WI-38 human fibroblasts during aging in vitro. *Exp. Cell Res.* **252**, 20-32.

Boren E, Gershwin ME (2004). Inflamm-aging: Autoimmunity, and the immune-risk phenotype. *Autoimmun. Rev.* **3**, 401-406.

Boyce M, Bryant KF, Jousse C, Long K, Harding HP, Scheuner D, Kaufman RJ, Ma D, Coen DM, Ron D, Yuan J (2005). A selective inhibitor of eIF2-alpha dephosphorylation protects cells from ER stress. *Science* **307**, 935-939.

Braakman I, Bulleid NJ (2011). Protein folding and modification in the mammalian endoplasmic reticulum. *Annu. Rev. Biochem.* **80**, 71-99.

Broome CS, Kayani AC, Palomero J, Dillmann WH, Mestril R, Jackson MJ, McArdle A (2006). Effect of lifelong overexpression of HSP70 in skeletal muscle on age-related oxidative stress and adaptation after nondamaging contractile activity. *FASEB J.* **20**, 1549-1551.

Brunsing R, Omori SA, Weber F, Bicknell A, Friend L, Rickert R, Niwa M (2008). B- and T-cell development both involve activity of the unfolded protein response pathway. *J. Biol. Chem.* **283**, 17954-17961.

Brush MH, Weiser DC, Shenolikar S (2003). Growth arrest and DNA damage-inducible protein GADD34 targets protein phosphatase 1 alpha to the endoplasmic reticulum and promotes dephosphorylation of the alpha subunit of eukaryotic translation initiation factor 2. *Mol. Cell Biol.* **23**, 1292-1303.

Buchberger A, Bukau B, Sommer T (2010). Protein quality control in the cytosol and the endoplasmic reticulum: Brothers in arms. *Mol. Cell* **40**, 238-252.

Butterfield DA, Poon HF (2005). The senescence-accelerated prone mouse (SAMP8): a model of age-related cognitive decline with relevance to alterations of the gene expression and protein abnormalities in Alzheimer's disease. *Exp. Gerontol.* **40**, 774-783.

Campisi J, Andersen JK, Kapahi P, Melov S (2011). Cellular senescence: A link between cancer and age-related degenerative disease? *Semin. Cancer Biol.* **21**, 354-359.

Carra S, Seguin SJ, Landry J (2008). HspB8 and Bag3: A new chaperone complex targeting misfolded proteins to macroautophagy. *Autophagy* **4**, 237-239.

Carrard G, Bulteau AL, Petropoulos I, Friguet B (2002). Impairment of proteasome structure and function in aging. *Int. J. Biochem. Cell Biol.* **34**, 1461-1474.

Carvalho P, Stanley AM, Rapoport TA (2010). Retrotranslocation of a misfolded luminal ER protein by the ubiquitin-ligase Hrd1p. *Cell* **143**, 579-591.

Chakravarti B, Seshi B, Ratanaprayul W, Dalal N, Lin L, Raval A, Chakravarti DN (2009). Proteome profiling of aging in mouse models: Differential expression of proteins involved in metabolism, transport, and stress response in kidney. *Proteomics* **9**, 580-597.

Chalkiadaki A, Guarente L (2012). Sirtuins mediate mammalian metabolic responses to nutrient availability. *Nat. Rev. Endocrinol*. **8**, 287-296.

Chawla A, Chakrabarti S, Ghosh G, Niwa M (2011). Attenuation of yeast UPR is essential for survival and is mediated by IRE1 kinase. *J. Cell Biol.* **193**, 41-50.

Chen B, Retzlaff M, Roos T, Frydman J (2011). Cellular strategies of protein quality control. *Cold Spring Harb. Perspect. Biol.* **3**. a004374.

Chiang W-C, Ching T-T, Lee Hee C, Mousigian C, Hsu A-L HSF-1 regulators DDL-1/2 link insulin-like signaling to heat-shock responses and modulation of longevity. *Cell* **148**, 322-334.

Chillaron J, Haas IG (2000). Dissociation from BiP and retrotranslocation of unassembled immunoglobulin light chains are tightly coupled to proteasome activity. *Mol. Biol. Cell* **11**, 217-226.

Cho KA, Ryu SJ, Oh YS, Park JH, Lee JW, Kim HP, Kim KT, Jang IS, Park SC (2004). Morphological adjustment of senescent cells by modulating caveolin-1 status. *J. Biol. Chem.* **279**, 42270-42278.

Christianson JC, Olzmann JA, Shaler TA, Sowa ME, Bennett EJ, Richter CM, Tyler RE, Greenblatt EJ, Harper JW, Kopito RR (2012). Defining human ERAD networks through an integrative mapping strategy. *Nat. Cell Biol.* **14**, 93-105.

Christianson JC, Shaler TA, Tyler RE, Kopito RR (2008). OS-9 and GRP94 deliver mutant alpha1-antitrypsin to the Hrd1-SEL1L ubiquitin ligase complex for ERAD. *Nat. Cell Biol.* **10**, 272-282.

Claessen JHL, Ploegh HL (2011). BAT3 guides misfolded glycoproteins out of the endoplasmic reticulum. *PLoS ONE*. **6**, e28542.

Cohen E, Bieschke J, Perciavalle RM, Kelly JW, Dillin A (2006). Opposing activities protect against age-onset proteotoxicity. *Science* **313**, 1604-1610.

Colla E, Coune P, Liu Y, Pletnikova O, Troncoso JC, Iwatsubo T, Schneider BL, Lee MK (2012). Endoplasmic reticulum stress is important for the manifestations of alpha-synucleinopathy in vivo. *J. Neurosci.* **32**, 3306-3320.

Connell P, Ballinger CA, Jiang J, Wu Y, Thompson LJ, Hohfeld J, Patterson C (2001). The co-chaperone CHIP regulates protein triage decisions mediated by heat-shock proteins. *Nat. Cell Biol.* **3**, 93-96.

Cross BC, McKibbin C, Callan AC, Roboti P, Piacenti M, Rabu C, Wilson CM, Whitehead R, Flitsch SL, Pool MR, High S, Swanton E (2009a). Eeyarestatin I inhibits Sec61-mediated protein translocation at the endoplasmic reticulum. *J. Cell Sci.* **122**, 4393-4400.

Cross BCS, Sinning I, Luirink J, High S (2009b). Delivering proteins for export from the cytosol. *Nat. Rev. Mol. Cell Biol*. **10**, 255-264.

Cuervo AM, Dice JF (2000). Age-related decline in chaperone-mediated autophagy. *J. Biol. Chem.* **275**, 31505-31513.

Dantuma NP, Lindsten K, Glas R, Jellne M, Masucci MG (2000). Short-lived green fluorescent proteins for quantifying ubiquitin/proteasome-dependent proteolysis in living cells. *Nat. Biotechnol.* **18**, 538-543.

David DC, Ollikainen N, Trinidad JC, Cary MP, Burlingame AL, Kenyon C (2010). Widespread protein aggregation as an inherent part of aging in *C. elegans. PLoS Biol*. **8**, e1000450.

David Y, Ternette N, Edelmann MJ, Ziv T, Gayer B, Sertchook R, Dadon Y, Kessler BM, Navon A (2011). E3 ligases determine ubiquitination site and conjugate type by enforcing specificity on E2 enzymes. *J. Biol. Chem.* **286**, 44104-44115.

de Magalhaes JP, Curado J, Church GM (2009). Meta-analysis of age-related gene expression profiles identifies common signatures of aging. *Bioinformatics* **25**, 875-881.

de Virgilio M, Weninger H, Ivessa NE (1998). Ubiquitination is required for the retro-translocation of a short-lived luminal endoplasmic reticulum glycoprotein to the cytosol for degradation by the proteasome. *J. Biol. Chem.* **273**, 9734-9743.

Dhahbi JM, Tsuchiya T, Kim HJ, Mote PL, Spindler SR (2006). Gene expression and physiologic responses of the heart to the initiation and withdrawal of caloric restriction. *J. Gerontol. A. Biol. Sci. Med. Sci.* **61**, 218-231.

Dillin A, Cohen E (2010). Ageing and protein aggregation-mediated disorders: from invertebrates to mammals. *Philos. Trans. R .Soc. Lond. B. Biol. Sci.* **366**, 94-98.

Ding WX, Yin XM (2008). Sorting, recognition and activation of the misfolded protein degradation pathways through macroautophagy and the proteasome. *Autophagy* **4**, 141-150.

Douglas PM, Dillin A (2010). Protein homeostasis and aging in neurodegeneration. *J.Cell Biol.* **190**, 719-729.

Drori A, Misaghi S, Haimovich J, Messerle M, Tirosh B (2010). Prolonged endoplasmic reticulum stress promotes mislocalization of immunoglobulins to the cytoplasm. *Mol. Immunol.* **47**, 1719-1727.

Drummond DA, Wilke CO (2009). The evolutionary consequences of erroneous protein synthesis. *Nat. Rev. Genet.* **10**, 715-724.

Duennwald ML, Lindquist S (2008). Impaired ERAD and ER stress are early and specific events in polyglutamine toxicity. *Genes Dev.* **22**, 3308-3319.

DuRose JB, Tam AB, Niwa M (2006). Intrinsic capacities of molecular sensors of the unfolded protein response to sense alternate forms of endoplasmic reticulum stress. *Mol. Biol. Cell* **17**, 3095-3107.

Edwards MG, Anderson RM, Yuan M, Kendziorski CM, Weindruch R, Prolla TA (2007). Gene expression profiling of aging reveals activation of a p53-mediated transcriptional program. *BMC Genomics.* **8**, 80.

Erickson RR, Dunning LM, Holtzman JL (2006). The effect of aging on the chaperone concentrations in the hepatic, endoplasmic reticulum of male rats: the possible role of protein misfolding due to the loss of chaperones in the decline in physiological function seen with age. *J. Gerontol. A. Biol. Sci. Med. Sci.* **61**, 435-443.

Eriksson KK, Vago R, Calanca V, Galli C, Paganetti P, Molinari M (2004). EDEM contributes to maintenance of protein folding efficiency and secretory capacity. *J. Biol. Chem.* **279**, 44600-44605.

Ferrington DA, Husom AD, Thompson LV (2005). Altered proteasome structure, function, and oxidation in aged muscle. *FASEB J.* **19**, 644-646.

Finley D (2009). Recognition and processing of ubiquitin-protein conjugates by the proteasome. *Annu. Rev. Biochem*. **78**, 477-513.

Fons RD, Bogert BA, Hegde RS (2003). Substrate-specific function of the translocon-associated protein complex during translocation across the ER membrane. *J. Cell Biol.* **160**, 529-539.

Frank-Cannon T, Alto L, McAlpine F, Tansey M (2009). Does neuroinflammation fan the flame in neurodegenerative diseases? *Mol. Neurodegener*. **4**, 47.

Gallastegui N, Groll M (2010). The 26S proteasome: assembly and function of a destructive machine. *Trends Biochem*. *Sci.* **35**, 634-642.

Gallione CJ, Rose JK (1985). A single amino acid substitution in a hydrophobic domain causes temperature-sensitive cell-surface transport of a mutant viral glycoprotein. *J. Virol.* **54**, 374-382.

Gamerdinger M, Hajieva P, Kaya AM, Wolfrum U, Hartl FU, Behl C (2009). Protein quality control during aging involves recruitment of the macroautophagy pathway by BAG3. *EMBO J.* **28**, 889-901.

Gamerdinger M, Kaya AM, Wolfrum U, Clement AM, Behl C (2011). BAG3 mediates chaperone-based aggresome-targeting and selective autophagy of misfolded proteins. *EMBO J.* **12**, 149-156.

Gardner BM, Walter P (2011). Unfolded proteins are Ire1-activating ligands that directly induce the unfolded protein response. *Science* **333**, 1891-1894.

Gidalevitz T, Ben-Zvi A, Ho KH, Brignull HR, Morimoto RI (2006). Progressive disruption of cellular protein folding in models of polyglutamine diseases. *Science* **311**, 1471-1474.

Gillon AD, Latham CF, Miller EA (2012). Vesicle-mediated ER export of proteins and lipids. *Biochim. Biophys. Acta* **1821**, 1040-1049.

Godbout JP, Chen J, Abraham J, Richwine AF, Berg BM, Kelley KW, Johnson RW (2005). Exaggerated neuroinflammation and sickness behavior in aged mice following activation of the peripheral innate immune system. *FASEB J.* **19**, 1329-1331. .

Gorlich D, Hartmann E, Prehn S, Rapoport TA (1992). A protein of the endoplasmic reticulum involved early in polypeptide translocation. *Nature* **357**, 47-52.

Guerriero CJ, Brodsky JL (2012). The delicate balance between secreted protein folding and endoplasmic reticulum-associated degradation in human physiology. *Physiol. Rev*. **92**, 537-576.

Gupta S, Deepti A, Deegan S, Lisbona F, Hetz C, Samali A (2010). HSP72 protects cells from ER stress-induced apoptosis via enhancement of IRE1alpha-XBP1 signaling through a physical interaction. *PLoS*. **8**, e1000410.

Gupta S, Jie S, Colby DW (2011). Protein misfolding detected early in pathogenesis of transgenic mouse model of Huntington disease using amyloid seeding assay. *J. Biol. Chem.* **287**, 9982-9989.

Gurevich VV, Pokrovskaya ID, Obukhova TA, Zozulya SA (1991). Preparative in vitro mRNA synthesis using SP6 and T7 RNA polymerases. *Anal. Biochem*. **195**, 207-213.

Halaschek-Wiener J, Khattra JS, McKay S, Pouzyrev A, Stott JM, Yang GS, Holt RA, Jones SJ, Marra MA, Brooks-Wilson AR, Riddle DL (2005). Analysis of long-lived C. elegans daf-2 mutants using serial analysis of gene expression. *Genome Res.* **15**, 603-615. .

Hamasaki M, Noda T, Baba M, Ohsumi Y (2005). Starvation triggers the delivery of the endoplasmic reticulum to the vacuole via autophagy in yeast. *Traffic* **6**, 56-65.

Hampton RY, Sommer T (2012). Finding the will and the way of ERAD substrate retrotranslocation. *Curr. Opin. Cell Biol*. **24**, 460-466.

Han D, Lerner AG, Vande Walle L, Upton JP, Xu W, Hagen A, Backes BJ, Oakes SA, Papa FR (2009). IRE1alpha kinase activation modes control alternate endoribonuclease outputs to determine divergent cell fates. *Cell* **138**, 562-575.

Harding HP, Novoa I, Zhang Y, Zeng H, Wek R, Schapira M, Ron D (2000a). Regulated translation initiation controls stress-induced gene expression in mammalian cells. *Mol. Cell* **6**, 1099-1108.

Harding HP, Zhang Y, Bertolotti A, Zeng H, Ron D (2000b). Perk is essential for translational regulation and cell survival during the unfolded protein response. *Mol. Cell* **5**, 897-904.

Harding HP, Zhang Y, Ron D (1999). Protein translation and folding are coupled by an endoplasmic-reticulum-resident kinase. *Nature* **397**, 271-274.

Harding HP, Zhang Y, Zeng H, Novoa I, Lu PD, Calfon M, Sadri N, Yun C, Popko B, Paules R, Stojdl DF, Bell JC, Hettmann T, Leiden JM, Ron D (2003). An integrated stress response regulates amino acid metabolism and resistance to oxidative stress. *Mol. Cell* **11**, 619-633.

Hartl FU, Bracher A, Hayer-Hartl M (2012). Molecular chaperones in protein folding and proteostasis. *Nature* **475**, 324-332.

Hasnain SZ, Lourie R, Das I, Chen AC, McGuckin MA (2012). The interplay between endoplasmic reticulum stress and inflammation. *Immunol. Cell Biol.* **90**, 260-270.

Hayase K, Yokogoshi H (1994). Age affects brain protein synthesis in rats. *J. Nutr.* **124**, 683-688.

Hayashi-Nishino M, Fujita N, Noda T, Yamaguchi A, Yoshimori T, Yamamoto A (2009). A subdomain of the endoplasmic reticulum forms a cradle for autophagosome formation. *Nat. Cell Biol.* **11**, 1433-1437.

Haze K, Yoshida H, Yanagi H, Yura T, Mori K (1999). Mammalian transcription factor ATF6 is synthesized as a transmembrane protein and activated by proteolysis in response to endoplasmic reticulum stress. *Mol. Biol. Cell* **10**, 3787-3799.

He C, Klionsky DJ (2009). Regulation mechanisms and signaling pathways of autophagy. *Annu. Rev. Genet*. **43**, 67-93.

He CH, Gong P, Hu B, Stewart D, Choi ME, Choi AMK, Alam J (2001). Identification of activating transcription factor 4 (ATF4) as an Nrf2-interacting protein. *J. Biol. Chem*. **276**, 20858-20865.

Hebert DN, Bernasconi R, Molinari M (2010). ERAD substrates: Which way out? *Semin. Cell Dev. Biol*. **21**, 526-532.

Hebert DN, Molinari M (2007). In and out of the ER: Protein folding, quality control, degradation, and related human diseases. *Physiol. Rev*. **87**, 1377-1408.

Hegde RS, Kang SW (2008). The concept of translocational regulation. *J. Cell Biol.* **182**, 225-232.

Hegde RS, Voigt S, Rapoport TA, Lingappa VR (1998). TRAM regulates the exposure of nascent secretory proteins to the cytosol during translocation into the endoplasmic reticulum. *Cell* **92**, 621-631.

Henis-Korenblit S, Zhang P, Hansen M, McCormick M, Lee SJ, Cary M, Kenyon C (2010). Insulin/IGF-1 signaling mutants reprogram ER stress response regulators to promote longevity. *Proc. Natl. Acad. Sci. USA* **107**, 9730-9735.

Herbig U, Ferreira M, Condel L, Carey D, Sedivy JM (2006). Cellular senescence in aging primates. *Science* **311**, 1257.

Herczenik E, Gebbink MFBG (2008). Molecular and cellular aspects of protein misfolding and disease. *FASEB J*. **22**, 2115-2133.

Hessa T, Sharma A, Mariappan M, Eshleman HD, Gutierrez E, Hegde RS (2011). Protein targeting and degradation are coupled for elimination of mislocalized proteins. *Nature* **475**, 394-397.

Hetz C (2012). The unfolded protein response: Controlling cell fate decisions under ER stress and beyond. *Nat. Rev. Mol. Cell Biol*. **13**, 89-102.

Hetz C, Bernasconi P, Fisher J, Lee AH, Bassik MC, Antonsson B, Brandt GS, Iwakoshi NN, Schinzel A, Glimcher LH, Korsmeyer SJ (2006). Proapoptotic BAX and BAK modulate the unfolded protein response by a direct interaction with IRE1alpha. *Science* **312**, 572-576.

Heydari AR, You S, Takahashi R, Gutsmann-Conrad A, Sarge KD, Richardson A (2000). Age-related alterations in the activation of heat shock transcription factor 1 in rat hepatocytes. *Exp. Cell Res.* **256**, 83-93.

Hipp MS, Patel CN, Bersuker K, Riley BE, Kaiser SE, Shaler TA, Brandeis M, Kopito RR (2012). Indirect inhibition of 26S proteasome activity in a cellular model of Huntington's disease. *J. Cell Biol.* **196**, 573-587.

Hollien J, Lin JH, Li H, Stevens N, Walter P, Weissman JS (2009). Regulated Ire1-dependent decay of messenger RNAs in mammalian cells. *J. Cell Biol*. **186**, 323-331.

Hollien J, Weissman JS (2006). Decay of endoplasmic reticulum-localized mRNAs during the unfolded protein response. *Science* **313**, 104-107.

Holzenberger M, Dupont J, Ducos B, Leneuve P, Geloen A, Even PC, Cervera P, Le Bouc Y (2003). IGF-1 receptor regulates lifespan and resistance to oxidative stress in mice. *Nature* **421**, 182-187.

Hoozemans JJ, van Haastert ES, Nijholt DA, Rozemuller AJ, Eikelenboom P, Scheper W (2009). The unfolded protein response is activated in pretangle neurons in Alzheimer's disease hippocampus. *Am. J. Pathol.* **174**, 1241-1251.

Hosokawa N, Tremblay LO, Sleno B, Kamiya Y, Wada I, Nagata K, Kato K, Herscovics A (2010). EDEM1 accelerates the trimming of alpha1,2-linked mannose on the C branch of N-glycans. *Glycobiology* **20**, 567-575.

Hsu AL, Murphy CT, Kenyon C (2003). Regulation of aging and age-related disease by DAF-16 and heat-shock factor. *Science* **300**, 1142-1145.

Hubbard V, Valdor R, Macian F, Cuervo A (2011). Selective autophagy in the maintenance of cellular homeostasis in aging organisms. *Biogerontology* **13**, 21-35.

Huppa JB, Ploegh HL (1997). The alpha chain of the T cell antigen receptor is degraded in the cytosol. *Immunity* **7**, 113-122.

Hussain SG, Ramaiah KV (2007). Reduced eIF2alpha phosphorylation and increased proapoptotic proteins in aging. *Biochem. Biophys. Res. Commun*. **355**, 365-370.

Huzil JT, Pannu R, Ptak C, Garen G, Ellison MJ (2007). Direct catalysis of lysine 48-linked polyubiquitin chains by the ubiquitin-activating enzyme. *J. Biol. Chem*. **282**, 37454-37460.

Iwakoshi NN, Lee AH, Vallabhajosyula P, Otipoby KL, Rajewsky K, Glimcher LH (2003). Plasma cell differentiation and the unfolded protein response intersect at the transcription factor XBP-1. *Nat. Immunol.* **4**, 321-329.

Jedlicka P, Mortin MA, Wu C (1997). Multiple functions of Drosophila heat shock transcription factor in vivo. *EMBO J.* **16**, 2452-2462.

Jessop CE, Watkins RH, Simmons JJ, Tasab M, Bulleid NJ (2009). Protein disulphide isomerase family members show distinct substrate specificity: P5 is targeted to BiP client proteins. *J. Cell Sci*. **122**, 4287-4295.

Jiang H-Y, Wek RC (2005). Phosphorylation of the alpha-subunit of the eukaryotic initiation factor-2 (eIF2 alpha) reduces protein synthesis and enhances apoptosis in response to proteasome inhibition. *J. Biol. Chem*. **280**, 14189-14202.

Johnson N, Vilardi F, Lang S, Leznicki P, Zimmermann R, High S (2012). TRC-40 can deliver short secretory proteins to the Sec61 translocon. *J. Cell Sci*.**125**, 3612-20.

Johnson TE (1990). Increased life-span of age-1 mutants in Caenorhabditis elegans and lower Gompertz rate of aging. *Science* **249**, 908-912.

Juhasz G, Erdi B, Sass M, Neufeld TP (2007). Atg7-dependent autophagy promotes neuronal health, stress tolerance, and longevity but is dispensable for metamorphosis in Drosophila. *Genes Dev.* **21**, 3061-3066.

Kabeya Y, Mizushima N, Ueno T, Yamamoto A, Kirisako T, Noda T, Kominami E, Ohsumi Y, Yoshimori T (2000). LC3, a mammalian homologue of yeast Apg8p, is localized in autophagosome membranes after processing. *EMBO J*. **19**, 5720-5728.

Kabeya Y, Mizushima N, Yamamoto A, Oshitani-Okamoto S, Ohsumi Y, Yoshimori T (2004). LC3, GABARAP and GATE16 localize to autophagosomal membrane depending on form-II formation. *J. Cell Sci*. **117**, 2805-2812.

Kaneko M, Nomura Y (2003). ER signaling in unfolded protein response. *Life Sci*. **74**, 199-205.

Kang HT, Lee KB, Kim SY, Choi HR, Park SC (2011). Autophagy impairment induces premature senescence in primary human fibroblasts. *PLoS*. **6**, e23367.

Kang SW, Rane NS, Kim SJ, Garrison JL, Taunton J, Hegde RS (2006). Substrate-specific translocational attenuation during ER stress defines a pre-emptive quality control pathway. *Cell* **127**, 999-1013.

Kaushik S, Bandyopadhyay U, Sridhar S, Kiffin R, Martinez-Vicente M, Kon M, Orenstein SJ, Wong E, Cuervo AM (2011). Chaperone-mediated autophagy at a glance. *J. Cell Sci.* **124**, 495-499.

Kawaguchi Y, Kovacs JJ, McLaurin A, Vance JM, Ito A, Yao T-P (2003). The deacetylase HDAC6 regulates aggresome formation and cell viability in response to misfolded protein stress. *Cell* **115**, 727-738.

Keller JN, Huang FF, Markesbery WR (2000). Decreased levels of proteasome activity and proteasome expression in aging spinal cord. *Neuroscience* **98**, 149-156.

Kelly SM, Vanslyke JK, Musil LS (2007). Regulation of ubiquitin-proteasome system mediated degradation by cytosolic stress. *Mol. Biol. Cell* **18**, 4279-4291.

Kenyon C (2010a). A pathway that links reproductive status to lifespan in Caenorhabditis elegans. *Ann. N Y Acad. Sci*. **1204**, 156-162.

Kenyon C, Chang J, Gensch E, Rudner A, Tabtiang R (1993). A C. elegans mutant that lives twice as long as wild type. *Nature* **366**, 461-464.

Kenyon CJ (2010b). The genetics of ageing. *Nature* **464**, 504-512.

Kern A, Roempp B, Prager K, Walter J, Behl C (2006). Down-regulation of endogenous amyloid precursor protein processing due to cellular aging. *J. Biol. Chem*. **281**, 2405-2413.

Kikkert M, Hassink G, Barel M, Hirsch C, van der Wal F , Wiertz E (2001). Ubiquitination is essential for human cytomegalovirus US11-mediated dislocation of MHC class I molecules from the endoplasmic reticulum to the cytosol. *Biochem. J.* **358**, 369-377.

Kil IS, Lee YS, Bae YS, Huh TL, Park JW (2004). Modulation of NADP(+)-dependent isocitrate dehydrogenase in aging. *Redox Rep*. **9**, 271-277.

Kim HM, Yu Y, Cheng Y (2011). Structure characterization of the 26S proteasome. *Biochim. Biophys. Acta* **1809**, 67-79.

Kim I, Xu W, Reed JC (2008). Cell death and endoplasmic reticulum stress: disease relevance and therapeutic opportunities. *Nat. Rev. Drug Discov*. **7**, 1013-1030.

Kim SJ, Mitra D, Salerno JR, Hegde RS (2002). Signal sequences control gating of the protein translocation channel in a substrate-specific manner. *Dev. Cell* **2**, 207-217.

Kimura Y, Nakazawa M, Yamada M (1998). Cloning and characterization of three isoforms of OS-9 cDNA and expression of the OS-9 gene in various human tumor cell lines. *J. Biochem.* **123**, 876-882.

Klapper M, Ehmke M, Palgunow D, Bohme M, Matthaus C, Bergner G, Dietzek B, Popp J, Doring F (2011). Fluorescence-based fixative and vital staining of lipid droplets in Caenorhabditis elegans reveal fat stores using microscopy and flow cytometry approaches. *J. Lipid Res*. **52**, 1281-1293.

Klee M, Pallauf K, Alcala S, Fleischer A, Pimentel-Muinos FX (2009). Mitochondrial apoptosis induced by BH3-only molecules in the exclusive presence of endoplasmic reticular Bak. *EMBO J.* **28**, 1757-1768.

Koga H, Kaushik S, Cuervo AM (2010). Protein homeostasis and aging: The importance of exquisite quality control. *Ageing Cell* **10**, 205-215. .

Kourtis N, Tavernarakis N (2011). Cellular stress response pathways and ageing: intricate molecular relationships. *EMBO J*. **30**, 2520-2531.

Kriegenburg F, Ellgaard L, Hartmann-Petersen R (2012). Molecular chaperones in targeting misfolded proteins for ubiquitin-dependent degradation. *FEBS J*. **279**, 532-542.

Lakkaraju AK, Thankappan R, Mary C, Garrison JL, Taunton J, Strub K (2012). Efficient secretion of small proteins in mammalian cells relies on Sec62-dependent posttranslational translocation. *Mol. Biol Cell* **23**, 2712-2722. .

Lamark T, Johansen T (2012). Aggrephagy: Selective disposal of protein aggregates by macroautophagy. *Int. J. Cell Biol*. **2012**, 736905.

Lang S, Benedix J, Fedeles SV, Schorr S, Schirra C, Schauble N, Jalal C, Greiner M, Hassdenteufel S, Tatzelt J, Kreutzer B, Edelmann L, Krause E, Rettig J, Somlo S, Zimmermann R, Dudek J (2012). Different effects of Sec61alpha, Sec62 and Sec63 depletion on transport of polypeptides into the endoplasmic reticulum of mammalian cells. *J. Cell Sci*. **125**, 1958-1969.

Larsen PL (1993). Aging and resistance to oxidative damage in Caenorhabditis elegans. *Proc. Natl. Acad. Sci. USA* **90**, 8905-8909.

Lawson WE, Cheng DS, Degryse AL, Tanjore H, Polosukhin VV, Xu XC, Newcomb DC, Jones BR, Roldan J, Lane KB, Morrisey EE, Beers MF, Yull FE, Blackwell TS (2011). Endoplasmic reticulum stress enhances fibrotic remodeling in the lungs. *Proc. Natl. Acad. Sci. USA* **108**, 10562-10567.

Lee A-H, Scapa EF, Cohen DE, Glimcher LH (2008). Regulation of hepatic lipogenesis by the transcription factor XBP1. *Science* **320**, 1492-1496.

Lee AH, Iwakoshi NN, Glimcher LH (2003). XBP-1 regulates a subset of endoplasmic reticulum resident chaperone genes in the unfolded protein response. *Mol. Cell Biol*. **23**, 7448-7459.

Lee C-K, Klopp RG, Weindruch R, Prolla TA (1999). Gene expression profile of aging and its retardation by caloric restriction. *Science* **285**, 1390-1393.

Lee CK, Weindruch R, Prolla TA (2000). Gene-expression profile of the ageing brain in mice. *Nat. Genet.* **25**, 294-297.

Lee JY, Koga H, Kawaguchi Y, Tang W, Wong E, Gao YS, Pandey UB, Kaushik S, Tresse E, Lu J, Taylor JP, Cuervo AM, Yao TP (2010). HDAC6 controls autophagosome maturation essential for ubiquitin-selective quality-control autophagy. *EMBO J.* **29**, 969-980.

Lewerenz J, Maher P (2009). Basal levels of eIF2alpha phosphorylation determine cellular antioxidant status by regulating ATF4 and xCT expression. *J. Biol. Chem.* **284**, 1106-1115.

Leznicki P, Clancy A, Schwappach B, High S (2010). Bat3 promotes the membrane integration of tail-anchored proteins. *J. Cell Sci*. **123**, 2170-2178.

Li H, Korennykh AV, Behrman SL, Walter P (2010). Mammalian endoplasmic reticulum stress sensor IRE1 signals by dynamic clustering. *Proc. Natl. Acad. Sci. USA* **107**, 16113-16118.

Li J, Holbrook NJ (2004). Elevated gadd153/chop expression and enhanced c-Jun N-terminal protein kinase activation sensitizes aged cells to ER stress. *Exp. Gerontol*. **39**, 735-744.

Lilley BN, Gilbert JM, Ploegh HL, Benjamin TL (2006). Murine polyomavirus requires the endoplasmic reticulum protein Derlin-2 to initiate infection. *J. Virol*. **80**, 8739-8744.

Lilley BN, Ploegh HL (2004). A membrane protein required for dislocation of misfolded proteins from the ER. *Nature* **429**, 834-840.

Lin JH, Li H, Yasumura D, Cohen HR, Zhang C, Panning B, Shokat KM, LaVail MM, Walter P (2007). IRE1 signaling affects cell fate during the unfolded protein response. *Science* **318**, 944-949.

Lin JH, Li H, Zhang Y, Ron D, Walter P (2009). Divergent effects of PERK and IRE1 signaling on cell viability. *PLoS ONE*. **4**, e4170.

Lindquist SL, Kelly JW (2011). Chemical and biological approaches for adapting proteostasis to ameliorate protein misfolding and aggregation diseases: progress and prognosis. *Cold Spring Harb. Perspect. Biol*. **3**, a004507.

Lippincott-Schwartz J, Bonifacino JS, Yuan LC, Klausner RD (1988). Degradation from the endoplasmic reticulum: disposing of newly synthesized proteins. *Cell* **54**, 209-220.

Lisbona F, Rojas-Rivera D, Thielen P, Zamorano S, Todd D, Martinon F, Glavic A, Kress C, Lin JH, Walter P, Reed JC, Glimcher LH, Hetz C (2009). BAX inhibitor-1 is a negative regulator of the ER stress sensor IRE1alpha. *Mol. Cell* **33**, 679-691.

Lithgow GJ, White TM, Melov S, Johnson TE (1995). Thermotolerance and extended life-span conferred by single-gene mutations and induced by thermal stress. *Proc. Natl. Acad. Sci. USA.* **92**, 7540-7544.

Litovchick L, Friedmann E, Shaltiel S (2002). A selective interaction between OS-9 and the carboxyl-terminal tail of meprin. *J. Biol. Chem*. **277**, 34413-34423.

Liu Y, Choudhury P, Cabral CM, Sifers RN (1997). Intracellular disposal of incompletely folded human alpha1-antitrypsin involves release from calnexin and post-translational trimming of asparagine-linked oligosaccharides. *J. Biol. Chem.* **272**, 7946-7951.

Low P (2011). The role of ubiquitin - proteasome system in ageing. *Gen. Comp. Endocrinol*. **172**, 39-43.

Luders J, Demand J, Hohfeld J (2000). The ubiquitin-related BAG-1 provides a link between the molecular chaperones Hsc70/Hsp70 and the proteasome. *J. Biol. Chem.* **275**, 4613-4617.

Luo D, He Y, Zhang H, Yu L, Chen H, Xu Z, Tang S, Urano F, Min W (2008). AIP1 is critical in transducing IRE1-mediated endoplasmic reticulum stress response. *J. Biol. Chem.* **283**, 11905-11912.

Ma K, Vattem KM, Wek RC (2002). Dimerization and release of molecular chaperone inhibition facilitate activation of eukaryotic initiation factor-2 kinase in response to endoplasmic reticulum stress. *J. Biol. Chem*. **277**, 18728-18735.

Ma Y, Shimizu Y, Mann MJ, Jin Y, Hendershot LM (2009). Plasma cell differentiation initiates a limited ER stress response by specifically suppressing the PERK-dependent branch of the unfolded protein response. *Cell Stress Chaperones*. **15**, 281-293.

Majumder M, Huang C, Snider MD, Komar AA, Tanaka J, Kaufman RJ, Krokowski D, Hatzoglou M (2012). A novel feedback loop regulates the response to endoplasmic reticulum stress via the cooperation of cytoplasmic splicing and mRNA translation. *Mol. Cell Biol*. **32**, 992-1003.

Marciniak SJ, Ron D (2006). Endoplasmic reticulum stress signaling in disease. *Physiol. Rev*. **86**, 1133-1149.

Marciniak SJ, Yun CY, Oyadomari S, Novoa I, Zhang Y, Jungreis R, Nagata K, Harding HP, Ron D (2004). CHOP induces death by promoting protein synthesis and oxidation in the stressed endoplasmic reticulum. *Genes Dev.* **18**, 3066-3077.

Mariappan M, Li X, Stefanovic S, Sharma A, Mateja A, Keenan RJ, Hegde RS (2010). A ribosome-associating factor chaperones tail-anchored membrane proteins. *Nature* **466**, 1120-1124.

Martin JA, Buckwalter JA (2002). Human chondrocyte senescence and osteoarthritis. *Biorheology* **39**, 145-152.

Martoglio B (2003). Intramembrane proteolysis and post-targeting functions of signal peptides. *Biochem. Soc. Trans.* **31**, 1243-1247.

Mazroui R, Di Marco S, Kaufman RJ, Gallouzi I-E (2007). Inhibition of the ubiquitin-proteasome system induces stress granule formation. *Mol. Biol. Cell* **18**, 2603-2618.

McArdle A, Dillmann WH, Mestril R, Faulkner JA, Jackson MJ (2004). Overexpression of HSP70 in mouse skeletal muscle protects against muscle damage and age-related muscle dysfunction. *FASEB J.* **18**, 355-357.

McKibbin C, Mares A, Piacenti M, Williams H, Roboti P, Puumalainen M, Callan AC, Lesiak-Mieczkowska K, Linder S, Harant H, High S, Flitsch SL, Whitehead RC, Swanton E (2012).

Inhibition of protein translocation at the endoplasmic reticulum promotes activation of the unfolded protein response. *Biochem*. *J.* **442**, 639-648.

Mebius RE, Kraal G (2005). Structure and function of the spleen. *Nat. Rev. Immunol*. **5**, 606-616.

Mehnert M, Sommer T, Jarosch E (2010). ERAD ubiquitin ligases. *BioEssays* **32**, 905-913.

Merksamer PI, Trusina A, Papa FR (2008). Real-time redox measurements during endoplasmic reticulum stress reveal interlinked protein folding functions. *Cell* **135**, 933-947.

Metzger MB, Michaelis S (2009). Analysis of quality control substrates in distinct cellular compartments reveals a unique role for Rpn4p in tolerating misfolded membrane proteins. *Mol. Biol. Cell* **20**, 1006-1019.

Meyer H, Bug M, Bremer S (2012). Emerging functions of the VCP/p97 AAA-ATPase in the ubiquitin system. *Nat. Cell Biol*. **14**, 117-123.

Mezzacasa A, Helenius A (2002). The transitional ER defines a boundary for quality control in the secretion of tsO45 VSV glycoprotein. *Traffic* **3**, 833-849.

Michalak M, Opas M (2009). Endoplasmic and sarcoplasmic reticulum in the heart. *Trends Cell Biol.* **19**, 253-259.

Miesbauer M, Pfeiffer NV, Rambold AS, Muller V, Kiachopoulos S, Winklhofer KF, Tatzelt J (2009). alpha-Helical domains promote translocation of intrinsically disordered polypeptides into the endoplasmic reticulum. *J. Biol. Chem.* **284**, 24384-24393.

Min JN, Whaley RA, Sharpless NE, Lockyer P, Portbury AL, Patterson C (2008). CHIP deficiency decreases longevity, with accelerated aging phenotypes accompanied by altered protein quality control. *Mol. Cell Biol.* **28**, 4018-4025.

Misra V, Lee H, Singh A, Huang K, Thimmulappa RK, Mitzner W, Biswal S, Tankersley CG (2007). Global expression profiles from C57BL/6J and DBA/2J mouse lungs to determine aging-related genes. *Physiol. Genomics* **31**, 429-440.

Mizushima N (2007). Autophagy: process and function. *Genes Dev.* **21**, 2861-2873.

Molinari M, Calanca V, Galli C, Lucca P, Paganetti P (2003). Role of EDEM in the release of misfolded glycoproteins from the calnexin cycle. *Science* **299**, 1397-1400.

Molinari M, Helenius A (2000). Chaperone selection during glycoprotein translocation into the endoplasmic reticulum. *Science* **288**, 331-333.

Moreno JA, Radford H, Peretti D, Steinert JR, Verity N, Martin MG, Halliday M, Morgan J, Dinsdale D, Ortori CA, Barrett DA, Tsaytler P, Bertolotti A, Willis AE, Bushell M, Mallucci GR (2012). Sustained translational repression by eIF2alpha-P mediates prion neurodegeneration. *Nature* **485**, 507-511.

Morimoto RI (2002). Dynamic remodeling of transcription complexes by molecular chaperones. *Cell* **110**, 281-284.

Morimoto RI (2008). Proteotoxic stress and inducible chaperone networks in neurodegenerative disease and aging. *Genes Dev*. **22**, 1427-1438.

Morley JF, Brignull HR, Weyers J, Morimoto RI (2002). The threshold for polyglutamine-expansion protein aggregation and cellular toxicity is dynamic and influenced by aging in Caenorhabditis elegans. *Proc. Natl. Acad. Sci*. USA **99**, 10417-10422.

Morley JF, Morimoto RI (2004). Regulation of logevity in Caenorhabditis elegans by heat shock factor and molecular chaperones. *Mol. Biol. Cell* **15**, 657-664.

Morrow G, Samson M, Michaud S, Tanguay RM (2004). Overexpression of the small mitochondrial Hsp22 extends Drosophila life span and increases resistance to oxidative stress. *FASEB J*. **18**, 598-599.

Mosmann T (1983). Rapid colorimetric assay for cellular growth and survival: Application to proliferation and cytotoxicity assays. *J. Immunol. Methods* **65**, 55-63.

Muller P, Ruckova E, Halada P, Coates PJ, Hrstka R, Lane DP , Vojtesek B (2012). C-terminal phosphorylation of Hsp70 and Hsp90 regulates alternate binding to co-chaperones CHIP and HOP to determine cellular protein folding/degradation balances *Oncogene* doi: 10.1038/onc.2012.314.

Mura CV, Gong X, Taylor A, Villalobos-Molina R, Scrofano MM (1996). Effects of calorie restriction and aging on the expression of antioxidant enzymes and ubiquitin in the liver of Emory mice. *Mech. Ageing Dev*. **91**, 115-129.

Nadanaka S, Okada T, Yoshida H, Mori K (2007). Role of disulfide bridges formed in the luminal domain of ATF6 in sensing endoplasmic reticulumstress. *Mol. Cell Biol*. **27**, 1027-1043.

Naeem A, Fazili N (2011). Defective protein folding and aggregation as the basis of neurodegenerative diseases: the darker aspect of proteins. *Cell Biochem. Biophys*. **61**, 237-250.

Naidoo N, Ferber M, Master M, Zhu Y, Pack AI (2008). Aging impairs the unfolded protein response to sleep deprivation and leads to proapoptotic signaling. *J. Neurosci*. **28**, 6539-6548.

Nardai G, Csermely P, Soti C (2002). Chaperone function and chaperone overload in the aged. A preliminary analysis. *Exp. Gerontol*. **37**, 1257-1262.

Nguyen T, Huang HC, Pickett CB (2000). Transcriptional regulation of the antioxidant response element. Activation by Nrf2 and repression by MafK. *J. Biol. Chem*. **275**, 15466-15473.

Nishio K, Inoue A (2005). Senescence-associated alterations of cytoskeleton: extraordinary production of vimentin that anchors cytoplasmic p53 in senescent human fibroblasts. *Histochem. Cell Biol.* **123**, 263-273.

Nishitoh H, Kadowaki H, Nagai A, Maruyama T, Yokota T, Fukutomi H, Noguchi T, Matsuzawa A, Takeda K, Ichijo H (2008). ALS-linked mutant SOD1 induces ER stress- and ASK1-dependent motor neuron death by targeting Derlin-1. *Genes Dev.* **22**, 1451-1464.

Nishitoh H, Matsuzawa A, Tobiume K, Saegusa K, Takeda K, Inoue K, Hori S, Kakizuka A, Ichijo H (2002). ASK1 is essential for endoplasmic reticulum stress-induced neuronal cell death triggered by expanded polyglutamine repeats. *Genes Dev*. **16**, 1345-1355.

Novoa I, Zeng H, Harding H, Ron D (2001). Feedback inhibition of the unfolded protein response by GADD34-mediated dephosphorylation of eIF2 alpha. *J. Cell Biol*. **153**, 1011-1022.

Nowis D, McConnell E, Wojcik C (2006). Destabilization of the VCP-Ufd1-Npl4 complex is associated with decreased levels of ERAD substrates. *Exp. Cell Res.* **312**, 2921-2932.

Nuss JE, Choksi KB, DeFord JH, Papaconstantinou J (2008). Decreased enzyme activities of chaperones PDI and BiP in aged mouse livers. *Biochem Biophys Res Commun*. **365**, 355-361.

Oda Y, Hosokawa N, Wada I, Nagata K (2003). EDEM as an acceptor of terminally misfolded glycoproteins released from calnexin. *Science* **299**, 1394-1397.

Oda Y, Okada T, Yoshida H, Kaufman RJ, Nagata K, Mori K (2006). Derlin-2 and Derlin-3 are regulated by the mammalian unfolded protein response and are required for ER-associated degradation. *J. Cell Biol*. **172**, 383-393.

Ohtsuka H, Takahashi R, Goto S (1995). Age-related accumulation of high-molecular-weight ubiquitin protein conjugates in mouse brains. *J. Gerontol. A. Biol. Sci. Med Sci.* **50A**, 277-281.

Okada T, Yoshida H, Akazawa R, Negishi M, Mori K (2002). Distinct roles of activating transcription factor 6 (ATF6) and double-stranded RNA-activated protein kinase-like endoplasmic reticulum kinase (PERK) in transcription during the mammalian unfolded protein response. *Biochem. J.* **366**, 585-594.

Okuda-Shimizu Y, Hendershot LM (2007). Characterization of an ERAD pathway for nonglycosylated BiP substrates, which require Herp. *Mol. Cell* **28**, 544-554.

Oliver JD, van der Wal FJ, Bulleid NJ, High S (1997). Interaction of the thiol-dependent reductase ERp57 with nascent glycoproteins. *Science* **275**, 86-88.

Olzscha H, Schermann SM, Woerner AC, Pinkert S, Hecht MH, Tartaglia GG, Vendruscolo M, Hayer-Hartl M, Hartl FU, Vabulas RM (2011). Amyloid-like aggregates sequester numerous metastable proteins with essential cellular functions. *Cell* **144**, 67-78.

Orenstein SJ, Cuervo AM (2010). Chaperone-mediated autophagy: molecular mechanisms and physiological relevance. *Semin. Cell Dev. Biol.* **21**, 719-726. .

Pagant S, Kung L, Dorrington M, Lee MC, Miller EA (2007). Inhibiting endoplasmic reticulum (ER)-associated degradation of misfolded Yor1p does not permit ER export despite the presence of a diacidic sorting signal. *Mol. Biol. Cell* **18**, 3398-3413.

Page LJ, Suk JY, Bazhenova L, Fleming SM, Wood M, Jiang Y, Guo LT, Mizisin AP, Kisilevsky R, Shelton GD, Balch WE, Kelly JW (2009). Secretion of amyloidogenic gelsolin progressively compromises protein homeostasis leading to the intracellular aggregation of proteins. *Proc. Natl. Acad. Sci. USA.* **106**, 11125-11130.

Panda S, Isbatan A, Adami GR (2008). Modification of the ATM/ATR directed DNA damage response state with aging and long after hepatocyte senescence induction in vivo. *Mech. Ageing Dev.* **129**, 332-340.

Papaconstantinou J, Deford JH, Gerstner A, Hsieh CC, Boylston WH, Guigneaux MM, Flurkey K, Harrison DE (2005). Hepatic gene and protein expression of primary components of the IGF-I axis in long lived Snell dwarf mice. *Mech. Ageing Dev.* **126**, 692-704.

Park E, Rapoport TA (2012). Mechanisms of Sec61/SecY-mediated protein translocation across membranes. *Annu. Rev.Biophys*. **41**, 21-40.

Partridge L, Piper MDW, Mair W (2005). Dietary restriction in Drosophila. *Mech. Ageing Dev*. **126**, 938-950.

Paz Gavilán M, Pintado C, Gavilán E, Jiménez S, Ríos RM, Vitorica J, Castaño A, Ruano D (2009). Dysfunction of the unfolded protein response increases neurodegeneration in aged rat hippocampus following proteasome inhibition. *Aging Cell* **8**, 654-665.

Paz Gavilan M, Vela J, Castano A, Ramos B, del Rio JC, Vitorica J, Ruano D (2006). Cellular environment facilitates protein accumulation in aged rat hippocampus. *Neurobiol. Aging* **27**, 973-982.

Perez VI, Buffenstein R, Masamsetti V, Leonard S, Salmon AB, Mele J, Andziak B, Yang T, Edrey Y, Friguet B, Ward W, Richardson A, Chaudhuri A (2009). Protein stability and resistance to oxidative stress are determinants of longevity in the longest-living rodent, the naked mole-rat. *Proc. Natl. Acad. Sci. USA.* **106**, 3059-3064.

Piec I, Listrat A, Alliot J, Chambon C, Taylor RG, Bechet D (2005). Differential proteome analysis of aging in rat skeletal muscle. *FASEB J.* **19**, 1143-1145.

Pincus D, Chevalier MW, Aragon T, van Anken E, Vidal SE, El-Samad H, Walter P (2010). BiP binding to the ER-stress sensor Ire1 tunes the homeostatic behavior of the unfolded protein response. *PLoS Biol*. **8**, e1000415.

Promlek T, Ishiwata-Kimata Y, Shido M, Sakuramoto M, Kohno K, Kimata Y (2011). Membrane aberrancy and unfolded proteins activate the endoplasmic reticulum stress sensor Ire1 in different ways. *Mol*. *Biol. Cell* **22**, 3520-3532. .

Rabek JP, Boylston WH, 3rd, Papaconstantinou J (2003). Carbonylation of ER chaperone proteins in aged mouse liver. *Biochem. Biophys. Res. Commun*. **305**, 566-572.

Rabu C, Wipf P, Brodsky JL, High S (2008). A precursor specific role for Hsp40/Hsc70 during tail-anchored protein integration at the endoplasmic reticulum. *J. Biol. Chem*. **283**, 27504-27513

Rane NS, Chakrabarti O, Feigenbaum L, Hegde RS (2010). Signal sequence insufficiency contributes to neurodegeneration caused by transmembrane prion protein. *J. Cell Biol*. **188**, 515-526.

Rane NS, Kang SW, Chakrabarti O, Feigenbaum L, Hegde RS (2008). Reduced translocation of nascent prion protein during ER stress contributes to neurodegeneration. *Dev Cell.* **15**, 359-370.

Rapoport TA (2007). Protein translocation across the eukaryotic endoplasmic reticulum and bacterial plasma membranes. *Nature* **450**, 663-669.

Ravikumar B, Sarkar S, Davies JE, Futter M, Garcia-Arencibia M, Green-Thompson ZW, Jimenez-Sanchez M, Korolchuk VI, Lichtenberg M, Luo S, Massey DCO, Menzies FM, Moreau K, Narayanan U, Renna M, Siddiqi FH, Underwood BR, Winslow AR, Rubinsztein DC (2010). Regulation of mammalian autophagy in physiology and pathophysiology. *Physiol. Rev*. **90**, 1383-1435.

Reimold AM, Iwakoshi NN, Manis J, Vallabhajosyula P, Szomolanyi-Tsuda E, Gravallese EM, Friend D, Grusby MJ, Alt F, Glimcher LH (2001). Plasma cell differentiation requires the transcription factor XBP-1. *Nature* **412**, 300-307.

Ren PH, Lauckner JE, Kachirskaia I, Heuser JE, Melki R, Kopito RR (2009). Cytoplasmic penetration and persistent infection of mammalian cells by polyglutamine aggregates. *Nat Cell Biol.* **11**, 219-225.

Reynders E, Foulquier Fo, Annaert W, Matthijs G (2011). How Golgi glycosylation meets and needs trafficking: the case of the COG complex. *Glycobiology* **21**, 853-863.

Ritter C, Helenius A (2000). Recognition of local glycoprotein misfolding by the ER folding sensor UDP-glucose:glycoprotein glucosyltransferase. *Nat. Struct. Biol.* **7**, 278-280.

Rodwell GE, Sonu R, Zahn JM, Lund J, Wilhelmy J, Wang L, Xiao W, Mindrinos M, Crane E, Segal E, Myers BD, Brooks JD, Davis RW, Higgins J, Owen AB, Kim SK (2004). A transcriptional profile of aging in the human kidney. *PLoS Biol.* **2**, e427.

Ron D, Walter P (2007). Signal integration in the endoplasmic reticulum unfolded protein response. *Nat. Rev. Mol. Cell Biol*. **8**, 519-529.

Rong J, Chen L, Toth JI, Tcherpakov M, Petroski MD, Reed JC (2011). Bifunctional apoptosis regulator (BAR), an endoplasmic reticulum (ER)-associated E3 ubiquitin ligase, modulates BI-1 protein stability and function in ER stress. *J. Biol. Chem*. **286**, 1453-1463.

Roth DM, Balch WE (2010). Modeling general proteostasis: proteome balance in health and disease. *Curr. Opin. Cell Biol.* **23**, 126-134. .

Roth J, Yam GH, Fan J, Hirano K, Gaplovska-Kysela K, Le Fourn V, Guhl B, Santimaria R, Torossi T, Ziak M, Zuber C (2008). Protein quality control: The who's who, the where's and therapeutic escapes. *Histochem. Cell Biol*. **129**, 163-177.

Rubinsztein DC, Marino G, Kroemer G (2011). Autophagy and aging. *Cell* **146**, 682-695.

Rubio C, Pincus D, Korennykh A, Schuck S, El-Samad H, Walter P (2011). Homeostatic adaptation to endoplasmic reticulum stress depends on Ire1 kinase activity. *J. Cell Biol*. **193**, 171-184.

Rutkevich LA, Cohen-Doyle MF, Brockmeier U, Williams DB (2010). Functional relationship between protein disulfide isomerase family members during the oxidative folding of human secretory proteins. *Mol. Biol. Cell* **21**, 3093-3105.

Rutkowski DT, Arnold SM, Miller CN, Wu J, Li J, Gunnison KM, Mori K, Sadighi Akha AA, Raden D, Kaufman RJ (2006). Adaptation to ER stress is mediated by differential stabilities of pro-survival and pro-apoptotic mRNAs and proteins. *PLoS Biol.* **4**, e374.

Rutkowski DT , Hegde RS (2010). Regulation of basal cellular physiology by the homeostatic unfolded protein response. *J.Cell Biol*. **189**, 783-794.

Sadighi Akha AA, Harper JM, Salmon AB, Schroeder BA, Tyra HM, Rutkowski DT , Miller RA (2011). Heightened induction of proapoptotic signals in response to endoplasmic reticulum stress in primary fibroblasts from a mouse model of longevity. *J. Biol. Chem.* **286**, 30344-30351.

Saraogi I, Shan S-o (2011). Molecular mechanism of co-translational protein targeting by the signal recognition particle. *Traffic* **12**, 535-542.

Sato BK, Schulz D, Do PH, Hampton RY (2009). Misfolded membrane proteins are specifically recognized by the transmembrane domain of the Hrd1p ubiquitin ligase. *Mol. Cell* **34**, 212-222.

Sato K, Nakano A (2007). Mechanisms of COPII vesicle formation and protein sorting. *FEBS Lett*. **581**, 2076-2082.

Scheuner D, Song B, McEwen E, Liu C, Laybutt R, Gillespie P, Saunders T, Bonner-Weir S, Kaufman RJ (2001). Translational control is required for the unfolded protein response and in vivo glucose homeostasis. *Mol. Cell* **7**, 1165-1176.

Schmitz A, Schneider A, Kummer MP, Herzog V (2004). Endoplasmic reticulum-localized amyloid beta-peptide is degraded in the cytosol by two distinct degradation pathways. *Traffic* **5**, 89-101.

Schmucker DL, Sanchez H (2011). Liver regeneration and aging: a current perspective. *Curr. Gerontol. Geriatr. Res*. **2011**, 8.

Schroeder F, Goetz I, Roberts E (1984). Age-related alterations in cultured human fibroblast membrane structure and function. *Mech. Ageing Dev.* **25**, 365-389.

Schubert U, Anton LC, Gibbs J, Norbury CC, Yewdell JW, Bennink JR (2000). Rapid degradation of a large fraction of newly synthesized proteins by proteasomes. *Nature* **404**, 770-774.

Seidel K, Vinet J, Dunnen WF, Brunt ER, Meister M, Boncoraglio A, Zijlstra MP, Boddeke HW, Rub U, Kampinga HH, Carra S (2011). The HSPB8-BAG3 chaperone complex is upregulated in astrocytes in the human brain affected by protein aggregation diseases. *Neuropathol. Appl. Neurobiol*. **38**, 39-53.

Shaffer AL, Shapiro-Shelef M, Iwakoshi NN, Lee AH, Qian SB, Zhao H, Yu X, Yang L, Tan BK, Rosenwald A, Hurt EM, Petroulakis E, Sonenberg N, Yewdell JW, Calame K, Glimcher LH, Staudt LM (2004). XBP1, downstream of Blimp-1, expands the secretory apparatus and other organelles, and increases protein synthesis in plasma cell differentiation. *Immunity* **21**, 81-93.

Shaid S, Brandts CH, Serve H, Dikic I (2012). Ubiquitination and selective autophagy. *Cell Death Differ*. **20**, 21-30.

Shamu CE, Walter P (1996). Oligomerization and phosphorylation of the Ire1p kinase during intracellular signaling from the endoplasmic reticulum to the nucleus. *EMBO J.* **15**, 3028-3039.

Shang J, Gao N, Kaufman RJ, Ron D, Harding HP, Lehrman MA (2007). Translation attenuation by PERK balances ER glycoprotein synthesis with lipid-linked oligosaccharide flux. *J. Cell Biol.* **176**, 605-616.

Shao S, Hegde RS (2011). Membrane protein insertion at the endoplasmic reticulum. *Annu. Rev.Cell Dev. Biol*. **27**, 25-56.

Shen J, Chen X, Hendershot L, Prywes R (2002). ER stress regulation of ATF6 localization by dissociation of BiP/GRP78 binding and unmasking of Golgi localization signals. *Dev. Cell* **3**, 99-111.

Shi Y, Vattem KM, Sood R, An J, Liang J, Stramm L, Wek RC (1998). Identification and characterization of pancreatic eukaryotic initiation factor 2 alpha-subunit kinase, PEK, involved in translational control. *Mol. Cell Biol.* **18**, 7499-7509.

Sifers RN, Brashears-Macatee S, Kidd VJ, Muensch H, Woo SL (1988). A frameshift mutation results in a truncated alpha 1-antitrypsin that is retained within the rough endoplasmic reticulum. *J. Biol. Chem.* **263**, 7330-7335.

Simonsen A, Cumming RC, Brech A, Isakson P, Schubert DR, Finley KD (2008). Promoting basal levels of autophagy in the nervous system enhances longevity and oxidant resistance in adult Drosophila. *Autophagy* **4**, 176-184.

Sinclair DA (2005). Toward a unified theory of caloric restriction and longevity regulation. *Mech Ageing Dev*. **126**, 987-1002.

Sisoula C, Gonos ES (2011). CHIP E3 ligase regulates mammalian senescence by modulating the levels of oxidized proteins. *Mech. Ageing Dev*. **132**, 269-272.

Smith MH, Ploegh HL, Weissman JS (2010). Road to ruin: targeting proteins for degradation in the endoplasmic reticulum. *Science* **334**, 1086-1090.

Soetandyo N, Wang Q, Ye Y, Li L (2010). Role of intramembrane charged residues in the quality control of unassembled T-cell receptor alpha-chains at the endoplasmic reticulum. *J. Cell Sci*. **123**, 1031-1038.

Sousa M, Parodi AJ (1995). The molecular basis for the recognition of misfolded glycoproteins by the UDP-Glc:glycoprotein glucosyltransferase. *EMBO J.* **14**, 4196-4203.

Sousa MC, Ferrero-Garcia MA, Parodi AJ (1992). Recognition of the oligosaccharide and protein moieties of glycoproteins by the UDP-Glc:glycoprotein glucosyltransferase. *Biochemistry* **31**, 97-105.

Stagg SM, Gurkan C, Fowler DM, LaPointe P, Foss TR, Potter CS, Carragher B, Balch WE (2006). Structure of the Sec13/31 COPII coat cage. *Nature* **439**, 234-238.

Starke-Reed PE, Oliver CN (1989). Protein oxidation and proteolysis during aging and oxidative stress. *Arch. Biochem. Biophys.* **275**, 559-567.

Tabas I, Ron D (2011). Integrating the mechanisms of apoptosis induced by endoplasmic reticulum stress. *Nat. Cell Biol*. **13**, 184-190.

Taipale M, Jarosz DF, Lindquist S (2010). HSP90 at the hub of protein homeostasis: emerging mechanistic insights. *Nat. Rev. Mol. Cell Biol.* **11**, 515-528.

Taneike M, Yamaguchi O, Nakai A, Hikoso S, Takeda T, Mizote I, Oka T, Tamai T, Oyabu J, Murakawa T, Nishida K, Shimizu T, Hori M, Komuro I, Takuji Shirasawa TS, Mizushima N, Otsu K (2010). Inhibition of autophagy in the heart induces age-related cardiomyopathy. *Autophagy* **6**, 600-606. .

Tatar M, Khazaeli AA, Curtsinger JW (1997). Chaperoning extended life. *Nature* **390**, 30-30.

Tatar M, Kopelman A, Epstein D, Tu MP, Yin CM, Garofalo RS (2001). A mutant Drosophila insulin receptor homolog that extends life-span and impairs neuroendocrine function. *Science* **292**, 107-110.

Taylor DJ, Devkota B, Huang AD, Topf M, Narayanan E, Sali A, Harvey S, Frank J (2009). Comprehensive molecular structure of the eukaryotic ribosome. *Structure* **17**, 1591-1604.

Taylor SC, Ferguson AD, Bergeron JJ, Thomas DY (2004). The ER protein folding sensor UDP-glucose glycoprotein-glucosyltransferase modifies substrates distant to local changes in glycoprotein conformation. *Nat. Struct. Mol. Biol.* **11**, 128-134.

Terman A, Brunk UT (2005). The aging myocardium: roles of mitochondrial damage and lysosomal degradation. *Heart Lung Circ.* **14**, 107-114.

Teske BF, Wek SA, Bunpo P, Cundiff JK, McClintick JN, Anthony TG, Wek RC (2011). The eIF2 kinase PERK and the integrated stress response facilitate activation of ATF6 during endoplasmic reticulum stress. *Mol. Biol. Cell* **22**, 4390-4405.

Torres-Gonzalez E, Bueno M, Tanaka A, Krug LT, Cheng D-S, Polosukhin VV, Sorescu D, Lawson WE, Blackwell TS, Rojas M, Mora AL (2012). Role of endoplasmic reticulum stress in age-related susceptibility to lung fibrosis. *Am. J. Respir. Cell Mol. Biol.* **46**, 748-756.

Toth ML, Sigmond T, Borsos E, Barna J, Erdelyi P, Takacs-Vellai K, Orosz L, Kovacs AL, Csikos G, Sass M, Vellai T (2008). Longevity pathways converge on autophagy genes to regulate life span in Caenorhabditis elegans. *Autophagy* **4**, 330-338. .

Tower J (2009). Hsps and aging. *Trends Endocrinol. Metab*. **20**, 216-222.

Trocoli A, Djavaheri-Mergny M (2011). The complex interplay between autophagy and NF-kappaB signaling pathways in cancer cells. *Am. J. Cancer Res.* **1**, 629-649.

Tsaytler P, Harding HP, Ron D, Bertolotti A (2011). Selective inhibition of a regulatory subunit of protein phosphatase 1 restores proteostasis. *Science* **332**, 91-94.

Urano F, Calfon M, Yoneda T, Yun C, Kiraly M, Clark SG, Ron D (2002). A survival pathway for Caenorhabditis elegans with a blocked unfolded protein response. *J. Cell Biol.* **158**, 639-646.

Urano F, Wang X, Bertolotti A, Zhang Y, Chung P, Harding HP , Ron D (2000). Coupling of stress in the ER to activation of JNK protein kinases by transmembrane protein kinase IRE1. *Science* **287**, 664-666.

Vabulas RM, Raychaudhuri S, Hayer-Hartl M, Hartl FU (2010). Protein folding in the cytoplasm and the heat shock response. *Cold Spring Harb. Perspect. Biol*. **2**, a004390.

van der Vlies D, Makkinje M, Jansens A, Braakman I, Verkleij AJ, Wirtz KW, Post JA (2003). Oxidation of ER resident proteins upon oxidative stress: effects of altering cellular redox/antioxidant status and implications for protein maturation. *Antioxid Redox Signal* **5**, 381-387.

van Heemst D (2010). Insulin, IGF-1 and longevity. *Aging Dis.* **1**, 147-157.

Varki A CR, Esko J (1999). Essentials of Glycobiology (2nd edition). In Chapter 40: Natural and Synthetic Inhibitors of Glycosylationed. Cold Spring Harbor (NY): Cold Spring Harbor Laboratory Press.

Vasserman G, Magal LG, Shepshelovich J, Elifaz E, Hirschberg K (2006). Processing of VSVG protein is not a rate-limiting step for its efflux from the Golgi complex. *Biochem. Biophys. Res. Commun.* **351**, 689-694.

Verbitsky M, Yonan AL, Malleret G, Kandel ER, Gilliam TC, Pavlidis P (2004). Altered hippocampal transcript profile accompanies an age-related spatial memory deficit in mice. *Learn Mem.* **11**, 253-260.

Vilchez D, Morantte I, Liu Z, Douglas PM, Merkwirth C, Rodrigues AP, Manning G, Dillin A (2012). RPN-6 determines C. elegans longevity under proteotoxic stress conditions. *Nature* **489**, 263-268.

Viswanathan M, Kim SK, Berdichevsky A, Guarente L (2005). A role for SIR-2.1 regulation of ER stress response genes in determining C. elegans life span. *Dev Cell*. **9**, 605-615.

Volovik Y, Maman M, Dubnikov T, Bejerano-Sagie M, Joyce D, Kapernick EA, Cohen E, Dillin A (2012). Temporal requirements of heat shock factor-1 for longevity assurance. *Aging Cell* **11**, 491-499.

Walker G, Houthoofd K, Vanfleteren JR, Gems D (2005). Dietary restriction in C. elegans: From rate-of-living effects to nutrient sensing pathways. *Mech. Ageing Dev*. **126**, 929-937.

Walker GA, Lithgow GJ (2003). Lifespan extension in C. elegans by a molecular chaperone dependent upon insulin-like signals. *Aging Cell* **2**, 131-139.

Walter P, Ron D (2011). The unfolded protein response: From stress pathway to homeostatic regulation. *Science* **334**, 1081-1086.

Wang C, Jurk D, Maddick M, Nelson G, Martin-Ruiz C, von Zglinicki T (2009a). DNA damage response and cellular senescence in tissues of aging mice. *Aging Cell* **8**, 311-323.

Wang Q, Liu Y, Soetandyo N, Baek K, Hegde R, Ye Y (2011). A ubiquitin ligase-associated chaperone holdase maintains polypeptides in soluble states for proteasome degradation. *Mol. Cell* **42**, 758-770.

Wang Q, Mora-Jensen H, Weniger MA, Perez-Galan P, Wolford C, Hai T, Ron D, Chen W, Trenkle W, Wiestner A, Ye Y (2009b). ERAD inhibitors integrate ER stress with an epigenetic mechanism to activate BH3-only protein NOXA in cancer cells. *Proc. Natl. Acad. Sci. USA.* **106**, 2200-2205.

Wang S, Kaufman RJ (2012). The impact of the unfolded protein response on human disease. *J. Cell Biol*. **197**, 857-867.

Weihofen A, Lemberg MK, Ploegh HL, Bogyo M, Martoglio B (2000). Release of signal peptide fragments into the cytosol requires cleavage in the transmembrane region by a protease activity that is specifically blocked by a novel cysteine protease inhibitor. *J. Biol. Chem.* **275**, 30951-30956.

Wiertz EJHJ, Tortorella D, Bogyo M, Yu J, Mothes W, Jones TR, Rapoport TA, Ploegh HL (1996). Sec6l-mediated transfer of a membrane protein from the endoplasmic reticulum to the proteasome for destruction. *Nature* **384**, 432-438.

Wilhelmus MM, Otte-Holler I, Wesseling P, de Waal RM, Boelens WC, Verbeek MM (2006). Specific association of small heat shock proteins with the pathological hallmarks of Alzheimer's disease brains. *Neuropathol. Appl. Neurobiol.* **32**, 119-130.

Wilson R, Allen AJ, Oliver J, Brookman JL, High S, Bulleid NJ (1995). The translocation, folding, assembly and redox-dependent degradation of secretory and membrane proteins in semi-permeabilized mammalian cells. *Biochem. J*. **307**, 679-687.

Wood JG, Rogina B, Lavu S, Howitz K, Helfand SL, Tatar M, Sinclair D (2004). Sirtuin activators mimic caloric restriction and delay ageing in metazoans. *Nature* **430**, 686-689.

Wordsworth D, Dunn-Walters DK (2011). The ageing immune system and its clinical implications. *Rev. Clin. Gerontol*. **21**, 110-124.

Xiao X, Zuo X, Davis AA, McMillan DR, Curry BB, Richardson JA, Benjamin IJ (1999). HSF1 is required for extra-embryonic development, postnatal growth and protection during inflammatory responses in mice. *EMBO J.* **18**, 5943-5952.

Yabuki A, Matsumoto M, Nishinakagawa H, Suzuki S (2003). Age-related morphological changes in kidneys of SPF C57BL/6Cr mice maintained under controlled conditions. *J. Vet. Med. Sci.* **65**, 845-851.

Yamamoto K, Sato T, Matsui T, Sato M, Okada T, Yoshida H, Harada A, Mori K (2007). Transcriptional induction of mammalian ER quality control proteins is mediated by single or combined action of ATF6alpha and XBP1. *Dev Cell.* **13**, 365-376.

Yan W, Frank CL, Korth MJ, Sopher BL, Novoa I, Ron D, Katze MG (2002). Control of PERK eIF2alpha kinase activity by the endoplasmic reticulum stress-induced molecular chaperone P58IPK. *Proc. Natl. Acad. Sci. USA.* **99**, 15920-15925.

Yang H, Liu C, Zhong Y, Luo S, Monteiro MJ, Fang S (2008). Huntingtin interacts with the cue domain of gp78 and inhibits gp78 binding to ubiquitin and p97/VCP. *PLoS ONE*. **5**, e8905.

Yang WL, Zhang X, Lin HK (2010). Emerging role of Lys-63 ubiquitination in protein kinase and phosphatase activation and cancer development. *Oncogene* **29**, 4493-4503. .

Yao T-P (2010). The role of ubiquitin in autophagy-dependent protein aggregate processing. *Genes Cancer*. **1**, 779-786.

Ye Y, Meyer HH, Rapoport TA (2001). The AAA ATPase Cdc48/p97 and its partners transport proteins from the ER into the cytosol. *Nature* **414**, 652-656.

Ye Y, Meyer HH, Rapoport TA (2003). Function of the p97-Ufd1-Npl4 complex in retrotranslocation from the ER to the cytosol: dual recognition of nonubiquitinated polypeptide segments and polyubiquitin chains. *J. Cell Biol*. **162**, 71-84.

Ye Y, Shibata Y, Yun C, Ron D, Rapoport TA (2004). A membrane protein complex mediates retro-translocation from the ER lumen into the cytosol. *Nature* **429**, 841-847.

Yla-Anttila P, Vihinen H, Jokitalo E, Eskelinen E-L (2009). 3D tomography reveals connections between the phagophore and endoplasmic reticulum. *Autophagy* **5**, 1180-1185.

Yokoyama K, Fukumoto K, Murakami T, Harada S, Hosono R, Wadhwa R, Mitsui Y, Ohkuma S (2002). Extended longevity of Caenorhabditis elegans by knocking in extra copies of hsp70F, a homolog of mot-2 (mortalin)/mthsp70/Grp75. *FEBS Lett.* **516**, 53-57.

Yoshida H, Matsui T, Yamamoto A, Okada T, Mori K (2001). XBP1 mRNA is induced by ATF6 and spliced by IRE1 in response to ER stress to produce a highly active transcription factor. *Cell* **107**, 881-891.

Younger JM, Chen L, Ren HY, Rosser MF, Turnbull EL, Fan CY, Patterson C, Cyr DM (2006). Sequential quality-control checkpoints triage misfolded cystic fibrosis transmembrane conductance regulator. *Cell* **126**, 571-582.

Yun C, Stanhill A, Yang Y, Zhang Y, Haynes CM, Xu CF, Neubert TA, Mor A, Philips MR, Ron D (2008). Proteasomal adaptation to environmental stress links resistance to proteotoxicity with longevity in Caenorhabditis elegans. *Proc. Natl. Acad. Sci. USA*. **105**, 7094-7099.

Zagari A, Nemethy G, Scheraga HA (1990). The effect of the L-azetidine-2-carboxylic acid residue on protein conformation. I. Conformations of the residue and of dipeptides. *Biopolymers* **30**, 951-959.

Zahn JM, Poosala S, Owen AB, Ingram DK, Lustig A, Carter A, Weeraratna AT, Taub DD, Gorospe M, Mazan-Mamczarz K, Lakatta EG, Boheler KR, Xu X, Mattson MP, Falco G, Ko MS, Schlessinger D, Firman J, Kummerfeld SK, Wood WH, 3rd, Zonderman AB, Kim SK, Becker KG (2007). AGEMAP: a gene expression database for aging in mice. *PLoS Genet*. **3**, e201.

Zhang C, Cuervo AM (2008). Restoration of chaperone-mediated autophagy in aging liver improves cellular maintenance and hepatic function. *Nat. Med*. **14**, 959-965.

Zhang Y, Nijbroek G, Sullivan ML, McCracken AA, Watkins SC, Michaelis S, Brodsky JL (2001). Hsp70 molecular chaperone facilitates endoplasmic reticulum-associated protein degradation of cystic fibrosis transmembrane conductance regulator in yeast. *Mol. Biol. Cell.* **12**, 1303-1314.

Zhong X, Pittman RN (2006). Ataxin-3 binds VCP/p97 and regulates retrotranslocation of ERAD substrates. *Hum. Mol. Genet*. **15**, 2409-2420.

Zuleta A, Vidal RL, Armentano D, Parsons G, Hetz C (2012). AAV-mediated delivery of the transcription factor XBP1s into the striatum reduces mutant Huntingtin aggregation in a mouse model of Huntington's disease. *Biochem. Biophys. Res. Commun.* **420**, 558-563. .

CHAPTER 8

Appendices

APPENDIX 1

Wider scans of immunoblots with the primary antibodies used in this study

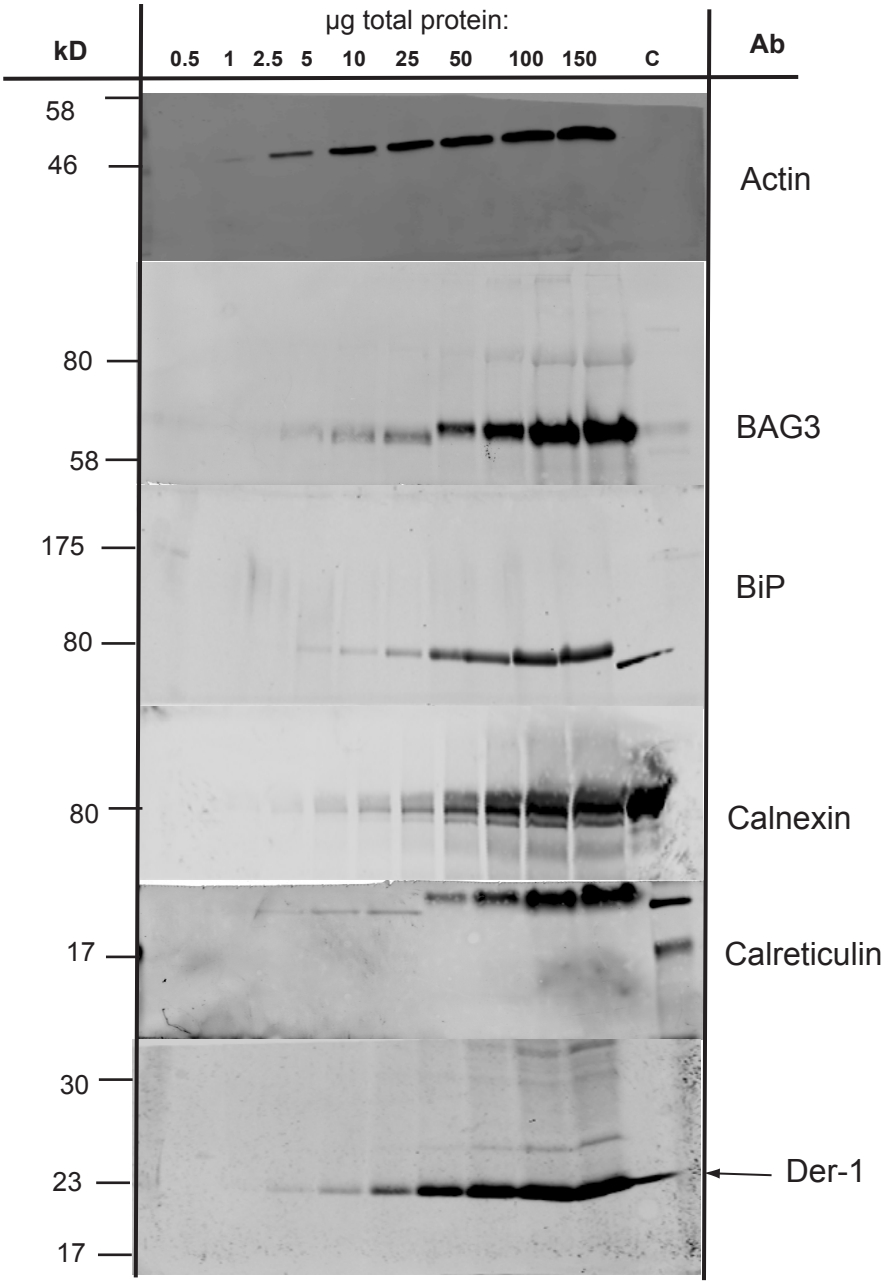

Wider scans of immunoblots

Using tissue and cells extracts, each antibody used in this study has been tested for its liniar range of fluorescence. A standard curve was designed, with concentrations of total protein from 0.5 to 150 µg. As positive control for the ER proteins, a small amount of microsome preparation was used. The samples were analysed by Western blotting with the indicated antibodies. Each band was quantified and plotted against the total protein concentration. The linar regression analysis gave the value of squared R, indicating the the linearity of the curve (see appendix 2).

.

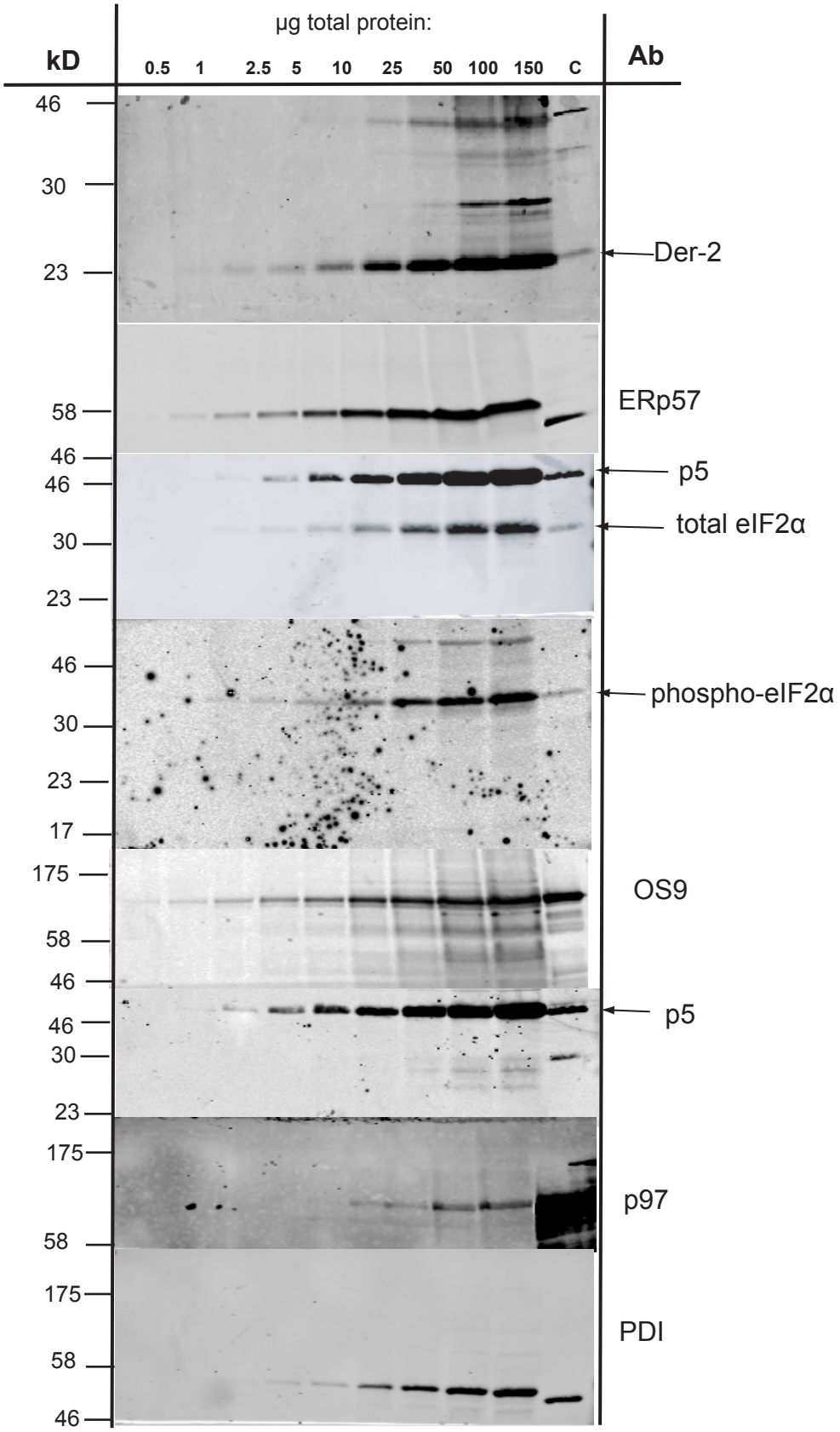
kD
µg total protein:
0.5
1
2.5
5
10
25
50
100
150
C
Ab
46
30
23
Der-2
58
ERp57
46
46
p5
30
total eIF2α
23
46
phospho-eIF2α
30
23
17
175
OS9
58
46
46
p5
30
23
175
p97
58
175
PDI
58
46

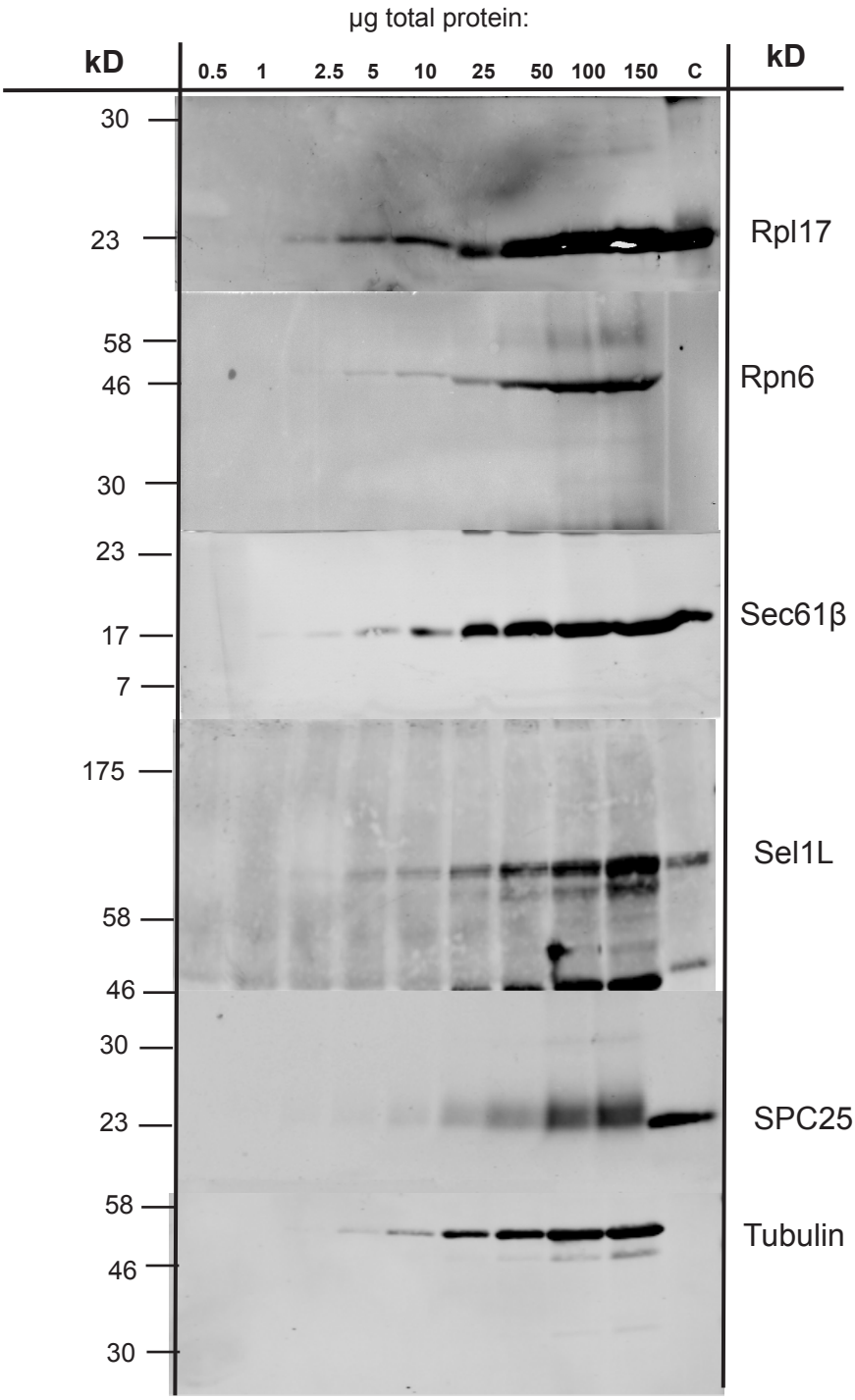
µg total protein:
kD
0.5
1
2.5
5
10
25
50
100
150
C
kD
30
23
Rpl17
58
46
30
Rpn6
23
17
7
Sec61β
175
58
46
Sel1L
30
23
SPC25
58
46
30
Tubulin

APPENDIX 2

Fluorescence linearity for the primary antibodies used in this study

The samples were prepared and analysed as described in section 2.5. Obtained data were plotted and the linearity was determined using the best-fit straight line and the associated goodness of fit (R-squared value)

Primary antibody	Linearity range µg total protein	R-squared value
actin	5 -150	0.98
BAG3	2.5 – 100	0.98
BAG6	–	–
BiP	2.5 – 150	0.97
calnexin	5 – 150	0.98
calreticulin	2.5 –150	0.95
Derlin-1	5 –150	0.97
Derlin-2	2.5 – 150	0.99
Phospho-eIF2α	5 – 150	0.99
Total eIF2α	10 - 150	0.97
ERp57	1 – 150	0.96
OS9	2.5 – 150	0.98
p5	2.5 – 100	0.96
p97	2.5 –150	0.97
PDI	2.5 – 150	0.99
Rpl17	2.5 – 25	0.95
Rpt6	5 - 25	0.96
Sec61β	50 - 150	9.99
Sel1L	5 – 150	0.99
SPC25	25 – 150	0.99
Tubulin	5 –150	0.96

APPENDIX 3: The specific band for BiP antibody in various tissues

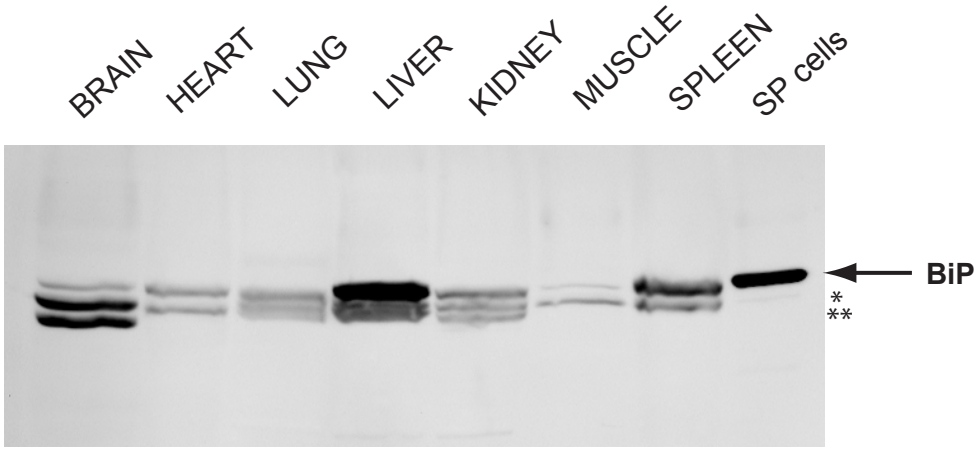

The specific band for BiP is the first top band in each of the used tissues. This is demonstrated by the SP cells sample where only a single band can be seen, therefore the other bands, marked * and ** are non-specific.

APPENDIX 4

Actin and tubulin relative to total protein for the *in vitro* and the *in vivo* aged cells

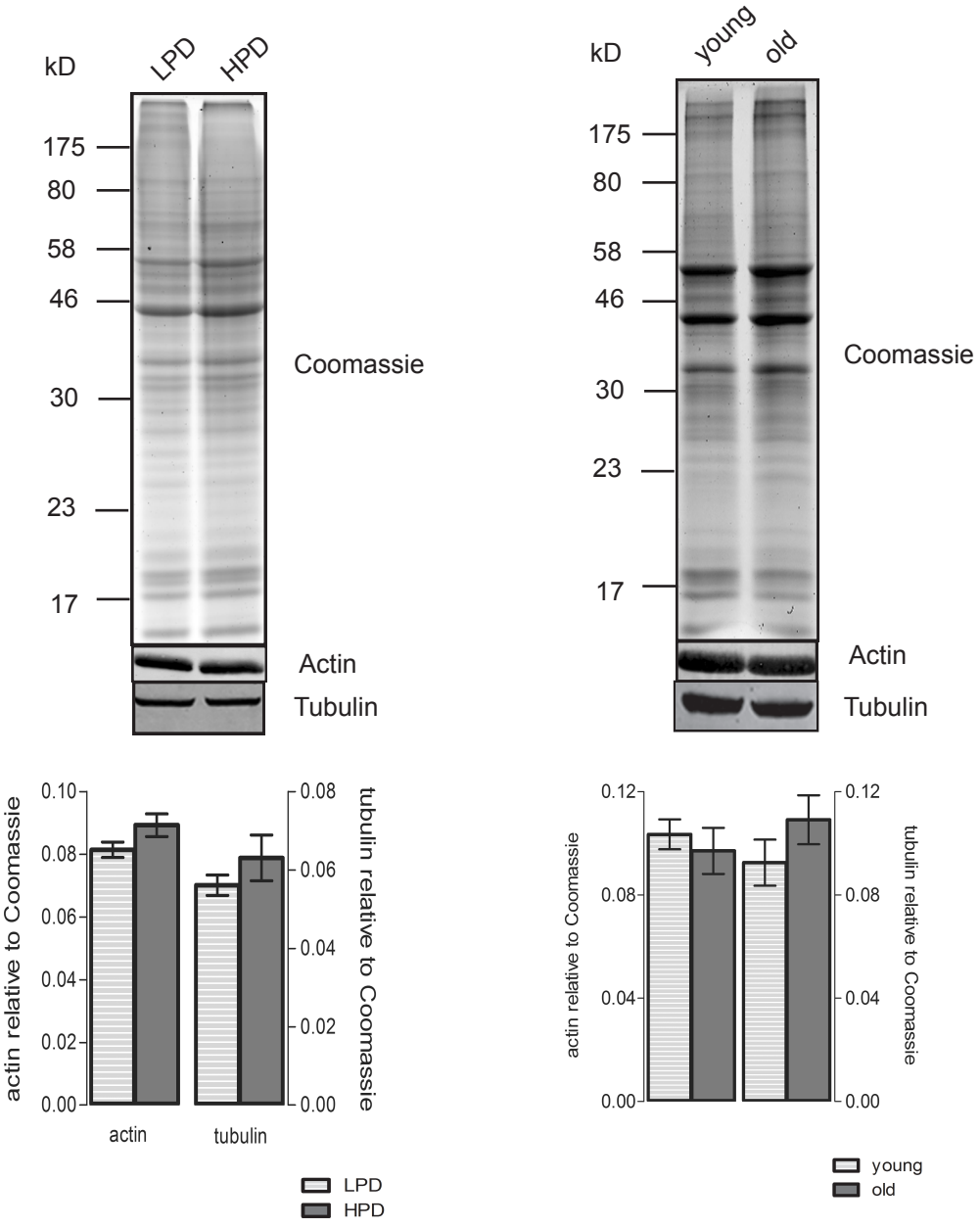

The level of actin and tubulin relative to total protein (Coomassie) was calculated for LPD and HPD cells, respectively for young and old cells and plotted as mean ± s.e.m. of three independent experiments.
No significant differences between the LPD and HPD, respectively young and old cells regarding the level of actin was observed, therefore the actin was used as loading control for all the immunoblotting experiments using cells.

APPENDIX 5
Full images of *in vitro* translation gels from this study

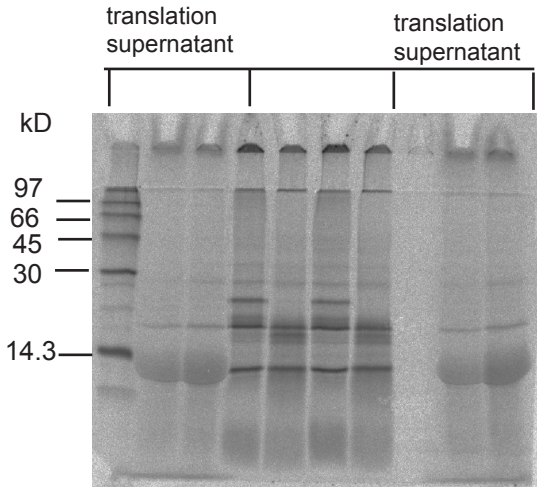

γ-INF

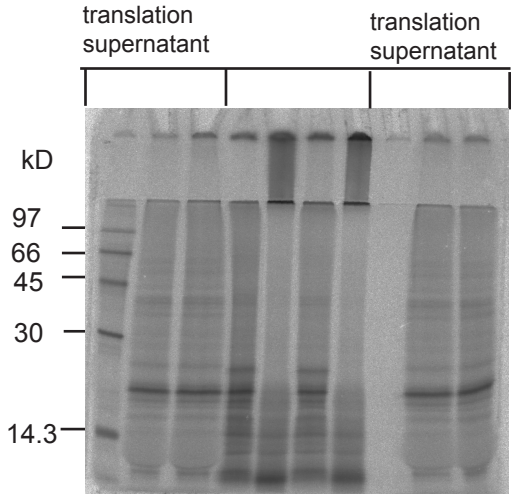

US2

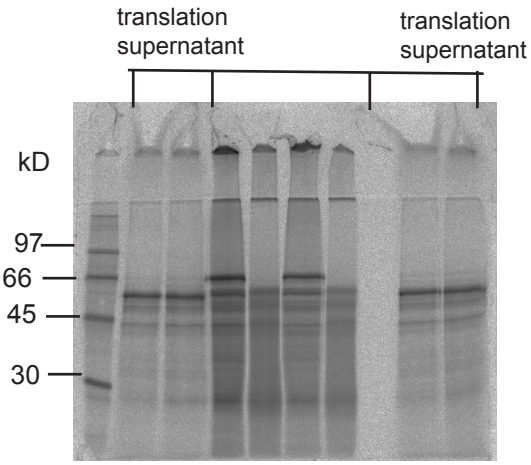

HA

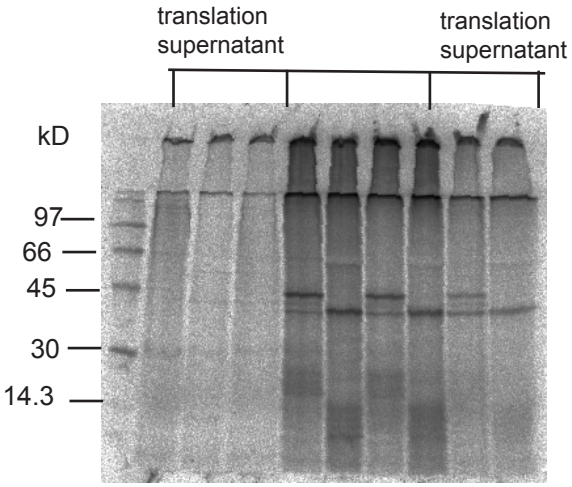

SPP

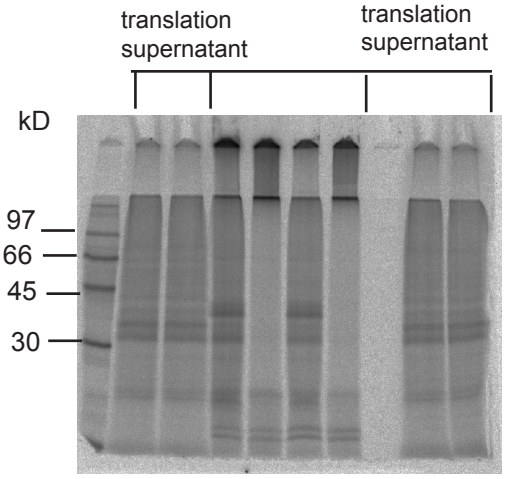

ops

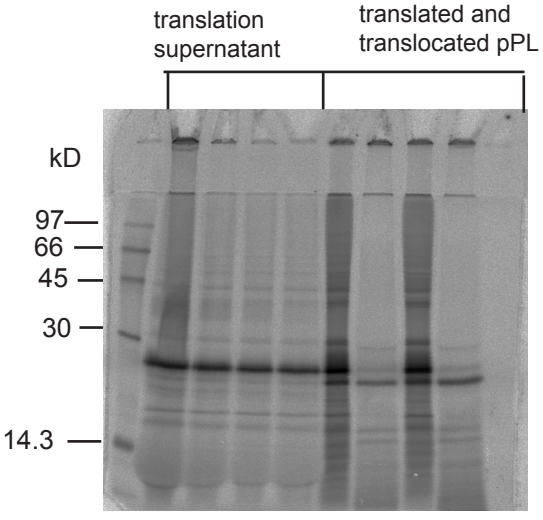

pPL